Iranica Journal of Energy & Environment 5 (3): 224-232, 2014
ISSN 2079-2115
IJEE an Official Peer Reviewed Journal of Babol Noshirvani University of Technology
DOI: 10.5829/idosi.ijee.2014.05.03.01

BUT

Attaining Optimum Tilts of Flat Solar Surfaces Utilizing Measured Solar Data: Case Study for Ilam, Iran

[1,2]H. Khorasanizadeh, [1]A. Aghaei, [1]H. Ehteram, [1]R. Dehghani Yazdeli and [1]N. Hataminasar

[1]Faculty of Mechanical Engineering, University of Kashan, Kashan, Iran
[2]Energy Research Institute, University of Kashan, Kashan, Iran

Date of Received: July 1, 2014; Date of Accepted in Revised Form: August 4, 2014

Abstract: The efficiency of the flat solar surfaces, such as thermal collectors and photovoltaic (PV) panels, depends on the received beam and diffuse radiation components and the angle of the beam incidence. In this study, based on the long term measured data tilt angle optimization of the flat solar surfaces in the city of Ilam, Iran, for the daily, monthly, seasonal and annual fixed adjustments have been performed. Study of characteristics of solar radiation showed that Ilam has 220 days in the year with horizontal global radiation in the range of 15-35 MJ/m^2 and 182 sunny or very sunny days having daily clearness index higher than 0.6. The optimum tilt for the fixed daily adjustment throughout the year varies between zero and 61° and the optimum tilt for the fixed monthly adjustment varies between 0° in June and July up to 60.1° in December. The optimum tilt for the fixed annual adjustment is 26°, which is close to latitude of Ilam (33.38°). Furthermore, the optimum tilt for the fixed seasonal adjustment in winter and autumn are 12.3 and 20° higher than the latitude of Ilam, respectively; whereas in spring and summer they are 30.3 and 21.1° less than the latitude, respectively.

Key words: Solar radiation · Optimum tilt angle · Flat solar surfaces · Collectors · Ilam

INTRODUCTION

Solar energy is the most important clean, free and unending renewable energy source which can be utilized in many parts of the world. The limitation and shortage of fossil fuels and the issues resulted from changes of world environmental and weather conditions have created a good opportunity for solar energy to compete with fossil based fuels. This is more important, in countries with high potential of solar radiation to be benefited from green and clean energy. Utilization of different kinds of solar energy technologies such as solar photovoltaic, concentrating solar thermal power, solar hot water/space heating systems, solar dryers, solar stills and solar ovens are becoming rapidly widespread. Aligned with recent augmented deployment of these technologies, many studies have been undertaken to enhance the performance of such technologies [1-5].

Flat-plate solar surfaces, such as thermal collectors and PV panels, have wide applications in domestic and industrial solar systems. A solar system, like any other system, must perform with the highest possible efficiency. This needs the correct design, manufacturing and installation of different components of the system. As for flat solar collectors, the best possible angle of the radiation incidence depends on their orientation and tilt angle; thus determining the proper installation is very vital in order to improve their performance. The optimum tilt angle is influenced by different factors such as the latitude, the clearness index, the air pollution and the distribution of the sunny days throughout the year [6-8]. Therefore, in order to design a solar energy system utilized by flat collectors in a region, performing solar radiation evaluation is essential for attaining suitable information about these factors. A study of this type has recently been undertaken by Khorasanizadeh *et al*. [9] for Yazd province of Iran.

There have been many studies on the optimum tilt and azimuth angles of solar surfaces around the globe, from which references are made here only to some of

Corresponding Author: H. Khorasanizadeh,University of Kashan, Kashan, Iran; Post Code: 87317-51167.
Tel: +98 361 55912449, Fax: +98 361 55912424.

Please cite this article as: H. Khorasanizadeh, A. Aghaei, H. Ehteram, R. Dehghani Yazdeli and N. Hataminasar, 2014. Attaining Optimum Tilts of Flat Solar Surfaces Utilizing Measured Solar Data: Case Study for Ilam, Iran . Iranica Journal of Energy and Environment, 5 (3): 224-232

them. Kern and Harris [10] explained the calculations related to the optimum slope angle based on the beam radiation. Chiou and EI-Naggar [11] carried out an investigation for many regions of the world using different techniques to attain the relation between the optimum slope angle and the latitude. Lewis [12] suggested two theoretical models for determining the optimum angle. In one model, he considered the cloudy and clearness indexes as variables and in another one he used Kern and Harris's model [10]. El-Kassaby [13] introduced an analytical equation for finding the optimum slope angle in any latitude and showed that it can be integrated to calculate the optimum slope angle for any period of time. Hj Mohd Yakup and Malik [14] and Skeiker [6], studied the issue of optimum slope angle in Brunei and Syria, respectively. They mentioned that in northern hemisphere the best orientation for the collectors is tilting them toward the south and the optimum tilt is only dependent on the latitude. Skeiker [6] developed an equation for calculating the optimum daily slope angle and computed the optimum daily slope angle for some cities in Syria. Hussein *et al.* [15] used the software TRNSYS and showed the optimum slope angle for annual fixed adjustment of collectors in Cairo, Egypt, is φ- 10. Ulgen [16] used a mathematical model and determined the monthly, seasonally and yearly optimum slope angles for collectors in Izmir, Turkey. He mentioned that the optimum slope angle varies between 0 and 61° for different months of the year. Gunerhan and Hepbasli [17] recommended that if a collector in Izmir is adjusted fixed for the whole year, its optimum slope angle is equal to the latitude. Furthermore, for seasonal fixed adjustment, they reported that the optimal slope angle isφ+15 for winter andφ-15 for summer. Calabro [18] showed the annual optimum slope angle in the area of southern-Italy (Sicily) is φ-10. Chenga *et al.* [19] indicated that the annual slope angle is approximately equal to the latitude for the regions below the equator line and for higher latitudes the angle is less than the latitude.

Using the genetic algorithm technique, Talebizadeh *et al.* [20] theoretically determined the surface azimuth and optimum tilt angles of collectors for installation in Kerman. By assuming that the collector surface is always facing toward the equator, Benghanem [21] determined the optimum slope of flat solar collectors in Madinah, Saudi Arabia. In order to calculate the optimum tilt angle, he used the measured values of daily total and diffuse solar radiations on a horizontal surface. He reported that annual optimum tilt angle is approximately equal to latitude, i.e. 23.5°. Also, he found that the optimum seasonal tilt angle in winter and summer are 37° and 12°, respectively. He reported that the loss of receiving energy is around 8% when adjusting the collector fixed with the annual optimum tilt angle compared with that of a collector adjusted monthly with the optimum tilt angle. In a recent study, Khorasanizadeh *et al.* [22] developed a horizontal diffuse radiation model for city of Tabass in Iran and determined the optimum tilt angle for south-facing solar surfaces for the fixed monthly, seasonal, semi-yearly and yearly adjustments.

Iran is located in a sunny region of the world enjoying high amount of solar radiation with 240-250 sunny days in the year. Tilt angle optimization of flat solar surfaces in the city of Ilam, the center of Ilam province of Iran, has not been yet carried out. Hence, in this study the seven years measured solar data have been utilized firstly to obtain the averaged daily horizontal total radiation (HGR) throughout the year. Then, based on these HGR values the daily clearness index, the monthly averaged HGR and clearness index values have been achieved. Finally, optimum tilt angles of flat solar surfaces have been obtained for the fixed daily, monthly, seasonal and annual tilt adjustments.

MATERIALS AND METHODS

In this section, the study region and the method utilized for applying the measured solar data are explained first. Then the mathematical models used for obtaining the solar radiation on inclined surfaces as well as well as clearness index are presented.

Figure 1 portrays the geographic location of the city of Ilam on the map of Iran, with the latitude of 33.38° and the longitude of 46.25°. The total daily solar radiation on horizontal surface, measured for seven years (2004-2010) in Ilam meteorological station, have been employed to obtain the average total daily radiation values,*H*, for all of days of the year. Then these values have been used to obtain the monthly averaged daily total radiation on horizontal surface for all of the months of a year. All further calculations for obtaining the daily as well as monthly averaged daily clearness indexes and optimum tilts of flat solar collectors are based on these averaged values.

Most of the solar radiation data are measured for horizontal surfaces; therefore it is necessary to calculate the solar radiation on a tilted surface through mathematical modeling. The total daily solar radiation on a tilted surface consists of [23].

Fig. 1: Geographic location of the city of Ilam on the map of Iran.

$$H_T = H_{bT} + H_{dT} + H_{gT} \quad (1)$$

where H_T is the average daily radiation on tilted surface and H_{bT}, H_{dT} and H_{gT} are the averaged daily beam, daily diffuse and ground-reflected radiations on the tilted surface, respectively. For calculating these terms, a method presented by Klein [24] has applied, by which the diffuse and the ground-reflected radiations are calculated using the isotropic model, stated as follows:

$$H_T = H_b R_b + H_d\left(\frac{1+\cos\beta}{2}\right) + H\rho_g\left(\frac{1-\cos\beta}{2}\right) \quad (2)$$

β is the collector slope angle and ρ_g is the ground reflectivity coefficient which is dependent on the kind of the ground around the tilted surface. H_b is the beam daily radiation on a horizontal surface and R_b is the ratio of the beam radiation on the tilted surface to that on a horizontal surface. For the northern hemisphere R_b is expressed as [24]:

$$R_b = \frac{\cos(\phi-\beta)\cos\delta\sin\omega_s' + \left(\frac{\pi}{180}\right)\omega_s'\sin(\phi-\beta)\sin\delta}{\cos\phi\cos\delta\sin\omega_s + \left(\frac{\pi}{180}\right)\omega_s\sin\phi\sin\delta} \quad (3)$$

where φ is the latitude and ω_s is the sunset hour angle for a horizontal surface, defined as [23]:

$$\omega_s = \cos^{-1}(-\tan\varphi\tan\delta) \quad (4)$$

δ is the declination angle defined as the angular position of the sun at solar noon with respect to the plane of the equator. δ is determined from following expression [24]:

$$\delta = 23.45\sin\left(360\frac{284+n}{365}\right) \quad (5)$$

n is the day number from the first of January. ω_s' is the sunset hour angle for an inclined surface and is defined as [24]:

$$\omega_s' = \min\begin{bmatrix}\cos^{-1}(-\tan\varphi\tan\delta)\\ \cos^{-1}(-\tan(\varphi-\beta)\tan\delta)\end{bmatrix} \quad (6)$$

To calculate H_b and H_d in equation (2), the K_T method [25] is used. K_T is the daily clearness index and is defined as the ratio of the terrestrial global daily radiation on a horizontal surface to the extraterrestrial radiation on a horizontal surface at the same latitude as [23]:

$$K_T = \frac{H}{H_o} \quad (7)$$

H_o is extraterrestrial radiation obtained from [23]:

$$H_o = \frac{24 \times 3600\, G_{sc}}{\pi}\left(1 + 0.033 \cos\frac{360n}{365}\right)\left(\cos\varphi \cos\delta \sin\omega_s + \frac{\pi\omega_s}{180}\sin\varphi \sin\delta\right) \quad (8)$$

G_{sc} is the solar constant equal to 1367 (W/m^2) [23]. After calculating K_T, H_d can be determined from [25]:
For $\omega_s \leq 81.4°$:

$$\frac{H_d}{H} = \begin{cases} 1.0 - 0.272 K_T + 2.4495 K_T^2 - 11.9514 K_T^3 + 9.3879 K_T^4 & \text{for } K_T < 0.715 \\ 0.143 & \text{for } K_T \geq 0.715 \end{cases} \quad (9)$$

and for $\omega_s \leq 81.4°$:

$$\frac{H_d}{H} = \begin{cases} 1.0 + 0.2832 K_T - 2.5557 K_T^2 + 0.8448 K_T^3 & \text{for } K_T < 0.722 \\ 0.175 & \text{for } K_T \geq 0.722 \end{cases} \quad (10)$$

Then H_b is obtained from:

$$H = H_b + H_d \quad (11)$$

To calculate the monthly averaged daily radiation on a tilted surface a similar procedure must be carried out, except that for obtaining R_b the values of ω_s, ω_s' and δ are calculated for the average day of that month. The average day of each month and the corresponding day number from the beginning of the year are presented in Table 1.

For each month, the monthly averaged daily radiation on a tilted surface is defined as [25]:

$$\bar{H}_T = \bar{H}_b \bar{R}_b + \bar{H}_d\left(\frac{1+\cos\beta}{2}\right) + \bar{H}\rho_g\left(\frac{1-\cos\beta}{2}\right) \quad (12)$$

$\bar{H}_d$ and $\bar{H}_b$ are the monthly averaged daily diffuse and beam radiations on a horizontal surface, respectively and $\bar{R}_b$ is the ratio of the beam radiation on the tilted surface to that on a horizontal surface on the average day of the corresponding month. For calculating $\bar{H}_d$, the monthly average clearness index is used, which is [26]:

$$\bar{K}_T = \frac{\bar{H}}{\bar{H}_o} \quad (13)$$

Table 1: The monthly average day of every month and its related day number [25].

Month	Monthly average day	n, for monthly average day
January	17	17
February	16	47
March	16	75
April	15	105
May	15	135
June	11	162
July	17	198
August	16	228
September	15	258
October	15	288
November	14	318
December	10	344

$\bar{H}_o$ is the monthly average daily extraterrestrial radiation calculated via Eq. (8) for the average day of each month for the latitudes in the range of -60≤ φ≤ 60.

For $\bar{K}_T$ in the range of 0.3 to 0.8, $\bar{H}_d$ could be obtained from [25]:
for $\omega_s \leq 81.4°$:

$$\frac{\bar{H}_d}{\bar{H}} = 1.391 - 3.560\,\bar{K}_T + 4.189\,\bar{K}_T^2 - 2.137\,\bar{K}_T^3 \quad (14)$$

and for $\omega_s \leq 81.4°$:

$$\frac{\bar{H}_d}{\bar{H}} = 1.311 - 3.022\,\bar{K}_T + 3.427\,\bar{K}_T^2 - 1.821\,\bar{K}_T^3 \quad (15)$$

After calculating $\bar{H}_d$ from the above equations, $\bar{H}_b$ can be determined from:

$$\bar{H} = \bar{H}_b + \bar{H}_d \quad (16)$$

To calculate the optimum tilt angle for different adjustment strategies a computer program was prepared in FORTRAN software.

This program utilizes the calculated values of averaged daily global radiation on a horizontal surface to obtain the beam and diffuse components via Eqs. (7) to (11). Then for obtaining the optimum slope angle for the fixed daily adjustment it changes β from 0° to 90° with interval of 0.1°. In order to obtain H_T for every day and every β, the program employs Eqs. (3) to (6) to calculate the terms in right hand side of Eq. (1). At last the β which causes the maximum value of H_T is chosen by the program as the optimum tilt angle for that day. For the fixed monthly adjustment the program firstly utilizes the calculated values of monthly mean daily global radiation to obtain the beam and diffuse components on a

horizontal surface via Eqs. (13) to (16). Then for obtaining the optimum slope angle for the fixed monthly adjustment the program employs Eq. (12) and changes β from 0° to 90° with interval of 0.1°. In the end the β which causes the maximum value of $\bar{H}_T$ is chosen by the program as the optimum tilt angle for that month. The same procedure is followed to obtain the optimum tilt angle for the fixed seasonal adjustment, except that $\bar{H}_T$ is computed for every β but for all of the months of that season. The angle for which the summation of $\bar{H}_T$ values related to all of the months of that season becomes maximum is considered as the optimum tilt angle of that season. Also for the fixed annual adjustment and after following the same procedure, the angle for which the summation of $\bar{H}_T$ values related to all of the months of a year becomes maximum is considered as the annual optimum tilt angle. The program makes an output file containing the optimum tilt for every selected individual adjustment period as well as the values of H_T for all of days of the year for the fixed daily adjustment and $\bar{H}_T$ for all of the months for the fixed monthly, seasonal and annual adjustment periods. In Ilam province most of the region are bare grounds, therefore ρ_g is considered to be 0.2 in all of the calculations [12].

RESULTS AND DISCUSSION

In this section, the results for the optimum tilt angle of flat solar surfaces in Ilam, for the fixed daily, monthly, seasonal and annual adjustments are presented.

Table 2 illustrates the frequency distribution of daily global radiation on horizontal surface, H, in different ranges in Ilam. There are 220 days in a year which have approximately solar radiation in the range of 15-35 MJ/m^2.

Passing through the earth atmosphere, the solar radiation is subjected to the atmosphere absorption and diffusion, the cloudy conditions, air pollution and other parameters. The impact of these parameters on solar radiation characteristics can be surveyed by studying the clearness index. To classify the level of clearness of sky, four different intervals for K_T have been recognized [27] as:

Cloudy : $0< K_T <0.2$
Partly cloudy : $0.2 \le K_T <0.6$
Sunny : $0.6 \le K_T <0.75$
Very sunny : $0.75 \le K_T < 1$

The frequency distribution of K_T in different ranges throughout the year is presented in Table 3. As shown in Table 3, there are 182 sunny or very sunny days in Ilam with a K_T higher than 0.6. This indicates the appropriate condition of this region for solar energy applications particularly utilization of flat plate solar thermal and photovoltaic collectors; hence the optimization of tilt angles of these solar surfaces is important.

Table 2: The frequency distribution of H in different ranges in Ilam.

Range of H (MJ/m^2)	Frequency distribution (days)
5-10	61
10-15	83
15-20	58
20-25	68
25-30	87
30-35	7
35-40	1

Table 3: The frequency distribution of K_T in different ranges in Ilam.

Range of K_T	Frequency distribution (days)
0.3-0.4	8
0.4-0.5	52
0.5-0.6	123
0.6-0.7	142
0.7-0.8	35
0.8-0.9	4
0.9-1.0	1

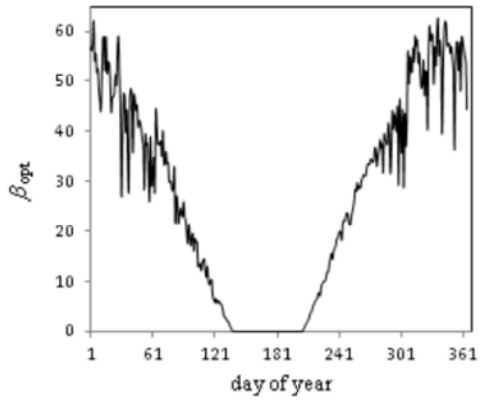

Fig. 2: The optimum slope angle for the fixed daily adjusted surface in Ilam.

Figure 2 shows the optimum tilt angle for different days of the year. The variation of the daily optimum tilt angel throughout the year between zero and 61° is notable. Winter, spring, summer and autumn seasons in the northern hemisphere consist of: (1) January, February and March; (2) April, May and June; (3) July, August and September; (4) October, November and December, respectively. In autumn and winter, the angle of the solar beam radiation has more deviation from the normal extension of the horizon because the solar declination angle is negative, thus the collector should be mounted toward south with a greater slope from the

Table 4: Optimum tilt angles and the corresponding monthly mean total solar radiations for different tilt adjustments in Ilam.

Monthly	$\bar{H}$ (MJ/m^2)	βopt (°)	$\bar{H}_T$ (MJ/m^2)	Seasonal	βopt (°)	$\bar{H}_T$ (MJ/m^2)	Yearly	βopt (°)	$\bar{H}_T$ (MJ/m^2)
Jan	9.79	57.70	15.86	Winter	45.7	15.56	Whole year	26.0	13.92
Feb	11.69	47.4	15.58			15.55			14.74
Mar	17.91	34.5	20.73			20.32			20.55
Apr	21.59	16.9	22.27	Spring	3	21.71			22.06
May	25.23	1.6	25.23			25.12			23.71
Jun	29.21	0.0	29.21			29.05			26.36
Jul	27.13	0.0	27.13	Summer	12.3	26.45			24.99
Aug	25.38	11.2	25.76			25.66			25.18
Sep	20.49	28.3	22.58			21.79			22.51
Oct	13.60	43	17.15	Autumn	53.4	16.84			16.57
Nov	11.22	56.2	17.90			17.78			15.84
Dec	9.15	60.1	15.80			15.61			13.51

horizon. In spring and summer, deviation of the solar beam radiation from the normal extension is less (declination is positive), thus the collector should be mounted with a lesser slope such that it is zero in the last days of May, the whole days of June and most days of July. The difference between the optimum angle of the first day and that of the last day of the year noticed in Figure 2 is related to the difference between the averaged values of the measured daily solar radiations in these days.

Figure 3 shows the monthly mean daily clearness index for different months of the year. The maximum $\overline{K_T}$ is 0.866 which corresponds to June. In general, the $\overline{K_T}$ values related to the middle months of the year (i.e. May, June and July) demonstrate a better clear sky, because they are higher than those related to other months.

Skeiker [6] computed the optimum tilt angle of solar collectors in the major Syrian zones for the fixed daily adjustment as well as other adjustment strategies such as monthly and seasonal. His results indicated that changing the tilt angle once every month (12 times in the year) keeps the total annual solar radiation received approximately near that of received by daily adjustment. Therefore, in the absence of utilizing a tracking system, the monthly adjustment of solar collectors and PV panels is a preferred strategy. The monthly optimum tilt angle along with the corresponding monthly mean daily total solar radiation on the optimally monthly adjusted surface together with the monthly mean daily total radiation on a horizontal surface in Ilam have been presented in Table 4. As shown, the maximum and minimum values of daily solar radiation on a horizontal surface are 29.2 and 9.15 MJ/m^2 which corresponds to June and December, respectively. However, the monthly optimum tilt is zero for June, while it is 60.1° in December and the total daily radiation received by the tilted surface in December is

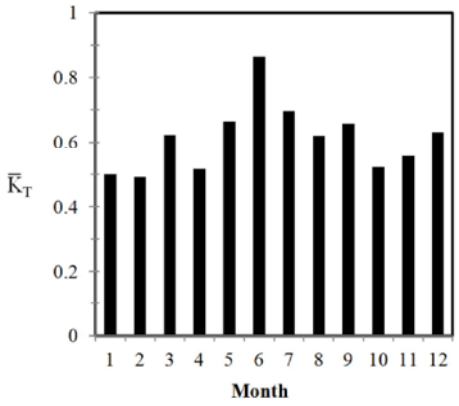

Fig. 3: The monthly averaged daily clearness index in Ilam.

73% more than that of a horizontal surface. As explained before, for the months of summer and spring seasons the solar declination angle is positive, thus their optimum monthly angles are lower compared to those of other months.

To show the effect of optimal tilt adjustment, the monthly averaged daily radiation on a horizontal surface and on an optimally tilted surface are shown together for different months of the year in Figure 4. As shown in Figure 4, employing the monthly adjustment demonstrates its maximum effect on the first and the last four months of the year. By utilizing this strategy the total gain of the monthly optimally tilted surface in these 8 months is 28% more than that of received by a horizontal surface in the same period. However, the relative annual extra gain of the monthly optimally tilted surface compared to that of horizontal surface is 14.75%.

For making comparison, the seasonal optimum tilts as well as the optimum tilt for the fixed annual adjustment along with the corresponding monthly mean daily total solar radiations on optimally adjusted surfaces are also presented in Table 4. It is observed from Table 4 that for

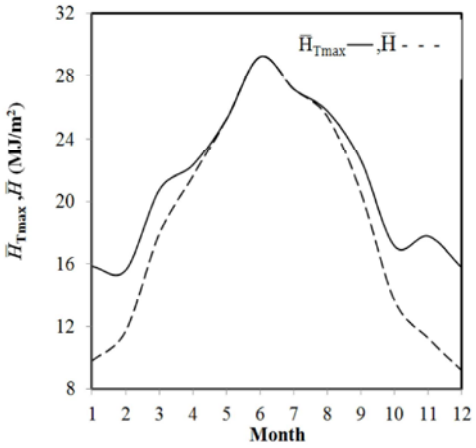

Fig. 4: The monthly averaged daily total radiation on horizontal and on optimally monthly adjusted surfaces in Ilam.

achieving the maximum radiation in autumn and winter the tilts of the collector should be approximately 20 and 12.3° higher than the latitude of Ilam (33.38 °), respectively and in spring and summer they should be 30.4 and 20.1° less than the latitude, respectively. The optimum angle for the fixed annual adjustment is 26°, which is close to the latitude of Ilam. Comparing the values of the monthly mean daily radiation on the optimally tilted surface in every month attained for different tilt adjustment strategies reveal the dependency of the received radiation to the selected tilt strategy. Therefore, the corresponding total annual solar gain is also dependent on the selected tilt adjustment strategy. The relative total annual extra solar gain of the seasonal optimally adjusted surface compared to that of horizontal surface is 13.06%, whereas for the optimally annually adjusted surface it is just 7.89%.

CONCLUSION

In this work, the solar data recorded for a period of seven years have been utilized to obtain the averaged daily horizontal total radiation (HGR) throughout the year in Ilam. Then, based on these HGR values the daily clearness index, the monthly averaged daily HGR and clearness index values have been obtained. At last optimum tilt angles of flat solar surfaces have been obtained for the fixed daily, monthly, seasonal and annual tilt adjustments. In Ilam, there are 220 days in the year with solar radiation in the range of 15-35 MJ/m^2 and 182 sunny and very sunny days with a K_T higher than 0.6; thus appropriate status of this region for utilization of flat plate solar thermal and photovoltaic flat collectors confirmed the necessity of tilt optimization. The optimum tilt for the fixed daily adjustment throughout the year varies between zero and 61° and the maximum optimum tilt for the fixed monthly adjustment is 60.1° for January and the minimum is zero for June as well as July, respectively. The optimum tilts for the fixed seasonal adjustment are 3°, 12.3°, 53.4° and 45.7° for spring, summer, autumn and winter, respectively. The optimum tilt for the fixed annual adjustment is 26°, which is close to the latitude of Ilam. Total yearly extra solar gain of the monthly, seasonal and annually optimally adjusted surfaces compared to that of horizontal surface are 14.75, 13.06 and 7.89%, respectively.

ACKNOWLEDGMENT

The authors are highly grateful to the Energy Research Institute of the University of Kashan for supporting this research (Grant No. 158576/12). Also thanks are extended to the Iranian meteorological organization (IMO) for providing the solar data.

REFERENCES

1. Panchal, H.N. and P.K. Shah, 2011. Char performance analysis of different energy absorbing plates on solar stills. Iranica Journal of Energy & Environment, 2(4): 297-301.
2. Azimi, A. and T. Tavakoli, 2012. Experimental study on eggplant drying by an indirect solar dryer and open sun drying. Iranica Journal of Energy & Environment, 3(4): 347-353.
3. Khalil, M.H., M. Ramzan, M.U. Rahman and M.A. Khan, 2012. Development and evaluation of a solar thermal collector designed for drying grain. Iranica Journal of Energy & Environment, 3 4): 380-384.
4. Mehrpooya, M. and S. Daviran, 2013. Dynamic modeling of a hybrid photovoltaic system with hydrogen/air PEM fuel cell. Iranica Journal of Energy & Environment, 4(2): 104-109.
5. Shah, N.A., M. Abbas, W.A. Syed and W. Mahmood, 2014. Physical properties of silver doped ZnSe thin films for photovoltaic applications. Iranica Journal of Energy & Environment, 5 (1): 87-93.
6. Skeiker, K., 2009. Optimum tilt angle and orientation for solar collectors in Syria. Energy Conversion and Management, 50: 2439-2448.

7. Keyanpour-Rad, M., H.R. Haghgou, F. Bahar and E. Afshari, 2000. Feasibility study of the application of solar heating systems in Iran. Renewable Energy, 20: 333-345.
8. GharakhaniSiraki, A. and P. Pillay, 2012. Study of optimum tilt angles for solar panels in different latitudes for urban applications. Solar Energy, 86: 1920-1928.
9. Khorasanizadeh, H., K. Mohammadi and A. Aghaei, 2014. The potential and characteristics of solar energy in Yazd province, Iran. Iranica Journal of Energy & Environment, 5(2): 173-183.
10. Kern, J. and L. Harris, 1975. On the optimum tilt of a solar collector. Solar Energy, 17: 97-102.
11. Chiou, J.P. and M.M. EI-Naggar, 1986. Optimum slope for solar insolation on a flat surface tilted toward the equator in the heating season, Solar Energy, 36: 471-478.
12. Lewis, G., 1987. Optimum tilt of solar collectors. Solar & Wind Energy, 4: 407-410.
13. El-Kassaby, M.M., 1988. Monthly and daily optimum tilt angle for south facing solar collectors; theoretical model, experimental and empirical correlations. Solar & Wind Technology, 5: 589-596.
14. HjMohdYakup, M.A. and A.Q. Malik, 2001. Optimum tilt angle and orientation for solar collector in Brunei Darussalam. Renewable Energy, 24: 223-234.
15. Hussein, H.M.S., G.E. Ahmad and H.H. El-Ghetany, 2004. Performance evaluation of photovoltaic modules at different tilt angles and orientations. Energy Conversion and Management, 45: 2441-2452.
16. Ulgen, K., 2006. Optimum tilt angle for solar collectors. Energy Sources, Part A: Recovery, Utilization and Environmental Effects, 28: 1171-1180.
17. Gunerhan, H. and A. Hepbasli, 2007. Determination of the optimum tilt angle of solar collectors for building applications. Building and Environment, 42: 779-783.
18. Calabro, E., 2009. Determining optimum tilt angles of photovoltaic panels at typical north-tropical latitudes. Journal of Renewable and Sustainable Energy, 1: Article ID 033104 doi:10.1063/1.3148272
19. Chenga, C.L., C.S.S. Jimenez and M. Lee, 2009. Research of BIPV optimal tilted angle, use of latitude concept for south orientated plans, Renewable Energy, 34: 1644-1650.
20. Talebizadeh, P., M.A. Mehrabian and M. Abdolzadeh, 2011. Prediction of the optimum slope and surface azimuth angles using the Genetic Algorithm. Energy and Building, 43: 2998-3005.
21. Benghanem, M., 2011. Optimization of tilt angle for solar panel: Case study for Madinah, Saudi Arabia. Applied Energy, 88: 1427-1433.
22. Khorasanizadeh, H., K. Mohammadi and A. Mostafaeipour, 2014. Establishing a diffuse solar radiation model for determining the optimum tilt angle of solar surfaces in Tabass, Iran. Energy Conversion and Management, 78: 805-814.
23. Duffie, J.A. and W.A. Beckman, (3rd edition) 2006. Solar engineering of thermal processes. New York: John Wiley & Son.
24. Klein, S.A., 1981. Calculation of monthly average insolation on tilted surfaces. Solar Energy, 10: 72-77.
25. Klein, S.A., 1978. Calculation of flat-plate collector utilizability. Solar Energy, 21: 393-402.
26. Liu, B.Y.H. and R.C. Jordan, 1960. The interrelationship and characteristic distribution of direct, diffuse and total solar radiation. Solar Energy, 4: 1-19.
27. Yousif, C., G.O Quecedo and J.B. Santos, 2013. Comparison of solar radiation in Marsaxlokk, Malta and Valladolid, Spain. Renewable Energy, 49: 203-206.

Nomenclature:

G_{sc} = Solar constant
H = Daily global radiation on horizontal surface (MJ/m^2)
$\overline{H}$ = Monthly mean daily global radiation on horizontal surface (MJ/m^2)
H_b = Daily beam radiation on a horizontal surface (MJ/m^2)
H_{bT} = Daily beam radiation on tilted surface (MJ/m^2)
$\overline{H}_b$ = monthly mean daily beam radiation on a horizontal surface (MJ/m^2)
H_d = Daily diffuse radiation on horizontal surface (MJ/m^2)
H_{dT} = Daily diffuse radiation on tilted surface (MJ/m^2)
$\overline{H}_d$ = Monthly mean daily diffuse radiation on a horizontal surface (MJ/m^2)
H_g = Daily ground-reflected radiation on horizontal surface (MJ/m^2)
H_{gT} = (MJ/m^2)
H_o = Daily extraterrestrial on horizontal surface (MJ/m^2)
$\overline{H}_o$ = Monthly mean daily extraterrestrial on horizontal surface (MJ/m^2)

H_T = Daily global radiation on a tilted surface (MJ/m^2)
$\overline{H}_T$ = Monthly mean daily global radiation on tilted surface (MJ/m^2)
K_T = Daily clearness index
$\overline{K}_T$ = Monthly mean daily clearness index
n = Number day
R_b = The ratio of the beam radiation on tilted surface to that on a horizontal surface

Greek Letters:

δ = Solar declination angle (°)
φ = Latitude of the location (°)
β = Tilt angle of the collector
β_{opt} = Optimum tilt angle of the collector
ρ_g = Ground reflectivity coefficient
ω_s = Sunset hour angle on horizontal surface (°)
ω_s = Sunset hour angle on a tilted surface (°)

Persian Abstract

DOI: 10.5829/idosi.ijee.2014.05.03.01

چکیده

راندمان سطوح تخت خورشیدی، شامل کلکتورهای حرارتی یا پانل‌های فتوولتاییک، به مولفه‌های تابش مستقیم و پخشی و همچنین به زاویه برخورد تابش مستقیم خورشیدی بستگی دارد. در این مطالعه، با استفاده از داده‌های اندازه‌گیری‌شده درازمدت، بهینه سازی شیب سطوح تخت خورشیدی در شهر ایلام برای تنظیم‌های ثابت روزانه، ماهیانه، فصلی و سالیانه انجام شده است. بررسی مشخصه‌های تابش خورشیدی نشان داد که ایلام دارای ۲۲۰ روز با تابش خورشیدی بین ۱۵ و ۳۵ MJ/m^2 و همچنین ۱۸۲ روز آفتابی یا خیلی‌آفتابی با شاخص روزانه صافی هوا بیشتر از ۰/۶ می‌باشد. زاویه بهینه شیب برای تنظیم ثابت روزانه در طول سال بین صفر و ۶۱ درجه تغییر می‌کند و این زاویه برای تنظیم ثابت ماهیانه از صفر در خرداد و تیر تا ۶۰/۱ درجه در آذر متغیر است. زاویه بهینه شیب برای تنظیم ثابت سالیانه برابر ۲۶ درجه و به عرض جغرافیایی ایلام (۳۳/۳۸ درجه) نزدیک است. همچنین زوایای بهینه شیب برای تنظیم فصلی در زمستان و پاییز به ترتیب ۱۲/۳ و ۲۰ درجه بیشتر از عرض جغرافیایی ایلام و در بهار و تابستان به ترتیب ۳۰/۳ و ۲۱/۱ درجه کمتر از عرض جغرافیایی ایلام هستند.

Iranica Journal of Energy & Environment 5 (3): 233-239, 2014
ISSN 2079-2115
IJEE an Official Peer Reviewed Journal of Babol Noshirvani University of Technology
DOI: 10.5829/idosi.ijee.2014.05.03.02

BUT

Photo Catalytic Decomposition of Malachite Green in Aqueous Solutions under UV Irradition Using Nano ZnO Rod

P. Rejani, Asha Radhakrishnan and B. Beena

Department of Chemistry, D.B. College, Sasthamcotta, Kollam, Kerala, India 690 521

Date of Received: February 12, 2014; Date of Accepted in Revised Form: August 2, 2014

Abstract: ZnO nano rod was prepared by microwave assisted method. The crystal structure of the nano powders were confirmed by X-Ray diffraction analysis and the mean particle size was estimated by the Scherrer's formula. The surface morphology of the nano particles were analyzed by SEM and TEM. The absorption spectrum of the material in the UV-Vis range was recorded. The prepared ZnO rod was used as a photocatalyst in presence of UV light against Malachite Green dye. The ZnO nanoparticle was found to be an efficient low cost photocatalyst which degraded Malachite Green dye in presence of UV light in a relatively short period of time.

Key words: Nanoparticles · Zinc oxide rod · Malachite Green dye · Photocatalytic activity

INTRODUCTION

Water contamination becomes a serious issue due to the fact that two percentages of dyes that are produced from different industries is discharged directly in aqueous effluent [1]. Recently, there has been an increasing concern, particularly in highly developed countries, about penetration of pharmaceuticals compounds into environment and related risks [2]. Nowadays, U.V. and visible light illuminated photo catalytic reaction has attracted great deal of attention for application in waste water treatment [3]. Photo catalytic decolorization process is one of the emerging advanced technology which are considered as alternative method for the degradation of dyes in wastewater [4]. Among advanced oxidation process (AOP), semiconductor assisted photo catalysis has attracted considerable attention as an alternative treatment method and a promising technique for treating dye contaminated waste water at low cost [5].

Photo catalysis is a process by which a semiconducting material absorbs light of energy more than or equal to its band gap; thereby generating holes and electrons, which can further generate free-radicals in the system to oxidize the substrate. The resulting free radicals are very efficient oxidizers of organic matter. The degradation of organic compound is the most widely used photo catalytic application of nano crystalline particles [6, 7]. The photo catalytic decolorization of many dyes has been extensively explored in many previous studies using various nano particles [8, 9]. Photo catalysis has been considered and proved as a cost effective alternate for the purification of dye containing wastewater [10].

Photo catalytic degradation of organic compounds by semi conducting materials such as TiO_2 [11, 12], ZnO [13], CdS [14] and SnO_2 [15] has been used for environmental cleaning. Photo catalytic degradation of organic pollutants in water using semi conductive particles such as TiO_2 and ZnO, has attracted extensive attention. ZnO is a suitable alternative to TiO_2 as it has a similar ban gap energy (3.2ev), larger quantum efficiency than TiO_2 and higher photo catalytic efficiency have been reported [16-22]. ZnO is a low cost alternative photo catalyst to TiO_2 for decolorization of organics in aqueous [23, 24].The presence of metals on semiconducting metal oxides which acts as electron-hole separation centers can enhance the degradation efficiency of photo catalytic reactions [25].

Here we are interested in the photo catalytic degradation of malachite green buying ZnO photo catalyst. The dispersion and surface area of zinc oxide depends on method of synthesis; that is important factor for determination of photocatalytic activity. Zinc oxide nanoparticles can be prepared by various methods,

Corresponding Author: B. Beena, Department of Chemistry, D.B. College, Sasthamcotta, Kollam, Kerala, India 690 521.

Please cite this article as: P. Rejani, Asha Radhakrishnan and B. Beena, 2014. Photo Catalytic Decomposition of Malachite Green in Aqueous Solutions under UV Irradition Using Nano ZnO Rod. Iranica Journal of Energy and Environment, 5 (3): 233-239

such as, alkali precipitation [26-28]], thermal decomposition [29], hydrothermal synthesis [30], organo-zinc hydrolysis [31], spray pyrolysis [11, 32, 33] and microwave irradiation [34, 35], etc.

The ZnO photo catalyst was synthesized via micro wave assisted method and the photo catalytic degradation of the dye was carried out using UV light irradiation.

MATERIALS AND METHODS

Experimental: All chemical $Zn(NO_3)_2.6H_2O$, hexamethylenetetramine $\{(CH_2)_6N_4\}$, HMT} and malachite green (MG) were purchased from Merck Company as analytical grade and were used as received.

Preparation of Nano ZnO Rod: ZnO nano rods were prepared from Zinc nitrate hexahydrate($Zn(NO_3)_2.6H_2O$). A 0.5g zinc nitrate hexahydrate salt was dissolved in 65 mL of demineralized water. Appropriate quantity of a moderate alkali namely hexamethylene tetramine$\{(CH_2)_6N_4)$,HMT} was mixed to reach the pH level 7. The prepared solution was then stirred well for 30min to obtain a homogeneously turbid liquid. Then the solution was microwave-heated by a 300W domestic microwave oven for 20 min to obtain a curdy white precipitate, which was cooled to room temperature, filtered, washed with water followed by drying in hot air oven.

Characterization: X-ray diffractogram (2θ=10-90°) was obtained on XPERT-PRO powder diffractometer with Cu-Ká radiation. The FTIR spectrum was recorded using KBr wafer on the Thermo Nicolet FTIR model AVATAR 370 DTGS. In the present study, SEM of the sample was recorded using a JED-2300 system and HRTEM was taken using 300kv HRTEM (FEI-Model). The absorption spectra were recorded at room temperature using SHIMADZU UV-2550 UV Visible spectrophotometer.

Evaluation of Photo Catalysis: Photo catalytic activity of nano ZnO rod was evaluated by determining the decolourization efficiency of MG photo degradation. An aqueous solution of MG were used as model pollutant for investigation of the photo catalytic activity of ZnO. Photo degradation experiments were carried out us keeping the dye solution of concentration 25ppm prepared using distilled water. A known concentration (0.1g) of photo catalytic ZnO was added in to the beaker containing 50 mL dye solution and mixture was stirred in the dark for 30 min to obtain uniform suspension. After that the beakers were kept in a UV-light irradiation using 40W UV tube lamp. During irradiation, agitation was maintained to keep the suspension homogeneous. The concentration of dye in each degraded sample was determined with UV-Vis spectrophotometer. The percentage of degradation was determined by using the following equation

$$Removal(R\%) = \frac{(c_o - c_t)}{c_o} \times 100 \quad (1)$$

where R% is the degradation efficiency of MG, C_o [mg L^{-1}] and C_t [mg L^{-1}] are initial and concentration of MG in aqueous solution at different reaction time, t [36].

RESULTS AND DISCUSSION

X-Ray Diffraction Patterns: The structure identity and purity of the prepared nano particles were verified by XRD. Fig. 1 show the XRD pattern for ZnO rod at different temperatures. The observed peaks of the nano crystallite match well with standard JCPDS files and no other crystalline phases were detected. The average crystallite size of the powders were determined by using Scherrer's formula,

$$D = 0.9\lambda/\beta Cos\theta \quad (2)$$

where D is the average crystallite size in nm, λ the wavelength of X-ray radiation, θ the Bragg's angle and â the full width at half maximum of the peak observed for the sample [37].

A hexagonal wurtzite crystalline structure with lattice parameters of a=3.2498 and c=5.2066 were observed. All peaks correspond to hexagonal ZnO without evidence of any other crystal phase or another material. ZnO of wurtzite crystal structure; has no center of inversion and an inherent asymmetry along the c-axis is present, which allows the anisotropic growth of the crystal along the (1000) direction [38, 39]. Here the major intensity of the peaks centered at 2θ=31.5 and 36.1 show a preferred growth in (1010) and (1011) directions, in agreement with the micro rods observed in SEM micrograph. The grain size of ZnO nano rod has been found to be 26nm.

FT-IR Spectra of ZnO: FT-IR spectra of ZnO is shown in Fig. 2. The room temperature spectrum shows bands in the region ~3485cm^{-1} and ~2355cm^{-1} due to the presence of adsorbed water molecules or surface hydroxyl groups and C=O residues, probably due to atmospheric moisture and CO_2 respectively. The spectrum also shows Zn-O absorption band near 480 cm^{-1}.

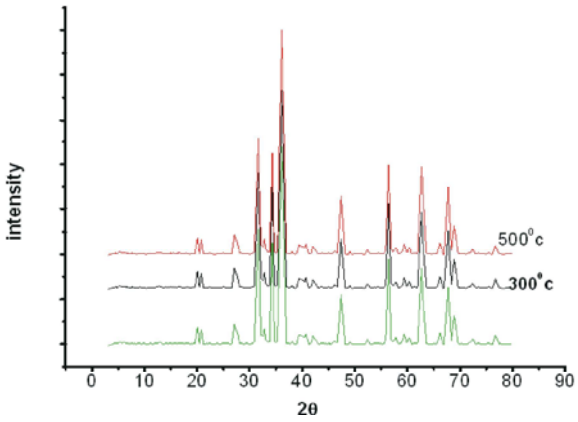

Fig. 1: XRD spectrum of ZnO rod at different annealing temperatures

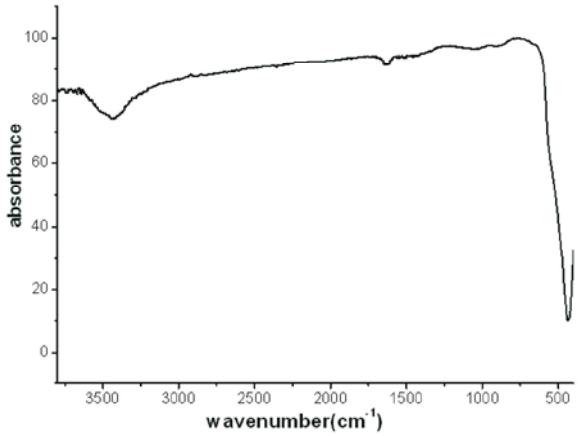

Fig. 2: FT-IR spectrum of ZnO nano rod

Surface Morphology of ZnO: The surface morphology of the as synthesized ZnO is revealed by scanning electron micrograph. Microwave irradiation might have played an important role in the fast synthesis of ZnO rods. As a polar material, ZnO may be significantly affected by microwave irradiation. The applied microwave field induces a rotation of polarized dipole of polar materials, which can generate heat due to molecular inner friction. The presence of an internal electric field also leads to orientation effects of dipolar molecules and hence reduces the action energy. The reduction in surface energy of the polar crystal may be the primary driving force for the faster nucleation, growth of the material and morphology evolution. The formation of the ZnO rods may be explained as follows. In the first stage OH^- ions are formed as a result of the reaction of H_2O with HMT and subsequently ZnO nuclei are formed. In the second stage, the formed ZnO nuclei grow preferentially along the (1000) direction, resulting in the formation of single-crystalline ZnO rods [38].

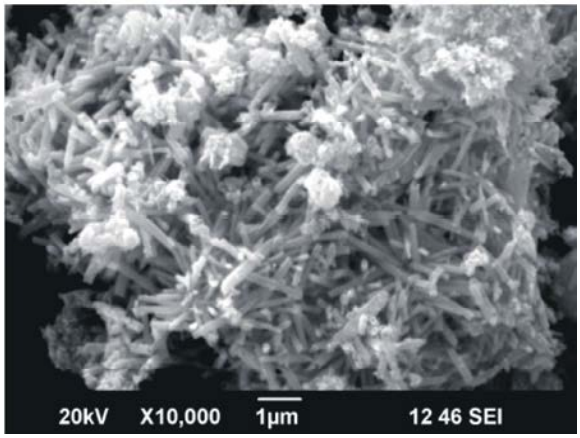

Fig. 3: SEM image of ZnO nano rod

In this study, hydroxide anions are provided by hydration of hexamethylenetetramine (HMT). When HMT is used as the hydroxide anion-generating agent, the reactions involved in the formation of ZnO crystals are believed to be as follows:

$$CH_2N_4 + 6H_2O \rightarrow 4NH_3 + 6CHO \quad (3)$$

$$NH_3 + H_2O \rightarrow NH^+_4 + OH^- \quad (4)$$

$$Zn^2 + 2OH^- \rightarrow ZnO + H_2O \quad (5)$$

Fig. 3 clearly shows ZnO crystals with rod like structure with average length of 1-2μm. Chemical composition by EDS indicate stoichiometry (Fig. 4). The resulting atomic-percent contents for ZnO rod was O 30.42%; Zn 69.58%. The high content of Zn indicates a high value of oxygen vacancies in their crystalline structures. The TEM micrograph, Fig. 5 of the sample revealed that the ZnO nano rod synthesized in this study have an average diameter of about 96 nm and an average length 400nm.

Evaluation of Photo Catalytic Activity: The variations in different experimental conditions affecting on photo catalytic oxidation of malachite green using the catalyst ZnO, such as, illumination time and amount of catalyst loaded were taken in to account to reach to integrated model for the photo catalytic degradation of malachite green.

Effect of Illumination Time: To investigate the effect of contact time on the decolorization efficiency of malachite green, the experiments were carried out with the contact time from 0 to 150 min. Fig. 6 shows time dependent

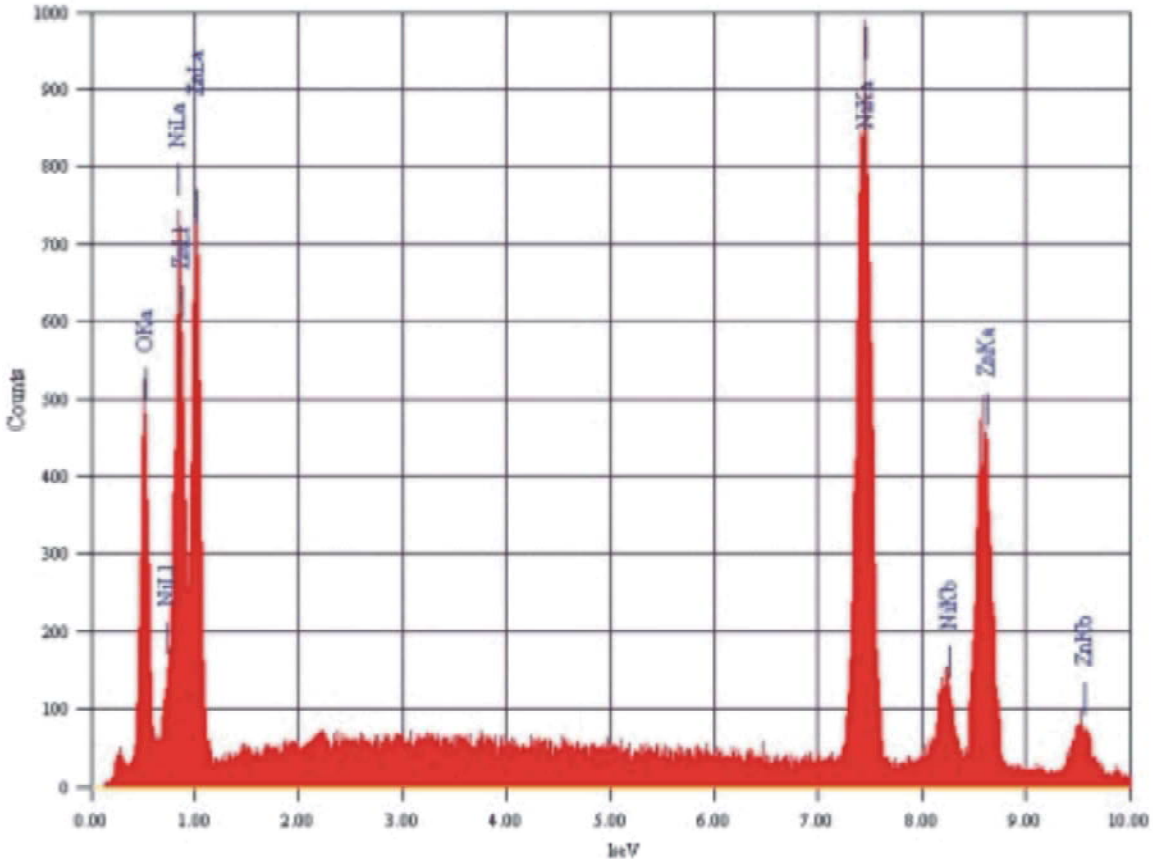

Fig. 4: EDS of ZnO nano rod

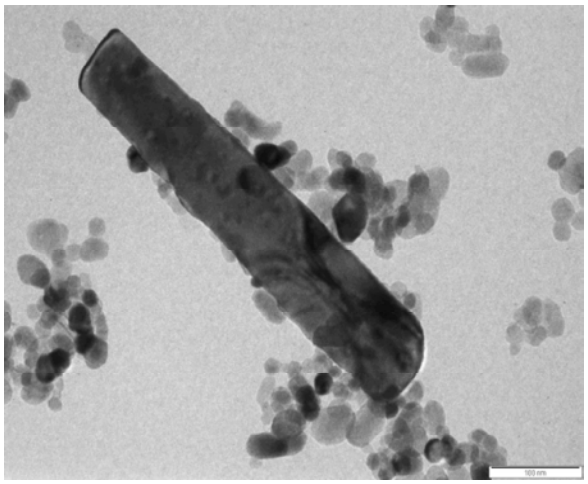

Fig. 5: TEM micrograph of ZnO nano rod

absorption spectra of the dye malachite green during the process. It can be seen that the intensity of absorption peak decreases with increases in the contact time, which indicate that the MG dye was decolorized as time prolonged.

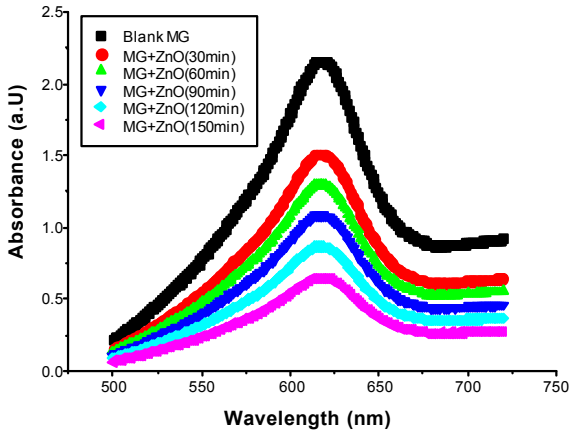

Fig. 6: Variation of absorbance of MG solution at various irradiation time

Effect of Catalytic Concentration: The amount of photo catalyst is another critical parameter to the degradation efficiency. In order to determine the effect of catalyst amount on the degradation of MG, a series of experiments were carried out by varying the catalyst amount from 0.025 to 0.125 g for 25 mg L^{-1} of malachite green solution

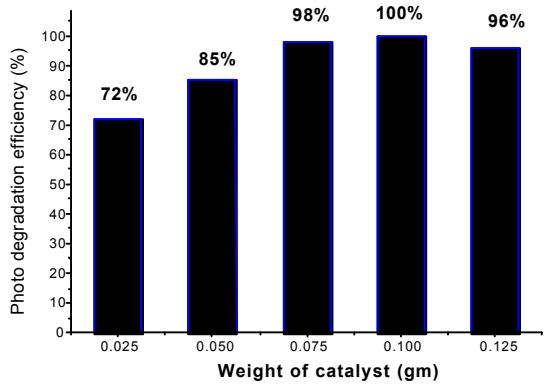

Fig. 7: Effect of catalyst dosage on the decolorization of MG using ZnO nano rod

keeping all other parameters identical and the results are presented in Fig. 7. As the photo catalytic amount increased from 0.0125 to 0.125g the degradation efficiency of MG enhanced and reached to maximum of 100% at 0.1g. The increase in amount of catalyst load increased the number of active sites on the photocatalytic surface, which in turn increased the number of hydroxyl radicals. Further increasing the loading of photocatalyst has increased the catalyst surface area and as a result increased the decolorization rate. It was assumed that furthur increase in photo catalyst may hindered the transmission of UV light in the reaction vessel if catalyst dosage was increased more than 0.1g and consequently decreased the decolorization rate [40].

Mechanism of photo catalytic decolorization

$$ZnO + h_3 \rightarrow ZnO(+h^+_{VB}) \quad (6)$$

$$h^+_{VB} + H_2O \rightarrow H^+ + OH^- \quad (7)$$

$$h^+_{VB} + OH^- \rightarrow OH^{\bullet} \quad (8)$$

$$OH^{\bullet} + MG \rightarrow \text{decomposed MG} \quad (9)$$

Upon exposure to UV – irradiation, ZnO is photo excited and an electron – hole pair is formed, where e^-_{CB} is the electron in the conduction band and h^+_{VB} is the hole in the valence band.

CONCLUSION

Pure hexagonal-phase ZnO nano rod was synthesized through fast and simple microwave irradiation method from the solution comprising Zinc nitrate and hexamethylenetetramine. The grain size of ZnO nano rod have been found to be 26nm. The nano rods structures were found to have an average diameter of about 96 nm and an average length 400nm from HRTEM. Photo catalytic degradation activities of MG have been studied using ZnO nano rod. It is to be found that at lower catalyst concentration the catalyst surface and adsorption of light on catalyst surface are the limiting factors. Thus, an increase in catalyst concentration greatly enhanced the process efficiency. On the other hand, at higher concentration, overlapping of adsorption site and deactivation of activated catalyst reduced the process efficiency.

REFERENCES

1. Rauf, M.A., I. Shehadeh, A. Ahmed and A. Al-Zamly, 2009. Removal of methylene blue from aqueous solution by using gypsum as a low cost adsorbent. World Academy of Science, Engineering and Technology, 55: 608-613.
2. Paola, A.D., M. Addamo, V. Augugliaro, E. García-López, V. Loddo, G. Marcì and L. Palmisano, 2006. Photodegradation of lincomycin in aqueous solution. International Journal of Photoenergy, 2006: Article ID 47418, 6 pages, http://www.hindawi.com/journals/ijp/2006/047418/abs/.
3. Min, S., F. Wang and Y. Han, 2007. An investigation on synthesis and photocatalytic activity of polyaniline sensitized nanocrystalline TiO_2 composites. J. Materials Science, 42(24): 9966-9972.
4. Zhao, M. and J. Zhang, 2009. Wastewater treatment by photocatalytic oxidation of nano-ZnO. Journal of Global Environmental Policy in Japan, 12(1): 88-95.
5. Comparelli, R., E. Fanizza, M. Curri, P. Cozzoli, G. Mascolo and A. Agostiano, 2005. UV-induced photocatalytic degradation of azo dyes by organic-capped ZnO nanocrystals immobilized onto substrates. Applied Catalysis B: Environmental, 60(1): 1-11.
6. Matthews, R.W., 1992. Photocatalytic oxidation of organic contaminants in water: An aid to environmental preservation. Pure and Applied Chemistry, 64(9): 1285-1290.
7. Seo, D.S., J.K. Lee and H. Kim, 2001. Synthesis of TiO_2 nanocrystalline powder by aging at low temperature. J. Crystal Growth, 233(1): 298-302.
8. Konstantinou, I.K. and T.A. Albanis, 2004. TiO_2-assisted photocatalytic degradation of azo dyes in aqueous solution: kinetic and mechanistic investigations: A review. Applied Catalysis B: Environmental, 49(1): 1-14.

9. Xiaodan, Y., W. Qingyin, J. Shicheng and G. Yihang, 2006. Nanoscale ZnS/TiO_2 composites: Preparation, characterization and visible-light photocatalytic activity. Materials Characterization, 57(4): 333-341.
10. Kansal, S.K., N. Kaur and S. Singh, 2009. Photocatalytic degradation of two commercial reactive dyes in aqueous phase using nanophotocatalysts. Nanoscale research Letters, 4(7): 709-716.
11. Komarneni, S., M. Bruno and E. Mariani, 2000. Synthesis of ZnO with and without microwaves. Materials Research Bulletin, 35(11): 1843-1847.
12. Chen, C., C. Lu, Y. Chung and J. Jan, 2007. UV light induced photodegradation of malachite green on TiO_2 nanoparticles. Journal of Hazardous Materials, 141(3): 520-528.
13. Bansal, P., N. Bhullar and D. Sud, 2009. Studies on photodegradation of malachite green using TiO_2/ZnO photocatalyst. Desalination and Water Treatment, 12(1-3): 108-113.
14. Sarmah, S. and A. Kumar, 2011. Photocatalytic activity of polyaniline-TiO_2 nanocomposites. Indian Journal of Physics, 85(5): 713-726.
15. Dodd, A., A. McKinley, M. Saunders and T. Tsuzuki, 2006. Mechanochemical synthesis of nanocrystalline SnO_2-ZnO photocatalysts. Nanotechnology, 17(3): 692-698.
16. Gouvea, C.A., F. Wypych, S.G. Moraes, N. Duran, N. Nagata and P. Peralta-Zamora, 2000. Semiconductor-assisted photocatalytic degradation of reactive dyes in aqueous solution. Chemosphere, 40(4): 433-440.
17. Khodja, A.A., T. Sehili, J.F.O. Pilichowski and P. Boule, 2001. Photocatalytic degradation of 2-phenylphenol on TiO_2 and ZnO in aqueous suspensions. Journal of Photochemistry and Photobiology A: Chemistry, 141(2): 231-239.
18. Dindar, B. and S. Icli, 2001. Unusual photoreactivity of zinc oxide irradiated by concentrated sunlight. Journal of Photochemistry and Photobiology A: Chemistry, 140(3): 263-268.
19. Sakthivel, S., B. Neppolian, M. Shankar, B. Arabindoo, M. Palanichamy and V. Murugesan, 2003. Solar photocatalytic degradation of azo dye: comparison of photocatalytic efficiency of ZnO and TiO_2. Solar Energy Materials and Solar Cells, 77(1): 65-82.
20. Mehrpooya, M. and S. Daviran, 2013. Dynamic modeling of a hybrid photovoltaic system with hydrogen/air PEM fuel cell. Iranica Journal of Energy & Environment, 4(2): 104-109.
21. Shah, N.A., M. Abbas, W.A. Syed and W. Mahmood, 2014. Physical Properties of Silver Doped ZnSe Thin Films for Photovoltaic Applications. Iranica Journal of Energy & Environment, 5(1): 87-93.
22. Peralta-Zamora, P., C.u.M. Pereira, E.R. Tiburtius, S.G. Moraes, M.A. Rosa, R.C. Minussi and N. DurÃ¡n, 2003. Decolorization of reactive dyes by immobilized laccase. Applied Catalysis B: Environmental, 42(2): 131-144.
23. Ekambaram, S., Y. Iikubo and A. Kudo, 2007. Combustion synthesis and photocatalytic properties of transition metal-incorporated ZnO. Journal of Alloys and Compounds, 433(1): 237-240.
24. Daneshvar, N., D. Salari and A. Khataee, 2004. Photocatalytic degradation of azo dye acid red 14 in water on ZnO as an alternative catalyst to TiO_2. Journal of Photochemistry and Photobiology A: Chemistry, 162(2): 317-322.
25. Chittofrati, A. and E. Matijevic, 1990. Uniform particles of zinc oxide of different morphologies. Colloids and Surfaces, 48: 65-78.
26. Chakrabarti, S., B. Chaudhuri, S. Bhattacharjee, P. Das and B.K. Dutta, 2008. Degradation mechanism and kinetic model for photocatalytic oxidation of PVC-ZnO composite film in presence of a sensitizing dye and UV radiation. Journal of hazardous materials, 154(1): 230-236.
27. Rodrýguez-Paéz, J., A. Caballero, M. Villegas, C. Moure, P. Duran and J. Fernandez, 2001. Controlled precipitation methods: formation mechanism of ZnO nanoparticles. Journal of the European Ceramic Society, 21(7): 925-930.
28. Trindade, T., J.L.D.P. De Jesus and P. O'Brien, 1994. Preparation of zinc oxide and zinc sulfide powders by controlled precipitation from aqueous solution. Journal of Materials Chemistry, 4(10): 1611-1617.
29. Shao, Z., C. Wang, S. Geng, X. Sun and S. Geng, 2006. Fabrication of nanometer-sized zinc oxide at low decomposing temperature. Journal of Materials Processing Technology, 178(1): 247-250.
30. Perez-Lopez, O.W., A.C. Farias, N.R. Marcilio and J. Bueno, 2005. The catalytic behavior of zinc oxide prepared from various precursors and by different methods. Materials Research Bulletin, 40(12): 2089-2099.
31. Milošević, O., B. Jordović and D. Uskoković, 1994. Preparation of fine spherical ZnO powders by an ultrasonic spray pyrolysis method. Materials Letters, 19(3): 165-170.

32. Jang, Y.J., C. Simer and T. Ohm, 2006. Comparison of zinc oxide nanoparticles and its nano-crystalline particles on the photocatalytic degradation of methylene blue. Materials Research Bulletin, 41(1): 67-77
33. Kominami, H., J.I. Kato, S.Y. Murakami, Y. Ishii, M. Kohno, K.I. Yabutani, T. Yamamoto, Y. Kera, M. Inoue and T. Inui, 2003. Solvothermal syntheses of semiconductor photocatalysts of ultra-high activities. Catalysis Today, 84(3): 181-189.
34. Parida, K., S. Dash and D. Das, 2006. Physico-chemical characterization and photocatalytic activity of zinc oxide prepared by various methods. Journal of Colloid and Interface Science, 298(2): 787-793.
35. Zhang, X.H., S.Y. Xie, Z.Y. Jiang, X. Zhang, Z.Q. Tian, Z.X. Xie, R.B. Huang and L.S. Zheng, 2003. Rational design and fabrication of ZnO nanotubes from nanowire templates in a microwave plasma system. The Journal of Physical Chemistry B, 107(37): 10114-10118.
36. Patil, K.C., S. Aruna and T. Mimani, 2002. Combustion synthesis: an update. Current Opinion in Solid State and Materials Science, 6(6): 507-512.
37. Klug, H.P. and L.E. Alexander, 1974. X-ray diffraction procedures: for polycrystalline and amorphous materials. X-Ray Diffraction Procedures: For Polycrystalline and Amorphous Materials, 2nd Edition, by Harold P. Klug, Leroy E. Alexander, pp: 992. ISBN 0-471-49369-4. Wiley-VCH, May 1974., 1.
38. Hu, X.L., Y.J. Zhu and S.W. Wang, 2004. Sonochemical and microwave-assisted synthesis of linked single-crystalline ZnO rods. Materials Chemistry and Physics, 88(2): 421-426.
39. Penn, R.L. and J.F. Banfield, 1998. Imperfect oriented attachment: dislocation generation in defect-free nanocrystals. Science, 281(5379): 969-971.
40. Madhusudhana, N., K. Yogendra and K.M. Mahadevan, 2012. Photocatalytic degradation of violet GL2B azo dye by using calcium aluminate nanoparticle in presence of solar light. Research Journal of Chemical Sciences, 2(5): 72-77.

Persian Abstract

DOI: 10.5829/idosi.ijee.2014.05.03.02

چکیده

نانولوله ZnO با استفاده از روشی بهره گیری از مایکروویو تهیه شد. ساختار کریستالی نانوپودر با استفاده از آنالیز پراش اشعه ایکس تایید شد و اندازه میانگین ذرات با استفاده از فرمول شرار تخمین زده شد. مورفولوژی سطح نانوذرات با استفاده از SEM و TEM آنالیز شد. نانولوله ZnO تهیه شده بعنوان یک فوتوکاتالیست در حضور نور UV برای رنگ سبز مالاشیت استفاده شد. نانوذرات ZnO بعنوان فوتوکاتالیستی ارزان قیمت و موثر، رنگ سبز مالاشیت را در حضور نور UV و در یک بازه زمانی نسبتا کوتاه تجزیه نمود.

Iranica Journal of Energy & Environment 5 (3): 240-246, 2014
ISSN 2079-2115
IJEE an Official Peer Reviewed Journal of Babol Noshirvani University of Technology
DOI: 10.5829/idosi.ijee.2014.05.03.03

BUT

Optimum Size for Clay Core of Alavian Earth Dam by Numerical Simulation

[1]Armin Farzampour, [2]Farzin Salmasi and [2]Behnam Mansuri

[1]Maragheh Azad University, Civil engineering faculty,
Water Engineering Department, Maragheh, Iran
[2]University of Tabriz, Agricultural faculty, Water engineering department, Tabriz, Iran

Date of Received: July 1, 2014; Date of Accepted in Revised Form: August 4, 2014

Abstract: Seepage in embankment dams is one of the important factors in stability and dam's maintenance. Core in earth dam is essential for waterproofing and controlling of seepage. Therefore, selection of proper materials and sizes for core of earth dam are very important. Thick clay core is proper for waterproofing but because of low shear strength of the clay, it would be dangerous for dam's stability. The optimal core would be the core which has proper waterproofing, stability safety factor and also with economic condition. In this study, the aim is to determine the optimum size for clay core of Alavian dam near Maragheh city in steady state seepage condition. For this purposes, Geo-Studio pack is used for numerical simulation. In addition, simulation of seepage and slope stability for the built maps of the dam, 11 more models of the dam with different size of cores were tested to find the optimum core thickness. From these models, data required for objective function and constraints using regression techniques for seepage, hydraulic gradient and stability safety factor were provided. Results showed that optimized volume of the core is 35% smaller than the present core.

Key words: Earth dam · Optimization · Clay core · Excel solver · Geo-Studio

INTORDUCTION

Dams are one of the most important structure made by human that destruction of it may caused excessive costs and sometimes irreparable. Destruction of the dams may be due to seepage from dam is one of the most important ones. Seepage itself is not a destructive phenomenon and happens in all dams. But the point that makes it dangerous is lack of proper controlling and forecasting of dam resistances. In non-homogeneous earth dams, waterproofing is a task for dam core. Use of clay core for waterproofing the dam is most common. In the other hands, shear strength of the fine materials like clay is low and it would decrease the stability of the dam against slope sliding. Therefore, use of thick cores is a good choice for minimizing seepage and prevention from internal erosion; on the other hand, thick core would decrease dam slope stability [1]. In another study by Fadaei Kermani and Barani [1], finite difference method (FDM), the five-point approximation technique, has been demonstrated to deal with seepage problem in earth dams. The grid system, with computational boundary being coincident with the physical boundary, was numerically obtained by solving Laplace equation. The method was applied to analyze the steady seepage in an earth dam. In this study, three different grid types were considered and the results were compared with ones obtained by analyzing with Geostudio [2] software. It showed that by choosing small enough increments, the results are satisfactory. Hasani *et al*. [3] used geo-studio software for seepage analysis in Ilam earth fill dam. In order to evaluate the type and size of mesh on total flow rate and total head through the dam cross section, four mesh size such as coarse, medium, fine and unstructured mesh were considered. Results showed that average flow rate of leakage under the different mesh size for Ilam dam equal to 0.836 liters per second for the entire length of the dam [3].

Corresponding Author: Farzin Salmasi, University of Tabriz, Agricultural Faculty,
Water Engineering Department, Tabriz-Iran.

Please cite this article as: Armin Farzampour, Farzin Salmasi and Behnam Mansuri, 2014. Optimum Size for Clay Core of Alavian Earth Dam by Numerical Simulation. Iranica Journal of Energy and Environment, 5 (3): 240-246

Many researchers had effectively investigated in this field. Investigation on optimization of the dam core took place in 1979 to 1985 [4]. Kasim and Jusoh [5] studied seepage analysis using Seep/w program. Relation between seepage discharge and reservoir water level was nonlinear and for different input data; also the function of hydraulic conductivity were different [5]. Abdul Hossain *et al*. [6] for optimizing homogenous earth dam used multiple target function optimization by weighted method. Optimization is based on stability restrictions and distance between upstream water levels and downstream water levels. Function of seepage discharge, permeated surface and design restrictions are virtual functions of design parameters [6].

Salmasi and Mansuri [7] studied on effect of homogeneous earth dam hydraulic conductivity ratio (K_x/K_y) with horizontal drain on seepage. Results showed that the provision of the filter nearer the upstream side results in higher seepage losses and an increment in the required filter length. If the filter is located away from upstream face, i.e., near the downstream toe, though seepage gets reduced, the saturated zone is increased, resulting in a reduction of the dry zone. Mansuri and Salmasi [8] studied the effectiveness of using horizontal drain and cutoff wall in reducing seepage flow from an assumed heterogeneous earth dam. Seepage analysis, hydraulic gradient and uplift pressure, are computing by numerical simulation, using Seep/w software. Results showed that increasing horizontal drain length, caused slightly in increasing seepage rate and increasing hydraulic gradient. Optimum location of cut off wall for reduction of seepage rate and piping is in the middle of dam foundation. Different location of cut off wall in dam foundation has little effect on exit hydraulic gradient and always it is less than unity. Installation of cut off wall in middle of foundation, results in 19.68 percent decrease in hydraulic gradient respect to existent of cut off wall in upstream of dam.

In a study, Gotvand-Olya dam seepage analysis was numerically performed using 2-D FEM transient analysis [9]. As a particular boundary condition for an analysis, the water level fluctuation was incorporated to simulate the daily changes. As a result, various seepage phenomena were quantified such as hydraulic gradient, seepage vector and pore water pressure distribution at the corresponding time of interest as the water level rises and recedes. At steady state analysis, the seepage flux at high water level in downstream area was predicted to be 78 l/s. The result of this study proves that there was no sign of hazardous sources contributing to the possibility of piping, internal erosion and excess leakage through the dam body [9]. In another study, critical hydraulic gradient for sediment transport through rockfill dam was determined [10]. Results from dynamic pressure fluctuations in stepped three-side spillway showed that the proposed form of ogee profile caused a significant reduction in turbulence intensity within the side channel. On the other hand, the stepped Ogee profiles of three-side spillways caused to simple construction and ease of operation [11]. Other materials in this subject can be found in the reported literature [12, 13].

The aim of present study is to determine the optimal sizes for core within consideration of enough upstream slope stability safety factor. The executive restrictions are controlled seepage, acceptable hydraulic gradient, safety factor against sliding for upstream slope of dam and proper dam crest width. For this purpose, two part of Geo-Studio package, i.e. Seep/w and Slope /w programs were used for numerical simulation. The data required for regression modeling was obtained and regression models provided by SPSS software. In addition, optimization for minimizing the core volume was successfully carried out by Solver tool in Excel.

MATERIAL AND METHODS

Geo-Studio Software Pack: With Geo-Studio software pack analysis such as stress-strain, seepage, stability of slopes, dynamical analysis and condition of sudden drop of reservoir water level were preformed. In this study, Seep/w program for seepage analysis and Slope/w program for slope stability were used.

Finite element numerical methods are based on the concept of subdividing a continuum into small pieces, describing the behavior or actions of the individual pieces and then reconnecting all the pieces to represent the behavior of the continuum as a whole. This process of subdividing the continuum into smaller pieces is known as discretization or meshing. The pieces are known as finite elements.

In Geo-Studio Seep/w, the geometry of a model is defined in its entirety prior to consideration of the discretization or meshing. Furthermore, automatic mesh generation algorithms have now advanced sufficiently to enable a well behaved, numerically robust default discretization often without additional effort by the user. Of course, it is still wise to view the default generated mesh but any required changes can easily be made by changing a single global element size parameter, by changing the number of mesh divisions along a geometry line object, or by setting a required mesh element edge size.

The information required like dam geometry, property of material geotechnical parameters for dam and foundation are gathered from Regional Water Authority of Eastern Azerbaijan, RWAEA [14]. Selected dam is Alavian earth dam located in Eastern Azerbaijan in Iran near Maragheh city.

Seep/w program: Seep/w is geotechnical software based on finite element method. Equation (1) represents seepage discharge based on Darcy's law.

$$q = -kA(\partial h / \partial l) \quad (1)$$

where, q is seepage (m^3/s), k is hydraulic conductivity of soil (m/s), A is cross-section area of seepage flow (m^2) and $\partial h/\partial l$ is hydraulic gradient of flow (dimensionless).

Combining continuity equation with Darcy' law results in Poisson equation.

$$k_x \frac{\partial^2 h}{\partial x^2} + k_y \frac{\partial^2 h}{\partial y^2} = q \quad (2)$$

where k_x and k_y are horizontal and vertical hydraulic conductivities of soil (m/s), h is water potential head in soil (m) and q is input or output discharge of soil mass ($m^3/s.m^2$). Solving Poisson equation is a difficult problem in mathematics and so numerical methods are used to solve this differential equation. Seep/w uses finite element method.

Slope/w program: This program unlike the other program of Geo-Studio is not based on finite element. This program includes graphical method for analysis of stability of slopes. The process is done by limited equilibrium methods. The Slope/w has ability to analyses within most of the equilibrium methods such as Morgenstern-price, Bishop and etc. One of the cons of this program is possibility of direct modelling of common reinforcements like geo-fabrics, bearing rein and nailing for improving the safety of slopes.

Location of Alavian Earth Dam: Alavian dam is an earth dam with clay core, made on Sufi-Chay River 3.5 km of northern west of Maragheh city in eastern Azerbaijan, Iran. The main aim from Alavian dam construction is to collect surface river flows and controlling Sufi-Chay River for purposes like supplying drinking water of Maragheh city, development agriculture lands and hydroelectric uses as well. Fig. 1 shows a view of the Alavian earth dam.

The height of dam from bed rock is 76 meters, the dam has 935 meters length, the width of crest is 10 meters, total volume of dam's soil material is 4.8 million cubic meters, the crest elevation is 1572 meters from mean free surface of sea, the reservoir volume in normal level is 60 million cubic meters and dead volume is 3 million cubic meters [14].

Required Information for Modeling: The required information for numerical modeling and analysis of the cross sections of dams are listed as the following items:

- Dam layout map and cross-section profiles
- Permeability of all materials used in dam
- Strata under the dam (alluvium of the river) with its hydraulic conductivity
- Saturated and dry specific weight of materials
- Soil shear strength parameters, like internal friction angle and soil cohesion

Fig. 2 is the biggest cross-section view of the Alavian earth dam with finite elements mesh generation. Hydraulic conductivity of the different materials is shown in Table 1.

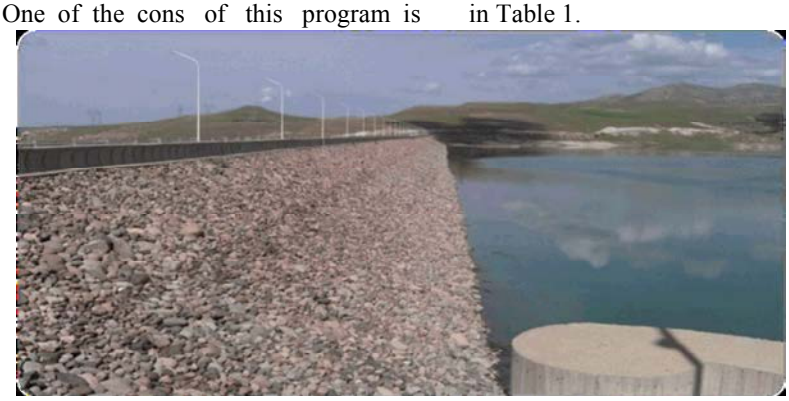

Fig. 1: Upstream slope of Alavian reservoir dam

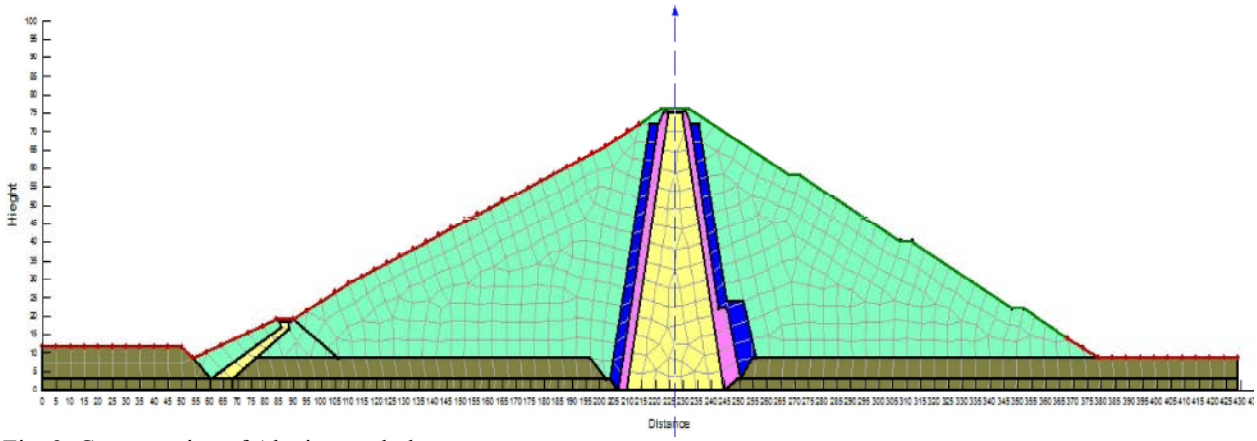

Fig. 2: Cross-section of Alavian earth dam

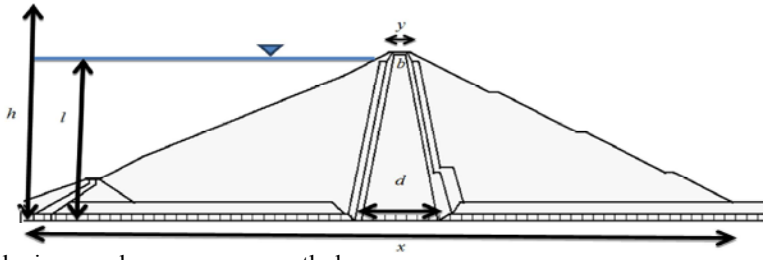

Fig. 3: Geometry of the Alavian non-homogeneous earth dam

Table 1: Hydraulic conductivity of different materials used in Alavian dam [14]

Layer	Hydraulic conductivity (*m/s*)
Core	$2 * 10^{-10}$ to $5 * 10^{-11}$
Filter 1	$1.8 * 10^{-5}$ to $4.5 * 10^{-6}$
Filter 2	$1.8 * 10^{-4}$ to $4.5 * 10^{-5}$
Shell	$1.1 * 10^{-4}$ to $4.1 * 10^{-5}$
Foundation	$2.69 * 10^{-9}$ to $3.32 * 10^{-10}$

Table 2: Shear strength proprieties of the material used in Alavian earth dam

Material	$\gamma_w (kN/m^3)$	$\gamma_{sat} (kN/m^3)$	φ_{UU}(Degree)	φ_{CU}(Degree)	φ_{CD}(Degree)	C_{UU} (kPa)	C_{CU} (kPa)	C_{CD} (kPa)
Core	19	20	10	22	28	50	37	0
Filter 1	21	22	35	0	0	0	0	0
Filter 2	21	22	40	0	0	0	0	0
Shell	21	22	43	0	0	0	0	0
Foundation	19	20	25	0	0	170	0	0

The values of soil specific wet weight, specific saturated weight, internal friction angle and cohesion of the materials in the studied dam are presented in Table 2, which is used for numerical simulation.

Fig. 3 shows the non-homogeneous embankment dam within needed parameters. In Fig. 3, *h* is the dam's height (m), *l* is upstream water level (m), *d* is the core width on foundation (m), *b* is the core crest width (m), *x* is the dam width on the foundation (m) and *y* is the crest width of the dam (m).

Initially, the Alavian dam was modeled in Seep/w and Slope/w just like how it built in reality. Then 11 more assumed models with different core sizes (thicker and thinner than the normal condition) and according to design criteria and the same material were created. The assumed geometrical data of the simulated models is in Table 3. After simulating 12 models, the required data for seepage regression equation, hydraulic gradient and stability of safety factor are obtained via SPSS software.

Table 3: Geometrical data of the 12 simulated models according to Fig. 3

Model	b (m)	d (m)	l (m)	h (m)
1	3	33	72	76
2	4	34	72	76
3	6	36	72	76
4	7	37	72	76
5	5	42.5	72	76
6	5	50	72	76
7	5	27.5	72	76
8	3	35	72	76
9	8	35	72	76
10	5	35	72	76
11	5	72	72	76
12	3	25	72	76

Numerical simulation with Seep/w and Slope/w resulted in for seepage, *q;* (m^2/s), hydraulic gradient (i*)* and stability safety factor (*SF)*. The dimensionless design parameters were selected are *q/kl, b/h, b/l, d/l, SF and d/x*.

Optimizing by Solver in Excel: Solver has capability for optimization when target function and constraints are known. For obtaining optimum Maragheh dam core, definition of target function and constraints are stated as following:

Target Function: Because of the need for less permeability of core, it is required to be made of fine-grained materials and because of this fact, shear strength of the core is less than the other parts of the dam. Sometimes while determining the proper sizes for the core, due to important design parameters and factors like: *q, i* and *SF*, the geometry would not be economic. For this reason, determining the optimized core size while observing the design criteria, physical and geo-technical characteristics of the material, should be economically justified. In order to minimize the volume of the clay core for embankment dams matching the design criteria, a model using *Solver* tool has been created in *Excel* to optimize the issue. In this study, volume of the clay core material is considered as target/objective function. For minimizing volume of clay core, Eq. 8 is used.

$$V = \left(\frac{d+b}{2} * h \right) \tag{3}$$

Constraints: Most of the designers believed that acceptable seepage in full reservoir condition must be less than a cubic foot per second or 30 liters per second. For minimizing the seepage from dam and its foundation, Eq. 4 is introduced using regression technique by SPSS software.

$$\frac{q}{kl} = -49791\frac{b}{h} + 7942.4 \tag{4}$$

To prevent soil particle migration in dam and piping, hydraulic gradient (*i*) constraint was applied according to Eq. 5.

$$i = 1.624 - 1.96\frac{b}{l} - 0.346\frac{d}{l} \; and \; 1 \le i \le 3 \tag{5}$$

Safety factor (*SF*) of stability against sliding derived in total simulated 12 models. Usually in earth dam design, *SF* was select more than 1.5. Eq. 6 is used for this purpose.

$$SF = 2.792 - 2.271\frac{d}{x} - 0.139\frac{b}{y} \quad , \; SF \ge 1.5 \tag{6}$$

RESULTS AND DISCUSSION

Simulated model of the Alavian dam (in present condition) is shown in Fig. 4. The phreatic line, equpotential lines and seepage amount are also shown on Fig. 4.

For analysis of the stability safety factor of the 12 models of Alavian dam, these models are simulated according to the design criteria. According to Fig. 5, stability safety factor of the upstream slope of Alavian dam at steady state condition is 2.488.

In this study, the optimized sizes of the clay core for Alavian dam are analyzed in steady flow condition. As it is mentioned in optimization part, the aim is to minimize the core's volume for dam unit length. Comparison between Tables 4 and 5 demonstrate that in optimized condition, volume of Alavian dam core would be 35% less than the present one. So it could be mentioned as a conclusion that optimizing the clay core of Alavian dam while observing design criteria would be more economic.

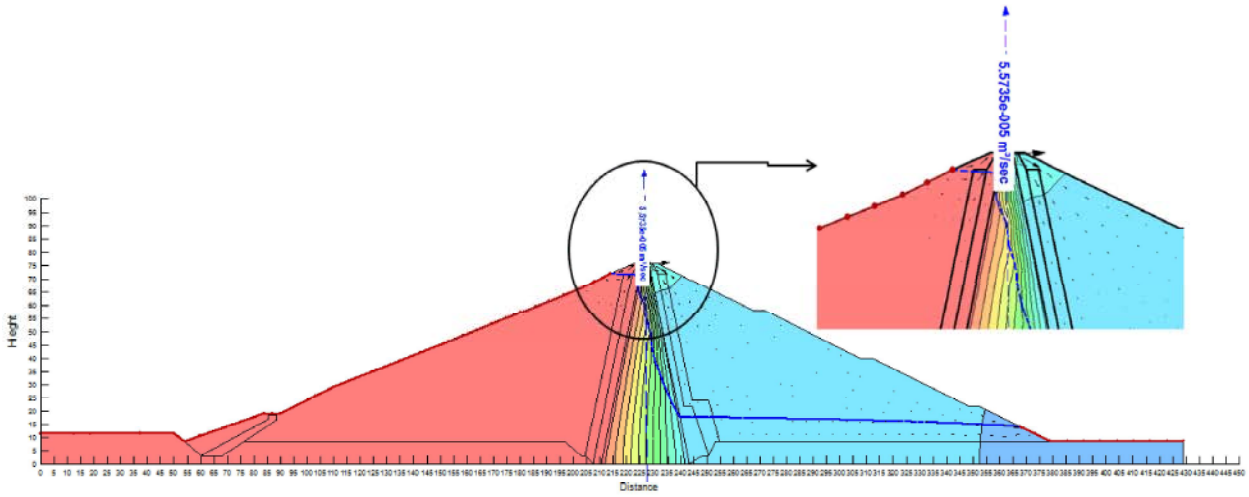

Fig. 4: Simulated model of the Alavian dam

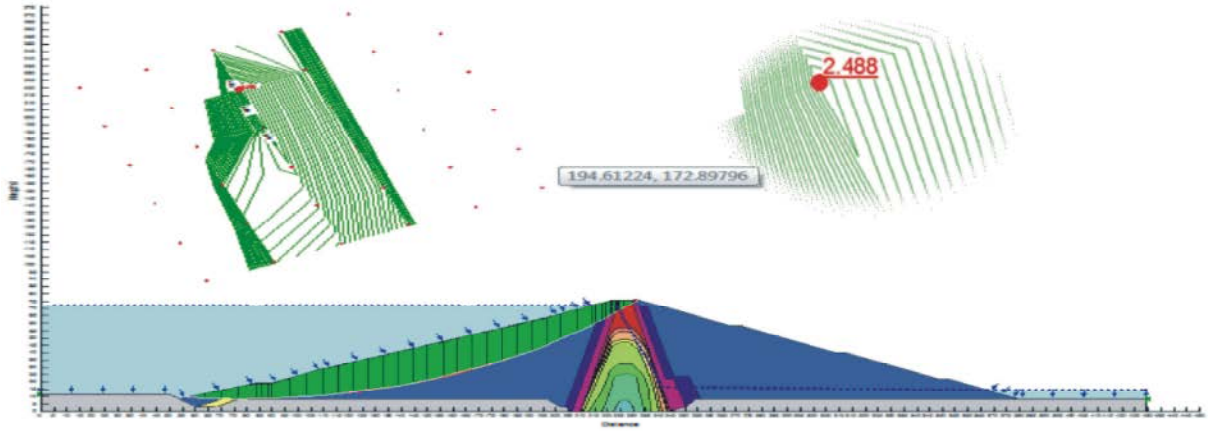

Fig. 5: Simulated model of Alavian dam and stability safety factor (present dam)

Table 4: Optimized sizes of the Alavian core dam

b (m)	*d (m)*	*h (m)*	*l (m)*	*x (m)*	*y (m)*	*i*	*q* ($m^3/s/m$)	*SF*	*Volume* (m^3/m)
3	22.8	76	72	10	329	1.43	0.000054	2.59	980.4

Table 5: Present sizes of the Alavian core dam

b (m)	*d (m)*	*h (m)*	*l (m)*	*x (m)*	*y (m)*	*i*	*q* ($m^3/s/m$)	*SF*	*Volume* (m^3/m)
5	35	76	72	10	329	1.37	0.00004	2.49	1520

CONCLUSION

In design of an earth dam, thicker clay core results less seepage amount and less hydraulic gradient due to low permeability of clay. This condition is proper for dam from prevention of piping phenomenon view point. In other hands, thicker clay core causes to reduce upstream slope safety factor against sliding (because of clay's low shear strength). The purpose of this study was to introduce a method for optimum design of an earth dam by taking consideration of the following criteria:

- Having minimum volume of clay as an objective function (Eq. 3).
- Safety factor against upstream sliding be more than 1.5, i.e., $SF>1.5$ (Eq. 6).
- Hydraulic gradient be less than 3 and more than unit, i.e. $1<i<3$ (Eq. 5).

- Seepage (q) from dam and foundation has to be less than 30 lit/s.m (Eq. 4).

Results demonstrate that in optimized condition for dam clay core, volume of Alavian dam core will be 35% less than the present condition. So in design of earth dams, using optimization technique with consideration of all hydraulic or geo-technique criteria, resulted in economic plan.

REFERENCES

1. USBR. 1987. Design of Small Dams, U. S. Bureau of Reclamation. Department of Interior, Col. USA.
2. Fadaei Kermani, E. and G.A. Barani, 2012. Seepage Analysis through Earth Dam Based on Finite Difference Method, Journal of Basic and Applied Scientific Research, 2(11): 11621-11625, ISSN 2090-4304.
3. Hasani, H., J. Mamizadeh and H. Karimi, 2013. Stability of Slope and Seepage Analysis in Earth Fills Dams Using Numerical Models (Case Study: Ilam DAM-Iran), World Applied Sciences Journal, 21(9): 1398-1402, ISSN 1818-4952, DOI: 10.5829/idosi.wasj.2013.21.9.1313.
4. Golding, A.L. and L.N. Rasskzov, 1992. Design of earth dams. A.A. Balkema Publisher, Rotterdam, Netherlands.
5. Kasim, P.F. and S.N.B. Jusoh, 2003. Effects of permeability disparity on seepage pattern of earth fill dam, Pertanika Journal of Science & Technology. University Technology Malaysia, 17(2): 384-395.
6. Abdul Hussein, I.A., D. Kashyap and K.S. Hariprasad, 2007. Seepage modeling assisted optimal design of a homogenous earth dam: procedure evolution. Journal of Irrigation and Drainage Engineering, ASCE, (9): 205-231.
7. Salmasi, F. and B. Mansuri, 2013. Effect of Homogeneous Earth Dam Hydraulic Conductivity Ratio (Kx/Ky) with Horizontal Drain on Seepage, Indian Geotechnical Journal, DOI 10.1007/s40098-013-0087-x.
8. Mansuri, B. and F. Salmasi, 2013. Effect of Horizontal Drain Length and Cutoff Wall on Seepage and Uplift Pressure in Heterogeneous Earth Dam with Numerical Simulation, Journal of Civil Engineering and Urbanism, 3(3): 114-121, ISSN-2252-0430.
9. Beheshti, A., A. Kamanbedast and H. Akbari, 2013. Seepage Analysis of Rock-Fill Dam Subjected to Water Level Fluctuation: A case study on Gotvand-Olya Dam, Iranica Journal of Energy & Environment, 4(2): 155-160.
10. Chapokpour, J. and E. Amiri Tokaldany, 2012. Critical hydraulic gradient for sediment transport through rock fill structures. Iranica Journal of Energy & Environment, 3(2): 197-201, DOI: 10.5829/ idosi.ijee.2012.03.02.1228.
11. Taghizadeh, H., S.A.A. Salehi Neyshabour and F. Ghasemzadeh, 2012. Dynamic pressure fluctuations in stepped three-side spillway, Iranica Journal of Energy & Environment, 3(1): 78-87, DOI: 10.5829/ idosi.ijee.2012.03.01.3567.
12. Mansouri, B., 2013. Earthquake Damage Detection in Built Environment: An Object-Oriented Approach Using Radar Imagery, Iranica Journal of Energy & Environment, 4 {(3) Geo-hazards and Civil Engineering)}: 289-293. DOI: 10.5829/ idosi.ijee.2013.04.03.16.
13. Nateghi, F. and N. Parsaeifard, 2013. Studying the Effect of Initial Damage on Failure Probability of One Story Steel Buildings, Iranica Journal of Energy & Environment 4 {(3) Geo-hazards and Civil Engineering)}: 258-264, DOI: 10.5829/ idosi.ijee.2013.04.03.12.
14. RWAEA, Regional Water Authority of Eastern Azerbaijan, 1991. Alavian dam, Technical report. Energy ministry, Repot No. 158-19.

Persian Abstract

DOI: 10.5829/idosi.ijee.2014.05.03.03

چکیده

یکی از مهمترین عوامل موثر در پایداری و نگهداری از سدهای خاکی مسئله نشت از بدنه و پی سد می باشد. معمولا هسته رسی مرکزی در سد خاکی کنترل کننده حد مجاز نشت از بدنه است. لذا انتخاب مصالح رسی مناسب و نیز ضخامت هسته جزو پارامتر های مهم طراحی هستند. هسته با ضخامت زیاد از نظر کاهش مقدار نشت مفید است ولی به دلیل مقاومت برشی کم مصالح رسی، هر چقدر هسته نازک تر باشد مناسب تر خواهد بود. تصمیم گیری در مورد ضخامت بهینه هسته رسی جزو کار طراحان این گونه سدها بوده و دارای اهمیت زیادی است. در این تحقیق هدف یافتن ضخامت بهینه هسته رسی سد علویان در نزدیکی شهر مراغه می باشد. برای این منظور از بسته نرم افزاری Geo-Studio جهت شبیه سازی عددی استفاده شده است. ابتدا بر اساس نقشه های همچو ساخت سد خاکی علویان، مقدار نشت و ضریب اطمینان در برابر لغزش شیب بالادست سد بررسی شده و سپس ۱۱ مقطع فرضی دیگر با ضخامت های مختلف هسته رسی شبیه سازی گردید. پس از شبیه سازی عددی این ۱۲ مدل از سد خاکی، معادلات مربوط به میزان نشت، گرادیان هیدرولیکی و پایداری شیب بالادست توسط تکنیک رگرسیون بدست آمده و به صورت تابع هدف و قید ها بکار رفتند. نتایج نشان دادند که حجم هسته رسی بهینه شده حدود ۳۵ درصد نسبت به وضعیت کنونی آن کاهش می یابد.

Iranica Journal of Energy & Environment 5 (3): 247-258, 2014
ISSN 2079-2115
IJEE an Official Peer Reviewed Journal of Babol Noshirvani University of Technology
DOI: 10.5829/idosi.ijee.2014.05.03.04

BUT

Analysis of Ecological Condition of Lakes Burabai and Ulken Shabakty in Republic of Kazakhstan

[1]A.A. Ismailova, [1]A.K. Zhamangara, [2]Park S. Ya,
[2,3]A.I. Abakumov, [1]A.A. Adamov and [1]R.M. Muratov

[1]L.N. Gumilyov Eurasian National University, Astana, Kazakhstan
[2]Institute of Automation and Control Processes, FEB RAS, Vladivostok, Russia
[3]Far Eastern Federal University, Vladivostok, Russia

Date of Received: July 4, 2014; Date of Accepted in Revised Form: August 4, 2014

Abstract: The information-analytical system (IAS) "Monitoring of aquatic ecosystems" was developed for the analysis of ecological lakes condition in Kazakhstan. It consists of a database on hydrochemical and hydrobiological characteristics for lakes Burabai and Ulken Shabakty in Shchuchinsk-Borovoye resort area of the Republic of Kazakhstan, as well as a set of statistical data processing methods. Qualitative analysis of data was made on the lakes. Data on biogenic substances for the years 2007-2013 were analyzed based on statistics. Dynamic characteristics and seasonal features of changes were identified in the concentrations of biogens. There is an absence of significant relationships between the concentrations of various biogenic substances in lakes and between lakes. Nitrogen substances were compared. The phosphorus compounds have a large stability that can contribute to a more stable life of phytoplankton species which are related to phosphorus.

Key words: Statistical analysis · Hydrobiology · Hydrochemistry · Classification of lakes · Mathematical modeling

INTRODUCTION

Shchuchinsk-Borovoye resort area has great recreational and tourist value. At the same time, the ecological status of the region is quite complicated. Pollution exceeding maximum permissible concentration (MPC) dozens of times are captured in a village Borovoye. Major complexes of recreation institutions, fixed on the coast lakes Burabai, Shuchye, Ulken (Big) and Kishi (Small) Shabakty and extends along the highways. As a result of irretrievable water intake for industrial and drinking and sanitary needs, plowing on the slopes, deforestation in the catchment area pollutants and organic substances are washed away, which increases the processes of lake siltation [1].

Compared to the surrounding areas, the territory of the state national park characterized by an abundance of water resources, mainly, fresh or brackish lakes, whose number reaches 22, fourteen of which are classified as large, such as Kishi Shabakty, Ulken Shabakty, Borovoye, Shuchye, Katarkol and so on.

Lakes are located in scenic locations in the foothills completely or partially surrounded by forests. The shores, on the one hand are steep, rocky, on the other - the lowest often sandy. Also the structure of lake shores correspond to the relief of their basins: in the cliffs lakes have the greatest depth and underwater slope is steep and precipitous.

Currently, the level of all lakes is lowering except Lake Borovoye, which maintained a constant water balance. Lakes are mainly fed by groundwater, but precipitation also plays a significant role in the nutrition of lakes.

Area is characterized by poor development of the river network. Small river basin of lakes Borovoye - Sarybulak and spring Imanaevsky are the most significant

Corresponding Author: A.I. Abakumov, Far Eastern Federal University, Vladivostok, Russia.

Please cite this article as: A.A. Ismailova, A.K. Zhamangara, Park S. Ya, A.I. Abakumov, A.A. Adamov and R.M. Muratov, 2014. Analysis of Ecological Condition of Lakes Burabai and Ulken Shabakty in Republic of Kazakhstan. Iranica Journal of Energy and Environment, 5 (3): 247-258

of watercourses, in the basins of lakes Shchuchye, Katarkol and Maybalik there's no watercourses, the basin of the lake is dominated by temporary streams of Kishi Shabakty. In the Lake Ulken Shabakty creek Arykpay is regulated, runoff in watercourses is practically absent; the runoff in the river Gromotukha depends on the threshold of flow from lake Borovoye. Rivers fed mainly due to spring snowmelt and summer rains, also partly due to groundwater.

Almost all lakes are characterized by the significant shrinkage of their water area in recent decades, with the speed of 14-17 cm per year. Apparently, the reasons are: reducing the inflow of melted water resulted by a small amount of snowfall in the winter and holdup melted water runoff by dams on the rivers and temporal watercourses, an increase of evaporation and water consumption by consumers.

MATHERIALS AND METHODS

Ecological and Geographical Description: Lake Burabai (Auliekol) - located within Kokshetau Highland, at the eastern foot of Kokshe, north of Lake Shchuchye (Fig. 1). Area of water surface is approximately 11 square kilometers. The average depth of the lake is 3.4 m, maximum depth is observed in the north and makes up to 7 m. Water surface of the lake is mostly open, only the western and north-western coasts covered with reeds and rushes.

The bottom is flat sloping to the north, the coast is sandy and rocky, silty in the middle and the power of silt in the northern part of the lake Burabai is 0.5-1.0 m, 1.6 m in the southern part. The lake has several small bays. In the northwestern gulf a rocky island "Sphinx" is located shaped like a fungus and towering over the water at 20 m. Southern, western and northern shores of the lake are composed of granite, sometimes rising above the water in the form of the cliffs. The eastern shore is sandy, gently sloping; there's a berm near the water's edge with width 2.5 m and height 1.5 m. Lake is flowing.

It is filled by the river Sary-Bulak in the southeast, creek Imanaevsky and two unnamed creek in the west. Lake Kurkureuk with 1.5 km long flows from the lake to its north-eastern part and discharge water into the nearby lake Aynakol. Monitoring observations on lakes had been conducting in North Kazakhstan hydrogeological station since September 1945 [1, 2].

Lake Ulken Shabakty (Aynakol) - the largest lake among Burabai group which is located 16.5 km to the north of Schuchinks (Fig. 1). Water surface area is about 23 square kilometers. The average depth of the lake is 11.1 m, maximum - 33.3 m. The lake is open without aquatic vegetation, which is explained by the presence of the great depths. The northern and eastern shores of the lake are gentle, southern and western shores are steep formed by the mountain massif slopes. There are several small islands on the lake which form seamounts and ridges. The bottom of the lake is composed of yellowish-brown clay, silt covered with capacity of up to 2 m. The lake is closed. In the western end of the lake there is a vast shallow to 1.5 meters deep bay, the soils of which are coarse sand and gravel. Pebble and gravel soils are also located around the ridge of islands, but they are highly silted. In the middle of the lake soils are presented as silts. There are mountains on the southern side covered with mixed forests with a predominance of conifers and hilly plain on the north side covered with steppe grasses [1, 2].

Information-analytical system "Monitoring of aquatic ecosystems": Information-analytical system (IAS) consists of information and analytical subsystems. Analytical subsystem is currently provided by the computer applications Microsoft Excel 2007 and STATISTICS which are connected to the information subsystem. An analysis of the aggregated data is carried out by standard statistical methods of research with the help of these packages [6-10]. Details about structures included in the methods of analytical subsystem are represented in the following sections together with an analysis of data on the lakes. Here are the structure and function of the information subsystem.

An information subsystem was created which consists of a database that contains geographical, hydrobiological and hydrochemical data on reservoirs of Kazakhstan. At the moment data on lakes Burabai and Ulken Shabakty are assembled and filled in [2].

Information subsystem includes two databases:

- Primary hydrobiological data;
- Hydrochemical data.

The data are dated and may be supplemented; the system monitors the correctness of records; extensions are given for data listed by user. The system requires a mandatory registering or logging in with passwords. To search, choose and view the information standard system is used to query the database with a specially designed system of menus and dialogs.

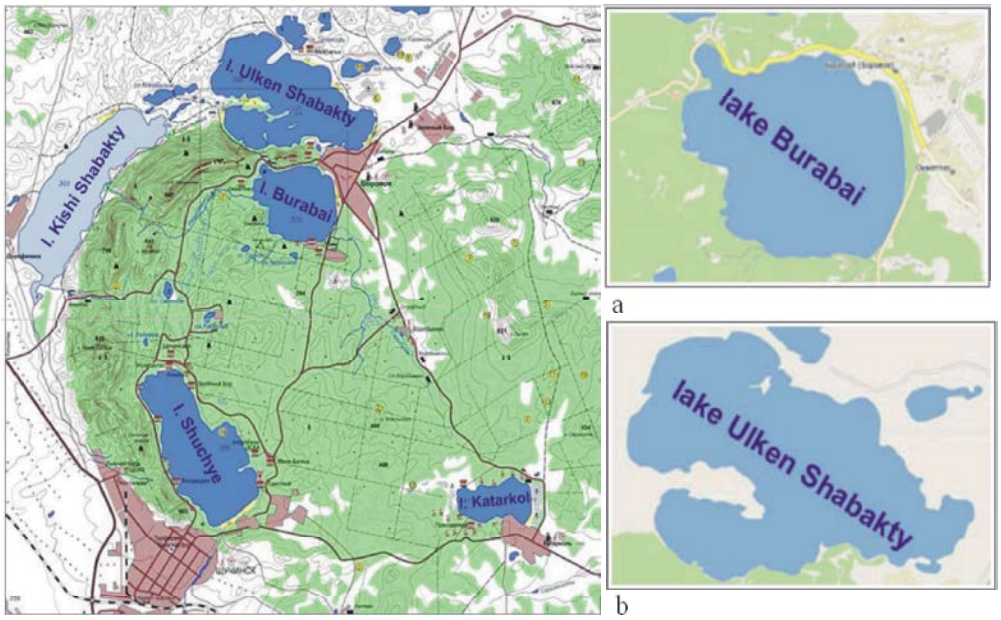

Fig. 1: Lakes in Shchuchinsk-Borovoye resort area: a - lake Burabai, b - lake Ulken Shabakty

The basic functionality of the information subsystem:

- Input, editing and processing information;
- Implementation of a variety of database queries, search for objects in the tables;
- Quick extract of required information (by years, by type, by name);
- Calculation of the maximum, average, total value of the selected search parameter;
- Calculation of period of time and values exceeding MPC of harmful substances for fishery reservoirs according to certain parameters;
- Output of results in various forms, including printing.

Subsystem includes comments and links to data sources.

Hydrobiological database includes primary hydrobiological data on the place, date and sampling conditions, taxonomic supplies quantity biomass, as well as ecological groups and functional characteristics of aquatic organisms (phytoplankton, zooplankton, bacterioplankton, periphyton, zoobenthos, pigment composition of microalgae, macrophytes) and the corresponding iconography.

Hydrochemical database consists of following main tables: "Information about system users", "Choice of reservoirs," "Properties, gas composition, major ions," "organic pollutants" "Biogenic components and inorganic contaminants".

The table "Biogenic components and inorganic contaminants" contains the following data: sampling time, date (dd / mm / yy), ammonium nitrogen (mg / l), nitrite nitrogen (mg / l), nitrate nitrogen (mg / l), the amount of nitrogen (mg / l), plumbum (mg / l), vanadium (g / l), molybdenum (µg / l), iron (3 +) (mg / l), cobalt (mg / l), mercury (mcg / l), phosphate (mg / l), silicon (mg / l), total phosphorus (mg / l), cadmium (mg / l), silver (mg / l), total iron (mg / l), iron (2 +) (mg / l), cuprum (mg / l), lead (mcg / l), manganese (mg / l), arsenic (g / l), zinc (mg / l), fluorides (mg / l), nickel (mg / l), cyanide (mg / l), total chromium (mcg / l), chromium 6 + (g / l), chromium 3 + (g / l), thiocyanates (mg / l), boron (mg / l).

The table "Properties, gas composition, major ions," contains the following data: sampling time, date (dd / mm / yy), width, depth (m), speed of current (m / s), water flow (cubic meters / s), the sample storing time (in days), the flow of waste water (m^3/s), smell (pts), salinity (mg / l), transparency (cm) temperature (°C), hydrogencarbonate (mg / l), suspended substances (mg / l), carbonates (mg / l), pH, sodium (mg / l), oxygen (mg / l), potassium (mg / l), oxygen saturation (%), calcium (mg / l), carbon dioxide (mg / L), transparency according to a DB (m), hydrogen sulfide (mg / l), magnesium (mg / l), chloride (mg / l), sulfates (mg / l).

The table "Contaminants organic" contains the following data: sampling time, date (dd / mm / yy), color, dichromate oxidation (µg / l) BOD5 (biochemical oxygen demand) (µg / l) volatile phenols (mg / l), alpha-HCH

(hexachlorocyclohexane) (g / l) resin and asphalt (µg / l), gamma-HCH (hexachlorocyclohexane) (µg / l), oil products (µg / l), Council-HCH (hexachlorocyclohexane) (µg / l), fats (µg / l), dicofol (mg / l), detergents (synthetic surfactants active ingredient) (µg / l) HCB (hexachlorobenzene) (µg / l), phenols sum (µg / l), xanthogenates (µg / l) carbohydrate (µg / l).

When creating a database of information subsystem MySQL 5.5.20 was used; this is included in WampServer 2.2 and operates harmoniously with technology Java. NetBeans was used - a free integrated development environment (IDE) on programming languages Java, Python, PHP, JavaScript, C, C + +, Ada and several others. In recent years cloud technologies are available for NetBeans and special plugins are required to set that make it easy to work with applications. Data may be stored in a cloud; it simplifies the management applications process. NetBeans IDE provides many opportunities for the DBMS. We can create a database on registered server directly from NetBeans, connect it immediately by opening the context menu of connection, to create a table, open it using the command View Data, go to the fill mode button InsertRecords and fill the table with all the required data [3, 4].

The created database is not final and may be supplemented by new data and other reservoirs.

The Data Analysis: Analytical subsystem consists of deterministic and statistical data processing methods [5-9]. Deterministic methods are limited to simple tools for sorting data averaging, calculating the maximum and minimum values. Statistical methods are presented in the form of sequence graph and contain the analysis of the type of probability distribution, point and interval estimation of parameters, hypothesis testing, regression and dispersion analysis and multivariate statistical methods.

In this paper information on biogenic substances are selected to illustrate the application of the methods. These mineral substances are based on nitrogen and phosphorus. They provide phytoplankton with food during photosynthesis and play an important role in the ecosystem of the reservoir [10]. Study of biogenic substances allows to identify patterns of condition and dynamics of hydrobiological indicators. In turn, this leads to an assessment of the environmental condition of the reservoir. The ratio of nitrogen to phosphorus compounds is particularly important. For the analysis concentration of nitrogen in the nitrite compounds, nitrates and ammonium salts and the total phosphorus in the two investigating lakes are selected. In addition, the dynamics of integrated concentration of biogenic elements have analyzed as reservoirs are interconnected. Data on their specific concentrations in the composition of samples taken per month for 7 years, from 2007 to 2013 were used to construct the seasonal dynamics of each of the observed elements. On Lake Ulken Shabakty data were analyzed for six years, starting from 2008. In the Figs. 2-5 below the vertical axis is the concentration of substance in mg/l and the horizontal axis - the time in months. Tables 3-7 are the concentrations of substances in mg/l.

RESULTS AND DISCUSSION

Classification of Lakes by Hydrochemical Indices: The water of lake Burabai is fresh, the mineralization of water is 216 - 251 mg/l. Ionic composition of the water refers to hydro-class sodium group of the first type. Environment reaction is slightly alkaline; pH in the range of 7.64 - 8.35. The lake water is soft; hardness does not exceed 2.23 mEq/l. BOD5 quantity (1.55 - 2.61 mg O_2/l), the oxygen content ranges from 8.57 to 9.28 mg O_2/l.

Lake Ulken Shabakty is salted, total mineralization of water is about 853 - 918 mg/l. Ionic composition of the lake water of Ulken Shabakty refers more to the first rather than the second type of hydro-class sodium group. Environment reaction is slightly alkaline - alkaline, pH is about 8.2. The water in lake has a medium hardness - 7.24 mEq/l. Biochemical oxygen demand (BOD5) (1.10 - 1.88 mg O_2/l), concentration of dissolved oxygen in water varies from 6.6 to 9.00 mg/l.

By the degree of pollution, the lakes Burabai and Ulken Shabakty can be currently classified as between "clean" and "moderately polluted" (Table 1). Font number indicates in Table 1 the status of the lake: normal font signifies very pure status, italic font signifies pure status, bold font signifies moderately polluted status. Not specified units are given in the description of the IAS.

It should be noted that in 2009, all indicators of the lakes belonged to the "pure" and in subsequent years, such parameters as dissolved oxygen, ammonia nitrogen and pH indicate some water pollution.

Data on phosphorus load presented in Table 2 show that in 2007-2008 lakes were close to oligotrophic and in 2012-2013 have already approached the mesotrophic reservoirs [2, 11, 12].

Currently, according to the classification of the content of total phosphorus, both lakes relate to mesosaprobic type [3, 5].

Table 1: Chemical, physical and organoleptic characteristics of condition of lakes Burabai and Ulken Shabakty in 2009-2013

	Dissolved oxygen in mg/l							
Lakes	Summer	Winter	% of saturation O_2	BOD5 mg/l	Ammonia nitrogen (mg/l)	Suspended substances	Smell	pH
2009								
Lake Burabai	9.18	11.4	89	1.2	0.06	10.3	0	8- 8.75
Lake Ulken Shabakty	9.18	11.4	87.8	1.5	0.06	10.3	0	8 - 8.75
2010								
Lake Burabai	8	8	75.5	1.6	0.2	9.33	0	6.25-8.65
Lake Ulken Shabakty	8	12.3	86.5	1.3	0.15	8	0	8.25-8.70
2011								
Lake Burabai	8.86	10.6	78	1.5	0.15	6.7	0	7.45-8.65
Lake Ulken Shabakty	8	11	85	1.04	0.23	5.9	0	8.50-9.25
2012								
Lake Burabai	8.81	10.28	82	1.7	0.2	2	0	7.25-8.55
Lake Ulken Shabakty	9.2	11.2	83.8	1.14	0.08	5	0	8.6-9.25
2013								
Lake Burabai		8.55	90	1.3	0.2	0.8_{min}-3.6_{max}	0	8.6 -8.7
Lake Ulken Shabakty	8	10.12	81	1.1	0.08	5.6	0	8.85-9.00

Table 2: Phosphorus load of lakes Burabai and Ulken Shabakty (2007-2013)

Years	2007	2008	2009	2010	2011	2012	2013
	Lake Burabai						
Annual average of total phosphorus, mg/l	0.011	0.013	0.014	0.024	0.023	0.025	0.033
	Lake Ulken Shabakty						
	-	0.009	0.010	0.020	0.023	0.021	0.026

Basic elements exceeding the maximum permissible concentrations in the lakes Ulken Shabakty and Burabai are sulfates, magnesium, fluoride, iron, aluminum, manganese and molybdenum. It is worth noting that according to data MPC the lake Ulken Shabakty has worse position. In the lake Burabai chemical elements, exceeding the norms MPC, comparatively less either by the quantity and the multiplicity of exceedance [2].

Lake Burabai in 2007-2008 in terms of water pollution index (WPI) classified as "pure" [13, 14]; there are no substances exceeding MPC during this period. In 2009, only fluoride exceeded MPC with the maximum excess of 16 times in June. Beginning from 2010 to 2011, in addition to fluoride, MPC exceeds copper, general iron and less often manganese. According to the WPI, the lake transit from "pure" to the class three, "moderately polluted". In the second quarter of 2012 in the lake Burabai the number of substances exceeding MPC increases significantly: fluoride, copper, total iron, zinc, total phosphorus, aluminum, cobalt, chemical oxygen consumption (COC). In the following months of 2012 exceeding of the MPC of such elements as zinc, cobalt and total phosphorus were not marked. In 2013, the list of substances with a high MPC includes only fluoride, molybdenum, manganese and total iron.

In the lake Ulken Shabakty in 2007 - 2008 years there is an excess of the maximum permissible concentration (MPC) of sulfate from 1.0 to 2.5 with the highest values in March and November. From 2009 to 2011 sulfates exceed the MPC 2.2 times, 2.6 times the magnesium and fluoride 17.7 times. Deterioration in water body begins with the second quarter of 2012. It is observed that there is an excess of MPC in not only previously mentioned magnesium, copper, sulphate, fluoride and also in total iron, aluminum, manganese, molybdenum and chemical oxygen consumption (COC). Heightened concentrations of these elements (except aluminum and indicators COC) were established also in 2013. Lake Ulken Shabakty, according to its water pollution index (WPI), refers to pollution class 4 [12]. It should be noted that the biogenic substances in both lakes do not exceed the norm.

Trend analysis of biogenic substances: We analyzed the smoothed dynamics of biogenic substances concentrations as trends. Data on nitrite, nitrate, ammonium and phosphorus from 2007 to 2013 were used for the statistical analysis of lakes condition. Samples were made monthly. To smooth the data over time, firstly, we examined the trends (moving averages) for four of these substances. Figs. 2 and 3 show moving averages with "windows" of averaging for 3 and 12 months. Averaging over three months allows you to see the seasonal features of the dynamics of substance concentrations. Averaging over 12 months shows interannual dynamics.

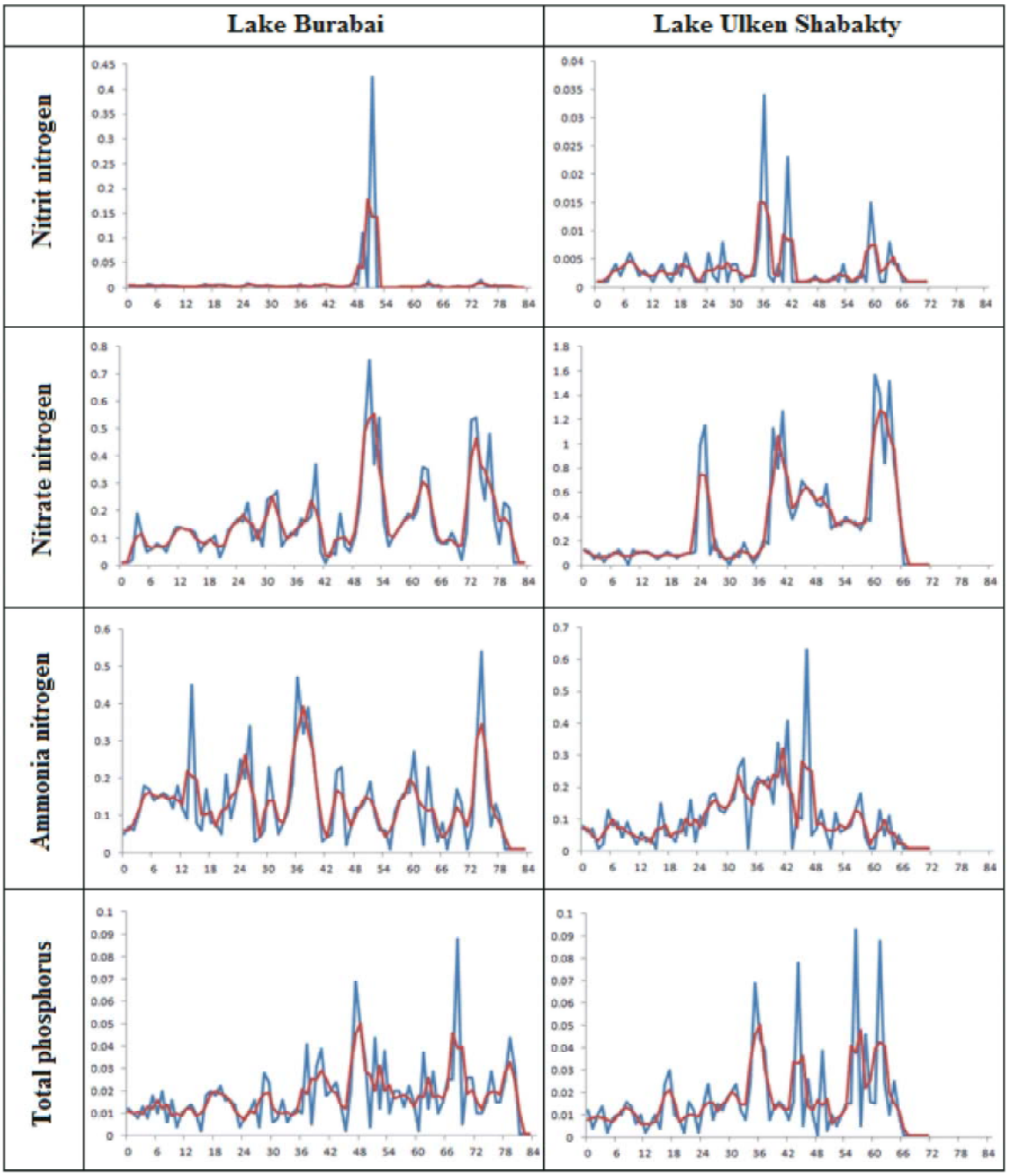

Fig. 2: Trends of biogens concentrations in two lakes with a three-month averaging

Seasonal fluctuations are amplified in the second half of the considered period. It is possible to assume that this effect indicates the increased human activity in the second decade of the XXI century.

Again, there is some increase in interannual estimation of substance concentrations in the second half of review period.

Averaging the assessment of standard deviations, they all, except nitrates, have the same order as the average values. For nitrates deviations are an order less than the trend values. By increasing the "window" of averaging from three to twelve months, standard deviations, of course, increase, but not significantly. For nitrates the increase is slightly higher. These facts indicate that the monthly deviations are large enough.

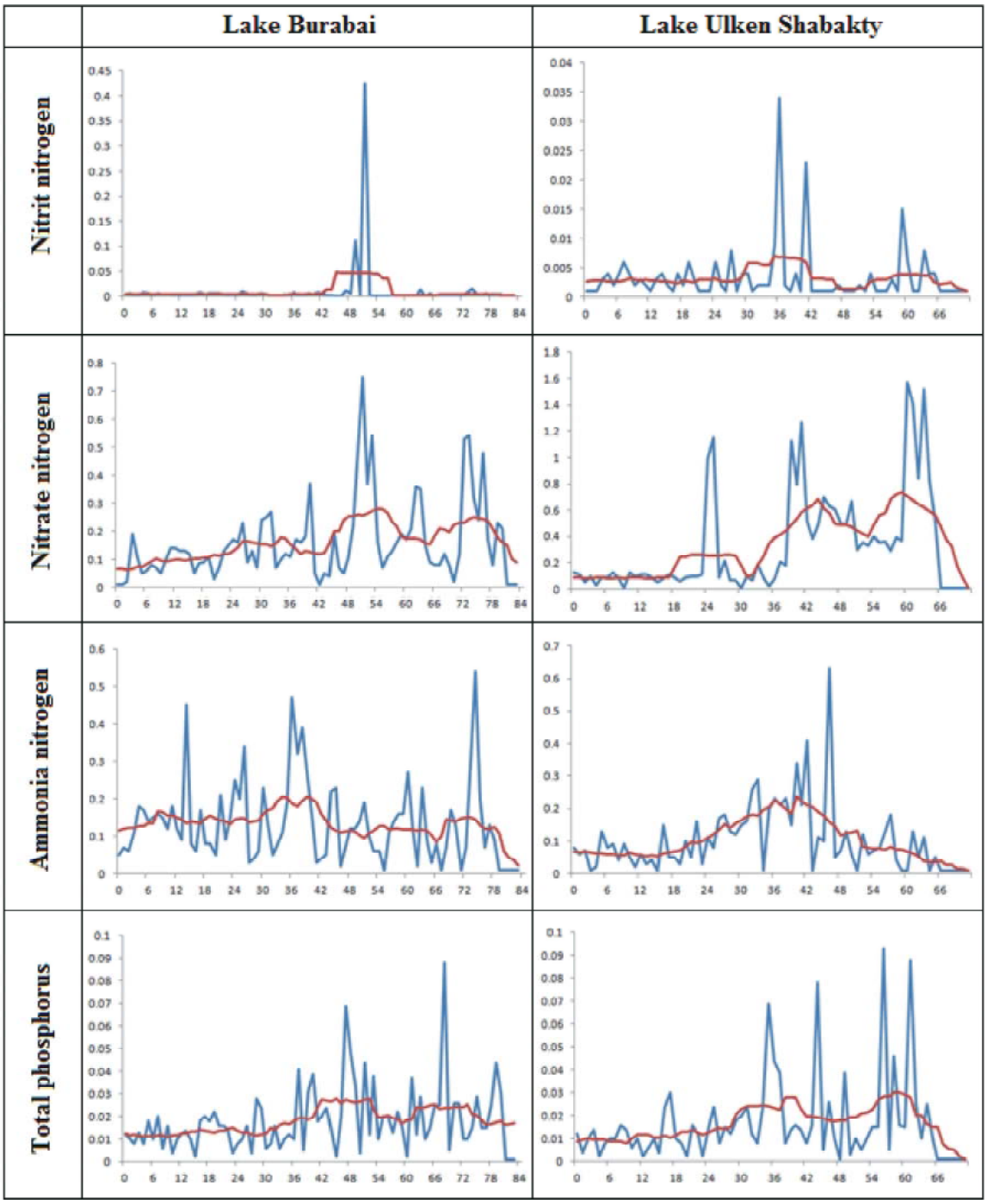

Fig. 3. Trends of biogenics concentrations in the two lakes with the twelve-month averaging

It is known that in different seasons in the reservoir ecosystem is dominated by various types of phytoplankton. Among other factors this is due to the amount of available mineral nutrition. However, there is a question for research which remains open about the qualitative composition of the substrate consumed by phytoplankton. In particular, it is useful to evaluate how significant seasonal fluctuations in concentrations of individual biogens in compare to their interannual variability. To construct such evaluations one way ANOVA (analysis of variance) scheme was used. These evaluation results are shown in Table 3.

Table 3: The value of Fisher criterion obtained in compare to intra annual variations

	Nitrite nitrogen	Nitrate nitrogen	Ammonia nitrogen	Total phosphorus	Limit value at the level of 0.05
Lake Burabai	1.460	1.604	1.639	1.699	1.93
Lake Ulken Shabakty	1.914	1.434	0.987	0.503	1.94

Table 4: Pearson criterion values for the lognormal distribution compared to the limit values for the two levels of significance

					Limit value for degrees of freedom 4 and 3	
	Nitrite nitrogen	Nitrate nitrogen	Ammonia nitrogen	Total phosphorus	At a significance level of 0.05	At a significance level of 0.01
Lake Burabai	25.8982	4.9588	4.6859	2.5660	9.49 (7.81)	13.3 (11.3)
Lake Ulken Shabakty	8.6031	9.8137	2.9480	5.5084		

The results also show that the seasonal fluctuations are large enough compared to the interannual. Seasonal factor plays a significant role in changing biogenic substances concentrations.

Statistical Data Analysis on Two Lakes: Trend analysis showed that seasonal oscillations of concentrations of substances are sufficiently large. In an attempt to answer the question about the reliability of the data, we tested the hypothesis about their lognormal distribution (which is quite reasonable to assume for the tested data) and the number of "unnatural" values in the data. The presence of the lognormal distribution provides to use traditional criteria Student, Pearson, Fisher, etc. to analyze the data in a logarithmic scale [5, 6].

Assuming that the detection of a component in the sample is limited by the sensitivity of the device-analyzer, zero concentration approximated to the minimum value of the observed multi corresponding element. At the beginning, data from all four biogens are tested on the lognormal distribution for each lake. We use Pearson criterion for this test.

The frequencies for the concentrations of nitrite nitrogen distributed with three degrees of freedom, other substances with four.

The lognormal distribution can be questioned with a sufficiently low level of significance for nitrates and nitrites. Perhaps such behavior of data associated with the drainless of the second lake and therefore, a small number of factors affecting the concentration of nitrogen. We will use them to the traditional criteria, maintaining alertness, indicated in Table 4.

Further, interval estimations of the annual dynamics of biogens concentrations are built for each of the lakes and lakes for both together (Fig. 4). For each lake and for both of them together averaged dynamics of year and its interval estimations were constructed.

In the averaged year dynamics of biogens are more diverse in the spring and early summer compared with the second half of the year, although "outbursts" do happen in the ammonium and phosphorus in the fall and early winter (Figs. 4 and 5). Spring effects may be associated with the arrival of melt water and intensive development of phytoplankton. Flashes also occur in autumn in the phytoplankton biomass, which can affect the concentrations of ammonium and phosphorus.

Data which are not included in the confidence intervals were allocated. When data were reanalyzed it is revealed that there are indicators, the absolute values of which lie outside the boundaries of the confidence intervals. The proportion of such points varies from 0.083 to 0.286. These deviations do not have any natural character of manifestations; that is they do not depend on the season or on the reservoir in which they are recorded. Number of such points is almost always within 20%. In our view, this indicates a satisfactory quality of data collection and a good reliability.

Further, two lakes were compared with each other on the object identity of their dynamics to the same general set (Table 5). On the one hand, a small river flows from the lake Borovoye into the lake Ulken Shabakty. This can contribute to a synchronous behavior of the concentration of substances in both lakes. On the other hand, the lake Ulken Shabakty is drainless that, in general, contributes to the increased biogens content in it. Statistically, the task of comparing lakes can be formulated as follows: Is the set of specific concentrations of some element of the two lakes samples from the same set or not? To do this, we used Student's test (Table 5) [6, 7].

For all substances, except for nitrates, the hypothesis about one general set confirmed. The number of degrees of freedom in all cases is in the range from 105 to 145.

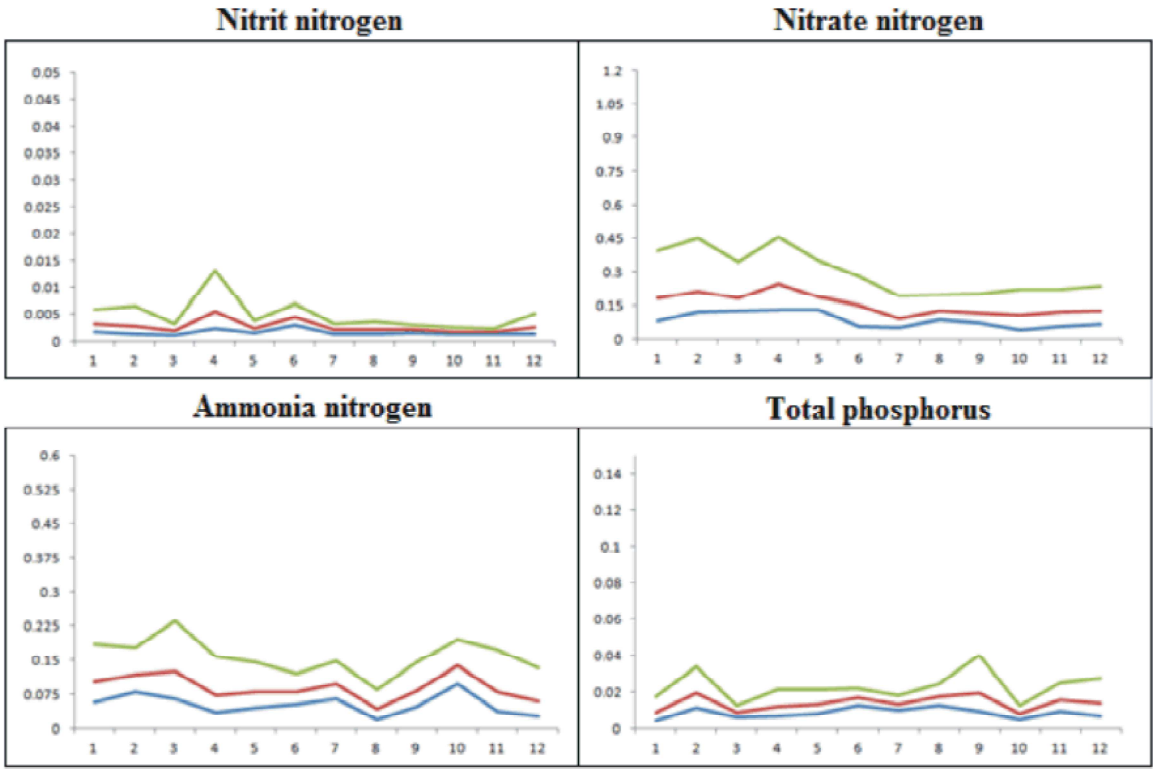

Fig. 4: Average annual dynamics of biogens with confidence intervals at a significance level of 0.05 over both lakes. Red denotes the average long-term. Green and blue colors represent lower and upper bounds of interval estimations

Table 5: Values of Student's criterion for the two lakes

	Nitrite nitrogen	Nitrate nitrogen	Ammonia nitrogen	Total phosphorus
Value of Student's test	0.905	4.090	1.291	0.194

Table 6: The correlation matrix of biogens communication for the lakes Burabai (above the main diagonal) and Ulken Shabakty (below the main diagonal)

	Nitrite nitrogen	Nitrate nitrogen	Ammonia nitrogen	Total phosphorus
Nitrite nitrogen	1.000	0.465	0.072	0.233
Nitrate nitrogen	0.154	1.000	0.216	0.137
Ammonia nitrogen	0.116	0.157	1.000	-0.123
Total phosphorus	0.134	0.236	0.204	1.000

Table 7: The correlation matrix of biogens communication in lakes

		Lake Burabai			
		Nitrite nitrogen	Nitrate nitrogen	Ammonia nitrogen	Total phosphorus
Lake Ulken Shabakty	Nitrite nitrogen	-0.029	0.018	-0.095	-0.013
	Nitrate nitrogen	-0.045	0.272	-0.036	-0.013
	Ammonia nitrogen	0.322	0.093	0.035	0.167
	Total phosphorus	-0.117	0.096	-0.011	0.042

The corresponding limit value of Student's t test for them is 1.98. Consequently, we can neglect the differences between lakes in concentrations of all substances except nitrate nitrogen compounds. The obtained value exceeds the limit criterion 3.37 even at a significance level of 0.001. This could be the termination of communication between the reservoirs in winter, as significant differences in the concentrations of nitrate nitrogen is observed between the lakes in the first half of the year, that is in spring and early summer period. After June there is a "leveling" of these indicators. The value of Student's t test obtained for total phosphorus, in contrast, is much less than the limit.

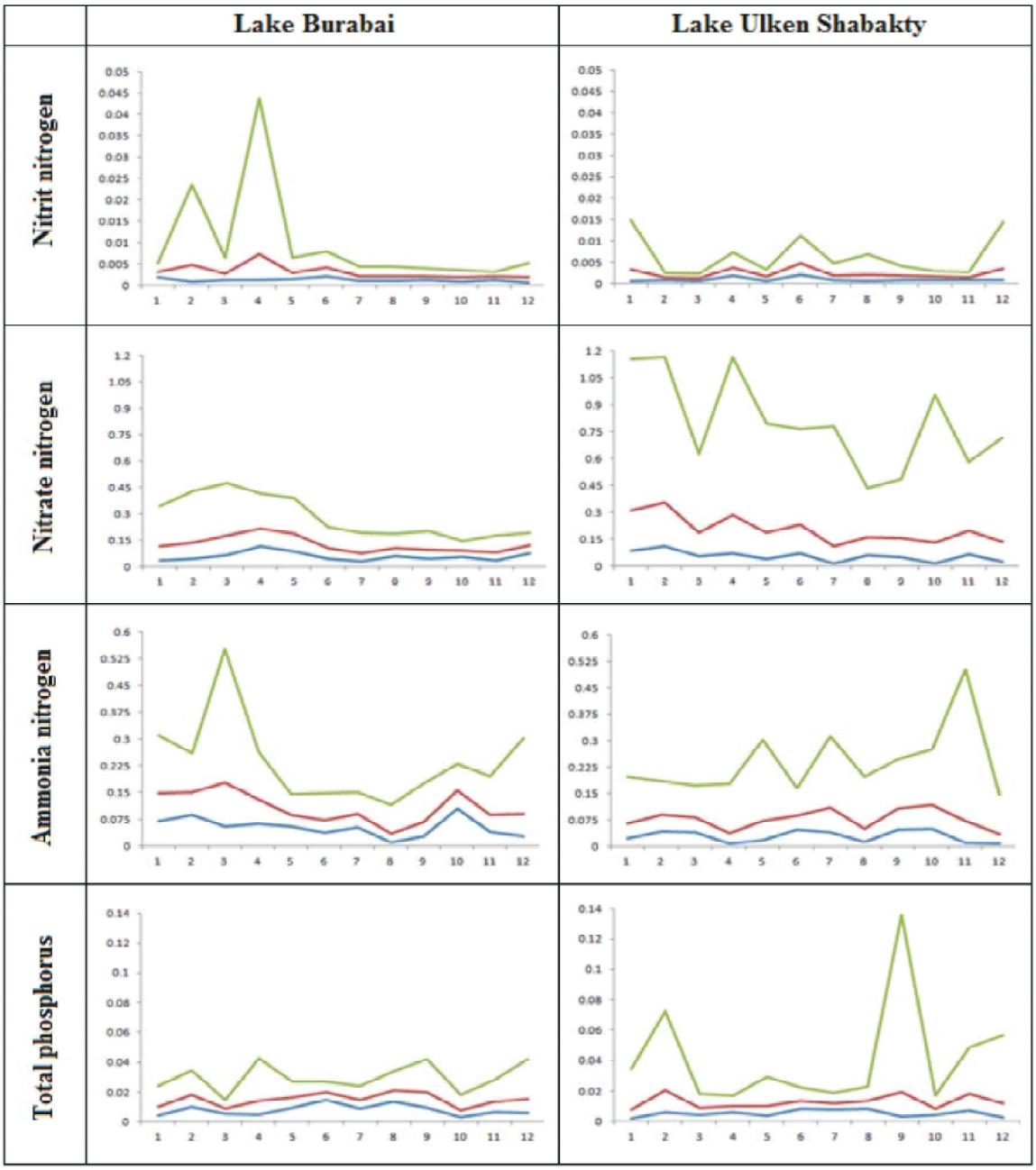

Fig. 5: Average annual dynamics of biogens for each lake with confidence intervals at a significance level of 0.05. Red color denotes the average long-term. Green and blue colors represent lower and upper bounds of interval estimations

This suggests that phosphorus compounds have approximately equal concentration changes in both lakes, not depending on the communications between them. Consequently, we can expect that those kinds of lake plant communities that have priority in phosphorus mineral nutrition, will be stable throughout the growing season.

Comparison of biogens: Biogenic substances come to lake with inflows at various concentrations, similar to the case with the outward flow. Concentrations of substances also change during evaporation. Phytoplankton is consumed at different speeds. They come into the water with different speeds as a result of destruction of organic matter by bacteria. At the same

time, the concentration of these substances in the lake can be correlated between them as a result of the total effect of all of these processes. The problem of such a correlation was considered for each lake and between lakes (Tables 6 and 7) [8].

Rigid links between the concentrations of substances in each lake are not separately identified, substances behave relatively independently. Only nitrates and nitrites of Burabai lake have significant connections (Table 6). The correlation matrix is symmetric, so the correlation coefficients in Table 6 for the lake Burabai are indicated above the main diagonal and for the lake Ulken Shabakty are below (italic).

This may mean that their delivery to the lake and phytoplankton consumption are not synchronized, that is substances come from various sources and converted with independent to each other speeds.

Visible connection between lakes is only seen in nitrates (Table 7). Nitrates are dominated by weight of among biogens; their connection has a great importance. The correlation coefficient in the nitrates which is 0.272 can mean interconnectedness of lakes and total dependence on the sources and nitrate runoff.

CONCLUSION

For the analysis of the ecological state of lakes in Kazakhstan the information-analytical system was developed. It consists of hydrochemical and hydrobiological data and analytical subsystem of deterministic and statistical methods of data processing.

The obtained results on trends indicate that seasonal variations are large enough compared to the interannual. Seasonal factor plays a substantial role in changing nutrient concentrations. Testing for normal distribution of the substance concentration logarithms shows that the lake Burabai "lives" mainly due to natural factors or many small artificial factors. In the lake Ulken Shabakty there are probably artificial sources of nitrites and nitrates, "concealing" lognormal distribution patterns.

In the averaged year dynamics of biogens are more diverse in the spring and early summer compared with the second half of the year, although there are "outbursts" in the ammonium and phosphorus which occur in the fall and early winter. Spring effects may be related to the intensive development of phytoplankton. Autumn is also an outbreak of phytoplankton biomass, which can affect the concentrations of ammonium and phosphorus. In general, the concentration of phosphorus compounds is more stable, which may favorably affect the life of phytoplankton species which are fond of phosphorus.

Intense links between the concentrations of substances have not been identified, substances behave relatively independently. This may mean that their delivery to lakes and phytoplankton consumption are not synchronized, that is, substances come from various sources and converted with independent to each other speeds.

Refilling the database on lakes would enhance data processing, including statistical data processing. It is anticipated that there is a possibility of using a dynamic mathematical model for the joint analysis of hydrobiological and hydrochemical information [10, 15-19]. These models give us the possibility for analysis of functioning of aquatic ecosystems in seas and lakes [17, 18, 20]. These ecosystems show by functioning many different effects.

REFERENCES

1. State Report, 2000. “A condition of natural resources and environment in the Republic of Kazakhstan”, 2000. Book 1. The general ecological state on the Republic and implementation of the plan of measures for 1998-2000 years. Kazakhstan.
2. Newsletter on a state of environment in Shchuchinsk-Borovoye resort area, 2013. For 2008-2013 years. Kazakhstan.
3. http://www.netbeans.org/.
4. Borovikov, V.P., 2001. Program “Statistics” for engineers. Moscow Computer Press.
5. Bendat, J.S. and A.G. Piersol, 1980. Engineering Applications of Correlation and Spectral Analysis. John Wiley & Sons.
6. Handbook of Applicable Mathematics, 1986. Volume VI: Statistics. John Wiley & Sons.
7. Aivazyan, S.A. and V.S. Mkhitaryan, 1998. Applied statistics and fundamentals of econometrics. Moscow YuNITI.
8. Dubrov, A.M., V.S. Mkhitaryan and L.I. Troshin, 1998. Multidimensional statistical methods. Moscow, Finance and Statistics.
9. Al-Badaii, F. and M. Shuhaimi-Othman, 2014. Heavy Metals and Water Quality Assessment Using Multivariate Statistical Techniques and Water Quality Index of the Semenyih River, Peninsular Malaysia. Iranica Journal of Energy & Environment, 5(2): 132-145.
10. Forecasting of Ecological Processes, 1986. Editor O. M. Kozhova. Novosibirsk Science Publ., Russia.

11. Vollenweider, R.A., 1968. The scientific basis of lake and stream eutrophication, with particular reference to phosphorus and nitrogen as eutrophication factors. Techical Report OECD. Paris DAS/CSI/68. 27: 1-83.
12. Datsenko, Yu S., 2007. Eutrophication of aquatic basins. Hydrological and hydrochemical aspects. Moscow State Univ., Geographical Department GEOS.
13. Schitikov, V. K., G.S. Rosenberg and T.D. Zinchenko, 2003. Quantitative hydroecology: methods of system identification. Tolyatti IEVB RAS, Russia.
14. Abakumov, V.A., N.G. Bulgakov, A.P. Levich, S.V. Mamikhin, E.P. Nikitina, V.A. Nikulin and S.V. Sukhov, 2000. Analitical information system "Ecology of Fresh Waters in Russia" as instrument for biological researches. Messenger of the Moscow State University. Biology Series, 2: 38-42.
15. Abakumov, A.I., V.A. Silkin and L.A. Pautova, 2012. Biomass dynamics of the phytoplankton under impact of the nutrient. 18th Biennial ISEM Conference On Ecological Modelling for Global Change and Coupled Human and Natural System. Book Series: Procedia Environmental Sciences, 13: 105-110.
16. Abakumov, A., A. Ismailova and A. Adamov, 2014. Modeling of Microbial Communities of Plant Organisms in Aquatic Ecosystem. Information. An International Interdisciplinary Journal, 17(1): 209-218.
17. Blenckner, T., 2008. Models as tools for understanding past, recent and future changes in large lakes. Hydrobiologia, 599: 177-182.
18. Silkin V.A., A.I. Abakumov, L.A. Pautova, A.S. Mikaelyan, V.K. Chasovnikov and T.A. Lukashova, 2011. Co-existence of non-native and the Black sea phytoplankton species. Invasion hypotheses discussion. Russian Journal of Biological Invasions, 2(4): 256-264.
19. Fathi, M. and A. Honarbakhs, 2012. River Channel Change Simulation of Khoshke Rud Farsan River and Bank Erosion Process Using a Numerical Depth Averaged Model, CCHE2D. Iranica Journal of Energy & Environment, 3(4): 299-306.
20. Jeppesen, E., J.P. Jensen, M. Sendergaard, T. Lauridsen and F. Landkildehus, 2000. Trophic structure, species richness and biodiversity in Danish lakes: changes along phosphorus gradient. Freshwater Biology, 45: 201-218.

Persian Abstract

DOI: 10.5829/idosi.ijee.2014.05.03.04

چکیده

سیستم اطلاعات تحلیلی (IAS) "نظارت بر اکوسیستم‌های آبی" برای تجزیه و تحلیل وضعیت دریاچه‌های اکولوژیکی در قزاقستان توسعه داده شد. این سیستم شامل یک پایگاه داده ویژگی‌های هیدروشیمی و هیدروبیولوژی برای دریاچه‌های Burabai و Ulken Shabakty در منطقه Shchuchinsk-Borovoye جمهوری قزاقستان است و مشابه مجموعه‌ای از روش‌های پردازش داده‌های آماری می‌باشد. تجزیه و تحلیل کیفی داده‌ها بر روی دریاچه انجام شده است. داده‌های مواد بیوژنیک برای سال ۲۰۰۷-۲۰۱۳ بر اساس آمار تجزیه و تحلیل شد. ویژگی‌های پویا و ویژگی‌های فصلی تغییر در غلظت بیوژن‌ها مشخص شد. رابطه مهمی بین غلظت مواد مختلف بیوژنیک در دریاچه‌ها و بین دریاچه‌ها وجود ندارد. در مقایسه با مواد نیتروژن دار، ترکیبات فسفردار پایداری زیادی دارند که می‌تواند به زندگی پایدارتر گونه‌های فیتوپلانکتون کمک کند.

Iranica Journal of Energy & Environment 5 (3): 259-269, 2014
ISSN 2079-2115
IJEE an Official Peer Reviewed Journal of Babol Noshirvani University of Technology
DOI: 10.5829/idosi.ijee.2014.05.03.05

BUT

Leachate Pollutants Adsorption Using Potassium Hydroxide and Surfactant Modified Bentonite for Possible Use as Slow Release Fertiliser

[1]Syafalni and [2]Roslina Mohd Rusli

[1]Department of Civil Engineering, Bina Nusantara University, Jakarta, Indonesia
[2]School of Civil Engineering, Engineering Campus, Universiti Sains Malaysia, 14300, Nibong Tebal, Penang, Malaysia

Date of Received: February 7, 2014; Date of Accepted in Revised Form: August 2, 2014

Abstract: Leachate pollutants adsorption using potassium hydroxide (KOH) and Surfactant Modified Bentonite (SMB) have been used as a new method for leachate treatment. KOH was used for removing the heavy metal elements and natural bentonite (NB) and SMB as adsorbents to adsorb ammoniacal-nitrogen, nitrate and phosphate. The suitable conditions for adsorbents are obtained using the percentage removal of colour, iron, COD, ammoniacal-nitrogen, nitrate and phosphate. The results obtained at optimum conditions for dosage and pH for NB was 233.3 g/L at pH 9. By comparison, for SMB they were 166.7 g/L at pH 8. For the contact time, using slow mixing and rapid mixing, SMB is better than NB. From the SEM-EDX analysis of weight percentage, after the NB and SMB treatments the elements of nitrogen, phosphorus and potassium for NB increased by 1.04, 1.32 and 5.13%; respectively; also for SMB 1.30, 2.25 and 6.81% respectively. It is clear that SMB gives better adsorption than NB and can be used for future application as a slow release fertiliser for plants.

Key words: Leachate · Natural bentonite · Surfactant modified bentonite · Adsorption · Fertiliser

INTRODUCTION

Landfill is one of the simplest methods for disposal of municipal solid waste around the world [1]. After solid waste is disposed into landfill, it undergoes physico-chemical and biological changes at the landfill site. Therefore, the degradation of the organic fraction of the waste is accomplished and this phenomenon generates a highly polluted wastewater called leachate [2, 3]. Leachate is defined as an aqueous effluent generated as a consequence of rainwater percolation through waste at the landfill site [4]. Leachate could contain a huge amount of pollutants such as organic substances measured as COD, biochemical oxygen demand (BOD), ammoniacal-nitrogen, heavy metals, major ions and inorganic salts [5].

In general, leachate generated from fresh acidogenic landfills; which is characterized by high BOD (3000-13000 mg/L), high strength COD (30000-60000 mg/L), high ammoniacal-nitrogen (500-2000 mg/L) and the ratio of BOD/COD is around 0.4 to 0.7. A high amount of COD and BOD concentration and high BOD/COD ratio in fresh leachate makes it a candidate for anaerobic treatment prior to any aerobic process [3, 6]. The composition of landfill leachate greatly varies, depends on waste quantity and composition, decomposition rate and age of the waste. Also, it depends on method of landfilling or applied technology. The spread of leachate contamination from a landfill site is unacceptable and must be collected and treated before it is discharged. It must be treated close to the site to promote a sustainable closed-loop treatment strategy. This creates a need to develop on-site leachate treatment systems [7, 8].

The removal of metals from contaminated effluent is a matter of great interest in the field of environmental restoration, especially in this era of environmental concern. Several conventional methods are available for the treatment of effluents containing metals such as chemical precipitation, chemical oxidation, ion exchange, reverse osmosis and membrane filtration. However, most of these methods are ineffective for the removal of low concentrations ($\leq$ 10 mg/L) of metal ions and resulted in

Corresponding Author: Syafalni, S., Civil Engineering Department, Bina Nusantara University, Palmerah 11480, Jakarta, Indonesia. Tel: +62215345830, Fax: +62215300244.

Please cite this article as: Syafalni and Roslina Mohd Rusli, 2014. Leachate Pollutants Adsorption Using Potassium Hydroxide and Surfactant Modified Bentonite for Possible Use as Slow Release Fertiliser. Iranica Journal of Energy and Environment, 5 (3): 259-269

toxic sludge production; which involves extra costs for treatment and disposal. On the other hand, adsorption is known as a cost effective and promising physico-chemical process for this purpose [9].

Currently, the adsorption process is believed to be a simple and effective method for water and wastewater treatment and the success of this method largely depends on the development of an efficient adsorbent. Activated carbon, clay minerals, biomaterials, zeolites and some industrial solid wastes have been widely used as adsorbents for adsorption of ions and organics in leachate treatment [10,11].

The aim of this study was to investigate the usage of SMB in adsorption process for the removal of ammoniacal-nitrogen, nitrate, phosphate and COD prior to eliminating the metals from the leachate. The generated sludge of adsorption can be used for the improvement of the soil fertility as slow release fertiliser.

MATERIALS AND METHODS

Sampling Location: Matang landfill is situated at 40°49'20.08" N and 100°40'44.08" E near the town of Taiping, Perak, Malaysia. The total area of this landfill site is about 12 hectare and it is equipped with a leachate detention pond. This landfill receives about 300 tonnes of solid waste daily and is classified as an improved anaerobic landfill. The landfilling operation started in 1995 and the landfill is now more than 17 years old [12].

The topography in the vicinity of the landfill is generally flat and low lying, with local elevations at the site ranging from 3.3 meters above sea level to as low as 1.8 meters. The climate of the area is classified as typical of Peninsular Malaysia, characterized by uniform temperature (daily mean minimum and maximum of 30 and 34°C, respectively) and high humidity (80 to 90%). This area is one of the wettest areas in Malaysia due to high average annual rainfall (4000 mm). Larut River and its tributary, Batu Tegoh River form the boundary of the landfill site on the south and east, respectively [13].

Leachate Sampling: Landfill leachate was collected manually from the leachate detention pond at an approximate depth of 1.0 m. The samples were kept in 25-litre plastic containers of high density polyethylene (HDPE). The samples were transported within 1 hour to the environmental laboratory and placed in a cool room (4°C) prior to experimental use, to minimise biological and chemical reactions in accordance with the Standard Methods for the Examination of Water and Wastewater [14]. The on-site parameters were prepared in situ, to represent the actual condition of the raw leachate. Sensitive parameters of leachate such as total dissolved solids (TDS), electrical conductivity (EC), salinity, dissolved oxygen (DO), temperature and pH were determined during on-site sampling using YSI Multiparameter Probe. The metals in the landfill leachate were determined using Inductive Coupled Plasma (ICP) test method. Thereafter, only the highest metal concentration was considered in the leachate before and after treatment.

Preparation of Surfactant Modified Bentonite (SMB): In this study, the amphoteric surfactant used is Miranol C2MSF 2M which is a very soft amphoteric surface-active agent, compatible with anionic, cationic (conditioning agent, germicides) and non-ionic materials [15]. The SMB was prepared with 0.02 mole (25.6 ml) of an amphoteric surfactant (Miranol C2MSF) that was mixed with 100 g NB and 1000 ml distilled water. Before the surfactant was mixed with the NB, the NB was washed several times with distilled water to avoid contamination. The mixtures were subjected to mechanical stirring for 4 hours at 250 rpm. After that, the mixture of SMB was left in a beaker for 3 days. After 3 days, the solution was filtered the solid residue was double washed with distilled water and then dried at 105 °C for about 24 hours. After being dried, the SMB was crushed to get the desired particle size and sieved using a mechanical shaker and 63µm sieve.

Leachate Treatment using KOH, NB and SMB: Characterisations of the raw leachate before treatment were conducted as soon as possible after sampling. Measurement of the parameters was conducted in triplicate, according to the Standard Methods of Water and Wastewater [16]. In this experiment, KOH was used as a chemical reagent for the process of chemical precipitation. Four mole of KOH solution was used from a stock solution throughout the experiments. Chemical precipitation was performed with conventional jar test apparatus (Stuart Flocculator, Model: SW6, UK) comprising of six paddle rotors (2.1 cm × 7.5 cm) each equipped with six 1000 mL beakers, using a variable speed mixer (0 to 350 rpm). The leachate samples were left for 2 hours at ambient temperature before each experiment was conducted. For each experiment, each beaker used for testing was filled with 300 mL of leachate sample. Jar test equipment in the physico-chemical treatment experiments was used to investigate the effect of KOH at various pH on removing the iron, colour, COD and turbidity content

of the leachate. During the treatment, the pH of the leachate sample was readjusted to the desired level using the KOH reagent. The pH varied from pH 9 to 13. One beaker was used as a control. Rapid mixing for 4 min (200 rpm), slow mixing for 20 min (60 rpm) and 30 min settling time was applied sequentially in the chemical precipitation. The supernatant of leachate from the treatment with KOH was filtered with a glass microfiber filter (90 mm) using the filtered media before analysis of the iron, colour and COD removal according to the standard methods using a DR2800 Spectrophotometer. The percentage removal of all the parameters versus pH coagulant was plotted. The highest removal point indicated the suitable pH condition for the leachate treatment with KOH. After the suitable pH from the leachate treatment with KOH was obtained, the supernatant from the chemical precipitation process was subjected to adsorption tests with NB and SMB. Before the leachate underwent the second stage of treatment with NB and SMB; the leachate effluent was filtered again to make sure that the suspended solids were removed. The batch studies for NB and SMB were conducted in order to find suitable conditions for dosage, pH and contact time. The dosages ranged between 10 to 90 g for both NB and SMB in the batch studies. After the suitable dosage was obtained, the leachate treatment was continued with batch studies for pH variation in the range of 6 to 11. The application of contact time by rapid mixing, slow mixing and the settling time were the same as in the KOH treatment. After treatment with NB and SMB, the effluent was filtered again with a glass microfiber filter (size 90 mm) before the concentration of colour, COD, iron, ammonia, phosphate and nitrate was measured.

RESULTS AND DISCUSSION

Landfill Leachate Characterisation: According to the Standard Methods for the Examination of Water and Wastewater, the characterisation of the raw leachate, such as pH, turbidity, colour, BOD_5, COD, ammoniacal-nitrogen, nitrate, phosphate, potassium and metals such as iron, copper, nickel, manganese and zinc were determined before the leachate was treated. Table 1 shows the raw leachate characterisation of Matang landfill from the laboratory analyses. The characteristics of the landfill leachate from this study were obtained before the landfill leachate treatment stage commenced. From Table 1, the colour, COD, BOD, NH_4-N, arsenic, manganese and nickel concentrations exceeded the parameter limits of standard discharges of leachate. Iron with maximum concentration 6.41 mg/L had the highest concentration of all measured metals in the leachate.

The leachate collected could be classified as alkaline since the pH values varied from 7.86 to 8.43. Generally, the pH of a stabilised leachate is higher than a fresh leachate. The pH for fresh leachate is less than 6.5, intermediate leachate is in the range of 6.5 to 7.5 and stabilized leachate is greater than 7.5 [17]. Moreover, the data obtained indicated that despite the short landfill lifetime, some parameters such as high pH (on average 8.15), low COD concentration (<2000 mg/L COD), low BOD_5/COD ratio (<0.4) and low heavy metal concentration indicated that the landfill was already characterised by methanogenic conditions at the beginning of the monitoring period [18].

The colour of the leachate sample in this study was orange brown or dark brown. The maximum value of colour for Matang landfill leachate was 8510 Pt-Co, while the minimum value was 4200 Pt-Co. The high concentration of colour in the landfill leachate is due to the high presence of organic substances. In general, the leachate produced by an old landfill with low biodegradability is classified as stabilised leachate. Stabilised leachate contains a high level of organic substances such as humic and fluvic compounds, which can be indicated by leachate colour [19]. Landfill leachate is a very dark coloured liquid formed primarily by the percolation of precipitation through open landfill or through the cap of the completed site. The decomposition of organic matter such as humic acid may cause the water to be yellow, brown or black [20].

From the characterisations of the landfill leachate, it was shown that the concentrations of arsenic, manganese, nickel and zinc were relatively low on average 0.21, 0.26, 0.27 and 0.36 mg/L respectively. Meanwhile the concentration of iron was the highest among the heavy metal elements contained in landfill leachate which average 4.62 mg/L. In general, the concentration of heavy metals in landfill leachate is fairly low. The concentration of heavy metals in landfill is generally higher at the earlier stages because of greater metal solubility as a result of low pH caused by production of organic acids [18].

The COD value for the landfill leachate varied from 867 to 1572 mg/L. The landfill for this study can be classified as a stabilised landfill as the COD value was less than 4000 mg/L, in accordance with results of a previous study on stabilized landfill [19]. The COD values obtained from our study seem to have exceeded the permissible limits issued by the Environmental Quality

Table 1: Characterisation of raw landfill leachate

Parameter	Units	Value				
		Minimum	Maximum	Average*	Standard Deviation	Standard**
pH	-	7.86	8.43	8.15	0.26	6.0-9.0
Turbidity	NTU	136	177	156.5	19.10	-
Colour	PtCo	4200	8510	6355	1878.45	100
Chemical Oxygen Demand (COD)	mg/L	867	1572	1219.5	324.01	400
Biological Oxygen Demand (BOD_5)	mg/L	108	360	234	114.34	20
Ratio BOD/COD	-	0.12	0.23	0.18	-	-
Ammoniacal Nitrogen (NH_4-N)	mg/L	1145	1620	1382.5	221.75	5
Nitrate (NO_3^-)	mg/L	45	80	62.5	14.72	-
Phosphate (PO_4^{3-})	mg/L	88	160	124	31.82	-
Potassium (K)	mg/L	725	909	817	65.71	-
Arsenic (As)	mg/L	0.10	0.32	0.21	0.09	0.05
Iron (Fe)	mg/L	2.83	6.41	4.62	1.52	5.00
Manganese (Mn)	mg/L	0.23	0.28	0.26	0.02	0.20
Nickel (Ni)	mg/L	0.14	0.40	0.27	0.11	0.20
Zinc (Zn)	mg/L	0.21	0.46	0.36	0.11	2.00

*Average reading for the period of leachate sampling between January and March 2013

** Environmental Quality (Control of Pollution from Solid Waste Transfer Station and Landfill) Regulations 2009 (PU (A) 433), Second Schedule (Regulation 13), Acceptable Conditions for Discharge of Leachate

(Control of Pollution from Solid Waste Transfer Station and Landfill) Regulations 2009 (PU (A) 433), Second Schedule (Regulation 13), Acceptable Conditions for Discharge of Leachate wherein the acceptable COD value standard is 400 mg/L. A contributing factor to the high COD level could be attributed to non-biodegradable compounds and inorganic oxidisable compounds [21].

The concentration of ammoniacal-nitrogen is in the range of 1145 to 1620 mg/L. This high concentration of untreated ammonia leads to stimulated algae growth, decreased performance of biological treatment systems, accelerated eutrophication, promoted dissolved oxygen depletion and increased toxicity of living organisms in water bodies [22]. Nitrogen removal is important to control eutrophication and adsorption is an efficient treatment process.

The concentration of nitrate in the leachate from this landfill site was 62.5 mg/L. The nitrate concentration from this study was higher than previous studies published by Aziz *et al.* [23]. Microbial decomposition of organic carbon influenced many processes of the nitrogen cycle. With time, the nitrogen concentration decreased due to microbial utilisation of nitrate compounds and there was denitrification of ammonia gas [19]. The phosphate concentration in this study varied from 88 to 160 mg/L and potassium was 817 mg/L. The phosphate value in this study was consistent with previous studies with a range of 57 to 197 mg/L [22].

Batch Studies for First Stage of Leachate Treatment: Batch studies for the first stage of leachate treatment were started using KOH as a chemical precipitation process and Granular Activated Carbon (GAC) as an adsorption process to remove heavy metals and COD [24]. This treatment used jar test equipment with three types of contact time applied: rapid mixing at 200 rpm for 4 min; slow mixing at 60 rpm for 20 min; and settling time for 30 min. The percentage removal of iron, colour and COD using KOH and GAC were compared to determine the suitable conditions for proceeding to the second stage of leachate treatment using NB and SMB as adsorbents. Fig. 1 shows the percentage removal of colour, iron, COD, turbidity, ammonia, nitrate and phosphate against the pH for KOH. Meanwhile Fig. 2 shows the percentage removal of colour, iron, COD, ammonia, nitrate and phosphate against the GAC dosage.

The initial concentration of raw leachate for colour, iron, COD, ammonia, nitrate and phosphate before treatment with KOH were 8350 Pt-Co, 6.27, 1000, 696.67, 65 and 41.83 mg/L, respectively. Fig. 2 shows the highest percentage removal of colour, iron, COD, nitrate and phosphate were 40.12, 46.12, 10.0, 27.87 and 33.86% at pH 13, respectively. The highest percentage removal of ammonia was 48.72% at pH 11. From the pattern of the graph shown, it can be seen that increasing the pH of the leachate with KOH caused the percentage removal of colour, iron, COD, turbidity, nitrate and phosphate to increase.

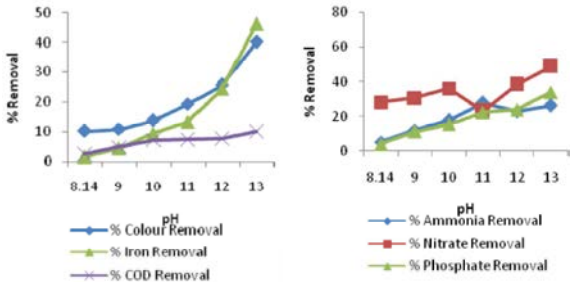

Fig. 1: Percentage removal of colour, iron, COD, turbidity, ammonia, nitrate, and phosphate against dosage for KOH

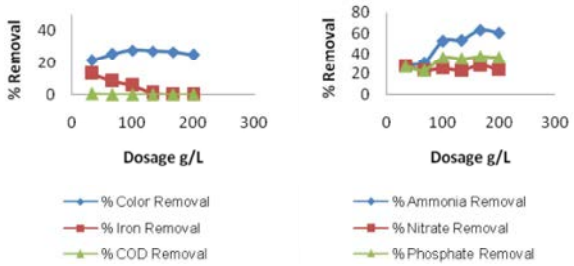

Fig. 2: Percentage removal of colour, iron, COD, ammonia, nitrate, and phosphate for GAC

The initial concentration of raw leachate for colour, iron, COD, turbidity, ammonia, nitrate and phosphate before treatment with GAC were 8350 Pt-Co, 6.12, 1271 mg/L, 187 NTU, 696.67, 65 and 41.83 mg/L, respectively. Fig. 2 shows the highest percentage removal of colour, iron, COD, ammonia, nitrate and phosphate were 28.14, 13.26, 0.66, 63.25, 28.21 and 37.30%, respectively. The graph shows that the percentage removal of colour, iron and COD decreased when the dosage increased. The percentage removal of ammonia, nitrate and phosphate increased when the dosage was increased.

Batch Studies for Second Stage of Leachate Treatment: After comparing the percentage removal of colour, iron, COD and turbidity between landfill leachate treatment with KOH and GAC, it was found that the leachate treatment with KOH was much better than GAC in removing colour, iron, COD and turbidity. Meanwhile, GAC was better for adsorption of ammonia, nitrate and phosphate than KOH. The aims for this study in the first stage of leachate treatment were to remove more colour, iron, COD and turbidity and less adsorption of ammonia, nitrate and phosphate. This was because more adsorption of ammonia, nitrate and phosphate were needed in the leachate treatment with NB and SMB in order to make NB and SMB into a slow release fertiliser product for future application.

Before the second stage of leachate treatment commenced, the leachate was treated with KOH at pH 13 and then the effluent in the leachate was filtered using filtering media to remove suspended solids. After filtering, the leachate was treated using NB and SMB as adsorbents. For these batch studies, there were three factors that were considered: the effect of dosage, pH and contact time (rapid mixing, slow mixing and settling time). The suitable conditions for dosage, pH and contact time were determined in order to compare the adsorption process of ammonia, nitrate and phosphate between NB and SMB.

Effect on Dosage: Fig. 3 shows the percentage removal of colour, iron and COD against dosage using NB and SMB. The dosage was varied from 133.3 to 300 g/L for NB and from 116.7 to 200 g/L for SMB. The leachate sample used in this treatment was 300 mL for both adsorbents. The adjusting pH for these batch studies was pH 8.5 and the pH of the raw leachate averaged pH 8.15. The least chemical reagent was used for adjusting the pH in the leachate treatment as it resulted in a saving in the cost of the reagent. The constant rapid mixing was 200 rpm for 4 min, the slow rapid mixing was 60 rpm for 20 min and the settling time was 30 min.

Fig. 3 also shows the percentage removal of colour, iron and COD increased when the dosage increased. The highest colour removal percentages for NB and SMB were 64.95 and 61.18% at dosage 233.3 and 166.7 g, respectively. The highest percentage removal of iron for NB and SMB were 71.18 and 66.88% at dosage of 266.7 and 166.7 g/L, respectively. The percentage removal of colour and iron, at more than 50%, while the highest percentage removal of COD for NB and SMB were only 35.17 and 18.8% at dosage 166.7 and 183.3 g, respectively. From the results, it can be seen that NB produces a higher percentage removal of colour, iron and COD than SMB. However, in terms of the amount of dosage used to achieve the most suitable conditions, the SMB was considered to be an excellent adsorbent, since it obtains a higher removal of colour, iron, COD and turbidity with a lower adsorbent dosage when compared to NB.

Fig. 4 shows the percentage removal of ammonia, nitrate and phosphate for NB and SMB with an increase in the dosage. The highest percentage removal

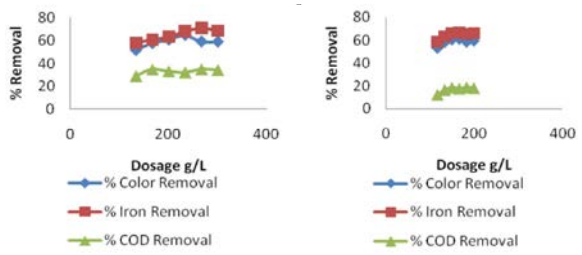

(a) (b)

Fig. 3: Percentage removal of colour, iron, COD, and turbidity against dosage for (a) NB and (b) SMB

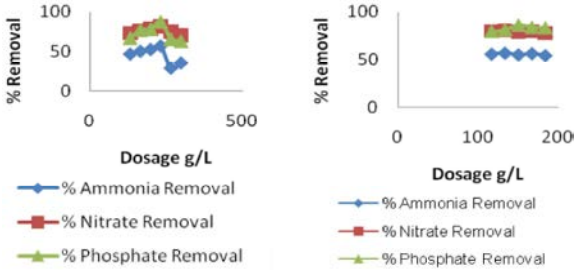

(a) (b)

Fig. 4: Percentage removal of ammonia, nitrate, and phosphate against dosage for (a) NB and (b) SMB

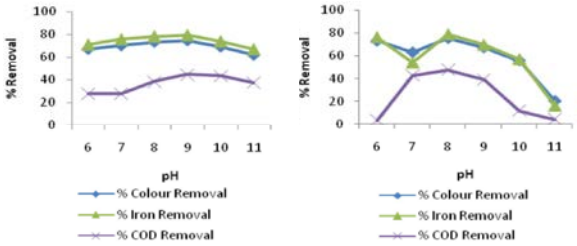

(a) (b)

Fig. 5: Percentage removal of colour, iron, and COD against pH for (a) NB and (b) SMB

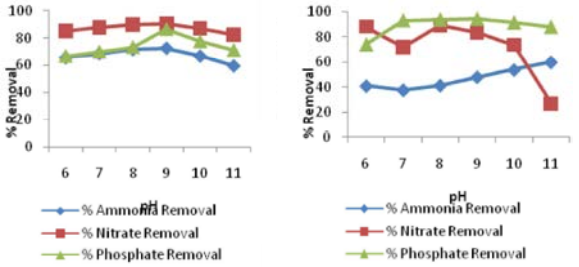

(a) (b)

Fig. 6: Percentage removal of ammonia, nitrate, and phosphate against pH for (a) NB and (b) SMB

2of ammonia, nitrate and phosphate for NB was 57.1, 88 and 81.66% at dosage 233.3 g/L, respectively. The highest percentage removal of ammonia, nitrate and phosphate for SMB was 56.88, 79.98 and 86.47% at dosage 133.3, 166.7 and 150 g/L, respectively. SMB has a higher percentage removal for phosphate than NB. Meanwhile for ammonia and nitrate, NB has a higher percentage removal than SMB.

SMB can be excellent adsorbents in terms of adsorption of ammonia, nitrate and phosphate since it can adsorb at a lower dosage when compared to NB. The SMB, as an adsorbent for ammonia, nitrate and phosphate in this study, can be used for future application as a slow release fertiliser for plants, since they need nitrogen, phosphorous and potassium for growth. After considering all the parameters in terms of removal, the suitable dosages were 233.3 and 166.7 g/L for NB and SMB, respectively. For the effect of dosage, the general patterns of colour, iron, COD, turbidity, ammonia, nitrate and phosphate removal were consistent and increased with larger dosages. However, an exception was the removal of COD by NB and ammonia by SMB, which both decreased rapidly and fluctuated when the dosages were increasing.

Effect on pH: Fig. 5 shows the percentage removal of colour, iron, COD and turbidity against pH for NB and SMB. The pH was varied from pH 6 to pH 11. The suitable dosages of 233.3 and 166.7 g were applied for NB and SMB, respectively. The contact time applied in this treatment was the same as in the previous experiment on the effect on dosage.

Fig. 5 shows the highest percentage removal of colour, iron and COD for NB were 75.05, 79.4 and 44.85%, at pH 9, respectively. Meanwhile for SMB, the highest percentage removal of colour, iron and COD were 75.44, 78.85 and 47.61% at pH 8, respectively. The percentage removal of colour and iron for SMB fluctuated at pH 7 and decreased rapidly at a higher pH. Meanwhile, the graph of NB was smooth and the percentage removal of colour, iron and COD increased slowly and was higher than for SMB.

Fig. 6 shows the percentage removal of ammonia, nitrate and phosphate for NB and SMB with an increased pH. The highest percentage removal of ammonia, nitrate and phosphate for NB was 72.71, 90.6 and 86.67% at pH 9, respectively. The highest percentage removal of ammonia, nitrate and phosphate for SMB was 59.97, 89.58 and 94.25% at pH 11, 8 and 9, respectively.

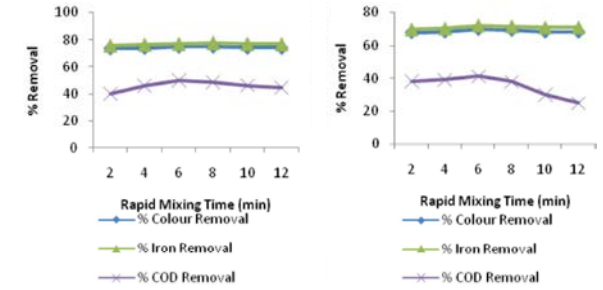

(a) (b)

Fig. 7: Percentage removal of colour, iron, COD, and turbidity against rapid mixing time for (a) NB and (b) SMB

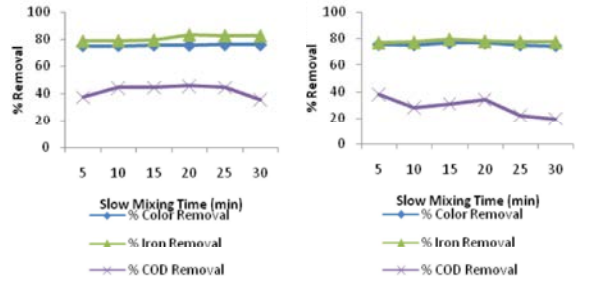

(a) (b)

Fig. 9: Percentage removal of colour, iron, and COD against slow mixing time for (a) NB and (b) SMB

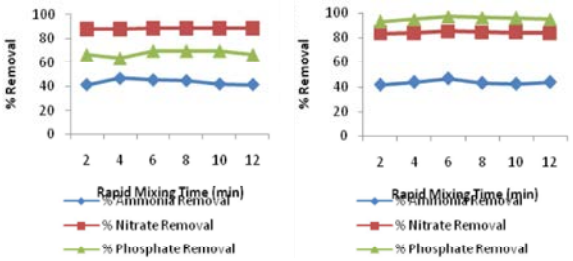

(a) (b)

Fig. 8: Percentage removal of ammonia, nitrate, and phosphate against rapid mixing time for (a) NB and (b) SMB

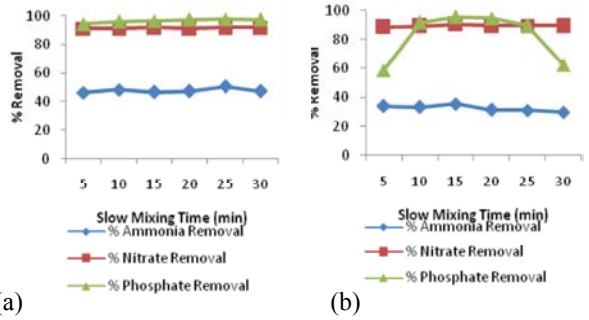

(a) (b)

Fig. 10: Percentage removal of ammonia, nitrate, and phosphate against slow mixing time for (a) NB and (b) SMB

In comparing NB and SMB, NB is better than SMB in adsorption of ammonia and nitrate. Meanwhile SMB is better than NB in adsorption of phosphate. The pH value needed for plant growth is in the range of 6-9. Therefore, NB and SMB are able to be used as a slow release fertiliser since they can supply the nutrients plants need, which are nitrogen, phosphorus and potassium. The suitable pH for NB and SMB were 8 and 9, respectively after considering all the parameter removals.

Effect on Contact Time

Rapid Mixing Time: Figures 7 and 8 show the percentage removal of colour, iron, COD, ammonia, nitrate and phosphate at the rapid mixing time for NB and SMB. The ranges of rapid mixing time were 2 to 12 min at 200 rpm. The adsorbent dosage and pH were adjusted to their suitable condition determined previously, where the dosage and pH applied for NB in rapid mixing was 233.3 g/L at pH 9. However, for SMB the dosage and pH applied was 166.7 g/L at pH 8. Figures 7 and 8 show the percentage removal increased as time increased, but with little difference. The highest percentage removal of colour, iron and COD for NB was 75.21, 77.67 and 50.09% and for SMB was 69.68, 72.15 and 41.21%, respectively. The highest percentage removal of ammonia, nitrate and phosphate for NB was 46.75, 88.49 and 69.67% and for SMB was 46.5, 85.07 and 96.91%, respectively.

Slow Mixing Time: Figures 9 and 10 show the percentage removal of colour, iron, COD, turbidity, ammonia, nitrate and phosphate at the slow mixing time for NB and SMB. The range of slow mixing time was between 5 and 35 min at 60 rpm. The adsorbent dosage, pH and slow mixing times were adjusted to their suitable condition determined previously, where the dosage, pH and slow mixing time for NB was 70g, pH 9 and 8 min, respectively. For SMB, the suitable dosage, pH and slow mixing time were 50 g at pH 8 and 6 min.

Based on Figures 9 and 10, the percentage removal increased as time increased but there was little difference in the percentage removal between the intervals of slow and rapid mixing times. The highest percentage removal of colour, iron and COD for NB was 75.97, 83.44 and 45.66% and for SMB were 76.73, 79.56 and 33.81%, respectively.

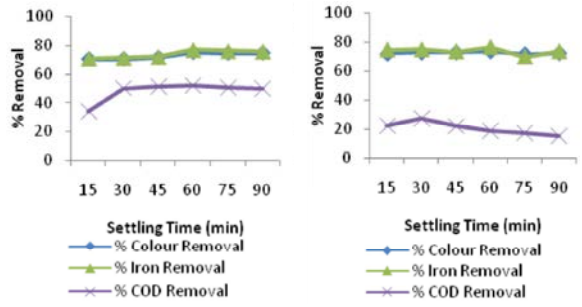

(a) (b)

Fig. 11: Percentage removal of colour, iron, and COD against slow settling time for (a) NB and (b) SMB

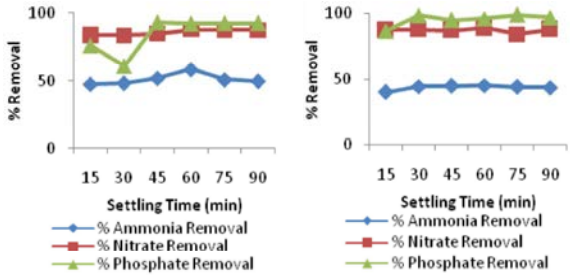

(a) (b)

Fig. 12: Percentage removal of ammonia, nitrate, and phosphate against settling time for (a) NB and (b) SMB

The highest percentage removal of ammonia, nitrate and phosphate for NB was 50.67, 97.49 and 91.77% and for SMB it was 35.6, 95.69 and 90.52%, respectively.

Settling Time: Figures 11 and 12 show the percentage removal of colour, iron, COD, turbidity, ammonia, nitrate and phosphate against settling time for NB and SMB. The range of settling time was from 15 to 90 min. The adsorbent dosage, pH, rapid mixing time and slow mixing time were adjusted to their suitable condition determined previously. For NB the suitable dosage, pH, rapid mixing time and slow mixing time applied in settling time were 233.3 g/L, pH 9, 8 min and 25 min, respectively. For SMB the suitable dosage, pH, rapid mixing time and slow mixing time were 50 g, pH at 8 for 6 and 15 min, respectively.

Based on Figures 11 and 12, the percentage removal increased as time increased with little difference of percentage removal between settling time in rapid and slow mixing times. The highest percentage removal of colour, iron and COD for NB was 74.92, 76.87 and 51.8% and for SMB was 73.96, 76.53 and 27.49%, respectively. Meanwhile, the highest percentage removal of ammonia, nitrate and phosphate for NB was 58.65, 88.04 and 93.37% and for SMB was 45.16, 88.85 and 98.71%, respectively. For the effect of contact time, we can conclude that it has less influence on all parameters for removal. For the effect on dosage and pH, it has considerable influence on all parameters for removal, since the percentage removal for variation of dosage and pH were higher than the effect on contact time.

Analysis of Scanning Electron Microscopy (SEM) and Energy Dispersive X-ray (EDX): In this study, samples of NB and SMB before and after treatment were analysed ted using SEM and EDX. The SEM analysis defined the morphology of shape and structure of NB and SMB while the EDX analysis defined their chemical compositions. SEM-EDX analyses are conducted in order to show the different elements contained in NB and SMB before and after treatment. These analyses were performed on clean surfaces to avoid any contamination.

Fig. 13 shows the surface of NB before treatment (x 10000, SEM) and is approximately 14 µm in size. The result of the SEM analysis shows that the shape of NB before treatment has a smooth surface and coating. The biggest constituent elements in NB before treatment were silicon and oxygen, with an average of 43.27 and 31.45% by weight. Meanwhile, other element content such as carbon, aluminium and magnesium in NB in terms of percentage by weight are shown in Table 2.

Fig. 14 shows the surface of NB after treatment (x 5000, SEM) and is approximately 20 µm in size. The shape of NB after treatment is rough. This is because of the increase of ions in the adsorption process and pollutant ions from the leachate are attached to the raw NB morphology structure. The biggest constituent elements in NB after treatment are silicon and oxygen and these are 44.98 and 33.65%, respectively (Table 3). The elements in NB after treatment are increased, with the presence of nitrogen, phosphorus and potassium. This indicates that the process of adsorption has occurred in the leachate treatment using NB.

Fig. 15 shows the surface of SMB before treatment (x 5000, SEM) and is approximately 22 µm in size. The SEM micrographs and the shape of SMB before treatment is different to the raw NB. The surface of the raw NB was disturbed by the added surfactant. The anionic and cationic surfactant has changed the shape of the raw NB. The greatest constituent elements in SMB before

Table 2: Elements in NB before treatment

Element	Wt %	At %
Carbon (C)	16.6	24.49
Oxygen (O)	31.45	37.67
Magnesium (Mg)	2.02	1.60
Aluminium (Al)	6.65	4.73
Silicon (Si)	43.27	29.52

Table 3: Elements in NB after treatment

Element	Wt %	At %
Carbon (C)	2.9	5.24
Nitrogen (N)	1.04	1.61
Oxygen (O)	33.65	45.60
Magnesium (Mg)	2.59	2.31
Aluminium (Al)	8.39	6.74
Silicon (Si)	44.98	34.73
Phosphorus (P)	1.32	0.92
Potassium (K)	5.13	2.84

Table 4: Elements in SMB before treatment

Element	Wt %	At %
Carbon (C)	4.79	8.53
Oxygen (O)	31.80	42.52
Magnesium (Mg)	2.61	2.30
Aluminium (Al)	11.22	8.89
Silicon (Si)	49.58	37.76

Table 5: Elements in SMB after treatment

Element	Wt %	At %
Carbon (C)	6.06	10.73
Nitrogen (N)	1.30	1.98
Oxygen (O)	31.71	42.13
Magnesium (Mg)	3.04	2.66
Aluminium (Al)	9.70	7.64
Silicon (Si)	39.11	29.60
Phosphorus (P)	2.25	1.54
Potassium (K)	6.82	3.71

treatment were silicon and oxygen with an average of 49.58 and 31.80%. Other elements such as carbon, oxygen and magnesiumin SMB in terms of percentage by weight are shown in Table 4.

Fig. 16 shows the surface of SMB after treatment (x 5000, SEM) and is approximately 20 µm in size. The shape of SMB after treatment is like NB after treatment. The biggest constituent elements in SMB after treatment are silicon and oxygen with a value of 39.11 and 31.71%, respectively (Table 5). The elements in SMB after treatment are also increased, with the presence of nitrogen, phosphorus and potassium. This shows that the process of adsorption of ammonia, nitrate, phosphate and potassium in leachate treatment using SMB had occurred, similar to NB. Nevertheless, percentage weight of elements nitrogen, phosphorus and potassium in SMB

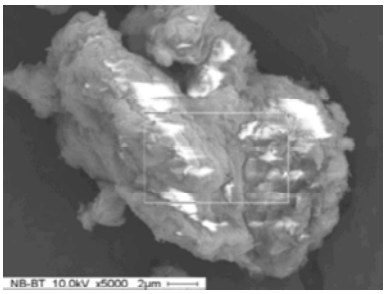

Fig. 13: SEM analysis for NB before treatment

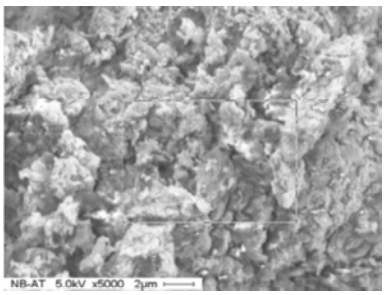

Fig. 14: SEM analysis for NB after treatment

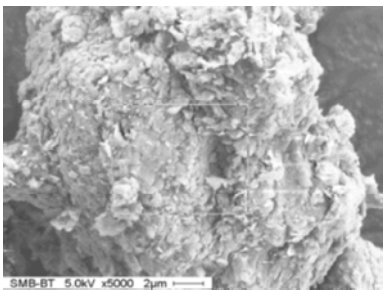

Fig. 15: SEM analysis for SMB before treatment

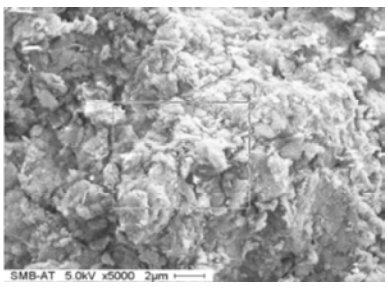

Fig. 16: SEM analysis for SMB after treatment

after treatment was greater than in NB with 1.30, 2.25 and 6.81%, respectively (Table 5). By comparison, in NB they were 1.04, 1.32 and 5.13%, respectively (Table 3).

CONCLUSION

From this study, in the first stage of leachate treatment by using KOH to remove the heavy metals and COD from raw leachate were achieved. The initial

concentrations in raw leachate of colour, iron, COD, ammonia, nitrate and phosphate were 8350 Pt-Co, 6.27, 1000, 696.67, 65 and 41.83 mg/L, respectively. Meanwhile, the highest percentage removal of colour, iron, COD, nitrate and phosphate were 40.12, 46.12, 10.0, 27.87 and 33.86% at pH 13, respectively. The highest percentage removal of ammonia was 48.72% at pH 11. In the second stage was achieved by subjecting the KOH treated leachate to NB and SMB, which were used as adsorbents. After considering all the percentage removal parameters for NB, the suitable condition for dosage, pH and contact time of adsorption for ammoniacal nitrogen (NH_4-N), phosphate (PO_4^{3-}) and nitrate (NO_3^-) were at dosage 233.3 g/L, pH 9, 8 min (rapid mixing time), 25 min (slow mixing time) and 60 min (settling time). Meanwhile, for SMB they were at dosage 166.7 g/L, pH 8, 6 min (rapid mixing time), 15 min (slow mixing time) and 30 min (settling time). From SEM-EDX analysis, NB and SMB were an increase in elements (nitrogen, phosphorus and potassium) after pollutants leachate adsorption. The percentage weight of these elements in SMB were 1.3, 2.25 and 6.81% while for NB were 1.04, 1.32 and 5.13%, respectively.

ACKNOWLEDGEMENTS

This research was undertaken at the Environmental Laboratory, School of Civil Engineering, USM.

REFERENCES

1. Ghafari, S., H.A. Aziz, and M.H. Isa, 2005. Coagulation process for semi-aerobic leachate treatment using poly-aluminum chloride. AEESEAP International Conference 2005, University of Malaya, June 2005, Kuala Lumpur, Malaysia, pp: 1-6.
2. Ghafari, S., H.A. Aziz, M.H. Isa and A.A. Zinatizadeh, 2009. Application of response surface methodology (RSM) to optimize coagulation-flocculation treatment of leachate using poly-aluminum chloride (PAC) and alum. Journal of Hazardous Materials, 163: 650-656.
3. Hamzeh, A.J., H.M. Amir, N. Ramin, V. Foorogh and A.O. Ghasem, 2009. Combination of Coagulation-Flocculation and Ozonation Processes for Treatment of Partially Stabilized Landfill Leachate of Tehran. World Applied Sciences Journal, 5: (Special Issue for Environment), 9-15.
4. Rui, L.M., Z. Daud, and A.A.A. Latif, 2012. Coagulation-Flocculation In Leachate Treatment By Using Micro Zeolite. International Journal of Engineering Research and Application (IJERA), 2: 218-226.
5. Aziz, S.Q., H.A. Aziz, M.S. Yusoff and M.J. K. Bashir, 2011a. Landfill leachate treatment using powdered activated carbon augmented sequencing batch reactor (SBR) process: Optimization by response surface methodology. Journal of Hazardous Materials, 189: 404-413.
6. Nguyen Manh Khai and Hoang Thi Quynh Trang, 2012. Chemical Precipitation of Ammonia and Phosphate from Nam Son Landfill Leachate, Hanoi. Iranica Journal of Energy and Environment, 3(5): 32-36. ISSN 2079-2115
7. Vymazal, J., 2008. Wastewater Treatment, Plant Dynamics and Management in Constructed and Natural Wetlands, Springer. Institute of Systems Biology and Ecology, Czech Academy of Sciences, Tøeboò, Czech Republic, pp: 1-27.
8. Sri Darwati 2012. Sustainable Approach for Landfill Management at Final Processing Site Cikundul in Sukabumi City, Indonesia. Iranica Journal of Energy and Environment, 3(5): 79-84. ISSN 2079-2115.
9. Sandy, Maramis, V., A. Kurniawan, A. Ayucitra, J. Sunarso and S. Ismadji, 2012. Removal of copper ions from aqueous solution by adsorption using Laboratories-modified bentonite (organo-bentonite). 6(1): 58-66.
10. Wang, S. and Y. Peng, 2010. Natural zeolites as effective adsorbents in water and wastewater treatment. Chemical Engineering Journal, 156: 11-24.
11. Amer Sultan, I., 1998. Treating Metal Finishing Wastewater. Aquachem Inc. ● 4501 Cartwright Rd.Unit 605 ● Missouri City, pp: 1-7.
12. Zainol, N.A., H.A. Aziz and M.S. Yusoff, 2012. Characterization of Leachate from Kuala Sepetang and Kulim Landfills: A Comparative Study. Energy and Environment Research, 2(2): 45-52.
13. Zawawi, M.H., I. Syafalni Abustan and M.A.A. Nazri, 2012. Assessment of Hydrochemical and Isotopic Characteristics at Matang Landfill Site Using Multivariate Analysis. Procedia Engineering, 50: 333-342.
14. Wang, Y., S. Liu, Z. Xu, T. Han, S. Chuan and T. Zhu, 2006. Ammonia removal from leachate solution using natural Chinese clinoptilolite. Journal of Hazardous Materials, 136: 735-740.
15. Syafalni, Rohana Abdullah and P.S. Ushaa Nair, 2013. New Approach of Heavy Metal (Chromium, Iron, Copper and Nickel) Removal using Surfactant Modified Zeolite for Tin Mining Wastewater. World Applied Sciences Journal, 27(5): 614-620.

16. Eaton, A.D. and M.A.H. Franson, 2005. Standard methods for the examination of water and wastewater, American Public Health Association, p. S-1 to S-16, ISBN 087553047897808755304 75
17. Poznyak, T., G.L. Bautista, I. Chaírez, R.I. Córdova, and L.E. Ríos, 2008. Decomposition of toxic pollutants in landfill leachate by ozone after coagulation treatment. Journal of Hazardous Materials, 152: 1108-1114.
18. Kulikowska, D. and E. Klimiuk, 2008. The effect of landfill age on municipal leachate composition. Bioresource Technology, 99: 5981-5985.
19. Bhalla, B., M. Saini and M. Jha, 2012. Characterization of Leachate from Municipal Solid Waste (MSW) Landfilling Sites of Ludhiana, India: A Comparative Study. International Journal of Engineering Research and Applications (IJERA) 2: 732-745.
20. Aziz, H.A., S. Alias, M.N. Adlan Faridah, A.H. Asaari, and M.S. Zahari, 2007. Colour removal from landfill leachate by coagulation and flocculation processes. Bioresource Technology, 98: 218-220.
21. Moreno-Casillas, H.A., D.L. Cocke, J.A. Gomes, P. Morkovsky, J. Parga and E. Peterson, 2007. Electrocoagulation mechanism for COD removal. Separation and Purification Technology, 56: 204-211.
22. Aziz, S.Q., H.A. Aziz, M.S. Yusoff, M.J.K. Bashir and M. Umar, 2010. Leachate characterization in semi-aerobic and anaerobic sanitary landfills: A comparative study. Journal of Environmental Management, 91: 2608-2614.
23. Aziz, H.A., T.J. Ling, A.A.M. Haque, M. Umar and M.N. Adlan, 2011c. Leachate treatment by swim-bed bio fringe technology. Desalination, 276: 278-286.
24. Gaikwad, R.W., 2012. Removal of Lead by Reverse Fluidazation Using Granular Activated Carbon. Iranica Journal of Energy and Environment, 3(4): 314-319.

Persian Abstract

DOI: 10.5829/idosi.ijee.2014.05.03.05

چکیده

جذب آلاینده های شیرابه با استفاده از هیدروکسید پتاسیم (KOH) و سورفاکتانت بنتونیت اصلاح شده (SMB) به عنوان یک روش جدید برای عملیلات تصفیه شیرابه استفاده شده است. هیدروکسید پتاسیم به عنوان جاذب جهت حذف فلزات سنگین استفاده شده و همچنین بنتونیت طبیعی و سورفکتانت بنتونیت اصلاح شده جهت جذب نیتروژن آمونیاکی، نیترات و فسفات استفاده شده است. شرایط مناسب برای جاذب با استفاده از درصد حذف کلر، آهن، COD، نیتروژن آمونیاکی، نیترات و فسفات بدست آمده اند. نتایج بدست آمده در شرایط بهینه برای مقدار بنتونیت طبیعی برابر ۲۳۳/۳ گرم بر لیتر و pH برابر با ۹ می باشند. در مقابل، این مقادیر برای سورفکتانت بنتونیت اصلاح شده برابر ۱۶۶/۷ گرم بر لیتر و pH برابر با ۸ می باشند. در مورد زمان تماس با استفاده از اختلاط آهسته و تند، سورفکتانت بنتونیت اصلاح شده نسبت به بنتونیت طبیعی بهتر عمل کرده است. با استفاده از نتایج آنالیز SEM-EDX درصد وزنی، عناصر نیتروژن، فسفرو پتاسیم برای بنتونیت طبیعی به ترتیب برابر ۱/۰۴ ، ۱/۳۲ و ۵/۱۳ ٪ و برای سورفکتانت بنتونیت اصلاح شده به ترتیب برابر ۱/۳۰ ، ۲/۲۵ و ۶/۸۱ ٪ به دست آمده اند. نتایج نشان می دهند که سورفکتانت بنتونیت اصلاح شده نسبت به بنتونیت طبیعی، جذب بهتری نشان داده و می تواند در آینده به عنوان آزاد کننده آهسته کود شیمیایی برای نباتات به کار گرفته شود.

Iranica Journal of Energy & Environment 5 (3): 270-276, 2014
ISSN 2079-2115
IJEE an Official Peer Reviewed Journal of Babol Noshirvani University of Technology
DOI: 10.5829/idosi.ijee.2014.05.03.06

BUT

Raschig Rings Versus PVC as a Packed Tower Media in Scrubbing Ammonia from Air

[1]Mohammad Javad Jafari, [1]Leila Omidi, [1]Mansour Rezazadeh Azari,
[2]Mohammad Reza Massoudi Nejad and [3]Mahshid Namdari

[1]Department of Occupational Health,
School of Public Health, Shahid Beheshti University of Medical Sciences, Tehran, Iran
[2]Department of Environmental Health,
School of Public Health, Shahid Beheshti University of Medical Sciences, Tehran, Iran
[3]Department of Biostatic,
School of Paramedical Science, Shahid Beheshti University of Medical Sciences, Tehran, Iran

Date of Received: June 30, 2014; Date of Accepted in Revised Form: August 6, 2014

Abstract: The selection of the packing media is concerned when ammonia is going to be scrubbed through a packed tower. In this study, a packed tower with two types of packing including raschig rings and PVC were used to remove the ammonia gas from air stream. Three gas flow rates as well as three ammonia concentrations and three pH of scrubbing liquid were applied. The level of ammonia at the inlet and out let of the packed tower was measured through a direct reading device. The removal efficiency of column significantly increased in both modes, packed with raschig rings and PVC ($p<0.001$) as the inlet concentration of ammonia gas was increased. With decreasing pH of scrubbing liquid from 7 to 5, the removal efficiency of the tower packed with raschig rings significantly increased ($p< 0.01$). The head loss across the bed was significantly increased ($p< 0.001$) as air flow rate increased from 5 to 10 and 10 to 15 l/s. The head loss across the bed was also higher when column was packed with raschig rings rather than packed with PVC. The lower ammonia removal efficiency of PVC rings could be ignored considering their other advantages such as light weight, low headlosses, low initial and operating costs.

Key words: Raschig rings · PVC · Packed tower · Ammonia removal · Efficiency · pH

INTRODUCTION

Ammonia (NH_3) is a colorless gas with a sharp odor. It is soluble in water and very irritant gas. Exposure to ammonia gas can cause skin and eye irritations. Long term exposure to ammonia may cause lung injuries. Ammonia may be absorbed through skin rapidly because of its' high water solubility. Ammonia reacts with water leading to a highly irritant and caustic hydroxide [1]. Ammonia is an explosive gas when mixed with air in appropriate reaction rate. Explosion is the main risk dealt with ammonia gas [2]. The Environmental Protection Agency (EPA) classified ammonia in National Priorities List (NPL). EPA stated that the source of human exposure to ammonia may increase in future and evaluation program is needed to identify the source of exposure [3].

Ammonia can be removed from polluted air by several methods. The most common methods include biofiltration, condensation or distillation method, adsorption and gas scrubbing (absorption) method [4]. Absorption is a mass-transfer operation in which pollutant transfers from gas into liquid phase. That is, concentration is varying between gas and liquid phase [5].

Water is the most widely used liquid to clean polluted air in wet scrubbers [6]. In spite of very high water soluble quality of ammonia gas, scrubbing by water

Corresponding Author: Leila Omidi, Department of Occupational Health, School of Public Health, Shahid Beheshti University of Medical Sciences, Tehran, Iran.
Tel: +98 (21) 88951390, Fax: +98 (21) 88954781.

Please cite this article as: Mohammad Javad Jafari, Leila Omidi, Mansour Rezazadeh Azari, Mohammad Reza Massoudi Nejad and Mahshid Namdari 2014. Raschig Rings Versus PVC as a Packed Tower Media in Scrubbing Ammonia from Air. Iranica Journal of Energy and Environment, 5 (3): 270-276

depends on physical absorption [7]. It is the case that acidic solution such as sulfuric acid (H_2SO_4) and the like has been known as scrubbing liquids for ammonia gas. These put forward the further benefit of chemical absorption [7]. Sulfuric acid was added to the scrubbing liquid in the present study expecting the following results when it is contacted with ammonia in the tower [8].

$$2NH_3 + H_2SO_4 \rightarrow (NH_4)_2SO_4 \quad (1)$$

Ammonium sulfate ($(NH_4)_2SO_4$) formed in this reaction is soluble in water and it could be easily removed by the blow down [7]. Packed columns provide continuous contact between the scrubbing liquid and the polluted gas. The countercurrent packed column is the most widely used device in air pollution control techniques. This type of column is commonly used in the chemical and pollution control industries [9]. Erosion and corrosion are the major drawbacks in wet scrubbers [10]. Packing is the mass transfer unit. It is important to ensure from appropriate operation of mass transfer media. Selection of packing material should be accurate in features such as in stability, resistance to corrosion and efficiency. The basic requirement for choosing the packing material is the ability to carry out the required gas and liquid flow rates. Besides, it needs to be affordable [11]. Ceramic packed beds with various porosities are usually used in the chemical and petrochemical industries. Ceramic tower packing is very efficient in contact with a number of scrubbing liquid [12]. The existing accounts showed that the ceramic packing material can be used in the corrosive atmosphere.

PVC packing is cheaper than metal and ceramic packing materials [13]. In compare to ceramic raschig rings, PVC is often preferred because of its light weight and great resistance to breakage. Its low resistance to high temperatures is the major drawback of PVC. The maximum operating temperature of PVC is 150 °F (66°C) [14]. The main objective of this paper was to compare the removal efficiency of ammonia gas from contaminated air using two kinds of packing material including ceramic raschig rings and PVC in a packed column.

MATERIAL AND METHODS

General Description of Experiment: A counter flow packed column in laboratory scale with 20 cm diameter was used to remove ammonia gas from contaminated air.

Table 1: Characteristics of studied packed column

parameter	value
Column diameter (m)	0.20
Column height (m)	1.80
Packing depth (m)	0.30
Size of packing materials (in)	0.25 , 0.44
Air flow rate (l/s)	5, 10, 15
Gas mass flow rate (lb/ft² hr)	140.88, 281.77, 422.66
Gas temperature (?C)	25
Injected ammonia gas (ppm)	25±3, 42±3, 57±3
Liquid flow rate (l/min)	0.21, 0.43, 0.64
Liquid mass flow rate (lb/ft² hr)	84.13, 168.27,252.41

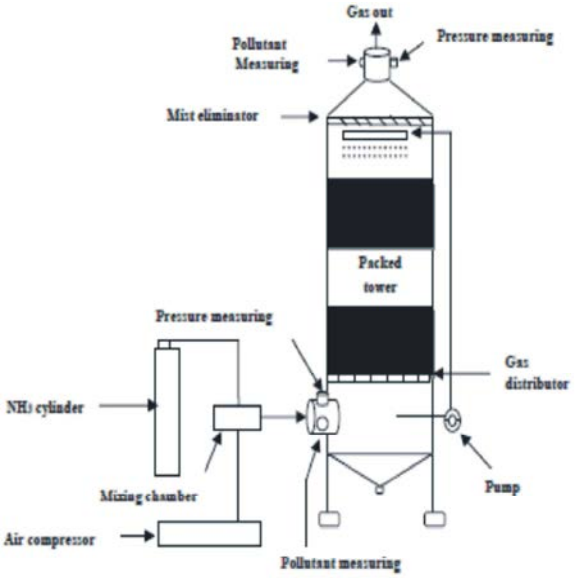

Fig 1: Packed column with auxiliary equipment

The column was randomly packed in 30 cm depth with 0.25 inch ceramic raschig rings and 0.44 inch PVC rings. Ammonia laden air was injected into the column at three air flow rates including 5, 10 and 15 l/s. Ammonia gas was applied to the column in three concentration ranges including 25±3, 42±3 and 57±3 ppm. A caustic scrubbing liquid at three pH including 5, 6 and 7 were used to scrub the polluted gas. Ammonia gas was measured with a direct reading instrument. Ammonia direct reading sensor used to measure ammonia gas in contaminated air [15]. All measuring instrumentation was calibrated prior to their use. The tower was operated at atmospheric pressure and room temperature. The results were analyzed by SPSS version 16 software package. Multi-way ANOVA test was used to analyze the data. Tukey's test was applied for multiple comparisons between variables. Table 1 shows the characteristics of packed column used in this study. Fig. 1 shows the packed column with auxiliary equipment.

Air Flow Rate and Pressure Drop: Required air flow rate for experiments were 5, 10 and 15 l/s. These air flow rates were supplied by a variable flow rate fan model HVDLT-MK2[1], UK air flow Company. A venture meter (G type) was used to measure air flow rate. The accuracy of venture was ± 5%. A monometer- Type 504 manufactured by UK air flow Company was used to measure the pressure losses. The measurement range of manometer was 0-5000 pa with an accuracy of ±10 pa.

Scrubbing Liquid Flow Rate and pH: The scrubbing liquid was free from ammonia at the beginning but it was recirculated by a pump with a maximum capacity of 6 l/min. The optimum volume of injected liquid was based on the exhaust gas flow rate defined in literature [16, 17]. The liquid-to-gas mass flow ratio $(L/G)_m$ was 0.6 based on ACGIH recommendations which is in the range of 0.6 to 1.2 for packed columns [18]. The pH values of scrubbing liquid were controlled by applying sulfuric acid and monitored with a pH meter. A Sartorius Basic Meter PB-11 with an accuracy of ±0.01 was used to measure the pH of scrubbing liquid.

Ammonia Supply and Measurement: A 45 kg gas cylinder was used to supply ammonia gas supply. Ammonia was blended with air prior to its injection to the packed tower. Ammonia concentration was measured through a direct reading using Crowcon Gasman single gas detector at the inlet and outlet of the column. This instrument had a measuring range of 0-100 ppm and detecting accuracy of ±1 ppm. All measuring instrumentations were calibrated prior to their application.

Ammonia removal efficiency (% eff.) was calculated based on given Eq. 2. The results were then averaged and reported [8].

$$\%\ Ammonia\ Eff.=\frac{InletConc.-OutletConc.}{InletConc.}\times 100 \quad (2)$$

RESULTS AND DISCUSSION

Air Flow Rate versus Removal Efficiency: Three air flow rates including 5, 10 and 15 l/s were introduced to the tower packed with ceramic raschig rings as well as PVC while other parameters were kept constant. The results of 162 experiments showed that the column packed with raschig rings had higher removal efficiency in all air flow rates than the column packed with PVC (Table 2).

In air flow rates variation, the results showed that the tower packed with ceramic raschig rings has higher ammonia removal efficiency than PVC rings. Higher gas flow rates leads to higher turbulent flow, introducing higher energy to the gas which consequently leads to higher removal efficiencies [18]. In present study, increasing the air flow rate from 5 to 10 l/s decreased the removal efficiency of ammonia gas in a tower packed with both packing materials but such decreases was not significant. These results are not consistent with results reported by Jafari *et al.* [16]. They used this packed column to remove sulfuric acid mist by scrubbing with caustic solution. Their results showed that increasing the air flow rate increased the removal efficiency of sulfuric acid mists. It seems that since the volume of the column was constant, an increase in air flow rate resulted in lower retention time [19] and decreases the removal efficiency of ammonia gas in the column. The retention time plays an important role in the absorption of pollutant into scrubbing solution [20]. However, in studied tower packed with both packing materials, by increasing the air flow rate from 10 to 15 l/s, the removal efficiency of ammonia gas was increased although the quantity was not significant.

Inlet Ammonia Concentration Versus Removal Efficiency: Three ranges of ammonia concentration including 25±3, 42±3 and 57±3 ppm were applied to investigate the influences of input concentration on

Table 2: Removal efficiency at different air flow rates

				Removal efficiency (%)		
Q_{air} (l/s)	V (m/s)	Type of packing	Test NO.	Ave± std	Min	Max
5	0.16	Raschig rings	27	95.38± 2.14	91.09	98.15
		PVC	27	92.43± 3.91	86.09	96.91
10	0.32	Raschig rings	27	92.24± 3.22	88.37	98.48
		PVC	27	92.11± 4.63	83.91	96.73
15	0.48	Raschig rings	27	94.35± 3.72	88.37	98.99
		PVC	27	93.80± 2.65	88.26	97.30

[1]High velocity ductwork leakage tester MK2

Table 3: Removal efficiency at different input ammonia concentration

C_{in} (ppm)	Type of packing	Test NO.	Removal efficiency (%) Ave± std
25±3	Raschig rings	27	91.09± 1.98
	PVC	27	87.93± 1.42
42±3	Raschig rings	27	95.73± 1.01
	PVC	27	94.27± 2.34
57±3	Raschig rings	27	97.23± 1.12
	PVC	27	96.11± 0.72

Table 4. Removal efficiency at different pH of scrubbing liquid

pH	Packingtype	Test NO.	Removal efficiency (%) Ave± std	Min	Max
5	Raschig rings	27	96.23± 2.55	91.89	98.99
	PVC	27	93.78± 3.64	86.96	97.09
6	Raschig rings	27	94.44± 2.8	89.53	97.3
	PVC	27	93± 3.6	86.09	96.36
7	Raschig rings	27	93.38± 3.08	87.98	96.29
	PVC	27	91.54± 4.07	83.91	95.82

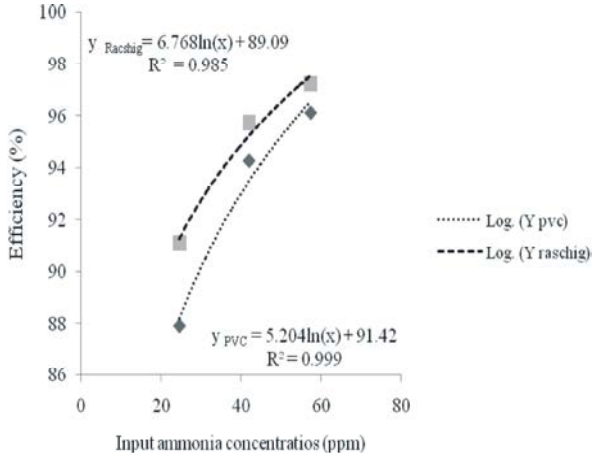

Fig 2: Removal efficiency versus input concentration

removal efficiency. The results revealed that the removal efficiency of column packed with ceramic raschig rings was higher than it when packed with PVC rings. The result of Tukey post-hoc test showed that with increases in the input concentration of ammonia gas, average removal efficiency in both media significantly increased (P-value <0.001). Table 3 shows the influences of inlet concentration of ammonia gas on packed tower removal efficiency. Fig. 2 shows the trend of ammonia removal efficiency of the tower at different ammonia input concentrations while packed with ceramic and PVC rings.

According to the results, increasing inlet ammonia concentration can increase tower removal efficiency. This is mainly because of high concentration of ammonia leads to a high driving force between gas and liquid phase which consequently increases the removal efficiency. A positive significant relationship (P-value<0.001) was observed between inlet ammonia concentration and the removal efficiency when using both packing materials. In a tower packed with ceramic raschig rings, increasing inlet ammonia concentration from 25±3 to 42±3 then to 57±3 the removal efficiency increased by 5.09% and 1.55% respectively. In similar situations for PVC packing materials, an increase in inlet concentration from 25±3 to 42±3 and then to 57±3 ppm, the removal efficiency increased by 7.9 and 1.94%, respectively.

The Scrubbing Liquid pH Versus Removal Efficiency: Sulfuric acid was added to water to have a caustic scrubbing liquid for better removal efficiencies. Three pH of scrubbing liquid including 5, 6 and 7 was used to scrub the ammonia gas. Table 4 shows the effect of pH of scrubbing liquid on removal efficiency of ammonia by the tower packed with ceramic raschig rings and PVC rings. Fig. 3 shows the trend of ammonia removal efficiency at different pH of scrubbing liquid in similar cases.

The result of Tukey post-hoc test showed that the removal efficiency of column packed with raschig rings significantly increased (P< 0. 01) as the pH of scrubbing liquid was reduced from 7 to 5. With decreasing the pH of scrubbing liquid from 7 to 5 in column packed with PVC, its removal efficiency increased but not significant quantities (P = 0.081). The trend is almost the same for both packing material.

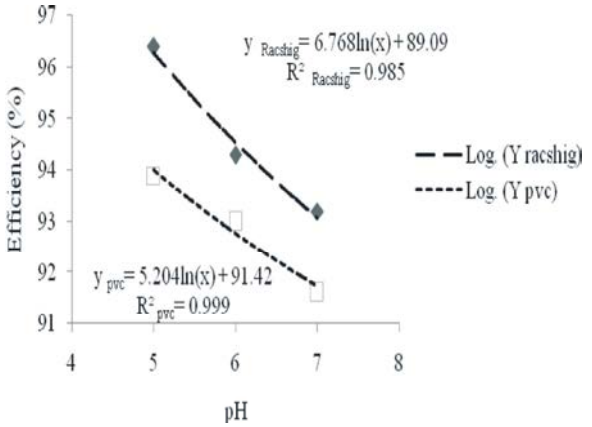

Fig 3: Removal efficiency versus scrubbing liquid pH

The acidity of scrubbing liquid plays a key role in chemical absorption. In such an absorption, the removal efficiency of a packed tower is expected to increase by decreasing the pH (increasing the acidity) of scrubbing liquid [8]. This is expected to be independent from the type of packing material. The results of the present study well agree with this fact. The results showed that removal efficiency of tower packed with raschig rings at studied pHs of 5, 6 and 7 was more than PVC by 1.95, 0.97 and 0.5%, respectively. That is not seems to be due to acidity of scrubbing liquid. At lower pH of 5, higher concentration of sulfuric acid more effectively reduces the ammonia gas from polluted air in packed column. The removal efficiency was consequently decreased with the increasing of pH of scrubbing liquid [8, 21].

The ammonia removal efficiency was independent from G/L ratio and inlet ammonia concentration when H_2SO_4 was applied as the absorbent. Adding H_2SO_4 to the scrubbing solution is recommended in order to have higher ammonia removal efficiencies in a packed tower which is consistent with Bunyakan *et al.* findings [21]. While the handling of scrubbing solutions with high acidity (e. g. pH of less than 4) is more difficult and expensive, the present study shows that at lower concentrations of H_2SO_4 (pH > 5), acceptable average removal efficiency of up to 96.23% is obtainable. This is in the range of removal efficiencies obtained by Melse and Ogink [22]. They have reported an average ammonia removal efficiency of 91 to 99% at pH of 4 [22].

The Influences of Air Flow Rates on Pressure Loss: As it was expected, head losses of packed tower were increased with increases in the air flow rate in both packing materials. Higher head loss was observed when the tower was packed with ceramic raschig rings rather than packed with PVC in all three air flow rates. Fig. 4 shows the effect of air flow rates on head losses of the tower with two types of packing material. The maximum head loss of 788 (pa) was observed at the air flow rate of 15 l/s when the column was packed with ceramic raschig rings.

Table 5: Head losses at different air flow rates

Type of packing	Q, l/s	ΔP, Pa	P-value
Raschig rings	5, 10	153.2	P<0.001
	10, 15	115.2	P<0.001
	5, 15	268.42	P<0.001
PVC	5, 10	7.41	P<0.001
	10, 15	6.07	P<0.001
	5, 15	13.48	P<0.001

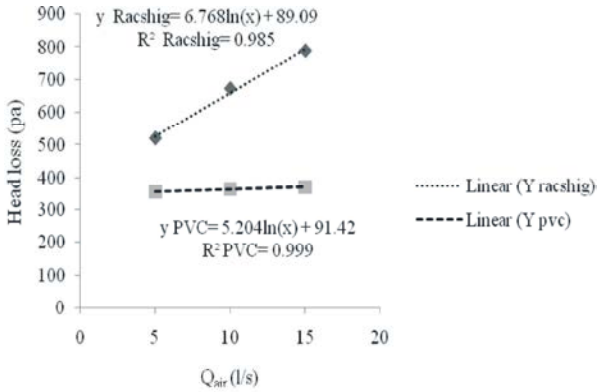

Fig 4: Tower head losses versus air flow rates

The results of Tukey post-hoc test indicated that changing air flow rates from 5 to 10 and 10 to 15 l/s caused a significant increase (P-value<0.001) in tower head loss with both packing materials. Table 5 shows the Tukey post- hoc analysis test to compare the effect of different air flow rates on the head loss of tower packed with two types of packing material.

By increasing air flow rate, the head loss across the bed packed with both packing materials significantly (P-value<0.001) increased which his in consistent with results of many investigations reported in literature [9, 11 and 16]. As the air velocity increases in the column, the head loss which depends on air velocity is expected to increase. The trends of head loss versus air flow rates in Fig. 4 show that the type of air flow in the column packed with Raschig rings is turbulent while it seems to be laminar flow when it is packed with PVC rings. This could be mainly due to smaller sizes of raschig rings in compare to PVC rings. Smaller packing sizes offer a larger surface area, thus enhancing absorption. However, smaller packing fits more tightly, which decreases the open area or void volume between packing, leading to high head losses across the packing bed [6, 9].

By increasing the air flow rate from 5 to 15 l/s, the head loss across the bed packed with Raschig rings increased by 51.63%, while it increased by only 3.79% when it was packed with PVC rings. This is a significant advantage of PVC rings over raschig rings. It may be concluded that the operating costs of air cleaning with packed towers using raschig rings will be much higher than PVC. Packed towers with 500 to 2500 Pascal pressure drops classified as medium-energy scrubbers [17]. The head loss of the studied packed tower packed with raschig rings was two times higher than PVC for the same removal efficiency which is a considerable credit for PVC rings.

CONCLUSION

Lower concentration of H_2SO_4 (pH > 5) is recommended to remove ammonia from polluted air. The lower ammonia removal efficiency of PVC rings could be ignored considering their other advantages of having less weight, low head loss, low initial and operating costs.

ACKNOWLEDGEMENTS

This paper is extracted from the results of a registered (registration No 1391-1-85-9578 dated 16 June, 2012) research project financially supported by Shahid Beheshti University of Medical Sciences as well as L. Omidi thesis supervised by M.J. Jafari. Authors are thankful for this support.

Conflict of Interest: The authors announce no conflict of interests.

REFERENCES

1. Leduc, D., P. Gris., P. Lheureux., P.A. Gevenois, P. De Vuyst. and J.C. Yernault, 1992. Acute and long term respiratory damage following inhalation of ammonia. Thorax., 47(9): 755-7.
2. Phillips, J, 1995. Control and pollution prevention options for ammonia emissions: VIGYAN, Inc., Vienna, VA (United States).
3. Agency for Toxic Substances and Disease Registry, 2004. Public Health Statement Ammonia, [cited 2014 04/04]. Available from: www.atsdr.cdc.gov/toxprofiles/tp126-c1-b.pdf.
4. Jafari, M., L. Omidi, M. Rezazadeh azari, M. Massoudi Nejad and M. Namdari, 2013. The comparison of ammonia removal from air by a wet scrubber packed with ceramic raschig rings and PVC. Tkj., 5 (3) :11-19. [In persion]
5. U.S. Environmental Protection Agency. Design Review of Absorbers Used for Gaseous Pollutants, 1998. Available from: www. yosemite.epa.gov/oaqps/eogtrain.nsf.gov. Accessed 5, 2012, pp: 1-15.
6. Wang, L.K., N.C. Pereira and T.Y. Hung, 2004. Air pollution control engineering: Humana press, pp: 197.
7. Monroe, Liquid Clarification Air/Gas Cleaning Systems, 2009. Michigan; Available from: www.mon-env.com. Accessed Jan 15, 2012.
8. Chungsiriporn, J., C. Bunyakan. and R. Thepchai, 2005. Ammonia Removal from Emission Air in Packed Column. Proceedings of The Fourth PSU Engineering Conference; Dec. 8-9; Songkhla,Thailand, pp: 49-53.
9. Theodore, L., 2008. Air Pollution Control Equipment Calculations. New Jersey: John Wiley & Sons, Inc; pp: 128.
10. Croll-Reynolds, 2013. Selecting Material for Wet Scrubbing Systems. Croll-Reynolds Co; Available from: www.croll.com/air-technicalbulletins-article6.html. Accessed may27, 2013.
11. Jiuan, Y.L., 2005. Evaluation of wet scrubber systems: University of southern Queensland, pp: 1-30.
12. Treybal R.E., 1980. Mass transfer operation. McGraw-Hill Publishing Co., 3rd ed., Tokyo, Japan.
13. U.S. EPA, 2010. APTI 415: Control of gaseous emissions. Absorption, Chapter 5, Air Pollution Training Institute, APTI, USA; pp: 5-7.
14. INTALOX, 2012. Packed tower systems. Plastic random packing. Bulletin KGPP-1.2M050EE; Available from: www.koch-glitsch.com.
15. Cordeiro, M., I. Tinôco, R. Vigoderis, P. Oliveira, R.S. Gates and H. Xin, 2005. Ammonia Concentration Evaluation in Deep-Bedded and Concrete Floor Housing Systems for Grow-Finish Swine in Brazil.
16. Jafari, M.J., R. Ghasemi, Y. Mehrabi, A.R. Yazdanbakhsh and M. Hajibabaei, 2012. Influence of liquid and gas flow rates on sulfuric acid mist removal from air by packed bed tower. Iranian Journal of Environmental Health Science and Engineering, 9(1): 20-7.
17. U.S. Environmental Protection Agency, 1998. Wet-Film (Packed Tower) Scrubbers; Available from: www. yosemite.epa.gov/oaqps/eogtrain.nsf.gov. Accessed 5, 2012, pp: 1-15.

18. ACGIH, 2010. Industrial ventilation a manual of practice Cincinnati, Ohio. USA: American conference of industrial hygienists.
19. Chungsiriporn, J., C. Bunyakan and R. Nikom, editors, 2005. Treatment of toluene using wet scrubber with sodium hypochlorite oxidation reaction. Proceedings of the PSU-UNS international conference on engineering and environment-ICEE, Novi Sad, Italy T11-31.
20. Ebert, F. and H. Büttner, 1996. "Recent investigations with nozzle scrubbers." Powder technology, 86(1): 31-36.
21. Bunyakan, C., J. Chungsiriporn and R. Thepchai, 2007. Treatment of ammonia in waste air using packed column coupling with chemical reaction. Journal of Science and Technology; 29(3): 825-36.
22. Melse, R. and N. Ogink, 2005. Air scrubbing techniques for ammonia and odor reduction at livestock operations: Review of on-farm research in the Netherlands. Transactions of the ASAE; 48(6): 2303-13.

Persian Abstract

DOI: 10.5829/idosi.ijee.2014.05.03.06

چکیده

انتخاب بستر پرکننده برای حذف گاز آمونیاک در ستون پرشده اهمیت زیادی دارد. در این مطالعه یک برج پرشده با دو نوع ماده پرکننده شامل حلقه‌های راشیگ سرامیکی و PVC برای حذف گاز آمونیاک از جریان هوا مورد استفاده قرار گرفت. هوا در سه گذر حجمی، گاز آمونیاک در سه دامنه‌ی تراکم، و مایع شستشو در سه pH بکار گرفته شد. غلظت گاز آمونیاک در ورودی و خروجی برج پرشده توسط تجهیزات قرائت مستقیم اندازه‌گیری گردید. راندمان حذف ستون پرشده با افزایش غلظت آمونیاک ورودی در هر دو نوع بستر پرشده بوسیله‌ی حلقه‌های راشیگ سرامیکی و PVC بطور معنی‌دار افزایش یافت ($P<$ 0.001). با کاهش pH مایع شستشو از ۷ به ۵ راندمان حذف ستون پرشده با حلقه‌های راشیگ سرامیکی بطور معنی‌دار افزایش یافت ($P<$ 0. 01). با افزایش گذر حجمی هوا از ۵ به ۱۰ و از ۱۰ به ۱۵ لیتر بر ثانیه، افزایش معنی‌داری ($P<$ 0.001) در افت فشار ستون در هر دو نوع بستر پرکننده مشاهده گردید اما این افت فشار افزایش یافته در ستون پر شده بوسیله‌ی حلقه‌های راشیگ سرامیکی بیشتر بود. با وجود راندمان حذف کمتر ستون پر شده توسط حلقه‌های PVC نسبت به حلقه‌های راشیگ سرامیکی، سایر مزایای این نوع پرکننده از قبیل وزن پایین‌تر، افت فشار کمتر و هزینه‌ی اولیه و نگهداری پایین‌تر سبب می‌شود بیشتر مورد پذیرش و استفاده قرار گیرد.

Iranica Journal of Energy & Environment 5 (3): 277-286, 2014
ISSN 2079-2115
IJEE an Official Peer Reviewed Journal of Babol Noshirvani University of Technology
DOI: 10.5829/idosi.ijee.2014.05.03.07

BUT

Adsorption of Chromium (IV) by a Low Cost Adsorbent Prepared from Neem Leaves

A.S. Kovo, S.C. Olu and E.S. Gwatana

Department of Chemical Engineering, Federal University of Technology, Minna

Date of Received: June 14, 2014; Date of Accepted in Revised Form: August 3, 2014

Abstract: The adsorption capacity of Neem Leaves powder (NLP) used as a low-cost adsorbent for the removal of Chromium (VI) from aqueous solutions was investigated. During the adsorption process, batch technique was used. The effects of initial metal ion concentration, adsorbent dose, temperature, pH and agitation/contact time on adsorption rate at constant solution pH of 6.4, under a constant temperature of 30°C were studied. The results were analyzed using three adsorption isotherm models; Freundlich, Langmuir and Temkin. Evaluating the correlation coefficients showed that Langmuir isotherm described the data more appropriately than the other isotherms. The adsorption capacity (q_m) from Langmuir isotherm for Chromium (VI) was found to be 125.83mg g^{-1}. The effectiveness of Neem Leave Powder (NLP) in the adsorption of the heavy metal (Chromium VI) from aqueous solution, kinetic studies showed that a pseudo second order model was more suitable than the pseudo first order model. It was concluded that Neem Leave Powder (NLP) can be used as an effective adsorbent for the removal of Chromium (VI) from aqueous solutions. The adsorption process was observed to be exothermic. The negative value of Gibb free energy indicates feasibility and spontaneity of the system while the negative values of the entropy and enthalpy indicate randomness and the exothermic nature of adsorption, respectively.

Key words: Neem leave · Adsorption isotherm · Adsorption kinetics · Chromium (IV) · Thermodynamic properties

INTRODUCTION

In recent year's toxic metals level in fresh waters have increased gradually due to release of untreated industrial effluent and municipal wastewaters into nearby fresh waters [1]. Chromium being a heavy metal which is often found in high proportion in untreated municipal wastewater and industrial effluent discharged from different industries such as leather tanning, electroplating, metal coating industries and paint industries. Mining, metal finishing and leather tanning are the major industrial activities that lead to chromium pollution [2].

Adsorption through the use of solid adsorbents can effectively and efficiently remove pollutants from both aqueous and gaseous municipal and industrial waste discharge and therefore, it is considered environmentally significant. It has been reviewed by number of resaerchers [3-8] that Activated carbon is the most popular adsorbent and it has been right from time traditionally used for the adsorption of odor, taste and colors, which are known as trace pollutants [9]. Its high removal capacity and versatility have expanded its scope of application in the area of treatment of numerous industrial waste streams. With these other commercial adsorbents, with increased reversibility, have been recently reviewed although their versatility and high removal capacity is generally not greater than those of activated carbon, but they are advantageous for certain applications.

Such low cost adsorbents, [10, 11] have been found that in laboratory scale they are applied in the treatment of various pollutants from water and wastewater.

The aqueous form of chromium can be majorly found as Chromium (III) and Chromium (VI) [2]. At low concentration Chromium (III) can be regarded as a biological-element since it is an important constituent in metabolism of plants and animals [2]. On the other hand, Chromium (VI) is very toxic even at very low concentration and it can result in to genetic alternation in

Corresponding Author: A.S. Kovo, Department of Chemical Engineering, Federal University of Technology, Minna.

Please cite this article as: A.S. Kovo, S.C. Olu and E.S. Gwatana, 2014. Adsorption of Chromium (IV) by a Low Cost Adsorbent Prepared from Neem Leaves. Iranica Journal of Energy and Environment, 5 (3): 277-286

plants and animals [2]. The adsorption of Chromium (VI) on so many locally prepared low cost adsorbents have been studied extensively as an alternative process for adsorbing Chromium (VI) from polluted fresh water [1], industrial effluent and municipal wastewater. Activated carbon being the most studied adsorbent and its high capacity for adsorbing Chromium (VI) is dependent upon the solution pH [12]. In the recent years the adsorption of Chromium (VI) on several low cost biological-adsorbents has been worked upon extensively. Some of the low cost biological-adsorbents studied include Eucalyptus, Agave lechugilla biomass; yohimbe and grape tree. The outcomes of the study have shown that these biological-adsorbents have a very high capacity of adsorbing Chromium (VI) from Chromium polluted water [1, 13].

The element Chromium occurs naturally in rocks, volcanic dust, gases, soil, plants and animals. Chromium (0) is the most common forms of chromium. Chromium (III) occurs freely in the environment and as an important nutrient that helps the use of protein, fat and sugar by the body. Chromium (VI) and chromium (0) are majorly fixed into the environment by industrial processes [14]. The element chromium (Cr (0)) is used for casting of steel [13]. Chromium (VI) and chromium (III) are used in chrome dyes and pigments, plating, wood preserving and leather tanning. Chromium (III) and Chromium (VI) is the form in which chromium enters the Air, water, soil [15]. Chromium compounds are present mostly in air in the form of fine dust particles, which gradually settle over land and water. Chromium is strongly attached to soil and only a small amount dissolves in water and penetrate deeper into soil particles and into underground waters. Skin ulcer is majorly caused by contact with some certain chromium (VI) compounds [16]. Some people sensitivity to chromium (VI) or chromium (III), results in an allergic reactions consisting of severe redness and swelling of the skin [17].

Adsorption is as a result of attraction forces between the individual atoms and ions of an adsorbate at the surface or interface or as a result of electromagnetic interactions [18]. The sum total dispersion, electrostatic and functional group interactions widely states the affinity of an adsorbent for a specific adsorbate is termed chemisorption. Series of parameters, affect adsorption [18]. For the adsorbate, molarity, molecular structure, molecular size, molecular weights, molecular polarity, configuration or steric form and competitive adsorption or the nature of background are important. Surface area, physicochemical nature of the surface, the availability of the surface to adsorptive molecules, the physical size [19], form of the adsorbent particles are the valuable characteristics of the adsorbent that determine equilibrium capacity and rate, other parameters such as pH and temperature can also influence adsorption to a large extent [20], the accumulation of solute at the surface of a solid is essentially based on adsorbate, van der waal forces are responsible for adsorbent interaction involving permanent dipoles, induced dipoles and quadruples [21].

MATERIAL AND METHOD

Preparation of Adsorbent: Neem leaves, were harvested from a tall matured Neem tree at Federal university of Technology minna Gidan kwano campus, Minna Niger state, Nigeria. Repeatedly washed with ordinary water to remove soluble impurities, dust and poured into a perforated bowl for the water to drain and then allowed to dry under room temperature or a shade. For the leaves to become crisp, the leaves were placed in an air oven at 80–90°C for 4hours (not to decompose the active principle, high temperature range should not be used [22] and therefore, the drying of the leaves is done only at 30–40°C above the ambient temperature), which was then grinded or blended into a fine powder in a mechanical grinder or blender. The (NLP) Neem Leaf Powder, sieved fraction was, less than or equal to 75 ìm, were selected for use as the adsorbent. These selected fraction was again washed 8 times with ordinary water till the washings is free of color and turbidity and finally with distilled water. After which the (NLP) Neem leave powder was dried for 4 days at room temperature, the Neem Leaf Powder (NLP) was preserved in glass bottles for use as an adsorbent.

Raman Spectroscopy Studies: IR and Raman are the most common vibrational spectroscopies for assessing molecular motion and finge printing species. Based on *inelastic* scattering of a monochromatic excitation source routine energy range between: 200 - 4000 cm^{-1}.

Adsorption Studies: The batch mode operation was used to study the removal of Chromium (VI) from the prepared Cr (VI) solution. 1.2 g adsorbent was placed in a conical flask with 50ml solution of metal ions of desired concentration. The mixture was shaken in temperature controlled water bath shaker for 120 minutes at 240rpm. The mixture was then filtered using (Whatman filter paper No. 41) and final concentration of metal ion was determined in the filtrate by atomic absorption spectrophotometer (AAS). The amount of metal ions adsorbed was calculated by subtracting final concentration from initial concentration.

Effect of pH: The effect of pH on the Adsorption of Cr (VI) was studied by batch process as follows: 50ml of the prepared metal ion solution was taken in beaker. 6.4 was the natural pH of the aqueous solutions of potassium dichromate prepared the desired pH of solution was adjusted by adding dilute solution of 0.1M HNO_3 and 0.1M NaOH. 50ml of the metal ion solution was taken in a conical flask and was treated with 1.2 g of Adsorbent, the pH ranges between 2.4-12 the final concentration of metal ions in this solution was then determined using Atomic Adsorption spectrophotometer (AAS) respectively.

Effect of Contact Time/ Agitation: A series of six 250ml conical flasks, each having 1.2 g adsorbent and 50ml of the prepared metal ion solution was shaken in temperature controlled water bath shaker at 240 rpm and at the predetermined time intervals (20, 40, 60, 80, 100 and 120min) the solution of the specified flask was taken out and filtered. The concentration of metal ions in the filtrate was determined by AAS. The amount of metal adsorbed in each case was then determined as described earlier.

Effect of Adsorbent Dose: A series of six 250ml conical flasks each containing 50ml of the prepared metal ion solution (1000mgl^{-1}) were treated at the same temperature by varying the amount of sorbent (0.2–1.2 g). The flasks were shaken in temperature controlled water bath shaker at 240 rpm and after equilibrium (2 hours) the solutions were filtered. The amount of metal ions in filtrate was then determined by AAS.

Effect of Temperature: A series of six 250ml conical flasks each containing 50ml of the prepared metal ion solution (1000mg l^{-1}) was treated at different temperatures ranging between (30-55°C) by keeping the amount of sorbent constant at 1.2 g and the natural pH of 6.4. The flasks were shaken in temperature controlled water bath shaker at 240 rpm and after equilibrium (2 hours) the solutions were filtered. The amount of metal ions in filtrate was then determined by AAS.

Effect of Initial Concentration: A series of six 250ml conical flasks each containing 50ml of the prepared metal ion solution of different initial metal ion concentration of the range within (70.7, 141.5, 212.24, 282.99, 353.74 and 424.49 mg dm^{-3}) equivalent to $K_2Cr_2O_7$ concentration of (200, 400, 600, 800, 1000 and 1200 mg dm^{-3}). (50mg l^{-1}) were treated at the same temperatures and the same amount of adsorbent (1.2 g) and pH of 6.4. The flasks were shaken in temperature controlled water bath shaker at 240 rpm and after equilibrium (2 hours) the solutions were filtered. The amount of metal ions in filtrate was then determined by AAS.

Blank sample where ran und similar condition of concentration, temperature, pH without adsorbent in all cases to correct any adsorption on the internal surface of flask.

The percentage of Chromium removal (R%) was determined by the expression

$$R\% = \frac{(E_i - E_e)}{E_i} \times 100 \quad (1)$$

where E_i and E_e are the initial and final concentration of Chromium in the solution respectively, q_e the adsorption capacity of an adsorbent which is obtained from the mass balance on the sorbent in a system with solution volume V is often used to acquire the experiment adsorption capacity of all the adsorbent for each concentration of Chromium ions at equilibrium were calculated as thus

$$q_e(mg\ g^{-1}) = (\frac{E_i - E_e}{M}) \times V \quad (2)$$

where V is the volume of solution and (M) is the mass of adsorbent in grams used

RESULT AND DISCUSSION

Raman Spectroscopy Analysis: Raman spectroscopy measurements for Neem leaves powder are shown in Fig. 1. The broad and strong bands around 2000-3200cm^{-1} were due to vibration of –OH, C=C-H, etc. At the wavelength neem leaves powder at 1200-2000 cm^{-1} (Fig. 1), corresponding to the vibration of the cyano group. On the other hand, more new bands appeared at wavelength less than 1000cm^{-1}in the Neem leaves powder (Fig. 4.1), which were characteristic of the –C=N, –C=N and –N–OH groups, respectively.

Effect of Agitation/Contact Time: The study of the kinetic of Cr (VI) Adsorption on (NLP) was carried out as a batch experiment with initial concentration of Cr (VI) metal ions of 353.74 mg l^{-1} at 303 K with 50ml of six different Cr (VI) samples of the constant concentration when the agitation time was varied from 20 to 120 minutes at intervals of 20 minutes in each case. A gradual increase in the extent of adsorption with time was observed (Fig. 2). The percentage Cr (VI) adsorption increased from 99.5 to 99.75% in the time interval of 20 to 120 minutes for an

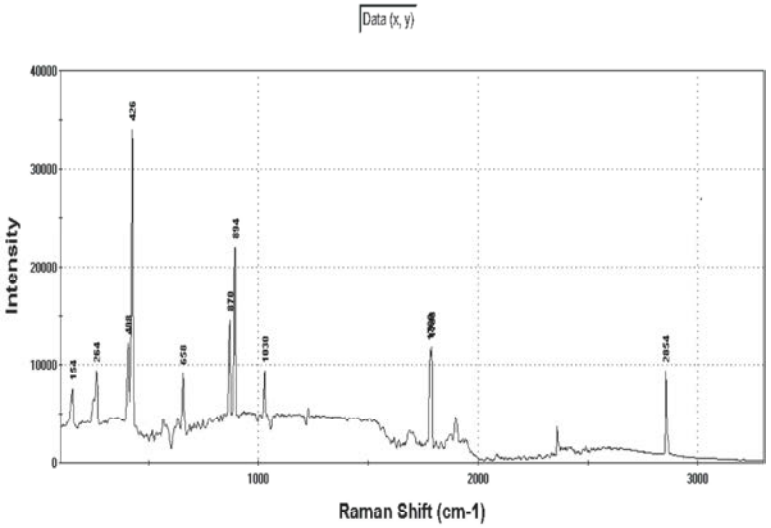

Fig. 1: Raman spectroscopy of Neem Leaves Powder

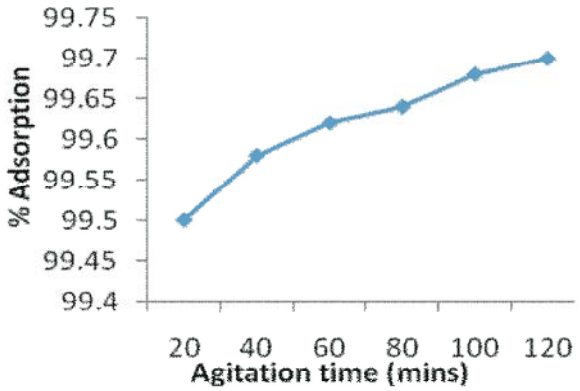

Fig. 2: Effect of agitation time of adsorption on percentage adsorption

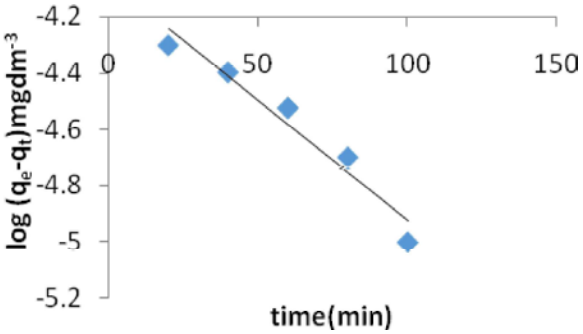

Fig. 3: Plot for pseudo first order kinetics

amount of 1.2 g NLP per dm^3. Such behavior is expected in a batch reactor with either constant adsorbent amount or varying initial adsorbate concentration or vice versa, based on the fact that the adsorbate have enough time to react with the adsorbent as the contact time increases [23].

Kinetic Study

First Order Kinetics: In this present work, the adsorption extent changed very slightly after 100 min and applying Lagergren pseudo first order kinetics, equilibrium conditions could be assumed at 100 min. The Lagergren's plots linearity range calculated to be, (Fig. 3, R value 0.95), this was obtained by plotting $\log(q_e-q_t)$ (mg dm^3) vs agitation time for the adsorption of Chromium (VI) from a prepared aqueous solution of concentration 353.74 mg dm^3 of the metal ions at 303K for the six different samples at different agitation time and of the adsorbent amount, indicated that the adsorption process maybe following the pseudo first order kinetics. The calculated rate constant, from the slopes of the best-fit lines, was gotten to be19.57×10^{-3} min^{-1} and $q_e=8.424\times10^{-5}$ not similar with the experimental value.It has been reported with very similar values for Chromium (VI) removal by *Dakiky* [24], *on* diverse kinds of adsorbents (cactus leaves 6.80×10-3 min^{-1}, wool 3.96×10^{-3} min^{-1}, sawdust 9.00×10-3 min^{-1}, olive cake 8.99×10-3 min^{-1}, almond 8.80×10-3 min^{-1}) at pH 2 and 30°C.

Describing the adsorption process for a large number of cases, Lagergren equation has been adequate [3, 10], although for a concrete mechanism of the adsorption process this equation does not provide such pictures. Besides, the experimental *log* q_e value of the present work, does not match with the *log* q_e value obtained from the intercept of the plot.

Second Order Kinetics: To give a good account of the kinetics of Chromium (VI) adsorption on Neem leave powder, the first order kinetics is thus inadequate.

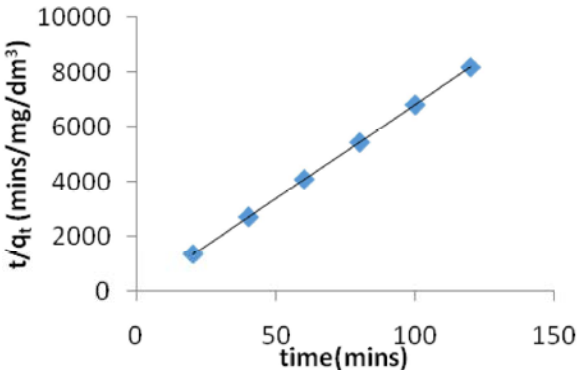

Fig. 4: Plot for the Pseudo-second order kinetics

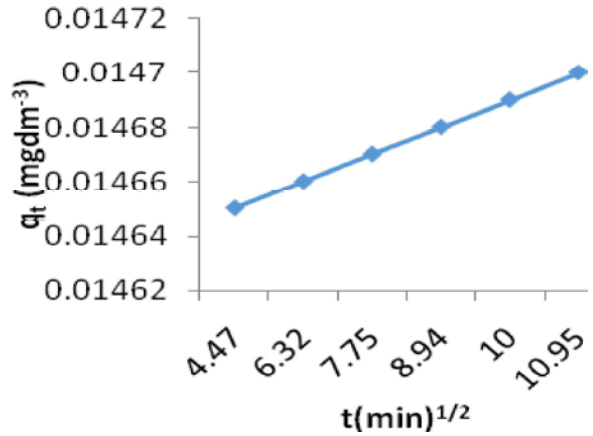

Fig. 5: Plot for intra-particle diffusion

Second order kinetics must be applied by plotting t/q_t *vs* t gave forth a better results (Fig. 4), with the second order rate constant k_2 gotten to be 984.09 $mg^{-1}min^{-1}$ (R for the lines ≈ 0.99). There is also now good agreement between experimental q_e (0.0147) values and those obtained from the slopes of the second order plots as given in the figure below, (Fig. 4).

Intra-Particle Diffusion: Intra-particle diffusion mechanism of adsorption the approach towards equilibrium is governed by the equation $(D.t/r^2)^{0.5}$, in which D is the diffusivity within the particle and r is the radius of the particle. From the plot of q_t (amount adsorbed in *mg* per unit mass (*g*) of the adsorbent after a contact time of *t* minutes) *vs* $t^{0.5}$ (Fig. 5) k_p, value as the constant of adsorption is discovered to be 7.721×10^{-6} The intra-particle diffusion is thus a very slow process its significance cannot be over emphasized. After the metal ions are adsorbed initially on the surface of the Neem leaves powder particles, the metal ions are slowly been transported into the interior of the particles and the kinetics of adsorption should be discussed in overall on the basis of both intra-particle diffusion and surface adsorption [25].

The intercept should have been zero by plotting t/q_t *vs* $t^{0.5}$ but the lines in the present work (Fig. 5) has the intercept of 0.0146. These proved that the mechanism for the adsorption process of Chromium (VI) on Neem leaves powder is not only governed by intra-particle diffusion. Adsorption process of chromium (VI) took place through initial diffusion followed by surface compound formation on a homogeneous mixture of wollastonites and fly ash [26]. A comparable condition cannot be ruled out in the present work as well. The metal ions diffuse from the aqueous solution to the exterior surface of the Neem Leaves Powder particles at a relatively high speed, then gradual diffuse into the interior surface and ultimately fix to the surface through chemisorptive bond formation.

Effect of Adsorbent Dosage: The amount of Neem Leaves Powder influenced the adsorption process of Chromium (VI). With Chromium (VI) concentration of 353.7*mg* dm^{-3}, the% adsorption increased from 99.45 to 99.70% while increasing the Neem Leaves Powder amount between the range of 200 to 1200 *mg* per dm^3 at a constant agitation time of 120 min at 303 K due to availability of more adsorption sites. On increasing the adsorbent dose from 200 to 1200*mg* dm^{-3} for constant Chromium (VI) metal ion concentration, the rate of adsorption process per unit mass indicated a decrease due to accessibility of fewer number of Chromium (VI) metal ions per adsorbent unit mass. Neem Leave Powder compared to some unconventional adsorbent has a larger adsorption capacity. Cactus leaves and pine needles at metal ion concentration of 0.1*mg* dm^{-3} at 303 K pH 2.0 adsorbents can respectively remove 19.8 and 42.9% [24]. Large number of OH-groups on the surface based cellulose plant material can bind easily to Chromium (VI) ions. Similar attribute can be apportioned to the large adsorption capacity of the NLP to easily access other groups for metal ion uptake and surface OH. The major chemicals contained in the Neem leaves, are namely, azadirachtin, meliantriol, nimbin, salannin and andnimbidin comprise of large number of Hydroxyl-groups that are probable to be the potential sorption sites for the metal ions. Fatty acids like linoleic acid, oleic acid, palmitic acid, steric acid, etc. are present in Neem Leaves [27]. FTIR measurements also indicated the existence of a large number of functional groups, OH, COOH, etc., in Neem leaves and these groups may give Neem leaves powder the excellent sorption properties it has [26].

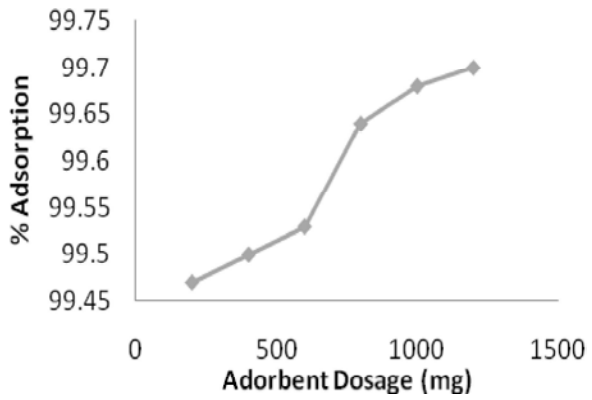

(V=50ml=0.05*l*, T=30°C, t=120mins, C_o=1000 *mg* l^{-1} = 353.74 *mg* $l^{-1}$of Cr metal Ions)

Fig. 6: Effect of adsorbent dose on percentage Adsorption

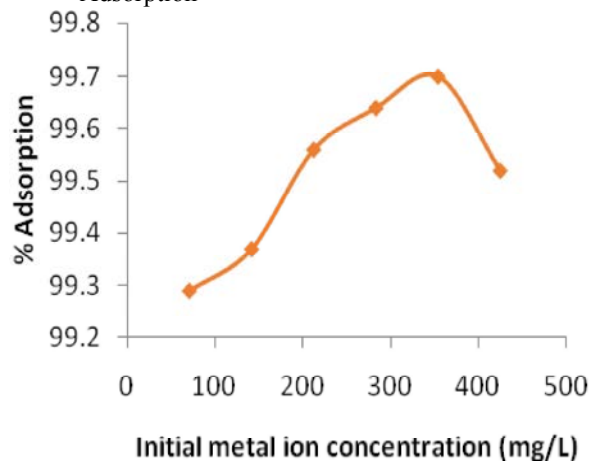

*(*V=50ml=0.05L, T=30°C, t=120mins, M=1.2g)

Fig. 6: Effect of Initial concentration on percentage Adsorption

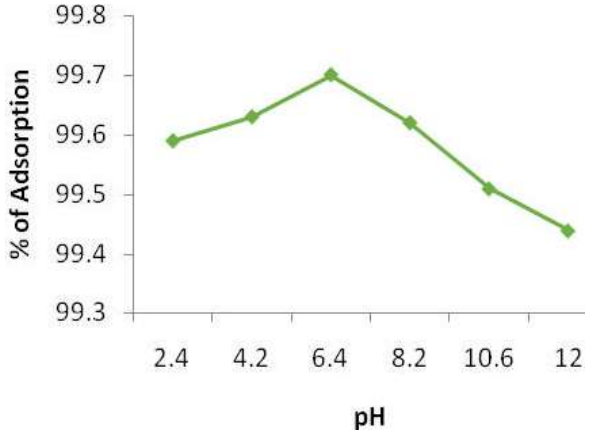

(V= 50 *ml* =0.05 *l*, T=30°C, t=120 min, M=1.2g, C_o=1000 *mg* l^{-1} =353.74 *mg* $l^{-1}$of Cr metal Ions)

Fig. 7: Effect of pH on Percentage of Adsorption

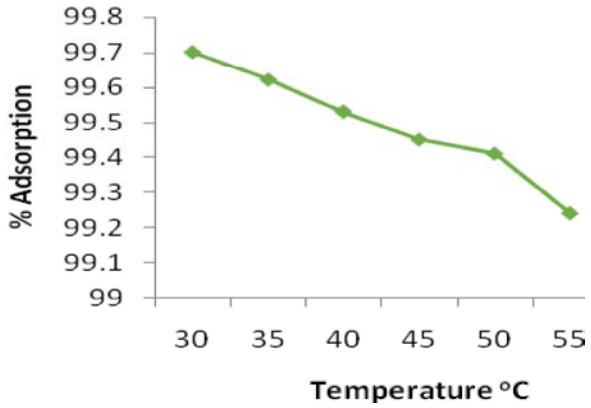

(V=*50ml* =0.05 *l*, t=120min, M=1.2g, C_o=1000 *mg* l^{-1}=353.74 *mg* $l^{-1}$of Cr metal Ions)

Fig. 8: Effect of Temperature on percentage adsorbed

Effect of Initial Concentration of Metal Ions: The effect of initial concentration of chromium is shown in (Figure 7). Results from these plots indicate that% removal decreases from 99.7 (353.7 *mg* g^{-1}) to 95.5% (424.5 *mg* g^{-1}) as the initial concentration of chromium is increased from 70.75 to 424.5 *mg* l^{-1} for 1.2 *g* of 75*im* size adsorbent at equilibrium agitation time of 120 minutes. However, the change in% removal increased for initial concentration between 70.72 to 353.74 *mg* l^{-1}. Maintenance a fixed number of binding sites in the dosage can be attributed as evidence to such a behavior while increasing the concentration. This kind of behavior are not usually found in literature but they are bound to happen only if the concentration of initial metal ion concentration needed exceeds the number of available sorption sites in the adsorbent [28]. The% removal of chromium is found to be maximums at (99.7%) for 1.2 *g* of 75 μm adsorbent sizes, where the adsorption sites on the fixed adsorbent mass had been exhausted; while, the% adsorption starts decreasing to 99.5%.

Effect of pH: pH is an important factor controlling the process of adsorption as it affects the surface charge of the adsorbents, the degree of ionization and the species of adsorbate.The effect of pH on adsorption of chromium is shown in Figure 4.8 the% removal of chromium increases from 99.59 to 99.70% for 1.2 g of 75μm adsorbent with an increase in pH from 2.4 to 12 as similarly reported earlier [13]. It is conformed that adsorption increases with the decrease in acidity. At low pH, hydrogen ions compete with chromium ions for appropriate sites on the adsorbent. As pH approaches to 7, the competition of hydrogen ions becomes negligible and more chromium ions are bound to the adsorbent.

Table 1: Kinetic parameters

Pseudo-First order			Pseudo-second order			Intra-particle diffusion		
R^2	$q_e(mg\ dm^{-3})$	slope	R^2	$q_e\ (mg\ dm^{-3})$	$K_2(mg^{-1}min^{-1})$	Kp	intercept	R^2
0.95	8.424×10^{-5}	19.57×10^{-3}	0.99	0.014705	984.09	7.72×10^{-6}	0.014613	0.99

Table 3.2: Coefficients calculated from Langmuir, Freundlinch and Temkin isotherm

	Langmuir isotherm			Feundlich isotherm				Temkin isotherm		
Parameters	R	$q_m\ (mg\ g^{-1})$	b($dm^3m\ g^{-1}$)	R_l	R	$K_f\ (dm^3\ g^{-1})$	n	A_T	b_T	R
Agitation time	0.99	104.6	0.00069	0.999	0.64	0.0148	-62.85	0	-0.0567	0.93
Adsorbent dose	0.99	128	0.0012	0.998	0.85	0.0123	0.405	1.048	89.9	0.97
Initial metal conc	0.98	126	0.0023	0.99	0.79	0.0111	0.469	2.38	12.0	0.98
pH	0.99	104.5	0.0021	0.997	0.94	0.0147	245.1	0	-0.0613	0.96
temperature	0.99	166.0	0.016	0.974	0.98	0.0147	202.02	0	-0.072	0.94

The values of k_f and n for the different parameters obtained from the intercept and slope of the plots of $log\ q_e$ *vs* $log\ C_e$ are also presented in Table 3.2. The values of k_f was calculated to be 14.8, 12.3, 11.1, 14.7, 14.7 mg/g for Agitation time, Adsorbent dose, Initial metal ion concentration, pH and Temperature respectively. k_f Is a measurement of adsorption capacity, all the values

The% removal decreases as pH increases beyond 7. The maximum removal of chromium was reported at a pH value of 6.4 for this present work. With chitosan as adsorbent [29], the maximum uptake capacity (50 $mg\ g^{-1}$) was noted at a pH of 5. The fungi biomass removed 64 $mg\ g^{-1}$at a pH of 4.8 [30]. The maximum removal of chromium was reported at a pH of 4 with cationic starch maleate [31].

Effect of Temperature: The effect of temperature on the adsorption of Cr (VI) on Neem leaves powder is depicted in Fig. 8 The percentage of adsorption at temperatures range from 30 to 55°C and pH = 6.4 plotted in this figure indicated that the Cr (VI) adsorption capacity of the Neem leaves powder diminished while increasing the temperature from 30 to 55°C. At an initial metal ion concentration of 353.74 $mg\ dm^{-3}$, the percentage adsorption of Cr (VI) adsorbed on the Neem Leaves Powder diminished steadily when the temperature was raised from 30 to 35°C and 35 to 40°C, respectively. Roberto *et al*. [1] reported that the adsorption capacity of the organobentonite decreased while increasing the temperature because the adsorption is exothermic. The heat of adsorption for the adsorption of Chromium (VI) on a bentonite modified with HDTMA was estimated to be ΔH_{ad} = -35.5 $kJ\ mol^{-1}$ this is similar to the report in this present work.

Isotherm Study

Langmuir and Freundlich Isotherm: Chromium (VI) adsorption on Neem Leave Powder isotherm was studied using both Langmuir Isotherm and Freundlich Isotherm. The adsorption coefficients and the correlation coefficients are given in Table 3.2. The Langmuir plots have good linearity (R: 0.99 to 1.00). The Langmuir monolayer adsorption capacity (q_m) was calculated to be 104.6, 128, 126, 104.5 and 166 $mg\ g^{-1}$ for agitation time, adsorbent dose, initial metal ion concentration, pH and temperature respectively, for the Neem Leaves Powder amount varying from 0.2 to 1.2 g dm^{-3} for adsorbent dose and for the remaining parameter the adsorbent dose was kept constant at 1.2 $g\ dm^{-3}$. The adsorption equilibrium parameter, b, was also calculated respectively for the individual parameter studied to be 0.00069, 0.0012,0.0023, 0.0021 and 0.016 $dm^{-3}\ g^{-1}$. The dimensionless parameter, R_L, remained between 0.974 and 0.999 ($0 < R_L < 1$) compiling with the requirement for a favorable adsorption process of n are between -62.85, 0.405, 0.469, -245.1 and -202.02. The values of n in the range of 2–10 represent good adsorption. From the results obtained, it is clear that the adsorption study is not too good [32]. The comparison of the experimental value with the calculated value from the equilibrium isotherm for chromium (VI) adsorption using Neem leaves powder as adsorbent. It is obvious that the adsorption capacities calculated from Langmuir isotherm are much closer to the experimental values of q_e than that of Freundlich isotherm. From Table 3.2, it also appears that Langmuir isotherm fitted the experimental results over the experimental parameters with a higher coefficient of correlation than that of Freundlich isotherm. These results indicated that the adsorption of Chromium (IV) onto Neem leaves powder as adsorbent follows Langmuir Isotherm better than Freundlich.

Temkin Isotherm: Temkin adsorption potential, A_T, of Neem Leaves Powder for Chromium (VI) adsorption are 0, 1.048, 2.38, 0 and 0 for Agitation time, Adsorbent dose, Initial metal ion concentration, pH and Temperature respectively, indicating a lower Neem Leaves Powder-

metal ion potential for Chromium (VI) probably due to its small ionic radius. The Temkin constant, b_T, related to heat of Adsorption for the Chromium (VI) metal ions were -0.0567, 89.9, 12, -0.0613 and -0.072 *kJ mol*$^{-1}$ for agitation time, Adsorbent dose, Initial metal ion concentration, pH and Temperature respectively. It has been reported [10], that the typical range of bonding energy for ion-exchange mechanism is 8-16 kJ/mol. The values in this study indicates a weak interaction between adsorbate and sorbent, supporting an ion-exchange mechanism for the present study. Dada *et al.,* [33] reported some estimated values as follows $A_T = 1.075\ l\ g^{-1}$, B=25.34 *J mol*$^{-1}$ which is an indication of the heat of sorption indicating a physical adsorption process and the R^2=0.62. Comparing this with the present work Agitation time, pH and Temperature with R^2 0.93, 0.98 and 0.98 are chemosorbed. While Adsorbent dose and Initial metal ion concentration with R^2= 0.64 and 0.98 are physical adsorption process.

Thermodynamic Studies: The thermodynamic parameters such as enthalpy change $\Delta H°$, change in entropy $\Delta S°$ and Gibb free energy $\Delta G°$ are helpful in determining the spontaneity, feasibility as well as the endothermic or exothermic nature of the adsorption process [34]. The thermodynamic parameters can also be correlated to the distribution coefficient by equations (3 and 4) as shown below:

$$\log \frac{q_e}{C_e} = \frac{\Delta S^\circ}{2.303R} - \left(\frac{\Delta H^\circ}{2.303R}\right)\frac{1}{T} \quad (3)$$

$$\Delta G^\circ = -RT \ln K_c \quad (4)$$

where $\Delta S°$ and $\Delta H°$ are the standard entropy and enthalpy for the adsorption process, q_e denotes the rate of adsorption (*mg g*$^{-1}$), $K_C = \frac{C_{ad}}{C_e}$, C_{ad} is the quantity of Chromium adsorbed and C_e denotes the quantity of chromium in the solution at equilibrium [35].

Fig. 9 is the plot of *log* (q_e/C_e) against *1/T* for 1000 (*mg l*$^{-1}$) initial concentration of Chromium (VI). The intercept and slope are used to evaluate the entropy change ΔS and enthalpy change ΔH, respectively. The values for entropy and enthalpy change is -4.715 and -118.766 (*kJ mol*$^{-1}$) for NLP sample. The values of change in enthalpy calculated from the plot suggest that the adsorption is exothermic in nature. The negative values of change in entropy also suggest decreasing randomness at the liquid-solid interphase. The change in Gibb's free

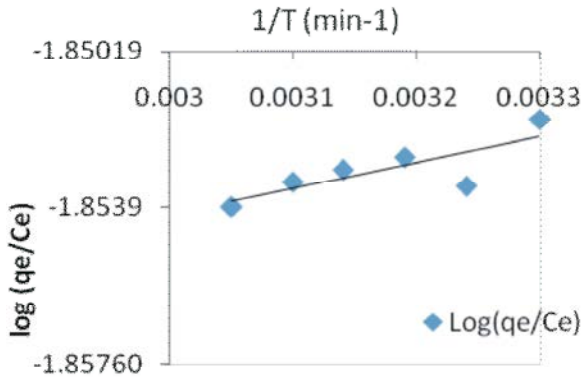

Fig. 9: Relationship between *1/T* and *log* (q_e/C_e)

energy values obtained via the above equation (4.2) are -615.96, -1217.44, -1659.57, -1846.74 and -2569.38 (*kJ mol*$^{-1}$). The negative values denoted a spontaneous and a feasible process.

CONCLUSION

The results of the study reveal that Neem Leaves Powder can be converted into an adsorbent with good adsorption capacity instead of its medicinal use it has been known for in time passed. The Neem Leaves Powder was used to study the removal of Chromium (VI) from aqueous solution and the adsorption percentage increased with an increase in Agitation time, Adsorbent Dose, increases with increase in Initial metal ion concentration to the maximum level and start decreasing after attaining it maximum adsorption capacity, adsorption is favorable at pH of 5-6.4, but decreased with the increase in temperature.

The studies of adsorption isotherms suggested that Langmuir isotherm generated the better agreement with the experimental data of Chromium (VI) adsorbed by Neem Leaves Powder than Freundlich isotherm. The values of the maximum adsorption capacity q_m calculated from Langmuir model were also closer to the experimental values of q_e than that of Frenudlich model, when studying the parameters. Some of the maximum adsorption capacity like Adsorbent Dose with Initial concentration of metal ion indicated the adsorption process of Chromium (VI) onto the Neem Leaves Powder was exothermic. And from Temkin isotherm coefficient of correlation there is a poor Neem Leaves Powder-metal ion interaction and adsorption process for Agitation time, pH and Temperature are chemosorbed while that for Initial metal ion concentration and adsorbent dose are physical adsorption process.

A pseudo-second-order model was more suitable than a pseudo first-order model with correlation coefficients greater than 0.999, which confirmed the exothermic nature of the adsorption process.

The intra-particle diffusion is a slow process and that the adsorption process is governed by slow transport into the interior of the particles, so the overall kinetics is based on both intra-particle diffusion and surface adsorption.

The adsorption process was observed to be exothermic. The negative value of Gibb free energy indicates feasibility and spontaneity of the system while the negative value of the entropy and enthalpy indicate randomness and the exothermic nature of adsorption. This also indicates that an increase in temperature decreases the overall sorption rate as well as amount of chromium (IV) ion adsorbed from aqueous solution by NLP.

REFERENCE

1. Roberto Leyva-Ramos, Araceli Jacobo-Azuara, Oliva L. Torres-Rivera, Rosa M. Guerrero-Coronado, Maria S. Berber-Mendoza and Pedro Alonso-Davila, 2008. Adsorption of chromium (vi) from water solution onto Organobentonite J. Environmental Engineering Management, 18(5): 311-317.
2. Bradl, H.B., C. Kim, U. Kramar and D. Stüben, 2005. Interactions of Heavy metals. In H.B. Bradl Ed.,Heavy Metals in the Environment: Origin, Interaction and Remediation. Elsevier Ltd., London, UK, pp: 104-107.
3. Ho, Y.S. and G. Mckay, 1998. A comparison of Chemisorption Kinetic Models Applied to Pollutant Removal on Various Sorbents, Transactions Industria Chemical Engineering, 76B: 332-340.
4. Hamideh Radnia, Ali Asghar Ghoreyshi and Habibollah Younesi, 2011. Isotherm and Kinetics of Fe(II) Adsorption onto Chitosan in a Batch Process, Iranica Journal of Energy and Environment 2(3): 250-257, DOI: 10.5829/idosi.ijee.2011.02.03.1837
5. Bharathi Kandaswamy Suyamboo and Ramesh Srikrishna Perumal, 2012. Equilibrium, Thermodynamic and Kinetic Studies on Adsorption of a Basic Dye by Citrullus Lanatus Rind, Iranica Journal of Energy and Environment, 3(1): 23-34, DOI: 10.5829/idosi.ijee.2012.03.01.0130
6. Sanaz. Monemtabary, Mojtaba Shariati Niasar, Mohsen Jahanshahi and Ali Asghar Ghoreyshi, 2013. Equilibrium and Thermodynamic Studies of Methane Adsorption on Multi-Walled Carbon Nanotube, Iranica Journal of Energy and Environment, 4(1) Special Issue on Nanotechnology: 17-23, DOI: 10.5829/idosi.ijee.2013.04.01.03
7. Mahalakshmi, K., S.K. Suja, K.Yazhini, S. Mathiya and G. Jayanthi Kalaivani, 2014. A Novel Approach to Investigate Adsorption of Crystal Violet from Aqueous Solutions Using Peels of Annona Squamosa, Iranica Journal of Energy & Environment, 5(2): 113-123, DOI: 10.5829/idosi.ijee.2014.05.02.02
8. Seyed Mahmoud Mehdinia, Khalilollah Moeinian and Tayyabeh Rastgoo, 2014. Rice Husk Silica Adsorbent for Removal of Hexavalent Chromium Pollution from Aquatic Solutions, Iranica Journal of Energy & Environment, 5(2): 218-223, DOI: 10.5829/ idosi.ijee.2014.05.02.15
9. Thomas, W. John, 1998. Crittenden, Barry, in Adsorption Technology and Design, Butterworth, Heinemann, Oxford.
10. Ho, Y.S. and G. Mckay, 1999. A comparison of Chemisorption Kinetic Models Applied to Pollutant Removal on Various Sorbents, Trans. IChemE., 76B: 332-340.
11. Bailey, S.E., T.J. Olin, R.M. Bricka and D.D. Adrian, 1999. A Review of Potentially Low Cost Sorbents for Heavy Metals, Walter Res., 33: 2469-2479.
12. Sh.Shahmohammadi-Kalalagh, H. Babazadeh, A.H. Nazemi and M. Manshouri, 2011. Isotherm and Kinetic Studies on Adsorption of Pb, Zn and Cu by Kaolinite. Caspian Journal of Environmental Sciences, 9(2): 243-255.
13. Sharma, A. and K.G. Bhattacharyya, 2004. Adsorption of Chromium (VI) on Azadirachta Indica (Neem) Leaf Powder, Adsorption, 10: 327-338.
14. ATSDR, 2013. Chromium Fact Sheet, Agency for Toxic Substances and Disease Registry (ATSDR), USA http://www.atsdr.cdc.go.
15. Monika Jain, V.K. Garg, K. Kadirvelu, 2009. Chromium (VI) removal from aqueous system using Helianthus annuus (sunflower) stem waste. Journal of Hazardous Materials, 162(1): 365-372.
16. Vinodhini V. and Nilanjana Das, 2009. Mechanism of Cr (VI) Biosorption by Neem Sawdust, American-Eurasian Journal of Scientific Research, 4(4): 324-329. ISSN 1818-6785.
17. US Department of Health and Human services, 2011. Toxicological profile for Chromium, Public Health services Agency for Toxic Substances and diseases Registry. Washington, DC.
18. Shuguang Deng, 2006. Sorbent Technology. Chemical Engineering Department, New Mexico State University, Las Cruces, New Mexico, U.S.A.
19. Gregg, S.J. and K.S.W. Sing, 1982. Adsorption, surface area and porosity, Academic Press, London.

20. Rifaqat Ali Khan Rao, Moonis Ali Khan, 2009. Biosorption of bivalent metal ions from aqueous solution by an agricultural waste: Kinetics, thermodynamics and environmental effects. Colloids and Surfaces A: Physicochem. Eng. Aspects, 332: 121-128.
21. Yu Jiang, Hao Pang and Bing Liao, 2009. Removal of copper(II) ions from aqueous solution by modified bagasse. Journal of Hazardous Materials, 164(1): 1-9.
22. Kraus, W., 1995. Biologically Active Ingredients, in The Neem Tree, H. Schmutterer (Ed.), pp: 35-92, VCH, Weinheim.
23. Chu, K.H., 2002. Removal of Copper from Aqueous Solution by Chitosan in Prawn Shell: Adsorption Equilibrium and Kinetics, Journal of Hazardous Materials, B90: 77-95.
24. Dakiky, M., M. Khamis, A. Manassra and M. Mereb, 2002. Selective adsorption of Cr (VI) in industrial wastewater using low cost abundantly available adsorbents. Advances in Environ. Res., 6: 533-540.
25. Wu, Feng-Chin, Tseng, Ru-Ling and Juang and Ruey-Shin, 2000. Comparative Adsorption of Metal and Dye on Flake- and Bead-Types of Chitosans Prepared from Fishery Wastes, Journal of Hazard Materials, B73: 63-75.
26. Panday, K.K., G. Prasad and V.N. Singh, 1984. Water Research, 19: 869-873.
27. Skellon, J.H., S. Thorburn, J. Spence and S.N. Chatterjee, 1962. The Fatty Acids of Neem Oil and their Reduction Products, Journal of Scientific Food Agriculture, 13: 639-643.
28. Mohanty, K., M. Jha, B.C. Meikap and M.N. Biswas, 2005. Removal of chromium (VI) from dilute solutions by activated carbon developed from Terminalia arjuna nuts ctivated with zinc chloride, Chemical Engineering Sciences, 60: 3049-3059.
29. Sarin, V. and K.K. Pant, 2005. Removal of chromium from industrial waste by using eucalyptus bark. Bioresource Technology, 97: 15-20.
30. Keskinkan, O., M.Z.L. Goksu, M. Basibuyuk and C.F. Forster, 2004. Heavy metal adsorption properties of a submerged aquatic plant, Bioresource Technology, 92: 197-200.
31. Xing, G.X., S.F. Zhang, B.Z. Ju and J.Z. Yang, 2006. Study on adsorption behaviour of crosslinked cationic starch maleate for chromium (VI), Carbohydrate Polymer, 66: 246-251.
32. McKay, G., M.S. Otterburn and A.G. Sweeney, 1980. The removal of colour from effluent using various adsorbents-III. Silica: rate processes, Water Research, 14: 15-20.
33. Dada, A.O., A.P. Olalekan and A.M. Olatunya, 2012. Langmuir, Freundlich, Temkin and Dubinin-Radushkevich Isotherms Studies of Equilibrium Sorption of Zn^{2+} Unto Phosphoric Acid Modified Rice Husk (IOSR-JAC), 3: 38-45.
34. Xiao-ming, L., W. Zheng, D. Wang, Q. Yang, J. Cao, X. Yue, T. Shen and G. Zeng, 2010. Removal of Pb (II) from aqueous solutions by adsorption onto modified areca waste: Kinetic and thermodynamic studies. Desalination, 258: 148-153.
35. Aksu, Z., 2002. Determination of equilibrium, kinetics and thermodynamic parameters of the batch Biosorption of nickel(II) ions onto chlorella vulgaris, process Biochemistry, 38: 89-96.

Persian Abstract

DOI: 10.5829/idosi.ijee.2014.05.03.07

چکیده

ظرفیت جذب پودر برگ نیم که به عنوان یک جادب ارزان قیمت برای حذف کروم از محلول‌های آبی استفاده می شود، مورد بررسی قرار گرفت. در طول فرایند جذب تکنیک ناپیوسته مورد استفاده قرار گرفته است. اثر غلظت اولیه یون فلزی ،میزان جاذب، دما ، pH ،اختلاط/زمان تماس روی سرعت جذب در ثابت ۶/۴ و دمای ثابت ۳۰ درجه سانتیگراد و pH مورد مطالعه قرار گرفت.نتایج با استفاده از ۳ مدل جذب هم دما، فرندلیچ ، لانگمایر و تمکین مورد ارزیابی قرار گرفت.ارزیابی ضرایب تصحیح نشان داد مدل هم دمای لانگمایر داده هارا به طور مناسب تری نسبت به سایر مدل ها عرضه می کند. ظرفیت جذب از مدل هم دمای لانگمایر برای کروم شش ظرفیتی ۱۲۵/۸۳ میلی گرم بر گرم بود. میزان موثر بودن پودر برگ نیم در جذب فلزات سنگین از محلول های آبی،مطالعات سینتیکی نشان داد که مدل شبه مرتبه ۲ از مدل شبه مرتبه ۱ مناسب تر بود. نتیجه گیری شد که پودر برگ نیم جاذب موثری برای حذف کروم شش ظرفیتی از محلول آبی را دارد.مشاهدات نشان میدهد که فرایند جذب گرما زاست. مقدار منفی انرژی آزاد گیبس نشانگر مقرون به صرفه بودن و خود به خودی بودن فرایند است. در حالیکه میزان منفی انتروپی و انتالپی به ترتیب نشانگر ماهیت تصادفی و گرمازای جذب هستند.

Iranica Journal of Energy & Environment 5 (3): 287-294, 2014
ISSN 2079-2115
IJEE an Official Peer Reviewed Journal of Babol Noshirvani University of Technology
DOI: 10.5829/idosi.ijee.2014.05.03.08

BUT

Development of Simple and Cost Effective Method for Arsenic(III) Removal

[1]Nur Zulaikha Yusof, [1]Mohd Azraai Kassim, [2]Razali Ismail and [1]Abdull Rahim Mohd Yusoff

[1]Department of Environmental Engineering, Faculty of Civil Engineering,
Universiti Teknologi Malaysia, 81310 Skudai, Johor, Malaysia
[2]Department of Chemistry, Faculty of Science, Universiti Teknologi Malaysia, 81310 Skudai, Johor, Malaysia

Date of Received: June 15, 2014; Date of Accepted in Revised Form: August 1, 2014

Abstract: In the present study, eight locally available low cost adsorbents (raw and heat treated) have been screening for its capability to remove As(III). The shale sedimentary rock (SSR) was selected as a good adsorbent based on high As(III) removal. The activation of adsorbent was carried out by heat (250 - 550°C) and acid treatment (0.1 - 1 M H_2SO_4) in order to chose the best treatment method for As(III) removal. Sorption experiments were conducted to examine the effect of initial As(III) concentration, contact time and initial pH on As(III) removal by SSR. Results show that, only by heating the adsorbent at 500°C for 1h, 0.2 g of SSR adsorbent capable to reduce the residual As(III) concentration below than maximum concentration limit (10µg/L) for initial concentration from 100 to 700 µg/L and optimum pH ranges between 3 to 9 after 24 h of contact time. The adsorption data fits well with Langmuir isotherm and yielded Langmuir monolayer capacity of 0.987 mg As(III)/g of SSR at pH 7. The SSR adsorbent has been successfully used for the removal of arsenic from seven real groundwater samples containing arsenic in the range of 20.2 to 697.34 µg/L with 86.73 to 97.86% removal efficiency.

Key words: As (III) removal · Shale sedimentary rock · Heat treatment · Langmuir isotherm · Adsorption

INTRODUCTION

Arsenic exists in natural water predominantly as inorganic arsenite (As(III)) and arsenate (As(V)) [1]. Arsenite is about 60 times more poisonous than arsenate and 70 times more toxic than the methylated species. Manifestation of higher doses of inorganic arsenic compounds in the human body leads to specific disease called arsenocosis. Arsenic contamination is of mostly geogenic origin and is known for its high toxicity and its ability to induce skin cancer on long-term ingestion [2]. Most treatment technologies, such as adsorption and precipitation, are effective in removing As(V) from waters because of positive charge on the surface of the adsorbents. On the other hand, under mildly reducing conditions such as in ground waters, As(III) is the thermodynamically stable form, which is presented as non-ionic form of arsenious acid (H_3AsO_3) at neutral pH [3]. Thus, As(III) is more difficult to be removed from water by means of adsorption and coprecipitation due to the lack of electrostatic attraction [4].

In the present work, 8 low cost adsorbents have been screening for the purpose of removing arsenic from water. The potential adsorbent such as shale sedimentary rock (SSR) was then activated by heat and acid treatment. The adsorption parameters, namely, initial As(III) concentration, shaking time and initial pH have been optimized with respect to arsenic spiked deionized water for As(III). Attempts have been made to ascertain appropriate adsorption isotherms. Finally, the SSR has been used for the removal of arsenic from seven real life arsenic contaminated groundwater samples. The overall objective of the present study was to ascertain the capability of the SSR for removing As(III) from water in a single step operation and without any pretreatment.

MATERIALS AND METHODS

Reagents and Glassware: All the reagents used, including acids, were of Analytical grade. HCl and HNO_3 solutions were prepared from concentrated stock solutions and NaOH solutions were prepared from pellets. Stock arsenic

Corresponding Aurthor: Mohd Azraai Kassim, Department of Environmental Engineering, Faculty of Civil Engineering, Universiti Teknologi Malaysia, 81310 Skudai, Johor, Malaysia.

Please cite this article as: Nur Zulaikha Yusof, Mohd Azraai Kassim, Razali Ismail and Abdull Rahim Mohd Yusoff, 2014. Development of Simple and Cost Effective Method for Arsenic(III) Removal. Iranica Journal of Energy and Environment, 5 (3): 287-294

solutions (1000 mg/l) were prepared for As (III) from sodium arsenite ($NaAsO_2$), using deionized water with water conductivity of 18.2 MÙ. All glassware and sample bottles used were soaked with 10% (v/v) HNO_3 and rinsed with deionized water three times. The procedure guarantees decontamination of glassware for working with As.

Preparation and Activation of Adsorbent Materials: A total of 8 different low cost materials were initially screening for their capability to remove As(III) from water. The materials comprise of natural occurring rocks (shale sedimentary rock (SSR) and river sand (RS)), ceramic factory by-products (porcelain glaze (PG), full body porcelain black (FBPB), ceramic glaze (CG), full body porcelain white (FBPW) and clay (C)) and common commercially available water purifier, activated carbon (AC). Some materials (clay and activated carbon) have been previously used for arsenic removal but others were of unknown potential. Natural occurring rocks were collected from residential college at Universiti Teknologi Malaysia, Johor Bharu, Malaysia and ceramic factory by-products were obtained from one of the ceramic manufacturing premises at Johor Bharu, Malaysia. The adsorbent materials obtained were washed with tap water in order to remove unwanted particle and dry in oven for 24 h at 100 °C. After drying process, the materials were crushed using mortar and pestle before being sieved through a 106 µm stainless steel siever. The material size between 106 to 75 µm was collected for adsorption study. In order to study the effect of heating on As(III) removal, all adsorbent material were heated at 180 °C for 1h. After heat treatment, weight loss was determined. For the screening purposes, the removal capacity of raw (RA) and heat treated (HTA) adsorbent were compared and the adsorbent with highest removal of As(III) was chosen for further study.

Heat and acid treatment methods were used to activate the SSR adsorbent in order to compare and select the best activation method for As (III) removal. For heat treatment method,1g of each SSR adsorbent was placed in porcelain dishes and calcined at various temperatures (250, 300, 400, 500, 550 and 600 °C) for 1 h, respectively. In order to find the optimum time for calcinations, the temperature that give high As(III) were chosen and 1 g of each SSR adsorbents were calcined at various time interval (10, 30, 60, 90, 120 min) respectively. At the end of heat treatment process, weight loss of each samples were determined. In the second method, SSR adsorbent was activated through acid treatment. For this purpose, 1 g of each SSR adsorbent were suspended in 20 mL of 0.2-1.0 M HCl solutions and the suspensions were shaken at 200 rpm for 3 h to allow a good contact between acid and adsorbent. The treated SSR adsorbent was separated from the acid solution by filtration and the adsorbent was washed three times with distilled water to remove the residual acid and soluble compounds. It was then dried at 100 °C for 24 h and used for adsorption study.

Batch Adsorption Study: Batch adsorption experiment were performed to examine the effect of initial As(III) concentration (100 -1000 µg /L), contact time (0 - 48h) and pH (pH 2 - 10) on adsorption performance. Adjustment of pH to 7 was done before addition of adsorbent by adding 0.1 M HCl solution. Unless otherwise stated, all experiments were carried out at room temperature 30°C using 0.2 g of adsorbent dose with particle size fraction between 75 to 106 µm. After introducing 100 mL of 500 µg/L As(III) bearing solution, the fiasks (250 mL) were placed on a orbital shaker and shaken for 24 h at the rate of 200 rpm (SW-20C, JULABO, Germany). After the required time, the suspension was filtered through a filter paper (Whatman No. 1) prior to analysis. All samples were analyzed using inductively coupled plasma-mass spectrometry (ICP-MS) (Perkin Elmer DRC-e). An average and standard deviation of three readings for each sample was reported. Samples were filtered through a filter paper (Whatman No. 1) before diluted to a maximum of 60 µg/L total arsenic and acidified to 1% (v/v) HNO_3. All data represents the mean of triplicates. The amount of As(III) adsorbed onto the adsorbents was calculated using the following equation:

$$q = V(C_i - C_t)/M \quad (1)$$

where q is the mass of As(III) adsorbed; V is volume of solution: C_i and C_t are initial As(III) concentration at time t respectively; and M is mass of adsorbent. All standard deviation were calculated using Microsoft Excel 2007.

Application of the Adsorbents to Real Life Groundwater Samples: The adsorbent studied was used for the removal of arsenic in six natural groundwater samples collected from Kandal Province and Kg. Cham, two of the most severe arsenic affected districts of Cambodia. The adsorbent (0.1 g) with particle size of 75 - 106 µm was mixed with 50 mL groundwater sample and shaken at 200 rpm, 30 °C for 24 h.

RESULT AND DISCUSSION

Screening of Low Cost Materials for As(III) Removal: From the screening tests, it was found that all materials were able to reduce As(III) concentration at different extent (Figure 1). The percentage removal range from as low as 0.4 to 60% for raw adsorbent and a slight increment was observed for the heated adsorbent (1.8 to 70%). The screening tests initially indicated that SSR was the best performing adsorbents (raw and heated) since it could remove 60 to 70% of 500 µg/L As(III) in the solution. From the experiment, it was found that, mild heating introduced could increase the removal efficiency of the adsorbent. For SSR adsorbent, the removal was efficiency was increase from 61.25 to 72.59% upon heating. This thing happen might be due to the contaminants present in natural occurring rocks. The present result (heated adsorbent > raw adsorbent) could well be related to the blockage of the rocks surface by the contaminants, thereby preventing access of As(III) to the adsorption site. Contaminants such as organic compound that burn along the heating process was evidence by the weigh loss of the adsorbent. After heating, the blockage by organic compound was reduced and this site now available for As(III) adsorption [5]. Studies by Altundogan *et al*. 2002 [6], revealed that thermal treatment of hydrous metal oxide (in this case iron oxide) strongly influenced the adsorption of metal ion. Therefore SSR was chosen for further adsorption study.

Effect of Method of Activation on as (III) Removal: Activation of SSR adsorbent was carried out to enhance As(III) adsorption. The removal efficiency of heat and acid treatment method was compared in order to select the best activation method for As(III) removal. From the Figure 2 (a) and (b), the removal efficiency of heat treated adsorbent was higher as compared to acid treated adsorbent. The removal efficiency for heat treated adsorbent calcined at 250 to 600 lies between 73 to 99.6%. It was clearly observed that, as the calcinations temperature increase, percentage removal also increased. This might be due to the decrease contaminant level in the adsorbent and provide an active site for As(III) removal. Other than that, calcinations at temperature above 350°C will change the properties of iron oxide present in the adsorbent where the amorphous state of iron oxide will converted to crystalline state. In this sense, the transformation from the amorphous to crystalline state may be advantageous for the long-term stability of the iron oxides and high affinity for As adsorption. Therefore, upon calcinations over 400°C, the residual As(III) concentration down below the MCL (Figure 2 (c)). However, heating above 550°C caused a slight reduction on As(III) removal. This could attribute to clogging of the pores by melted silica.

From the result of As(III) adsorption tests of SSR activated by acid treatment, the percentage removal vary between 71 to 81% with residual As(III) concentration of 78-145 µg/L. As observed from Figure 2(d), an increase in concentration of acid used in acid treatment up to 1.0 M causes an increase in adsorption efficiency of SSR adsorbent. Low As(III) adsorption using acid treated adsorbent might be due to covering the silicic acid of the active oxidic sites. Since heat treatment shows promising result as compare to acid treatment, therefore, heat treatment was chosen as the method for adsorbent activation. The optimum calcinations temperature used for subsequent study was 500°C. The study on the effect of calcinations time, the adsorbent was calcined at 10 to 120 min in order to determine the optimum time for adsorbent calcinations. As shown in Figure 3, all calcinations time show percentage removal greater than 99% with residue As(III) solution below MCL. Sixty minute calcinations time was chosen as an optimized calcinations time since it can lowest the As(III) concentration below 2 µg/L. Subsequent experiment was carried out using SSR adsorbent calcined at 500°C for 1 h.

Adsorption Study for As(III) Removal:

Effect of Initial As(III) Concentration: The effect of initial arsenic concentration was studied by varying the content of arsenic in the solution between 100 to 1000 µg/L. These concentrations were selected due to the results of groundwater sampling from Cambodia. The adsorption of As (III) with varying the initial As concentration are presented in Figure 4 (a) and (b), which represent the percentage As(III) removal, as well as the residual As concentration.

Interestingly, only by introducing 2g/L of SSR adsorbent, it can efficiently remove more than 99% of all As (III) concentration used. SSR adsorbent was able to remove As(III) from the solution to below the maximum concentration limit (MCL) for As (10 µg/L) as set by United State Environmental Protection Act (USEPA) for all concentration except for initial As(III) concentration of 1000 µg/L. As observed in Figure 4 (b), as the initial As(III) concentration increased, the residual As(III) concentration increased or in other word, increasing the

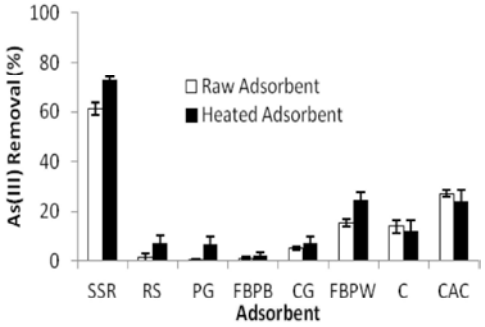

Fig. 1: As (III) removal performance of raw and heated low cost adsorbents.

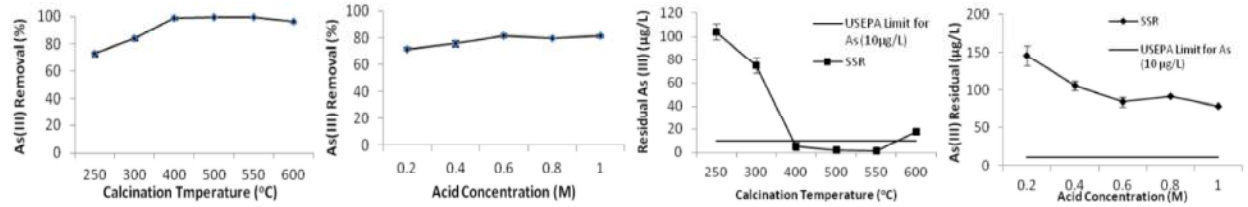

(a) (b) (c) (d)

Fig. 2: Effect of activation method on As(III) removal, (a)effect of heat treatment on As(III) removal, (b) effect of acid treatment on As(III) removal, (c) effect of heat treatment on residual As(III) concentration and (d) effect of acid treatment on residual As(III) concentration

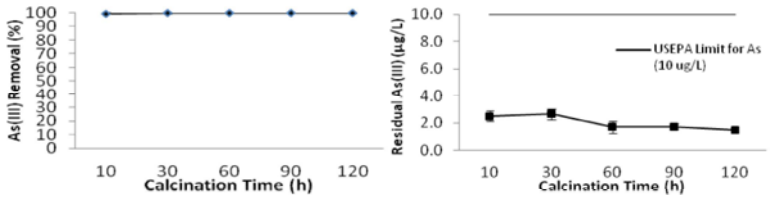

Fig. 3: Effect of calcinations time on As(III) removal and residual As(III) concentration

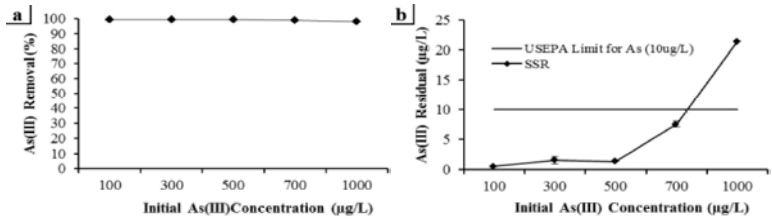

Fig. 4: Effect of initial As(III) concentration on SSR removal based on (a) percentage removal (b) As residual.

initial As concentration was decreased the removal efficiency of the adsorbent. This is because, high As(III) concentration will lead to more ion competing for the available binding sites and more ions are left unadsorbed in solution due to saturation of adsorption site. Contradict, at lower As(III) concentration, all As(III) ions present in the solution could interact freely with available binding site present in SSR adsorbent.

Effect of Initial pH on As(III) Removal: The solution pH is an important factor for all water and wastewater treatment processes because it affects, among others, the speciation of the metals in water. Therefore, experiments were performed in order to investigate the effect of initial pH of solution to be treated regarding and As(III) removal. From the result, the percentage removal of all pH solution vary from 97 to 99.6% (Figure 5 (a)) and the residual As present in the solution for all pH range were above MCL limit

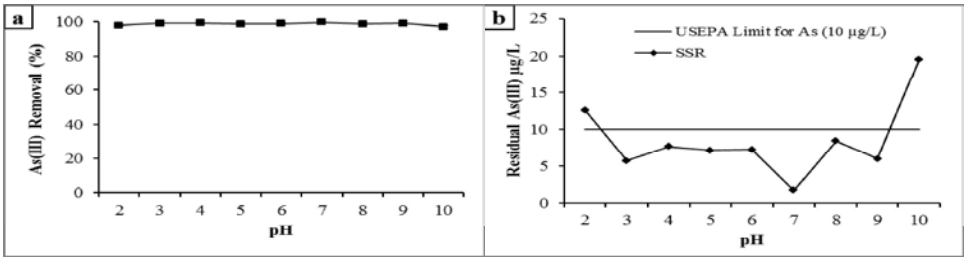

Fig. 5: Effect of initial pH on (a) percentage removal and (b) residual As concentration

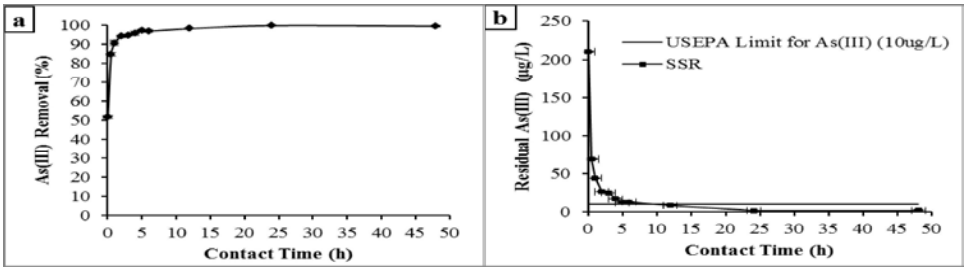

Fig. 6: Effect of contact time on (a) percentage removal and (b) residual As concentration.

except for solution at pH 2 and pH 10. The significant increase in percentage removal with the increase in pH between 2 and 3 was observed (Figure 5 (b)). At pH > 3, the adsorption capacity generally keeps constant. The results evidently show that the SSR adsorbent can efficiently adsorbed As(III) in a wide pH range.

The optimum pH for As(III) adsorption is at pH 7 and above this pH, arsenic removal was found to be decreased. This observation could be well correlated with the point of zero charge (PZC) of iron oxides. Pure iron oxides, whether they can be identified as having a particular crystal structure or not, typically have PZCs in the pH range 7-9 [7]. Over these PZC values, iron oxides are present in the monomeric anionic form [$Fe(OH)_4^-$], hence inappropriate for adsorbing anionic components. High As(III) residual in solution at pH 2 and 10 might be due to the electrostatic repulsion forces, which thrive between iron oxides and arsenic species over the PZC of hydrous ferric oxide [8]. H_3AsO_3 (uncharged form) dominates at pH 2.0-9.2 and the adsorption of this species to SSR adsorbents may occur as inner-sphere bidentate surface complexes with iron oxide surfaces [9]. H_2AsO^{3-} (monovalent anion) is dominant at pH 9.2-12.7. The adsorption of As(III) in this pH range is unfavorable. The negatively-charged monovalent anion becomes predominant and the oxide surface becomes negatively charged, resulting in electrostatic repulsion between As(III) and oxide surface [10].

Effect of Contact Time on As(III) Removal: It is clearly seen from Figure 6 that adsorption of As(III) on SSR adsorbent increases significantly with an increase in contact time. The adsorption rate is quite high in the first 30 min and gradually increases as the adsorption process continues (up to 6 h). The high adsorption rate attributes to the great amount of adsorption sites and the large gradient of As concentration between solution and solid at the beginning of the kinetic test. About 85% of As(III) is removed within 30 min, while only 5-10% in the following 48 h. The slow adsorption rate is likely due to the decrease in the adsorption sites on the surface of the adsorbents [11].

Actually, the adsorption achieves equilibrium in 120 min, when 94 % of As (III) is removed. However, the residue As concentration was lowered to below MCL after 24 h. Therefore a reaction time of 24 h is chosen for further studies. Three general stages normally occur for As adsorption onto solid particles. Firstly, As is transported to the external surface of the adsorbent from bulk solution across the boundary layer (external mass transfer); then As is adsorbed onto particle surfaces; and finally the adsorbed As is exchanged with the structural elements of adsorbent particles or diffused in the internal surfaces of porous materials (intra-particle diffusion) [12]. At the early stage of kinetic tests, first two steps would be predominated, which always happens very fast. However, major processes would be the intra-particle diffusion at the late stage, being considered to be slow [13].

Table 1: Arsenic concentration in real groundwater sample before and after adsorption

Sample	Sampling Location	[As](µg/L) $_{Before}$	[As](µg/L) $_{After}$	As Removal (%)
G1	Ecole Primaire Chong Koh, Kandal Province	697.34	15.1	97.36
G2	Villager at Kors Chamroeun, Kandal Province	99.71	6.44	93.54
G3	Villager at Kg. Siem District, Kg. Cham	20.2	2.68	86.73
G4	Villager at Koh Roka Village, Kg. Siem District, Kg. Cham	68.04	8.78	87.1
G5	Primary School, Kg. Siem District, Kg Cham	85.7	2.25	97.37
G6	Villager at Kg. Siem District, Kg. Cham	44.73	3.19	92.86
G7	As patient, Kg. Siem District, Kg Cham	200.59	4.29	97.86

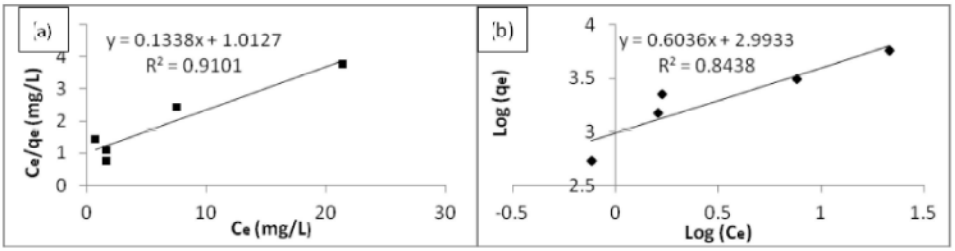

Fig. 7: Langmuir isotherm (a) and Freundlich isotherm (b) of As(III) adsorption on SSR adsorbent.

Application of the SSR Adsorbents to Real Life Groundwater Samples: Seven real groundwater samples obtained from Kandal Province and Kg. Cham were used in order to access the applicability of SSR adsorbent to remove As bearing groundwater. From the result, it can be seen that the As contents of real groundwater sample varied from 20.2 to 697.34µg/L (Table 1). In all water samples, 0.2 g of SSR adsorbent could bring down the As level well below the MCL level except for G1. SSR exhibit higher percentage removals of As in seven groundwater samples, achieving 86.73 to 97.86% efficiency. A slight reduction in As removal efficiency often occurred in ground water could due to the presence of other water contaminant such as Fe_2O_3, phosphate, nitrate and silica. Silica can interfere with the adsorption of As onto iron oxide by forming ferro-silicate.

Adsorption Isotherm: Adsorption isotherm correlate the equilibrium adsorption data with different mathematical models in order to describes a relationship between the amount of chemical adsorbed on adsorbent and the concentration of adsorbate in solution and it is critical in optimizing the use of adsorbents [14,15,16]. The fitness of the equilibrium data obtained from the experiment was evaluated using Langmuir and Freundlich isotherm model. These isotherm equations were used to quantitatively described the effect of increased aqueous As(III) concentrations on the surface loadings of As(III) on SSR adsorbent. The linear form of Langmuir equation is expressed as:

$$C_e/q_e = (C_e/q_m) + (1/K_L q_m) \quad (2)$$

Where q_e is the amount of As(III) uptake at equilibrium (mg/g), K_L is Langmuir constant related to energy of adsorption, C_e is the equilibrium concentration of As(III) in liquid phase (mg/L) and q_m is the monolayer maximum adsorption capacity (mg/g). The linear form of Freundlich model is given as:

$$\log q_e = \log K_f + (1/n) \log C_e \quad (3)$$

where K_f and n are Freundlich constants related to adsorption capacity and adsorption intensity respectively. Langmuir and Freundlich isotherms are plotted in Figure 7 (a) and (b) respectively.

The values of Langmuir parameters b and V_m are evaluated from the linear plot of C_e/q_e vs. C_e, while those of the Freundlich constants from the linear plot of log q_e vs. log C_e.. Results show that correlation coefficients (r^2) for both the isotherms range between 0.8438 and 0.9101, representing a good fit of observed data. In Freundlich model, the distribution coefficient (K) was 984.69 L/g while the Freundlich constant ($1/n$) was 0.6036. In Langmuir model, the adsorption constant b was 7.57 L/mol while the adsorption capacity (q_m) was 0.987 mg/g. As presented in Figure 7, the correlation coefficients (r^2) of Langmuir model were greater than those of Freundlich model, indicating that Langmuir isotherm was better than Freundlich isotherm at describing the experimental results. The dimensionless constant separation factor (R_L) which indicates whether

the adsorption process is unfavorable (R_L>1), linear (R_L=1), favorable (0< R_L<1) or irreversible (R_L=0) can be calculated as:

$$R_L = \frac{1}{1+bC_o} \quad (4)$$

The RL value was found to be less than 1 for adsorption of As(III) onto SSR adsorbent indication that the adsorption process was favorable [17,18]. The *n* value of Freundlich isotherm is related to the strength of adsorption. The calculated *n* is 1.657, denoting favorable adsorption of As(III) onto the SSR adsorbent. The greater the value of n, the stronger the adsorption bond is. The value of *n* usually lies between 1.4 and 5 for similar adsorption on soil [1]. Interestingly, the Langmuir isotherm for As(III) was characterized by a very strong adsorption bond energy as indicated by the constant 'b', typical of monolayer adsorption which clearly indicated that the present SSR was an adsorbent for As(III). This was further supported by a low q_m value which indicated a monolayer adsorption. A good fit of the data with Langmuir isotherm obtained suggest that the adsorption of As(III) is monolayer sorption. In this study, As(III) adsorption capacity of the SSR at 30 °C, estimated from Langmuir isotherm, is 0.987 mg/g. It has been reported that the values of q_m, the Langmuir constant related to saturated monolayer adsorption capacity for natural hematite [19], hematite [20], iron oxide coated sand [21], iron oxide coated cement [22] are 0.104, 0.18, 0.028 and 0.69 mg/g, respectively (synthetic siderite).

CONCLUSION

From the screening of potential low cost adsorbent for As(III) adsorbent, the adsorbent which gave high As(III) removal was chosen for further study namely SSR. Heat treatment method was found the best method for activation of SSR adsorbents based on its removal efficiency. The optimum condition for SSR adsorbent activation is at 500 °C for 1 h. From the adsorption study, 0.2 g of SSR adsorbent could reduce the residual As(III) concentration below than MCL for initial concentration from 100 to 700 µg/L and pH 3 to pH 9 with 24 h contact time. SSR adsorbent also manages to reduce As in real groundwater sample with 86.73 to 97.86% efficiency with the initial As concentration between 20.2 to 697.34 µg/L. A good fit of the data with Langmuir isotherm obtained suggest that the adsorption of As(III) is monolayer sorption.

ACKNOWLEDGEMENT

The authors acknowledge the Ministry of Higher Learning (MoHE), Malaysia for the MyBrain 15 scholarship awarded to Nur Zulaikha Yusof and Universiti Teknologi Malaysia (UTM) for the GUP grant.

REFERENCES

1. Cullen, W.R. and K.J. Reimer, 1989. Arsenic speciation in the environment, Chemical Review, 89: 713-764.
2. Ferguson, J.F. and J. Davis, 1972. A review of the arsenic cycle in natural waters. Water Research, 6: 1259-1274.
3. Smedley, P.L. and D.G. Kinniburgh, 2002. A review of the source, behaviour and distribution of arsenic in natural waters, Applied Geochemistry, 17: 517-568.
4. Streat, M., K. Hellgardt and N.L. Newton, 2007. Hydrous ferric oxide as an adsorbent in water treatment. Part 2. Adsorption studies, Process Safe Environment, 86: 11-20.
5. Li, Y., K. Zhao, Y. Ren, C. Wei and H. Guo, 2011. Removal of arsenite from water by synthetic siderite: Behaviors and mechanisms. Journal of Hazardous Materials. 186: 1847-1854.
6. Zhang, W., P. Singh, E. Paling and S. Delides, 2004. Arsenic removal from contaminated water by natural iron ores, Mine. Engineering, 17: 517-524.
7. Benjamin, M.M., R.S. Slatten, R.P. Bailey and T. Bennett, 1996. Sorption and filtration of metals using iron-oxide-coated sand. Water Research. 30: 2609-2620.
8. Altundogan, H.S., S. Altundogan, F. Tumen and M. Bildik, 2002. Arsenic adsorption from aqueous solutions by activated red mud. Waste Management, 22: 357-363.
9. Katsoyiannis, I.A. and A.I. Zouboulis, 2002. Removal of arsenic from contaminated water sources by sorption onto iron-oxide-coated polymeric materials. Water Research, 36: 5141-5155.
10. Manning, B.A., M.L. Hunt, C. Amrhein and J.A. Yarmoff, 2002. Arsenic(III) and Arsenic(V) reactions with zerovalent iron corrosion products. Environmental Science and Technology, 36(24): 5455-5461.
11. Gim´enez, J., M. Mart´ýnez, J. De Pablo, M. Rovira and L. Duro, 2007. Arsenic sorption onto natural hematite, magnetite and goethite. Journal of Hazardous Materials, 141(3): 575-580.

12. Chunming, S.and W.P. Robert, 2008. Arsenate and arsenite sorption on magnetite: Relations to groundwater arsenic treatment using zerovalent iron and natural attenuation, Water Air Soil Pollution, 193: 65-78.
13. Ho, Y.S. and A.E. Ofomaja, 2005. Kinetics and thermodynamics of lead ion sorption on palm kernel fibre from aqueous solution, Process Biochemistry, 40: 3455-3461.
14. Suyamboo, B.K. and R.S. Perumal, 2011. Equilibrium, thermodynamic and kinetic Studies on adsorption of a basic dye by Citrullus Lanatus Rind, Iranica Journal of Energy and Environment, 3(1): 23-34.
15. Monemtabary, S., M.S. Niasar, M. Jahanshahi and A.A. Ghoreyshi, 2013. Equilibrium and thermodynamic studies of methane adsorption on multi-walled carbon nanotube, Iranica Journal of Energy and Environment 4 (1) Special Issue on Nanotechnology, pp: 17-23.
16. Mehdinia, S.M., K. Moeinian and T. Rastgoo, 2014. Rice husk silica adsorbent for removal of hexavalent chromium pollution from aquatic solutions, Iranica Journal of Energy and Environment 5(2): 218-223.
17. Mahalakshmi, K., S.K. Suja, K.Yazhini, S. Mathiya and G. Jayanthi Kalaivani, 2014. A novel approach to investigate adsorption of crystal violet from aqueous solutions using peels of Annona Squamosa, Iranica Journal of Energy and Environment, 5(2): 113-123.
18., Radnia, H., A.A. Ghoreyshi and H. Younesi, 2011. Isotherm and kinetics of Fe(II) adsorption onto chitosan in a batch process, Iranica Journal of Energy and Environment, 2(3): 250-257.
19. Guo, H.M., D. Stuben and Z. Berner, 2007. Adsorption of arsenic(III) and arsenic(V) from groundwater using natural siderite as the adsorbent, Journal of Colloid Interface Sciences, 315: 47-53.
20. Gupta, V.K., V.K. Saini and N. Jain, 2005. Adsorption of As(III) from aqueous solutions by iron oxide-coated sand, Journal of Colloid Interface Sciences, 288: 55-60.
21. Kundu, S. and A.K. Gupta, 2007. Adsorption characteristics of As(III) from aqueous solution on iron oxide coated cement (IOCC), Journal of Hazardous Materials, 141: 97-104.
22. Singh, D.B., G. Prasad, R.D. Cupainwar and V.N. Singh, 1988. As(III) removal from aqueous solution by adsorption, Water Air Soil Pollution, 42: 373-386.

Persian Abstract

DOI: 10.5829/idosi.ijee.2014.05.03.08

چکیده

در مطالعه حاضر، هشت جاذب سطحی کم هزینه و محلی قابل دسترس (بصورت خام و تیمار شده با حرارت) به منظور تعیین قابلیت آن ها برای حذف آرسنیک(III) غربالگری شده اند. پوسته سنگ های رسوبی (SSR) به عنوان یک جاذب خوب بر اساس حذف بالای آرسنیک(III) انتخاب شده اند. فعال سازی جاذب به وسیله گرما (۵۵۰-۲۵۰ $^{\circ}C$) و تیمار اسیدی (H_2SO_4 ۱-۰/۱ M) به منظور بهترین انتخاب روش تیمار انجام شد. آزمایش های جذب برای بررسی اثر غلظت اولیه آرسنیک (III)، زمان تماس و pH ورودی بر روی حذف آرسنیک(III) بوسیله SSR صورت گرفت. نتایج نشان می دهد که، تنها با حرارت دادن جاذب در دمای ۵۰۰ $^{\circ}C$ به مدت ۱ ساعت، ۰/۲ گرم از SSR توانایی کاهش غلظت آرسنیک(III) باقیمانده به پایین تر از حداکثر غلظت محدود شده (۱۰ µg/L) برای غلظت ورودی ۱۰۰-۷۰۰ µg/L و محدوده pH بهینه ۳ تا ۹ بعد از ۲۴ ساعت از زمان واکنش را دارد. داده های جذب سطحی با معادله Langmuir isotherm به خوبی منطبق شده و تک لایه Langmuir ظرفیتی از ۰/۹۸۷ mg As(III) / g SSR در pH هفت را به همراه داشت. جاذب سطحی SSR به طور موفقیت آمیزی برای حذف آرسنیک از هفت نمونه آب زیرزمینی واقعی که شامل µg/L ۲۰/۲-۶۹۷/۳۴ آرسنیک بودند با بازدهی حذف ۸۶/۷۳ تا ۹۷/۸۶ درصد استفاده شد.

Iranica Journal of Energy & Environment 5 (3): 295-302, 2014
ISSN 2079-2115
IJEE an Official Peer Reviewed Journal of Babol Noshirvani University of Technology
DOI: 10.5829/idosi.ijee.2014.05.03.09

BUT

Purification and Biochemical Characterization of a β-glucosidase from *Penicillium commune* ITV01

[1]*Mariana Alvarez-Navarrete,* [2]*Jaime Alioscha Cuervo-Parra,*
[1]*Jorge Ricaño-Rodríguez and* [1]*Mario Ramírez-Lepe*

[1]Laboratorio de Genética. Unidad de Investigación y Desarrollo en Alimentos. Instituto Tecnológico de Veracruz. Av. Miguel Angel de Quevedo No.2779 Colonia Formando Hogar. Veracruz, Ver. C.P. 91897, Mexico. Tel/Fax 229-9345701 ext.107.
[2]Universidad Autónoma del Estado de Hidalgo. Carrera Pachuca Tulancingo km 4.5 Mineral de la Reforma. Hgo. C.P. 42090, Mexico

Date of Received: April 5, 2014; Date of Accepted in Revised Form: August 4, 2014

Abstract: β-glucosidases have attracted considerable attention in recent years due to their important roles in various biotechnological processes such as hydrolysis of isoflavone glucosides, the production of fuel ethanol from agricultural residues, the release of aromatic compounds from flavorless precursors, among others. In this study, extracellular β-glucosidase induced by cellulose from *Penicillium commune* ITV01 was purified to homogeneity by electrofocusing (IEF) and Sephadex G-100 gel filtration. The enzyme was characterized and the molecular weight was 144.2 kDa as estimated by SDS-PAGE. The isoelectric point determined by IEF was 4.73 and the enzyme was able to hydrolyze cellobiose and cellulose to glucose but not laminarine, xylan, starch, pullulan, colloidal chitin and carboxymethyl-cellulose. Optimal pH and temperature were detected at 5.0 and 50°C, respectively. Stability was observed at temperatures 30 to 50°C and pH values between 5 and 7 for 24 h. Enzyme activity was activated by K^{+}, Cu^{+}, Mn^{++}, Fe^{++}, Cu^{++}, Ca^{++} ions and significantly by Co^{++}. β-glucosidase was completely inhibited by Hg^{++}. In conclusion, the novel β-glucosidase purified from *P. commune* shows great potential for biotechnological uses.

Key words: Purification · Glucosidase · *Peniclillium* · Hydrolase · Fungi · Cellulolytic activity

INTRODUCTION

β-Glucosidases (β-D-glucoside glucohydrolase, EC 3.2.1.21) are an essential component of the cellulase complex [1]. That is widely distributed in nature acting as intermediary of several metabolic routes in animals, plants, yeast and bacteria. This enzyme belong to the glycosyl hydrolases GH1 and GH3 families and several β-glucosidases constitute critical components in enzymatic mixtures which also include endoglucanases and cellobiohydrolases intended for industrial saccharification [2].

β-glucosidases are capable of carrying out the hydrolysis of the β-glycosidic linkages or the aryl and alkyl substituents of the β-glucosides and in the oligosaccharides. β-glucosidases act on the β-link releasing glucose molecules as a byproduct [3]. Due to their hydrolytic characteristics their applications in biotechnological processes, β-glucosidases have a great potential for preparing products with high commercial value; for example, in the production of biofuels, the washed-out of dyes and in the paper industry [4]. In the food industry this enzyme is used to obtain glucosides for the release of aromatic compounds from fruits, to increase the isoflavone content during the fermentation process of soymilk [5] and in the conversion of phenolic antioxidants from defatted residues from the same soymilk [6]. In the pharmaceutical industry β-glucosidases are employed to hydrolyze the glucoside-isoflavones

Corresponding Author: Mario Ramírez-Lepe, Laboratorio de Genética. Unidad de Investigación y Desarrollo en Alimentos. Instituto Tecnológico de Veracruz. Av. Miguel Ángel de Quevedo No. 2779 Colonia Formando Hogar. Veracruz, Ver. C.P. 91897, Mexico. Tel/Fax: 229-9345701 ext.107

Please cite this article as: Mariana Alvarez-Navarrete, Jaime Alioscha Cuervo-Parra, Jorge Ricaño-Rodríguez and Mario Ramírez-Lepe, 2014. Purification and Biochemical Characterization of a β-glucosidase from Penicillium commune ITV01. Iranica Journal of Energy and Environment, 5 (3): 295-302

originating aglicones, which are simple phenols that act as natural antioxidants and at the same time promote their absorption [7].

Reports on the identification and characterization of β-glucosidases in fungi to investigate their potential use are limited. Relevant studies found on fungal β-glucosidases include: *Aspergillus terreus* [8], *Penicillium purpurogenum* [4], *Ceriporiopsis subvermispora* [9] and *Trichoderma harzianum* [3].

Moreover, a fungal source with the ability to produce enzyme with high hydrolytic activity are commonly microorganisms which have mycoparasitism activity [10]. Mycoparasitism happens when one fungus attacks another fungus and lytic enzymes have a fundamental role to hydrolyze the cell wall of the later one [11]. In a previous study, with the purpose of obtain fungal strains with high antagonistic activity on phytopathogenic fungi in our laboratory, we isolated nearly 80 strains from soil samples and from various parts of agricultural crop plants at the Cotaxtla Experimental Station near the city of Veracruz, Mexico. From these strains, we selected fungi with high cellulolytic and mycoparasitism activities. One of these strains (ITV01) with high cellulolytic activity was identified through the sequencing of its ribosomal DNA ITS1-5.8s-ITS2 region as *Penicillium commune*. In this study, we describe the purification and biochemical characterization of the β-glucosidase produced by this strain.

MATERIALS AND METHODS

Strain, Maintenance and Propagation: *Penicillium commune* ITV01 was isolated from soil samples from tomato crops in Cotaxtla Experimental Station (Cotaxtla, Ver. Mexico). For maintenance and propagation of the strain YPD medium (glucose 20 g/L, yeast extract 10 g/L, peptone 20 g/L) was used. To maintain viable cultures, the strain was replanted every 30 days.

β-glucosidase Production: To 100 mL of YPD medium contained in a 250 mL flask was added an inoculum of 1 x 10^6 spores. The inoculated medium was incubated in a Lab-Line rotary shaker at 200 rpm and 28°C for 50 hours. Mycelium from this flask was washed with sterile distilled water and was used to inoculate 1 L of minimal medium with 1% cellulose (Sigma). Minimal medium composition expressed as g/L was as follows: 2 K_2HPO_4, 14 $(NH_4)2SO_4$, $MgSO_4$.7HO 0.3 at pH 5.0 [12]. The medium was incubated in a 2 L flask at 150 rpm and 28°C for 75 hours.

β-glucosidase Activity: Standard assay for β-glucosidase activity was performed at 40°C in 150 mL of sodium citrate buffer 50 mM (pH 4.8) containing *p*-nitrophenyl-β-D-glucopyranoside (*Np*-β-Glu, Sigma) 1 mM and 50 µL of enzyme. The reaction was stopped by adding 50 µL of Na_2CO_3 (JT Baker) 1M after 15 minutes of incubation. The amount of *p*-nitrophenol generated was measured by reading the absorbance at 420 nm. One unit of enzyme activity (UI) was defined as the amount of enzyme that releases 1 µmol of *p*-nitrophenol equivalents per minute [3].

Protein Determination: The amount of soluble protein was determined by the method of Bradford, using bovine serum albumin as a standard [13]. Each assay was performed in duplicate.

Clarification of the Enzymatic Extract and Ultrafiltration: At the end of fermentation, the mycelium was separated from the supernatant by filtering with Whatman filter paper No. 1 and subsequently microfiltered through a 0.45µm membrane (Millipore). The filtrate was subjected to ultrafiltration (Amicon cell capacity: 350 mL) using a cutoff membrane of 500 kDa (Polyethersulfone, Millipore) according to manufacturer's instructions. The obtained filtrate was passed through another membrane cutoff of 10 kDa (Polyethersulfone, Millipore) and the concentrate was recovered. Ultrafiltration was carried out at 4°C with constant magnetic stirring and a pressure of 20 psi using nitrogen gas. The electrical conductivity of the concentrate was preserved in values lower than 780 µS/cm by adding deionized water and ultrafiltering with a 10 kDa membrane.

Isoelectrofocus: The concentrated enzyme obtained was injected into an isoelectrofocus cell of 58 mL capacity (Rotofor ® System, Bio-Rad). The applied power was 15 watts that remain constant during the separation. The temperature inside the cell was kept at 4°C and the separation required 5.5 hours. At the conclusion of the procedures, 20 fractions were recovered, to which were measured the final pH, protein content and β-glucosidase activity was determined. The isoelectric point (pI) of the enzyme was estimated by measuring the pH of the separated fractions by isoelectric focusing that showed β-glucosidase activity.

Gel Filtration Chromatography Sephadex G-100: Fractions with β-glucosidase activity were submitted to a fractionation by gel filtration chromatography using

Sephadex G-100 (Sigma). The gel was packed in a Bio-Rad column of 1.5 cm internal diameter and 120 cm length. The volume occupied by the packing was 190 mL. The column was equilibrated and eluted with 50 mM sodium citrate buffer at pH 4.8. The dead volume of the column was 56 mL, which was calculated using blue dextran 2000 (Sigma) at a concentration of 2 mg/mL. Separation was conducted at room temperature at a flow rate of 0.4332 mL/min. The buffer was fed into the column using a peristaltic pump (Millipore) and a flow adapter (Bio-Rad). The sample was applied using a micropipette onto the drained surface of the gel; after loading the sample a small amount of buffer was applied, drained and followed by filling the surface of the column with more buffer. The volume of the collected fractions was 2 mL. The protein content of each fraction was estimated by measuring their absorbance at 280 nm and interpolating on a graph of absorbance *vs* protein concentration of bovine serum albumin (Sigma) as standard. Fractions with β-glucosidase activity were lyophilized and analyzed by SDS-PAGE.

SDS-PAGE Gel Electrophoresis Staining and Molecular Weight Estimation: Electrophoresis was carried out according to Laemmli [14]. The sample was mixed in a 1:2 ratio with the buffer (Tris-HCl 0.5 M pH 6.8, β-mercaptoethanol, bromophenol blue, SDS 10% and glycerol) and loaded into a discontinuous gel: packing gel, 4% resolving gel, 12% polyacrylamide. Molecular weight markers used were: Kaleidoscope Pre-stained Standard (Bio-Rad) and Pre-stained SDS-PAGE Standards, Low Range (Bio-Rad). A Mini-Protean® 3 Cell (Bio-Rad) was employed and 100 V were applied for 120 minutes. After electrophoresis, the proteins were fixed with a solution of methanol (40%) and acetic acid (10%) with stirring for 30 min. Staining was performed using the revealed kit with silver nitrate and Coomassie (Bio-Rad). The molecular weight was calculated by the interpolation of the sample in the regression curve of the log molecular weight of each marker (log PM) against relative mobility R_f. For the estimation of molecular weight by gel filtration chromatography was applied 0.5 mL of marker (Gel Filtration Standard 151.1901, Bio-Rad) on the surface of the column and eluted with sodium citrate buffer 50 mM pH 4.8 at a rate of 0.4332 mL/min. and fractions of 2 mL were collected.

β-glucosidase Characterization

Effect of pH and Temperature on Enzymatic Activity: The effect of pH on enzymatic activity was assessed by incubating 21 mU of enzyme in 50 mM citrate-phosphate buffer at a pH range of 3.0 to 7.0 for 1 h at 50 °C. Enzyme activity was expressed as relative activity (%) in relation to the maximum enzyme activity value obtained. Temperature effect was evaluated by incubating 21 mU of enzyme in the same buffer at pH 5.0, at temperatures of 30 to 70°C at 10°C intervals. Subsequently, β-glucosidase activity was determined.

Effect of pH on enzyme stability: The enzyme (21 mU) was incubated at 50°C in 50 mM citrate-phosphate buffer in a pH range of 3.0 to 7.0 at one pH unit intervals during 24 h. To determine the stability of the enzyme, samples were incubated (21 mU) in the same buffer at pH 5.0 at a temperature range of 30 to 70°C. Subsequently, β-glucosidase activity was determined.

Effect of Metal Ions, SDS and EDTA on Enzymatic Activity: The solutions of the following metal ions were prepared in 50 mM sodium citrate buffer (pH 4.8): Hg^{2+}, Zn^{2+}, Ca^{2+}, Mg^{2+}, Co^{2+}, Mn^{2+}, K^{+}, Cu^{3+}, Fe^{2+}, SDS and EDTA. Final concentration was 5 mM. Enzyme (15.5 mU) was pre-incubated with each of these metal ions for 30 min at room temperature. Residual enzyme activity was evaluated by incubating the enzyme at 50°C and pH 5.0 in a 1% cellulose solution for 30 min. Each assay was performed in duplicate. After incubation, the reaction was stopped by adding 3 mL of the DNS reagent and the amount of reducing sugars released at 540 nm was determined [15]. ANOVA was applied followed of Tukey's tests. All the analyses were conducted using Statistix 9.0 software [16].

RESULTS AND DISCUSSION

β-glucosidase Enzyme Production: After 50 hours of incubation of *P. commune* ITV01 in 100 mL flask, abundant growth was observed in form of pellets. The culture was transferred to minimal medium with cellulose as the sole carbon source (1000 mL) and after 75 hours of incubation the enzymatic activity in the supernatant was determined. A specific activity of 79.72 U of β-glucosidase/mg protein in the fermentation product was measured. Table 1 shows the enzyme purification steps; the enzyme was partially purified with

Table 1: Purification steps of β-glucosidase enzyme isolated from *Penicillium commune* ITV01

Purification step	Volume (mL)	Total Protein (mg)	Total activity (mU)	Specific activity (mU/mg)	Purification fold	Yield (%)
Crude extract	1000	57.17	4,557	79.72	1	100
Clarified extract	950	54.31	4,329	79.72	1	95
Ultrafiltration (10-500 kDa)	58	28.8	4,264	148	1.86	93.56
Isoelectric-focusing (F7)	2	0.453	959	2,120	26.59	21.04
Gel filtration (F30)	2	0.35	873	2,496	31.3	19.16

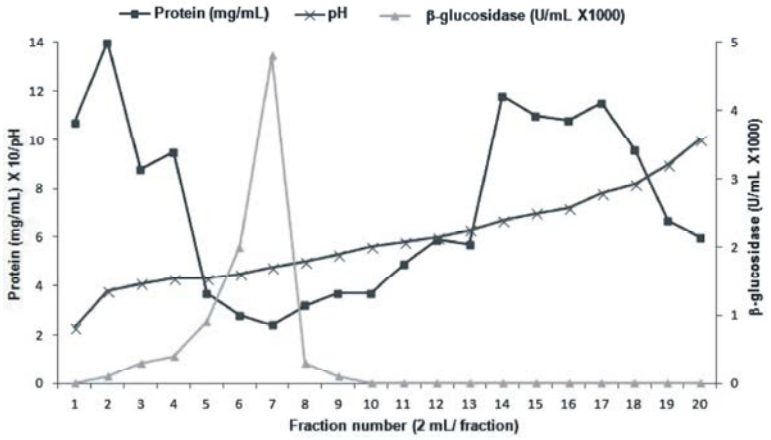

Fig 1: Profile of separation by electrofocusing of β-glucosidase from *P. commune* ITV01

a recovery of 19.16% and a purification factor of 31.3. The results for the β-glucosidase production suggest that this method of purification is favorable for the enzyme. β-glucosidases are not dependent on other enzymes to carry out their activity, as is the case of endoglucanases and exoglucanases, which act synergistically on cellulose degradation; therefore, its total activity was not drastically decreased as the purification advanced.

Ultrafiltration: In the ultrafiltration step the enzymatic activity and protein concentration were determined in fractions smaller than 10 kDa, in the 10-500 kDa fractions and in the fraction with molecular sizes greater than 500 kDa. Neither enzymatic activity nor proteins were detected in the fraction of less than 10 kDa. The highest enzymatic activity was detected in the 10-500 kDa fractions (4,254 U/mL and 0.497 mg protein/mL). However, in the highest fraction (500 kDa) 14% of the total activity of β-glucosidase was retained (600 U/mL, 0.210 mg protein/mL). It is suggested that the activity in the retainded is due to the formation of a layer on the surface of the membrane that prevents the enzymes with molecular weights smaller than 500 kDa pass through.

Isoelectric Focusing Fractionation (IEF): An enzyme concentrate of 58 mL was loaded to an isoelectric focusing fractionation equipment. The pH gradient formed by ampholytes was 2.2 to 10.0 (Figure 1). At this stage, 20 fractions were obtained of which three had β-glucosidase activity (F5, F6 and F7). Figure 1 shows that the distribution of protein is concentrated at both ends of the pH gradient. In the case of fractions with β-glucosidase activity, the protein content was low. According to the pH gradient obtained, the isoelectric point of the F7 (β-glucosidase) is 4.73. For isoelectric focusing fractionation, there are few studies that report the pI of this enzyme. In all of these, the values were low and consistent with our data. Accordingly, the pI value reported for β-glucosidase from *Aspergillus oryzae* is 4.9 [17] and for *Bacillus polymyxa* is 4.6 [18].

IEF Separation of Fraction 7 (F7) by Gel Filtration Chromatography with Sephadex G-100: Initially, the fraction 7(F7) of isoelectric focusing with high β-glucosidase activity, was separated on a gel filtration chromatography column Sephadex G-75. However, a significant amount of protein with β-glucosidase activity was detected in the void volume, so that separation was not efficient. These data suggests that the protein was greater than 80 kDa, which is the maximum separation limit of Sephadex G75. For this reason, a longer column was prepared loaded with a resin with a greater range for separation (Sephadex G-100 which can separate from 4 to 150 kDa, according to manufacturer's information). Therefore, F7 with β-glucosidase activity was applied

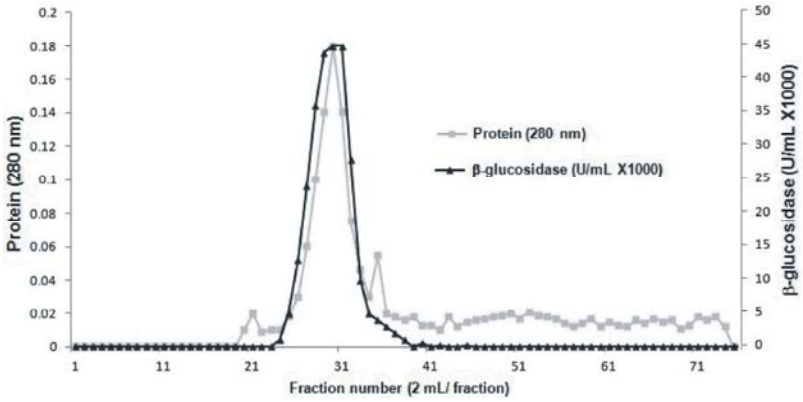

Fig 2: Profile of separation of β-glucosidase from *P. commune* ITV01 by gel filtration chromatography (Sephadex G100).

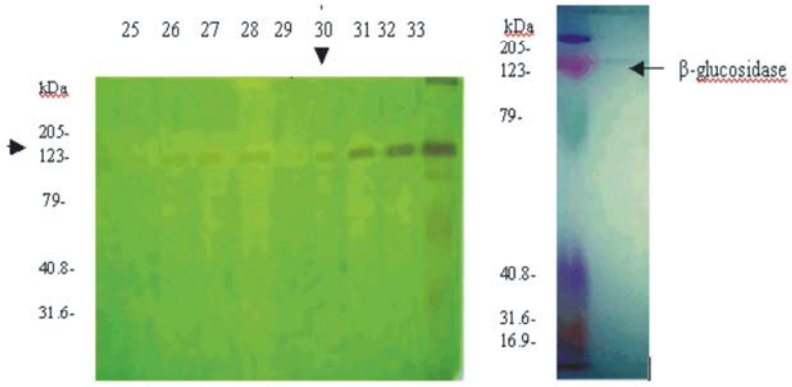

Fig 3: SDS-PAGE electrophoretic analysis of the β-glucosidase. (a) Silver staining gel of the fractions recovered from the filtration chromatography gel. The arrow indicates the fraction 30, which has the maximium β-glucosidase activity. (b) Gel revealed with Coomassie blue. The arrow indicate the purified β-glucosidase in lane 2. The marker used is the Kaleidospe of Bio-Rad (myosin, 205, β-galactosidase, 123; bovine serum albumin, 79; carbonic anhydrase, 40.8, soybean trypsin inhibitor, 31.6; lysozyme, 16.9; aprotinin, 6.6).

to this second gel filtration column (Sephadex G-100). The separation profile is shown in Figure 2. Starting from fraction 25, enzymatic activity was observed, reaching its maximum value in fraction 30.

Molecular Weight Estimation of β -glucosidase: The activity detected in fractions 25 to 33 collected from the column coincides with the approximate 140 kDa bands that were observed in the electrophoresis gel of the samples that was revealed with silver stain (Figure 3a). In the development of sample F30 with Coommassie blue (Figure 3b) a band corresponding to 144.2 kDa was found, as calculated with the Kaleidoscope marker (Bio-Rad). Furthermore, estimation of molecular weight using the gel filtration column was of 150.42 kDa (data not shown). The molecular weights estimated by both methods were very similar and the small differences can be attributed to the variability of each method. For the molecular weight estimation, values reported for β-glucosidase are 98kDa for *Trichoderma reesei* [19], 130kDa for *Aspergillus oryzae* [17] and 275kDa for *Pichia pastoris* [20]. A β-glucosidase 43kDa monomer of the fungus *Aspergillus oryzae*, is the smallest known β-glucosidase among the aerobic mushrooms [21]. In general, β-glucosidases of microbial origin have high molecular weights. By migration of the enzyme SDS-PAGE electrophoresis we suggest that the enzyme is monomeric. This result is consistent with those reported in the literature since the β-glucosidases of molecular weights of more than 200 kDa have more than one monomer. For example β-glucosidase from *Aureobasidium pullulans* with molecular weight of 340 kDa has two subunits [22], the enzyme of 275 kDa from *Pichia pastoris* has 4 subunits [20].

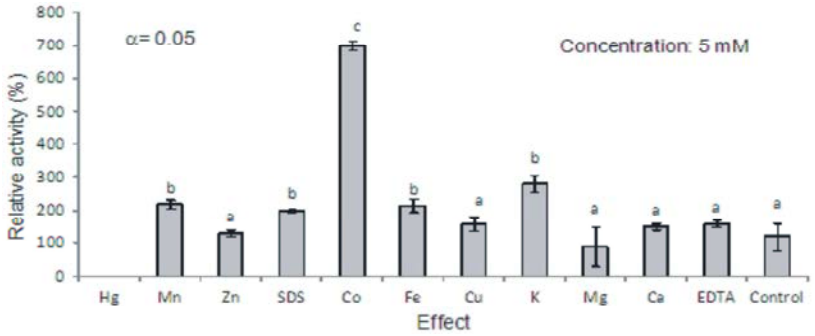

Fig 4: Effect of metal ions, EDTA and SDS on β-glucosidase activity

Effects of pH and Temperature on Enzymatic Activity and Stability: The influence of pH and temperature on β-glucosidase was determined. The optimum pH obtained was 5 after 24 h of incubation. At pH values of 5, 6 and 7, the enzymatic activity retained was greater than 70%, compared to the activity after 1 hour. With respect to temperature, the optimum was 50°C and the enzyme maintained stability greater than 70% at 30 and 40°C. β-glucosidase genes expressed in yeast are similar in pH and optimum temperatures; however, it may have more stability at higher temperatures. For example, the cloning of β-glucosidase in *P. pastoris* stabilizes the enzyme at pH values between 4 and 7 and is stable at 70°C [23].

Substrates, Effectors Effect on Enzymatic Activity of EG144 and Specificity Kinetic Parameters: β-glucosidase enzymes are heterogeneous; although there are no specific criteria for classification, substrate specificity and amino acid sequence can be used [24]. In this study β-glucosidase was tested on different substrates with α and β configurations. The enzyme preparation showed no activity on starch (α-1,4 and α-1,6 glucose), xylan (β-1,4 xylose), swarm (α-1,4), laminarin (β-1,3 glucose), colloidal chitin (β-1,4, N-acetylglucosamine) and CMC (β-1,4 CMC glucose). The substrates that showed activity were cellulose and cellobiose. According to Enari and Niku-Paavola [25] β-glucosidases are classified into three groups: (1) those with high affinity for aryl β-glucoside (2) those which hydrolyze oligosaccharides such as cellobiose and (3) those that are active on both substrates.

β-glucosidase of this study showed a higher activity in the presence of K^{+}, Cu^{+}, Mn^{++}, Fe^{++}, Cu^{++}, Ca^{++} ions and remarkably high with Co^{++}. EDTA did not significantly affect its activity, as also did not affect SDS and Mg^{++} and Zn^{++} ions (Figure 4). These results suggest that it is not a metalloenzyme, since it was not affected by EDTA [26]. Its activity decreased markedly in the presence of Hg^{++} ions. In numerous studies it has been reported that Hg^{++} ions have a negative effect on the activity of many enzymes [24]. The sensitivity to Hg^{++} suggests the existence of at least one catalytically important sulfhydryl group [27]. On the other hand, Co^{++} ions increased enzyme activity. In general cellulases are stimulated by these ions [28, 29].

The kinetic parameters, K_m and V_{max} values were determined using cellobiose as substrate. The estimated values for K_m and V_{max} were 2.3 mM and 670 U/mg, respectively. Joo *et al*. [30] reported values of K_m and V_{max} of 5.5 mM of 1120 U/mg of protein on cellulose. Ng *et al*. [31] reported a K_m of 1.2 mM and V_{max} of 85.93 U/mg of rice flour.

CONCLUSIONS

We purified and characterized a monomeric β-glucosidase from *P. commune* with important extracellular characteristics. It has good stability to pH and temperature, with a high affinity to cellulose, as shown by its low K_m value. These features could prove advantageous for easy recovery and shall provide potential uses in the food industry.

REFERENCES

1. Peshin, A and J.M.S. Mathur, 1999. Purification and characterization of β-glucosidase from Aspergillus niger strain 322, Letters in Applied Microbiology. 28(5): 401-404.
2. Bohlin, C., E. Praestgaard, M.J. Brauman, K. Borch, J. Praestgaard, N. Rune and M.P. Westh, 2013. A comparative study of hydrolysis and transglycosylation activities of fungal β-glucosidases. Applied Microbiology and Biotechnology, 97(1): 159-169.

3. Yun, S.I., C.S. Jeong, D.K. Chung and H.S. Choi, 2001. Purification and some properties of a β-glucosidase from Trichoderma harzanium Type C-4. Bioscience Biotechnology and Biochemistry Journal, 65(9): 2028-2032.
4. Dhake, A.D. and M.B. Patil, 2005. Production of ß-Glucosidase by Penicillium purpurogenum. Brazilian Journal of Microbiology, 36(2): 170-176.
5. Otieno, D.O. and N.P. Shah, 2007. Endogenous β-glucosidase and β-galactosidase activities from selected probiotic microorganisms and their role in isoflavone biotransformation in soymilk. Journal of Applied Microbiology, 103(4): 910-917.
6. McCue, P. and K. Shetty, 2003. Role of carbohydrate-cleaving enzymes in phenolic antioxidant mobilization from whole soybean fermented with Rhizopus oligosporus. Food Biotechnology, 27(l): 27-37.
7. Hendrich, S., 2002. Bioavailability of isoflavones. Journal of Chromatography, 777(1-2): 203-210.
8. Sidik, N.M., A.H. Abdul-Manan, R.M. Yazid and S.A. Sharifuddin, 2012. Gene cloning and characterization of a new glycosyl hydrolase family 3-β-glucosidase from Aspergillus terreus SUK-1. Australian Journal of Basic and Applied Sciences, 6(3): 106-111.
9. Magalhaes, P.O., A. Ferraz and A.F.M. Milagres, 2006. Enzymatic properties of two β-glucosidases from Ceriporiopsis subvermispora produced in biopulping conditions. Journal of Applied Microbiology, 101(2): 480-486.
10. Atanasova, L., S. Le Crom, S. Gruber, F. Coulpier, V. Seidl-Seiboth, C.P. Kubicek and I.S. Druzhinina, 2013. Comparative transcriptomics reveals different strategies of Trichoderma mycoparasitism. BMC Genomics, 14: 121-136.
11. López-Mondéjar, R., M. Ros and J.A. Pascual, 2011. Mycoparasitism-related genes expression of Trichoderma harzianum isolates to evaluate their efficacy as biological control agent. Biological Control, 56(1): 59-66.
12. Marcello, C.M., A.S. Steindorff, S.P. da Silva, R.N. Silva, L.A.M. Bataus and C.J. Ulhoa, 2010. Expression analysis of the exo-β-1,3 glucanase from the mycoparasitic fungus Trichoderma asperellum. Microbiological Research, 165(1): 75-81.
13. Bradford M.M., 1976. A rapid and sensitive method for the quantitation of microgram quantities of protein utilizing the principle of protein-dye binding. Analytical Biochemistry, 72(1-2): 248-254.
14. Laemmli, U.K., 1970. Cleavage of structural proteins during the assembly of the head of bacteriophage T4. Nature, 227(5259): 680-685.
15. Miller, G.L., 1959. Use of dinitrosalicylic acid reagent for determination of reducing sugar. Analytical Chemistry, 31(3): 426-428.
16. Analytical Software, 2008. Statistix 9. Analytical Software. Tallahassee, FL.
17. Riou, C., J.M. Salmon, M.J. Vallier, Z. Günata and P. Barre, 1998. Purification, characterization and substrate specificity of a novel highly glucose-tolerant β-Glucosidase from Aspergillus oryzae. Applied and Environmental Microbiology, 64(10): 3607-3614.
18. Painbeni, E., S. Valles, J. Polaina and A. Flors, 1992. Purification and characterization of a Bacillus polymyxa beta-glucosidase expressed in Escherichia coli. Journal of Bacteriology, 174(9): 3087-3091.
19. Saloheimo, M, J. Kuja-Panula, E. Ylösmäki, M. Ward and M. Penttilä, 2002. Enzymatic properties and intracellular localization of the novel Trichoderma reesei β-glucosidase BGLII (Cel1A). Applied and Environmental Microbiology, 68(9): 4546-4553.
20. Turan, Y. and M. Zheng, 2005. Purification and characterization of an intracellular β-glucosidase from the methylotrophic yeast Pichia pastoris. Biochemistry, 70(12): 1363-1368.
21. Saha, B.C. and R.J. Bothast, 1996. Production, purification and characterization of a highly glucose-tolerant novel β-glucosidase from Candida peltata, Applied and Environmental Microbiology, 62(9): 3165-3170.
22. Saha, B.C., S.N. Freer and R.J. Bothast, 1994. Production, purification and properties of a thermostable β-glucosidase from a color variant strain of Aureobasidium pullulans. Applied and Environmental Microbiology, 60(10): 3774-3780.
23. Liu, D., R. Zhang, X. Yang, S. Song, Y. Miao and Q. Shen, 2012. Characterization of a thermostable β-glucosidase from Aspergillus fumigatus Z5 and its functional expression in Pichia pastoris X33. Microbial Cell Factories, 11:25. doi:10.1186/1475-2859-11-25.
24. Singhania, R.R., A.K. Patel, R.K. Sukumaran, C. Larroche and A. Pandey, 2013. Role and signi?cance of beta-glucosidases in the hydrolysis of cellulose for bioethanol production. Bioresource Technology, 127: 500-507.

25. Enari, T.M. and M.L. Niku-Paavola, 1987. Enzymatic hydrolysis of cellulose: Is the current theory of the mechanism of hydrolysis valid? Critical Reviews in Biotechnology, 5(1): 67-87.
26. Elshafei, A.M., M.M. Hassan, M.A.E. Abouzeid, D.A. Mahmoud and D.H. Elghonemy, 2012. Purification, characterization and antitumor activity of L-asparaginase from Penicillium brevicompactum NRC829. British Microbiology Research Journal, 2(3): 158-174.
27. Singh, J., Batra, N. and R.S. Chander, 2004. Purification and characterization of alkaline cellulase produced by a novel isolate, Bacillus sphaericus JS1. Journal of Indian Microbiology and Biotechnology, 31(2): 51-56.
28. Story, S.V., C. Shah, F.E. Jr. Jenney and M.W.W. Adams, 2005. Characterization of a novel zinc-containing, lysine-specific aminopeptidase from the hyperthermophilic archaeon Pyrococcus furiosus. Journal of Bacteriology, 187(6): 2077-2083.
29. Saha, B.C., 2004. Production, purification and properties of endoglucanase from a newly isolated strain of Mucor circinelloides. Process Biochemistry, 39(12): 1871-1876. 67-87.
30. Joo, A.R., M. Jeya, K.M. Lee, H.J. Moon, Y.S. Kim and J.K. Lee, 2010. Production and characterization of β-1-4 glucosidase from a strain of Penicillium pinophilum. Process Biochemistry, 45(6): 851-858.
31. Ng, L.S., C.W. Li, S.P. Chan, J.L. Chir, P.T. Chen, C.G. Tong, S.M. Yu and H.T.K. David, 2010. High level production of a thermophilic β-glucosidase from Penicillium citrinum YS40-5 by solid-state fermentation with rice bran. Bioresource Technology, 101(4): 1310-1317.

Persian Abstract

DOI: 10.5829/idosi.ijee.2014.05.03.09

چکیده

بتا گلوکزیداز در سالهای اخیر توجه زیادی را با نقش مهم آن در فرآیندهای مختلف بیوتکنولوژی مانند هیدرولیز گلوزید ایزوفلاون ، تولید سوخت اتانولی از پسماندهای کشاورزی ، آزاد کردن ترکیبات آروماتیک از مواد اولیه طعم دار نشده و ... به خود جلب نموده است. در این مطالعه بتاگلوکزیداز خارج سلولی با تحریک *Penicillium commune ITV01* توسط سلولز تولید و توسط فرایند electrofocusing (IEF) با استفاده از فیلتراسیون ژل Sephadex G-100 ، خالص و همگن بدست آمده است. این آنزیم مشخصه یابی گردید و وزن مولکولی آن بوسیله SDS-PAGE برابر با ۱۴۴/۲ کیلودالتون تخمین زده شد. نقطه ایزوالکتریک با IEF ۴/۷۳ بدست آمد و همچنین این آنزیم قادر بود تا سلوبیوز و سلولز را به گلوکز هیدرولیز کند اما در مورد لامینارین ، زایلن ، نشاسته ، pullulan، کیتین کلوئیدی و کربوکسی متیل سلولز اینگونه نبود. pH و دمای بهینه به ترتیب ۵ و ۵۰ درجه سانتیگراد بود. همچنین در بازه دمایی ۳۰ تا ۵۰ درجه سانتیگراد و مقادیر pH بین ۵ تا ۷ به مدت ۲۴ ساعت پایدار بود. فعالیت آنزیمی توسط یونهای Ca^{++} , Cu^{++} , Fe^{++} , Mn^{++} , Cu^{+} ,K^{+} و بویژه Co^{++} فعال شد. بتاگلوکزیداز بطور کامل توسط Hg^{++} مهار گردید. در نتیجه بتاگلوکزیداز جدید خالص سازی شده از *P. commune* پتانسیل خوبی برای استفاده در بیوتکنولوژی دارد.

Iranica Journal of Energy & Environment 5 (3): 303-312, 2014
ISSN 2079-2115
IJEE an Official Peer Reviewed Journal of Babol Noshirvani University of Technology
DOI: 10.5829/idosi.ijee.2014.05.03.10

BUT

Extraction and Analysis of Pectin from Citrus Peels: Augmenting the Yield from *Citrus limon* Using Statistical Experimental Design

P. Kanmani, E. Dhivya, J. Aravind and K. Kumaresan

Department of Biotechnology, Kumaraguru College of Technology, Coimbatore - 641049, India

Date of Received: July 4, 2014; Date of Accepted in Revised Form: August 4, 2014

Abstract: Pectin is a structural hetero polysaccharide, commonly obtained from the peels of citrus fruits and finds prime commercial use as a gelling agent and stabilizer in food industries. In the present study, pectin was extracted using alcohol precipitation method from the peels of orange (*Citrus sinensis*), sweet lime (*Citrus limetta*) and lemon (*Citrus limon*). When the extraction conditions were varied one-at-a-time, a maximum yield of 36.71% was obtained from *C. limon*, after which the yield was further enhanced using the Box-Behnken Design of Response Surface Methodology. Optimum conditions for the extraction process were established to be pH 3.5, temperature 65°C and time 67.5 min. The interaction effects of these variables were studied using 3-D and contour plots. A 1.5-fold increase in pectin yield was obtained as a result of this experimental design. Analysis of variance indicated the significance of the model. The pectin obtained was then subjected to qualitative and quantitative analyses and found to contain desirable methoxyl, hyaluronic acid contents and degree of esterification. Functional groups present in the pectin were investigated using FTIR spectroscopy. The overall results point towards the amenability of the extracted pectin for industrial applications.

Key words: Pectin · *Citrus limon* · Yield · Optimization · Response surface methodology · FTIR.

INTRODUCTION

Pectin, a complex mixture of polysaccharides occurring in the primary cell walls of terrestrial plants, is a high value functional food ingredient. It consists of a linear backbone of α-(1-4)-D-galacturonic acid residues partially esterified with methanol, with periodic interruptions to L-rhamnose residues that make the backbone irregular and with some other neutral sugars present as side chains. The general makeup of the pectin content varies with the ripening of the fruit [1].

Pectin is produced commercially in the form of white to light brown powder, mainly extracted from citrus fruits and is used in food as a gelling agent particularly in jams and jellies. It is also used in fillings, sweets, as a stabilizer in fruit juices and milk drinks and as a source of dietary fiber [2]. Several studies have reported novel pectin usages, like biodegradable water-soluble films, bulking agents, coating agents, chelators, emulsifiers and viscosity modifiers.

The amount, structure and chemical composition of the pectin differs between plants, within a plant over time and in different parts of a single plant [3]. Although pectin occurs commonly in most of the plant tissues, the number of sources that may be used for commercial manufacture of pectin is limited. This is because the ability of pectin to form a gel depends on molecular size and the degree of esterification (DE).

At present, commercial pectins are almost exclusively derived from citrus peel or apple pomace, both of which are by-products of juice manufacturing units. Apple pomace contains 10-15% of pectin on a dry matter basis. Citrus peel contains relatively higher, i.e. 20-30% of pectin as compared to that of apples [4]. Among the physical properties, citrus pectins are light cream or light tan in color, whereas apple pectins are often darker.

Commercially, pectin is extracted by treating the raw material with hot dilute mineral acid at pH 2, for 2-4 h duration and pectic substances are precipitated using ethanol or isopropyl alcohol [5]. The precipitated pectin

Corresponding Author: P. Kanmani, Department of Biotechnology, Kumaraguru College of Technology, Coimbatore - 641049, India. Tel: +91422 2669401.

Please cite this article as: P. Kanmani, E. Dhivya, J. Aravind and K. Kumaresan, 2014. Extraction and Analysis of Pectin from Citrus Peels: Augmenting the Yield from Citrus limon Using Statistical Experimental Design. Iranica Journal of Energy and Environment, 5 (3): 303-312

is separated and washed with alcohol to remove impurities. It is dried, ground to a powder and blended with other additives, if necessary. The extracted pectin can be categorized into two major types depending on its degree of esterification (DE): high-methoxyl pectin (HMP, > 50% DE) and low-methoxyl pectin (LMP, < 50% DE).

The solubility and viscosity of pectin solution are related to the molecular weight, degree of esterification, concentration of the preparation, pH and presence of counter ions in the solution [6]. Viscosity, solubility and gelation are generally related to physical properties of the product. For example, factors that increase gel strength will increase the tendency to gel, decrease solubility and increase viscosity and vice versa. These properties of pectins are a function of their structure.

The present investigation aims to extract pectin from the peels of citrus fruits namely, *Citrus sinensis (*orange), *Citrus limon* (lemon) and *Citrus limetta* (sweet lime) using citric acid; to optimize the yield of pectin by varying one-factor-at-a-time (OFAT) and response surface methodology (RSM); and to characterize the extracted pectin by both qualitative and quantitative methods, thereby gauging its appropriateness for industrial usage.

MATERIALS AND METHODS

Chemicals: All reagents and chemicals used were of analytical grade. For the extraction process, citric acid was purchased from HiMedia, India and ethyl alcohol from SD Fine Chemicals, India.

Sample Preparation: Lemon, sweet lime and orange were purchased from the local market. They were split into four parts and the peels were removed, which were then cut into smaller pieces, shade dried, ground to a consistency intermediate to coarse and fine (for avoiding clumping during solvent extraction) and stored at ambient temperature for further use.

Pectin Extraction from Citrus Peels

Effects of pH and Temperature on the Extraction Process: The effects of these factors on the yield of pectin from different citrus peels were studied by varying one-factor-at-a-time, while keeping the other one constant. The optimum conditions giving a good yield from each source were ascertained in this preliminary study.

For the extraction process, a dry mass of 5 g was subjected to extraction by adding 90 mL of distilled water followed by 10 mL of citric acid of different pH values ranging from 1.2 - 4.2. The mixture was then heated at different temperatures of 40 - 90°C and continuously stirred for 1 hour. The hot acid extract was filtered through a Whatman No. 1 filter paper. The filtrate was coagulated using an equal volume of 95% ethanol and left for 2 h to allow the pectin to float on the surface. The gelatinous pectin flocculants were then skimmed off. The extracted pectin was then filtered and washed 2 - 3 times with ethyl alcohol to remove any remaining impurities [7]. Finally, the precipitate was dried at 35 - 40°C in hot air oven and percentage yield was calculated.

$$Ypec(\%) = \frac{P}{Bi} * 100 \quad (1)$$

where, Y_{pec} is the yield of pectin in (%), P is the amount of extracted pectin in g and B_i is the initial amount of fruit peel powder.

Optimization of Pectin Yield

Statistical Design Using Response Surface Methodology: Statistical process optimizations using RSM have been widely employed by a number of researchers [8, 9]. This statistical optimization was limited to the pectin from *C. limon*. Box-Behnken design of RSM was used to investigate the effects of different independent variables - pH, temperature (T) and extraction time (ET) on the response, pectin yield (Y_{pec}). The levels of these variables were selected based on preliminary experiments [10]. The experiments were performed in random order. All analyses were done using the software Design Expert 8.0 (trial version). The experimental design consisted of a set of points lying at the midpoint of each edge and the replicated center point of a multidimensional cube. The polynomial equation generated by the software is as follows:

$$Yi = b0 + b1X1 + b2X2 + b3X3 + b12X1X2 + b13X2X3 + b11X11 + b22X22 + b33X33 \quad (2)$$

where, Y_i is the dependent variable, b_0 is the intercept, b_1 to b_{33} are the regression coefficients and X_1 to X_{33} are the independent variables. The experimental design set up is summarized in Table 1.

Physicochemical Characterization of the Pectin Samples: The dried pectin samples obtained from all three fruit peels were subjected to the following qualitative and quantitative tests in order to characterize them.

Qualitative tests

Color

This was done by visual observation.

Table 1: Experimental design set up of RSM and responses obtained

	Independent Variables			Response
Run no.	pH	*T (°C)	*ET (min)	Y_{pec} (%)
1	3.5 (0)	90 (+1)	15 (-1)	21.45
2	3.5 (0)	65 (0)	67.5 (0)	55.76
3	5.5 (0)	40 (-1)	67.5 (0)	18.73
4	1.5 (-1)	65 (0)	15 (-1)	34.79
5	5.5 (+1)	65 (0)	15 (-1)	9.59
6	3.5 (0)	40 (-1)	15 (-1)	18.98
7	1.5 (-1)	90 (+1)	67.5 (0)	11.62
8	5.5 (+1)	90 (+1)	67.5 (0)	10.65
9	3.5 (0)	65 (0)	67.5 (0)	55.98
10	3.5 (0)	65 (0)	67.5 (0)	56.71
11	3.5 (0)	40 (-1)	120 (+1)	9.82
12	1.5 (-1)	65 (0)	120 (+1)	11.92
13	5.5 (+1)	65 (0)	120 (+1)	8.92
14	1.5 (-1)	40 (-1)	67.5 (0)	23.93
15	3.5 (0)	65 (0)	67.5 (0)	53.88
16	3.5 (0)	65 (0)	67.5 (0)	54.91
17	3.5 (0)	90 (+1)	120 (+1)	22.75

*T – temperature, ET – extraction time. Each one of the variables was studied at 3 different levels: -1, 0 and +1. Extraction was performed using citric acid in all cases

Solubility of Dry Pectin in Cold and Hot Water: A 0.25g of the pectin samples were separately placed in two conical flasks, followed by addition of 10 mL of 95% ethanol and 50 mL of distilled water. The mixture in the second flask was shaken vigorously to form a suspension which was then heated at 85-95°C for 15 min [11].

Solubility of Pectin Solution in Cold and Hot Alkali: To 1 mL of 0.1 N NaOH in two different conical flasks, 5ml of pectin solution was added and the second flask was heated at 85- 90°C for 15 min [12].

Quantitative Tests

Equivalent Weight (Titration A): Pectin sample (0.5 g) was weighed into a 250 mL conical flask and moistened with 5 mL ethanol. A 1.0 g NaCl was added to the mixture followed by 100 mL distilled water and few drops of phenol red indicator. Care was taken to ensure that all the pectin had dissolved and that no clumping occurred. The solution was then slowly titrated with 0.1 M NaOH to an end point of pale permanent pink color [13]. Equivalent weight was calculated using equation (3):

$$Equivalent\ Weight = \frac{(weight\ of\ pectin\ sample * Molarity\ of\ alkali)}{Volume\ of\ alkali} * 100 \quad (3)$$

Methoxyl Content (MeO) (Titration B): This was done using the neutralized solution obtained from equivalent weight determination, by the saponification of pectin followed by titration of the liberated acid. 25 mL of 0.25 M NaOH was added to the neutralized solution and the mixture was stirred thoroughly and allowed to stand for 30 min at ambient temperature. A 25 ml of 0.25N HCl was added and titrated with 0.1N NaOH to the same end point as earlier [14]. The percentage methoxyl content was calculated using equation (4):

$$Methoxyl\ content\% = \frac{Volume\ of\ alkali * weight}{Weight\ of\ pectin\ sample} * 100 \quad (4)$$

Moisture Content: An empty crucible was dried in an oven, cooled in a desiccator and weighed. A 5 g of pectin sample was transferred to it and placed in a hot air oven set at 100°C for 1 h. Thereafter the petri dish was removed, cooled in a desiccator and weighed. This process was repeated once. The moisture content was calculated using equation (5):

$$Moisture\ content\% = \frac{Weight\ of\ the\ Reside}{Weight\ of\ the\ sample} * 100 \quad (5)$$

Anhydrouronic Acid (AUA) Content: The AUA content was calculated using the values of equivalent weight and methoxyl content previously determined, according to equation (6) [13]:

$$AUA\% = \frac{176 * 100}{Z} \quad (6)$$

where, 176 is the molecular weight of AUA and

$$Z = \frac{Weight\ of\ sample\ (mg)}{meq\ of\ Titration\ A + meq\ of\ Titration\ B}$$

Degree of Esterification (DE): The DE of extracted pectin was calculated using equation (7), applying the data from methoxyl and anhydrouronic acid content determinations [15]:

$$DE(\%) = \frac{176 * MeO\% * 100}{31 * AUA\%} \quad (7)$$

Spectral Analysis: Subsequent to the above mentioned tests, the pectin from *C. limon* was further subjected to FTIR analysis (Shimadzu, IRAffinity-1) and the resulting spectrum was studied in order to understand the functional groups present.

RESULTS AND DISCUSSION

Pectin Extraction from Citrus Peels

Effects of pH and Temperature on Extraction Process: When the effects of these factors on pectin yield were

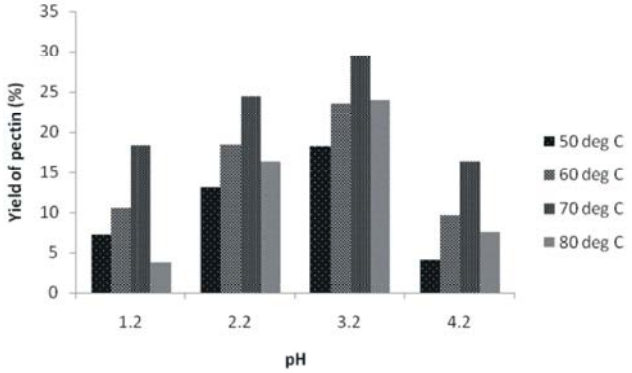

Fig. 1: Yield of pectin from *Citrus sinensis*
*The extractions were performed using citric acid under varying conditions of pH and temperature

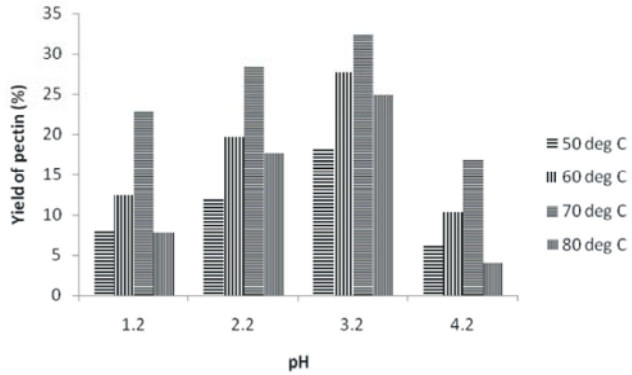

Fig. 2: Yield of pectin from *Citrus limetta*
*The extractions were performed using citric acid under varying conditions of pH and temperature

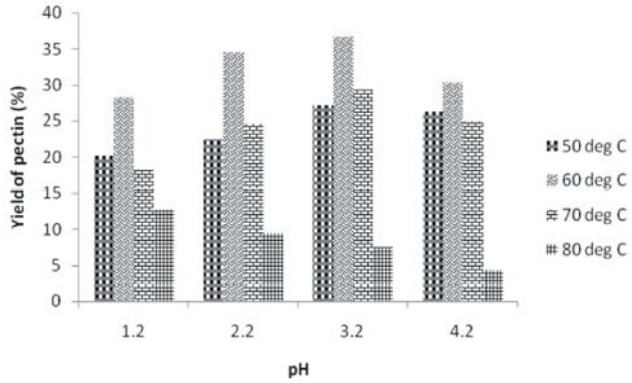

Fig. 3: Yield of pectin from *Citrus limon*
*The extractions were performed using citric acid under varying conditions of pH and temperature

monitored, the maximum yield from *C. sinensis* was found to be 29.41% at pH 3.2 and temperature of 70°C (Fig. 1). A 46.46% yield from orange peel residue after simple distillation of the orange oil has been reported in literature. Therefore, in the process of orange oil and pectin extraction, it has been recommended to first extract oil using simple distillation and then isolate pectin with acid hydrolysis technique [16]. In contrast to this, a very low yield of pectin obtained from dried orange peel using zeocarb as extractant at 85-90°C has also been reported [17].

When pectin present in *C. limetta* peel was extracted by citric acid based method, it showed a maximum yield of 32.42% at pH 3.2 and a temperature of 70°C (Fig. 2). Aina *et al*. have documented that the extraction from *C. limetta* resulted in a yield of 15.92% [18].

The extraction from *C. limon* resulted in a maximum yield of 36.71% at pH 3.2 and a temperature of 60°C (Fig. 3). In other studies, the percentage yield of pectin in wet weight basis from lemon has been observed to be 16.71% at pH 4.1 and a temperature of 60°C [18].

Thus, a pH of 3.2 appears to be optimum for the extraction of pectin from all the citrus peels studied. The optimum temperature for pectin extraction was observed to be 70°C for *C. sinensis* as well as *C. limetta*, except for *C. limon*, in which case, a lower temperature of 60°C was preferred. Further, on comparison of the above mentioned sources of pectin, it could be inferred that *C. limon* provided the highest yield and it was hence chosen for statistical optimization of the extraction process using design of experiments (DoE).

Optimization of Pectin Yield

Statistical Design Using Response Surface Methodology: The variables of pH, temperature (T) and extraction time (ET) were fitted for the Box-Behnken design of RSM. Yield of pectin for each individual run was determined by carrying out the acid based extraction method using citric acid. A maximum yield of 36.71% had been achieved prior to the process optimization. As a result of applying statistical optimization using RSM, a maximum yield of 56.81% was recorded in run 10. The desired conditions: pH, extraction time and extraction temperature were 3.5, 67.5 min and 65°C, respectively (Table 1). This represents a 1.5-fold increase in the yield of pectin. Kliemann *et al*. has obtained a yield of 61.32% at a pH of 1.9, temperature of 40°C and extraction time of 40 min [19].

The results obtained after the experimentation were fed into the Design Expert software, which generated the following regression equation:

$$Y = 55.58 - 4.25*A - 0.62*B - 3.97 * C + 1.06 * AB + 5.65 + AC + 2.61 * BC - 20.70 * A2 - 18.65 * B2 - 18.6 * C2$$

where, A- pH, B-temperature (°C) and C- extraction time (min).

Analysis of variance (ANOVA) indicated that the model F-value is 17.49, which implies that the model is significant. The model suggested for the yield of pectin from *C. limon* was a 'quadratic model'. The R^2 value of 0.9574 validates the accuracy of the model. This value provides a measure of how much variability in the observed response can be explained by the experimental factors and their interactions. It always lies between 0 and 1. The closer that the R^2 value is to 1.0, the stronger the model is and the better it predicts the response. The adjusted R^2 value was found to be a close 0.9027. The statistical analysis also determines which experimental factors generate signals which are large in comparison to the noise. This is measured as 'adequate precision' and a value of 9.791 means a good signal.

Three-dimensional response surface curves were plotted in order to understand the interactions between the variables and the optimum levels of each variable for maximum yield of pectin. The interaction between two variables, viz. pH and temperature is shown in Fig. 4. Significance of interaction between the corresponding variables is indicated by saddle nature of the contour plots. At lower and higher levels of both pH and temperature, decreased yield of pectin was observed. At intermediate concentrations, higher yield was obtained. Fig. 5 represents the interaction between pH and extraction time and its effect on the yield of pectin. In this case too, at intermediate levels of the variables, the yield was maximal. Fig. 6 depicts the interaction between extraction time and temperature. The yield was observed to be minimal at both lower and higher levels, whereas at intermediate levels, maximum yield was observed.

Physicochemical Characterization of the Pectin Samples

Qualitative and Quantitative Tests: The qualitative and quantitative characteristics of pectin are summarized in Table 2. The colour of pectin obtained from the orange peel sample was brown, whereas samples extracted from the other two sources were yellowish in colour. While pectins are usually light in colour, factors such as surface contamination or environmental factors might have contributed to the discrepancy in colour. This could also be due to the amount of alcohol used for precipitation or purification during the experiment not being enough [20]. In cold alkali (NaOH), the pectin suspensions formed a yellow precipitate, which dissolved when heated at 85-90°C for 15 min. Fishman *et al.* have stated that pectins are unstable in alkaline solutions, which agrees with the finding from our research [21].

The equivalent weight was found to be the highest for *C. sinensis* pectin and least for *C. limon* pectin. The methoxyl content of pectin usually varies from 0.2 - 12% depending on the source and mode of extraction. Among pectins from the three different sources studied, the methoxyl content varied from 6.8% (*C. sinensis*) to 2.3% (*C. limon*), the values thus falling within the range. Since all the values obtained experimentally were below 7%, the pectins are of low ester characteristic, indicating that they are desirable in terms of quality [12]. Anhydrouronic acid content of *C. limon* pectin was above 65%, indicating its purity.

Table 2: Qualitative and quantitative tests for pectin

	Source of Pectin		
Parameter	*C. sinensis*	*C. limetta*	*C. limon*
Qualitative tests:			
Color	Brown	Yellow	Yellow
Solubility of dry pectin in cold water	Insoluble, forms suspension	Insoluble	Soluble
Solubility of dry pectin at 85-90°C	Mixture dissolves	Mixture dissolves	Mixture dissolves
Solubility of pectin in cold alkali	Pectin forms a yellow precipitate	Pectin forms a yellow precipitate	Pectin forms a yellow precipitate
Solubility of pectin in hot alkali	Dissolved and turned milky	Dissolves	Dissolves
Quantitative tests:			
Equivalent weight	594.86	386.45	253.70
Methoxyl content (%)	6.840	4.460	2.348
Moisture content (%)	58.72	75.80	82.70
AUA (%)	68.74	42.80	39.48
DE (%)	3.50	2.98	1.50

*The samples were extracted using citric acid under optimum conditions of temperature and pH

Table 3: Functional groups present in *C. limon* pectin

Frequency (cm^{-1})	Bond	Functional group
3595.31 (s, sh)	O-H stretch, H-bonded	Alcohols, phenols
2931.80 (m)	C-H stretch	Alkanes
2862.36 (m)	C-H stretch	Alkanes
2222.00 (w)	C = C stretch	Alkynes
1728.22 (s)	C=O stretch	α,β-unsaturated ester
1319.31 (s)	C-O stretch	Alcohols, carboxylic acid, esters
1242.16 (s)	C-N stretch	Aliphatic amines
1149.57 (m)	C-H wag ($-CH_2X$)	Alkyl halides
1095.57 (m)	C-N stretch	Aliphatic amines
1056.99 (m)	C-N stretch	Aliphatic amines
1026.13 (m)	C-N stretch	Aliphatic amines
804.97 (m)	C-Cl stretch	Alkyl halides
840.98 (m)	C-Cl stretch	Alkyl halides

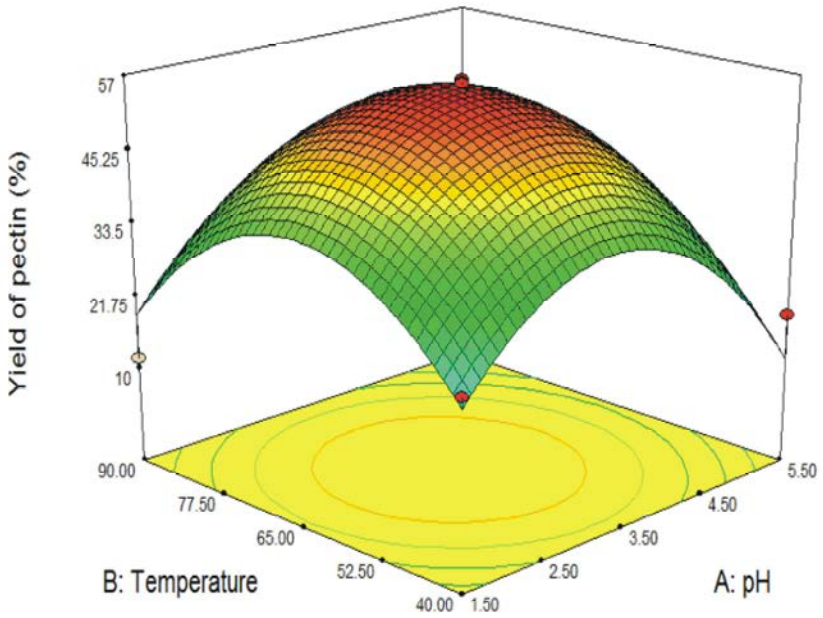

Fig. 4: Response surface curve showing interaction between pH and temperature

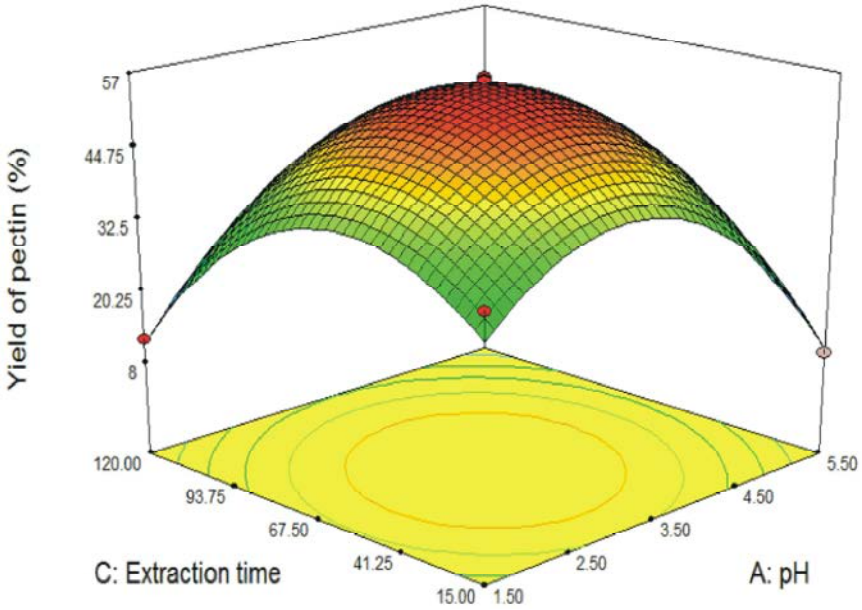

Fig. 5: Response surface curve showing interaction between pH and extraction time

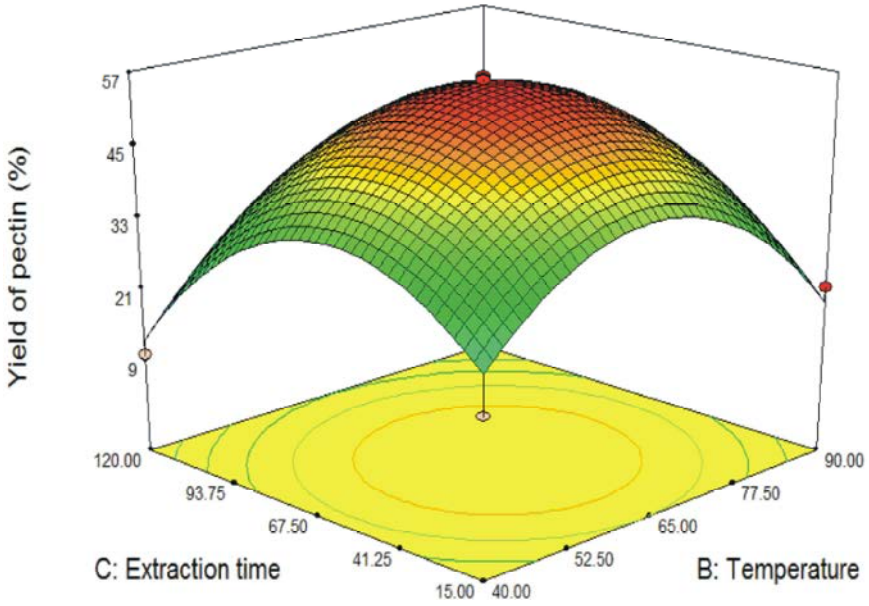

Fig. 6: Response surface curve showing interaction between temperature and extraction time

FTIR Spectral Analysis: The FTIR spectrum of *C. limon* pectin is presented in Fig. 7 and the corresponding functional groups are given in Table 3. From the results it could be inferred that the *C. limon* pectin exhibits sharp and strong peaks at 3595.31 cm^{-1} as O-H stretch, C-H stretch in the frequency 2830-2695 cm^{-1} shown as carbohydrate ring [22] and strong C=O stretch occurring at 1710-1665 cm^{-1}. The strong peak in the range of 1319.31 cm^{-1} suggests the stretching vibration of alcohols, carboxylic acid and esters [23]. Comparable study by Khule *et al*. has showed IR peaks at 4000-600 cm^{-1} for a sample of pectin present as a drug mixture [7]. Moreover, the presence of peaks at 1728.22 cm^{-1} and 1242.16 cm^{-1} indicate the existence of α, β-unsaturated esters and aliphatic amine functional groups.

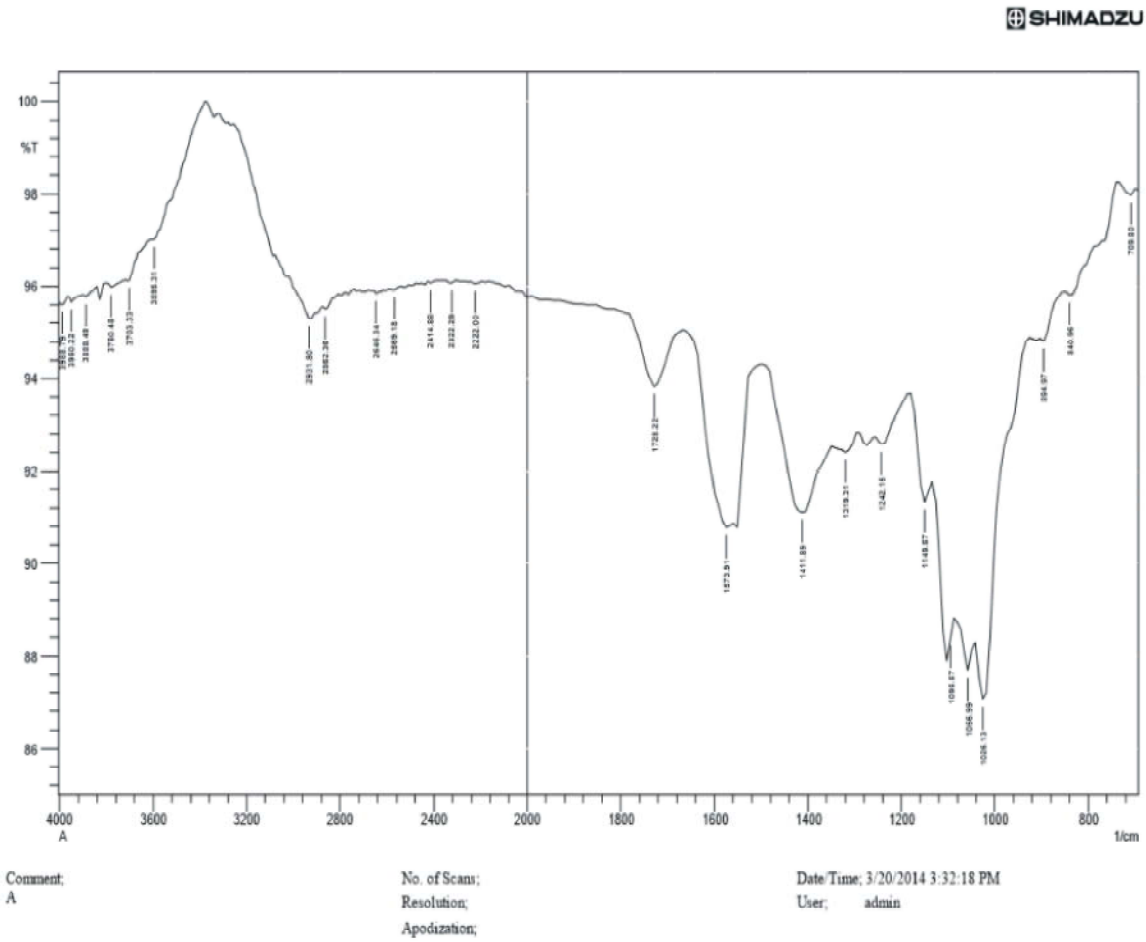

Fig. 7: FTIR spectrum of *C. limon* pectin

CONCLUSION

Our study has facilitated a detailed investigation on pectins from citrus peels, a product of enormous value for food-industry applications. Initially, the maximum yield of pectin was found to be 36.71% from *C. limon* at pH 3.2 and a temperature of 60°C. Process optimization for enhancing the yield of pectin was carried out using RSM statistical tool. pH, temperature and extraction time played a significant role in the yield of pectin and the levels of these factors were optimized. A 1.5-fold increase in pectin yield was achieved after optimization. Low p-value and high F-value indicated the significance of the model. The extracted pectins from all sources were characterized extensively in terms of solubility, equivalent weight, methoxyl and anhydrouronic acid contents and degree of esterification. Functional groups of *C. limon* pectin were analysed by FTIR spectroscopy. Thus, the work has facilitated the optimized production of pectins from different citrus peels and their characterization, with the pectins, especially the one from *C. limon*, exhibiting desirable properties for industrial applications.

ACKNOWLEDGEMENTS

The authors are thankful to the management of Kumaraguru College of Technology, Coimbatore, India, for providing the laboratory facilities to carry out this work.

REFERENCES

1. Wilkins, M.R., W.W. Widmer, R.G. Cameron and K. Grohmann, 2005. Effect of Seasonal Variation on Enzymatic Hydrolysis of Valencia Orange Peel Waste. Proceedings of the Florida State Horticulture Society, 118: 419-422.

2. Tobias, N.E., N.V. Eke, R.I. Okechukwu, R.N. Nwoguikpe and C.M. Duru, 2011. Waste to Health: Industrial Raw Materials. Potential of Peels of Nigerian Sweet Orange (*Citrus sinensis*). African Journal of Biotechnology, 10(33): 6257-6264.
3. Krishnamurthi, C.R. and K.V. Giri, 2003. Preparation, Purification and Composition of Pectin from Indian Fruits and Vegetables. Brazilian Archives of Biology and Technology, 44: 476-483.
4. Kulkarni, G.T., K. Gowthmarajan, B. Rao and B. Suresh, 2006. Evaluation of Binding Properties of *Blantago ovate* and *Trigonella foenum-graecum* mucilages. Indian Drugs, 39(8): 422-425.
5. Joye, D.D. and G.A. Luzio, 2000. Process for Selective Extraction of Pectin from Plant Material by Differential pH. Journal of Carbohydrate Polymer, 43(4): 337-342.
6. Pagan, J., A. Ibarz, M. Llorca and A. Paga, 2001. Extraction and Characterization of Pectin from Stored Peach Pomace. Food Research International, 34: 605-612.
7. Khule, R.N., B.M. Nitin, S.S. Dipak, M.R. Manisha and R.C. Sanjay, 2012. Extraction of Pectin from Citrus Fruit Peel and use as Natural Binder in Paracetamol Tablet. Scholars Research Library, 4(2): 558-564.
8. Asadi, A. and A.A.L. Ziantizadeh, 2011. Statistical Analysis and Optimization of an Aerobic SBR Treating an Industrial Estate Wastewater Using Response Surface Methodology (RSM). Iranica Journal of Energy and Environment, 2(4): 356-365.
9. Pishgar-Komleh, S.H., A. Keyhani, M.R. Mostofi-Sarkari and A. Jafari, 2012. Application of Response Surface Methodology for Optimization of Picker-Husker Harvesting Losses in Corn Seed. Iranica Journal of Energy and Environment, 3(2): 134-142.
10. Li, D., J. Shang, X. Ma, X. Zhu and Z. Li, 2013. Combined Influence of Extraction Parameters on Degree of Esterification of Sugar Beet Pulp Pectin, 35(5): 65-72.
11. Fishman, M.L., H.K. Chau, D.R. Coffin and A.T. Hotchkiss, 2003. A comparison of Lime and Orange Pectin which were Rapidly Extracted from Albedo. Advances in Pectin and Pectinase Research, 6: 107-122.
12. Joslyn, M.N., 1980. Methods of Food Analysis. Physical, Chemical and Instrumentation Method of Analysis, 2nd edn. Academic Press, New York, pp: 67-70.
13. Owens, H.S., R.M. Mc Cready, A.D. Shepherd, S.H. Schultz, E.L. Pippen, H.A. Swenson, J.C. Miers, R.F. Erlandsen and W.D. Maclay, 1952. Methods used at Western Regional Research Laboratory for Extraction and Analysis of Pectic Materials, AIC-340, Western Regional Research Laboratory, Albany, California.
14. Norziah, M.H., E.O. Fang and A.A. Karim, 2000. Extraction and Characterization of Pectin from Pomelo Fruit Peels. In P.A. Williams (Ed.), Gums and Stabilisers for the Food Industry, Cambridge, UK: The Royal Society of Chemistry, 10: 26-36.
15. Schultz, T., 1976. Methods in Carbohydrate Chemistry. In T. Schultz, Methods in Carbohydrate Chemistry, New York: Academic Press, pp: 189.
16. Shekhar, P. and M. Harshal, 2012. Separation of Oil and Pectin from Orange Peel and Study of Effect of pH of Extracting Medium on the Yield of Pectin. Journal of Engineering Research and Studies, 3(2): 6-9.
17. Joseph, M.J. and Hunang, 2001. Improved Method for the Extraction of Pectin. Proceedings of the Florida Horticultural Society, 3: 260-261.
18. Aina, V.O., M.B. Mustapha, Mamman, O.A. Zakari, H. Haruna, M.S. Umar and B.A. Yagana, 2012. Extraction and Characterization of Pectin from Peels of Grape Fruit (*Citrus paradisi*), Sweet Orange (*Citrus limetta*) and Lemon (*Citrus limon*). British Journal of Pharmacology and Toxicology, 3(6): 259-262.
19. Kleimann, E., N.S. Karina, R.A. Edna, S.P. Elane, F.T. Reinaldo, M.C. Ferreira and D.M. Renata, 2009. Optimization of Pectin Acid Extraction from Passion Fruit Peel (*Passiflora edulis-flavicarpa*) using Response Surface Methodology. International Journal of Food Science and Technol., 44: 476-483.
20. Mc Gready, R.M., 1996. Extraction of Pectin from Citrus Peels and Conversion to Pectin Acid. Academic Press, New York, 4: 167-170.
21. Fishman, M.L., P.E. Pferffer, R.A. Barford and K.W. Donar, 1991. Studies of Pectin Solution Properties by High Performance Exclusion Chromatography. Journal of Agricultural and Food Chemistry, 32(2): 372-378.
22. Silva, S., M. Sonia, A. Karmali, E. Rosa, 2012. Production, Purification and Characterization of Polysaccharides from *Pleurotus ostreatus* with Antitumor Activity. Journal of the Science of Food Science and Agriculture, 92: 1826-1832.
23. Thetsrimuang, C., S. Khammuang and R. Sarnthima, 2011. Antioxidant Activity of Crude Polysaccharides from Edible Fresh and Dry Mushroom Fruiting Bodies of *Lentinus* sp. strain RJ-2. International Journal of Pharmacology, 7: 58-65.

2 d 2 4 3

چکیده

پکتین پلی ساکاریدی با ساختار غیریکنواخت است که معمولا از پوست مرکبات بدست می آید و در سطح تجاری به عنوان عامل ژل کننده و پایدارکننده به کار می رود. در این پژوهش پکتین با روش ته نشینی با الکل از پوست پرتقال، لیموی شیرین و لیمو استخراج شد. هنگامی که شرایط استخراج به صورت جداگانه تغییر داده شد، حد اکثر بازده در حدود ۳۶/۷۱ درصد از لیمو بدست آمد و سپس بازده با استفاده از روش (در رابطه با روش شناسی پاسخ سطحی) بازده نیز افزایش داده شد. شرایط بهینه برای فرایند استخراج پکتین مربوط به ۳/۵ ، دمای ۶۵ درجه سانتی گراد و زمان ۶۷/۵ دقیقه می باشد. اثر متقابل این متغیرها بر یک دیگر با استفاده از منحنی 3 و منحنی های کانتوری بررسی شد. استفاده از این طراحی تجربی سبب افزایش ۱/۵ برابری در بازده تولید پکتین شد. آنالیز واریانس ها معنی دار بودن مدل را نشان داد. پکتین به دست آمده مورد آزمایشات کمی و کیفی قرار گرفت و این نتیجه حاصل شد که پکتین بدست آمده محتوی متوکسیل، هیالورونیک اسید و درجه استریفیکاسیون مطلوبی دارد. گروه های چند عملکردی موجود در پکتین با استفاده از مورد بررسی قرار گرفت. نتایج کلی حاصله نشان دهنده قابل استفاده بودن پکتین استخراج شده برای استفاده های صنعتی می باشد.

Iranica Journal of Energy & Environment 5 (3): 313-322, 2014
ISSN 2079-2115
IJEE an Official Peer Reviewed Journal of Babol Noshirvani University of Technology
DOI: 10.5829/idosi.ijee.2014.05.03.11

BUT

Quality Changes of Red Pitaya (*Hylocereus undatus*) Slices Dried in Hot Air, Microwave-Hot Air and Microwave-Vacuum Dryers

[1]M.F.M. Nordin, [2]I. Puspasari, [2]S.M. Tasirin, [2]W.R.W. Daud,
[3]Y. Gariépy, [2]M.Z.M. Talib, [3]G.S.V. Raghavan

[1]Faculty of Agro Based Industry, Universiti Malaysia Kelantan,
Jeli Campus Locked Bag 100, 17600 Jeli, Kelantan, Malaysia
[2]Department of Chemical and Process Engineering, Faculty of Engineering and Built Environment,
Universiti Kebangsaan Malaysia, 43600 Bangi, Selangor, Malaysia
[3]Department of Bioresource Engineering, Faculty of Agricultural and Environmental Sciences,
McGill University, Macdonald Campus, 21,111 Lakeshore,
Ste-Anne-de-Bellevue, Quebec, Canada H9X 3V9

Date of Received: May 19, 2014; Date of Accepted in Revised Form: August 4, 2014

Abstract: Quality changes of red pitaya (*Hylocereus undatus*) slices dried in hot air, microwave-hot air and microwave-vacuum dryers were investigated. The quality parameters were colour, water activity, shrinkage, rehydration ratio, ascorbic acid content and visual market quality. Microwave-vacuum produced pitaya with the best quality compared to hot air and microwave-hot air. Pitaya dried in microwave-vacuum had the highest rehydration ratio while the other methods presented similar rehydration ratios. Ascorbic acid in dried pitaya was also better retained when drying by microwave-vacuum. Apart from that, the drying time of pitaya dried in microwave-vacuum could be reduced by 83% compared to hot air.

Key words: Dragon fruit · Drying kinetics · Microwave convective drying · Microwave vacuum drying · Product quality

INTRODUCTION

Pitaya (*Hylocereus*) fruit is also known as dragon fruit due to the dragon-like appearance of the scales or bracts on its skin [1]. Pitaya is favoured fruit especially in Asian countries such as Vietnam, Taiwan, Malaysia and Philippines. Three commercial varieties of pitaya are *Hylocereus undatus* (Red Pitaya) which has red-skinned fruit with white flesh, *Hylocereus polyrhizus* which has red-skinned fruit with red flesh and *Hylocereus megalanthus* (Yellow Pitaya) which has yellow-skinned fruit with white flesh [2]. Peeled fruit slices are amongst the favoured after dinner desserts. It contains highly gelatinous carbohydrates such as cellulose, hemicellulose and simple saccharide polymers [3]. The flesh is mildly sweet. It is also converted into juice or used to flavour other beverages [4]. Many researchers have reported that pitaya fruit contains other antioxidant nutrients such as phenolic compounds and ascorbic acid, in addition to vitamin C which significantly contribute to its total antioxidant capacity [5-7].

Fresh fruits and vegetables contain a great deal of water and are rich with nourishment, which stimulates the growth of microorganisms resulting in putrefaction. Drying would remove the water within fruits and vegetables by evaporation of most of the water in the product. The reduction of moisture content inhibits or decreases microbial and enzymatic activity, being advantageous to dry long-term conservancy of the ware. But the drying process suffers from quality losses regarding colour, flavour and nutrient content and rehydration is often poor. Case hardening and shrinkage

Corresponding Author: Siti Masrinda Tasirin, Department of Chemical and Process Engineering, Faculty of Engineering and Built Environment, Universiti Kebangsaan Malaysia, 43600 Bangi, Selangor, Malaysia. Tel: +603-8921 6425.

Please cite this article as: M.F.M. Nordin, I. Puspasari, S.M. Tasirin, W.R.W. Daud, Y. Gariépy, M.Z.M. Talib, G.S.V. Raghavan, 2014. Quality Changes of Red Pitaya (Hylocereus undatus) Slices Dried in Hot Air, Microwave-Hot Air and Microwave-Vacuum Dryers. Iranica Journal of Energy and Environment, 5 (3): 313-332

are the main problems. In recent years, improvement of quality retention by dried products, by altering drying methods and/or process conditions, has been a major research goal [8].

Hot air drying is a conventional process used to preserve foods in which the solid to be dried is exposed to a continuously flowing hot stream of air where moisture evaporates. The phenomena underlying this process is a complex problem involving simultaneous mass and energy transport in a hygroscopic, shrinking system. Air-drying offers dehydrated products that can have an extended shelf life.

The efficiency of drying process increases with the arising of air temperature as it enhances the effectiveness of moisture diffusivity [9, 10]. However, this process also negatively impacts product quality, due to the long drying times and high temperatures employed. The quality of the dried product is often lower than that of the original foodstuff, with an impact on colour, rehydration ratio, texture and other characteristics [11, 12].

Microwave drying has gained popularity in food preservation industries due to the shorter drying time, improved product quality and flexibility in producing a wide variety of dried products. The energy absorption level is controlled by the wet products which can be used for selective heating of interior parts of the sample containing moisture and without affecting the exterior parts. Microwave energy combined with other drying methods can improve the drying efficiency as well as the quality of food products which is far better than that achievable by microwave drying only or by other conventional methods [13, 14].

Microwave assisted air drying is one of the methods where hot air drying is combined with microwave heating in order to enhance the drying rate. For drying of high moisture fruits and vegetables, a reduction in moisture content is time consuming especially in the final stage of drying. Microwave assisted drying as final stage of air drying overcomes these disadvantages with high thermal efficiency. Hot air drying does not improve moisture loss at the final stages of drying process, since the diffusion process is very slow. Besides increasing the drying rate, microwave assisted air drying enhances the rehydration capacity of dried products and also overcome shrinkage problems [13].

In the absence of convection, either conduction or radiation or microwaves can be combined with vacuum drying to improve its thermal efficiency. During vacuum drying, high energy water molecules diffuse to the surface and evaporate due to low pressure. Because of this, water vapour concentrates at the surface and the low pressure causes the boiling point of water to be reduced. Thus vacuum drying prevents oxidation due to the absence of air and thereby maintains the colour, texture and flavour of the dried products [14]. Microwave vacuum drying is applied for heat sensitive materials such as banana, carrot, potato, etc. The loss of nutritional qualities (vitamins, α and β-carotenes etc.) of food products by microwave vacuum drying is minimized due to non exposure of heat and oxygen [13].

The selection of the proper drying method can affect the final product quality and the drying economics [15]. The aim of this study was to evaluate the effects of different drying methods on the drying of red pitaya slices based on the drying parameters such as drying time, final moisture content and drying rate. Quality parameters such as changes in colour, water activity, shrinkage, rehydration capacity, ascorbic acid content and visual market quality were also compared.

MATERIALS AND METHODS

Materials: Ripe red pitaya (*Hylocereus undatus*) used in this study were purchased at a local store. These fruits were imported from Vietnam into Canada by Canada Herb, Toronto, Ontario. Before each experiment, the fruits were hand peeled and cut into cylinders of 3.5 cm in diameter and 1 cm thick. The fresh red pitaya fruits used for the drying trials were without visual sign of physical damage, disease or physiological disorders. The mean fruit mass was 576.5 ± 54.7 g and, on average, moisture content was 84.4 ± 2.6% wet basis. The colour of fresh red pitaya fruits, defined in terms of mean L^*, a^* and b^* values, were 45.6 ± 1.7, 38.3 ± 3.2 and 10.1 ± 1.9, respectively; for the purple red skins' color, while the white flesh's colour were 63.7 ± 3.6, -0.32 ± 0.1 and 3.8 ± 0.4. The mean of total soluble solid content for fresh fruits was 12.33 ± 1.06 °Brix, while their ascorbic acid content was 1.88 mg g^{-1} F.W.

Drying Methods

Hot Air Drying: A laboratory constant temperature and humidity chamber made by Jeio Tech. Co., Ltd (Korea) was used for the hot air drying trials. Hot air flowed through the bed at 45% relative humidity. Temperature of the hot air was controlled at 55 °C. Before starting the drying process, the dryer was run for 30 minutes to achieved steady-state conditions. The fruit slices were placed in a holder suspended in the centre of the oven cavity and attached to the analytical balance. Sample mass, air and sample temperatures were monitored and recorded at regular time interval. The samples were dried until they reached the final moisture content.

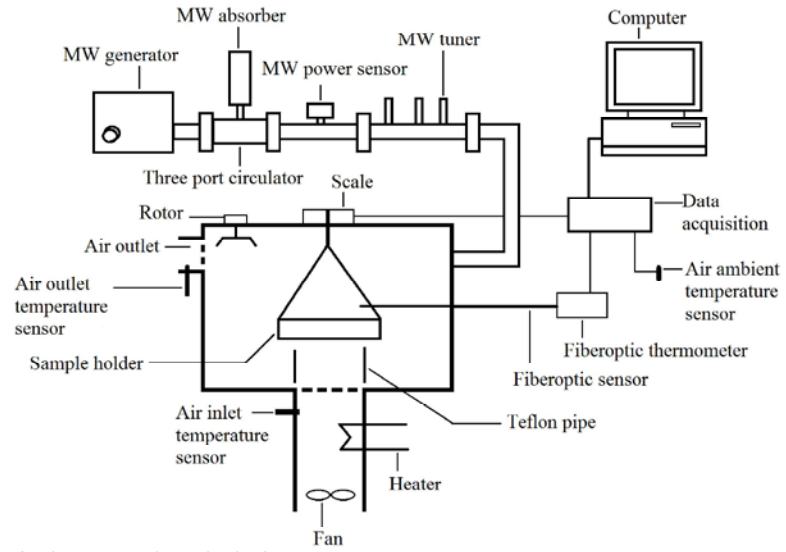

Fig. 1: Schematic diagram of microwave-hot air drying

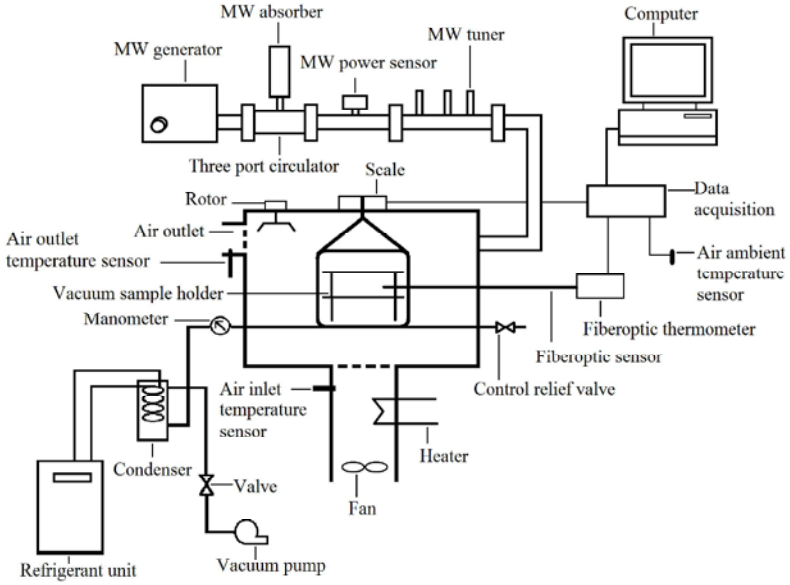

Fig. 2: Schematic diagram of microwave-vacuum drying unit

Microwave-Hot Air Drying: Microwave-hot air drying trials were performed using a laboratory scale drying unit at McGill University, Canada (Figure 1). It consisted of a 400 W microwave generator operating at 2,450 MHz, a three-port circulator, a microwave tuner, power meters, waveguides, a microwave absorber, a cavity and a data acquisition and controlled system. The dimension of the cavity was 490 mm by 250 mm by 380 mm. A motorized rotor was placed in the cavity to help distribute the microwave energy. Heated air was introduced into the cavity through a circular opening (diameter of 20 cm) made at the bottom of the cavity. A perforated metal grill was placed on the opening to prevent leakage of microwave. The sample holder consisted of a Teflon frame with a fine mesh screen. The holder was suspended to the load cell and located in the centre of the cavity. A microwave leakage detector model SMW-1, Microcheck (China) was used to detect any potential leakage. Agilent VEE Pro 8.0^{TM} was used to control the data acquisition system (Agilent model 34970A) and to monitor and record all process parameters. A fiber optic sensor (Emi-TS Series, Nortec Fibronic Inc., Quebec, Canada) was used to monitor product temperature during the drying process. The red pitaya slices were subjected to drying at temperature of 55 °C and microwave power density of 1 W/g.

Microwave-Vacuum Drying: Modifications were made to the microwave-hot air dryer to allow it to operate under vacuum. These modifications consisted of the addition of a vacuum pump, a digital vacuum gage, a condenser an airtight sample holder and a control relief valve (Figure 2). The vacuum was maintained in the sample holder with a belt driven Boekel Hyvac vacuum pump model 91308-001. The control relief valve was set to maintain a vacuum of 6.67 kPa absolute in the sample holder. A condenser cooled to -15°C with ethylene glycol was placed between the sample holder and the vacuum pump to capture water vapor. A Fisher Scientific Isotemp 1013S cooling unit was used to cool down and circulate the cooling liquid in the condenser. The sample holder consisted of a polycarbonate bell jar mounted on a polypropylene base and of Teflon™ trays. All drying trials were performed with microwave power level of 1 W/g of fruits.

Drying Kinetics: The experimental results from this work are presented as drying curves. Drying curve was constructed from the variation of moisture ratio (MR) as a function of time *t*. The moisture ratio shown in Eq. (1) was used so that the resulting drying curves for all of experiments are comparable [16]:

$$MR = \frac{X - X_{eq}}{X_o - X_{eq}} \quad (1)$$

where X_o is the initial moisture content and X_{eq} is the equilibrium moisture content. However, in this study, the equilibrium moisture content was relatively small compared to X or X_o and nearly approached the dry matter content, thus appearing negligible. This approximation was also used by Celma *et al*. [17] where they simplified the equation to:

$$MR = \frac{X}{X_o} \quad (2)$$

Quality Assessment

Colour: The product quality in terms of colour was determined by measuring the colour change before and after drying by using a Minolta Chromameter CR-300 (Konica Minolta, Japan). The colour testing method used was CIE-$L^*a^*b^*$ method where L^* stands for lightness and a^* and b^* stand for chromaticity. The sign of a^* and b^* indicate colour direction: $+a^*$ is the direction to red, $-a^*$ is direction to green, $+b^*$ is direction to yellow and $-b^*$ is direction to blue [18]. The colour change, ΔE, is given by the following equation:

$$\Delta E = \left[(\Delta L^*)^2 + (\Delta a^*)^2 + (\Delta b^*)^2 \right]^{1/2} \quad (3)$$

where

$$\Delta L^* = L^* - L_o^* \quad (4)$$

$$\Delta a^* = a^* - a_o^* \quad (5)$$

$$\Delta b^* = b^* - b_o^* \quad (6)$$

Water Activity: The water activity of fresh and dried red pitaya slices was measured room temperature using a water activity meter (AquaLab, Model Series 3TE, USA).

Shrinkage: Shrinkage caused by the drying process was expressed in terms of changes in sample volumes and measured using a displacement method in toluene [19]. Shrinkage was calculated as follows:

$$\Delta V = 1 - \frac{V}{V_o} \quad (7)$$

where V is sample volume and V_o is initial sample volume.

Rehydration Ratio: Rehydration capacity of the dried samples was determined following the method recommended by the US Department of Agriculture [20, 21]. A 5 g sample of the dried material was weighed and placed in a 500 mL beaker containing 150 mL of distilled water. The beaker was then placed on a hot plate and covered with a watch glass; the water was brought to boiling point in 3 min and allowed to boil for an additional 5 min. The sample was then transferred to a 7.5-cm Buchner funnel covered with Whatman No. 4 ?lter paper. Water was drained from the material by applying gentle suction until the dripping from the funnel had almost stopped. The sample was then removed and weighed.

Rehydration ratio was calculated as the ratio of rehydrated sample to that of dehydrated sample. The coefficient of rehydration, *COR*, was calculated using the following equation [21]:

$$COR = \frac{m_{rh}(100 - X_o)}{m_{dh}(100 - X_{dh})} \quad (8)$$

where m_{rh} is the mass of rehydrated sample, m_{dh} is the mass of dehydrated sample, X_o is the initial moisture content and X_{dh} is the moisture content of dehydrated sample.

Table 1: Quality Index (QI) used to assess the overall quality of dried pitaya slices

Index	Quality	Description
1	Excellent	Very good overall appearance, uniform drying, no colour change.
2	Good	Good appearance, less uniform drying, slight colour change.
3	Fair	Fair appearance, some slices are either over or under dried, browning becoming visible.
4	Poor	Poor appearance, more slices are either over or under dried, more intense browning of some slices.
5	Unsalable	Bad appearance, many slices are either over or under dried, intense browning of slices.

Ascorbic Acid Content: Ascorbic acid was measured by titration method, using phenolindo-2, 6-dichlorophenol (DPIP) as also used by Sahlin *et al*. [22]. The quantity of the ascorbic acid in the pitaya samples was then calculated using the following equation [23]:

$$\frac{\text{mg of ascorbic acid}}{\text{100 g fresh weight}} = \frac{(\text{sample} - \text{blank}) \times \text{dye factor} \times 100}{\text{sample mass} \times \text{aliquot}} \quad (9)$$

where

$$\text{dye factor} = \frac{\text{volume of ascorbic acid}}{0.5} \quad (10)$$

Quality Index: Sensory evaluation of a product, though subjective, is an important part of quality evaluation since it represents the same procedure that would be used by a consumer [24]. This analysis has been employed by Sunjka *et al*. [25] and Beaudry *et al*. [24] for dried cranberries, each had different sensory characteristics and its evaluation scale. In the present study, the appearance of the dried product was evaluated with a Quality Index (QI) scale ranging from 1 (highest quality) to 5 (lowest quality) as presented in Table 1.

Dielectric Properties: Dielectric properties of the samples were measured with an Agilent Network Analyzer model 8722ES (USA) equipped with an open-ended coaxial probe (model 85070D). Before the measurements, the instrument was calibrated using three different loads: air, short-circuited and distilled water at 20°C. The dielectric properties of the pitaya samples were measured by touching the surface samples with the flat face of open-ended probe.

RESULTS AND DISCUSSION

Drying Kinetics: The drying curves (moisture ratio versus time) of red pitaya slices dried by hot air drying, microwave-hot air drying and microwave vacuum drying are presented in Figure 3. It was clearly observed in Figure 3 that the difference on the drying time of red pitaya slices dried using different drying methods was significant. Drying time to 10% moisture content (db) for hot air drying was about 12 h, longer than drying using

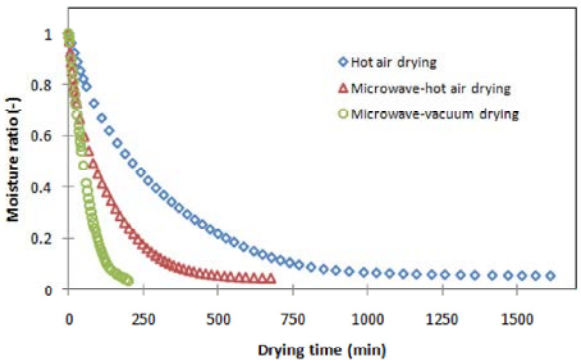

Fig. 3: Drying curves of red pitaya slices

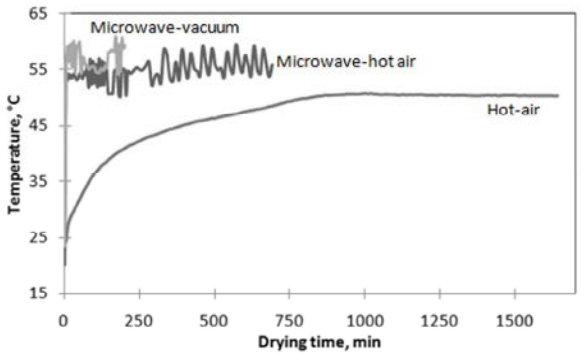

Fig. 4: Product temperature progressions during drying process

microwave-hot air and microwave-vacuum. It took only about 2 h for microwave-vacuum to dry the red pitaya slices, while drying in the microwave-hot air dryer required 6 h. The addition of the microwave energy to the hot air drying process enabled the drying time to be reduced by more than 50%. However, the drying time was reduced about 83% after application of a vacuum into the drying system. Similar result was obtained by Therdthai and Zhou [26] and Giri and Prasad [27] for the microwave vacuum drying and convective hot air drying of mint leaves and mushroom, respectively.

Temperature Progression During Drying Process: A comparison of the progressions of product temperature for hot air drying, microwave-hot air drying and microwave-vacuum drying (Figure 4) clearly indicated that the sample dried in the hot air dryer did not achieved

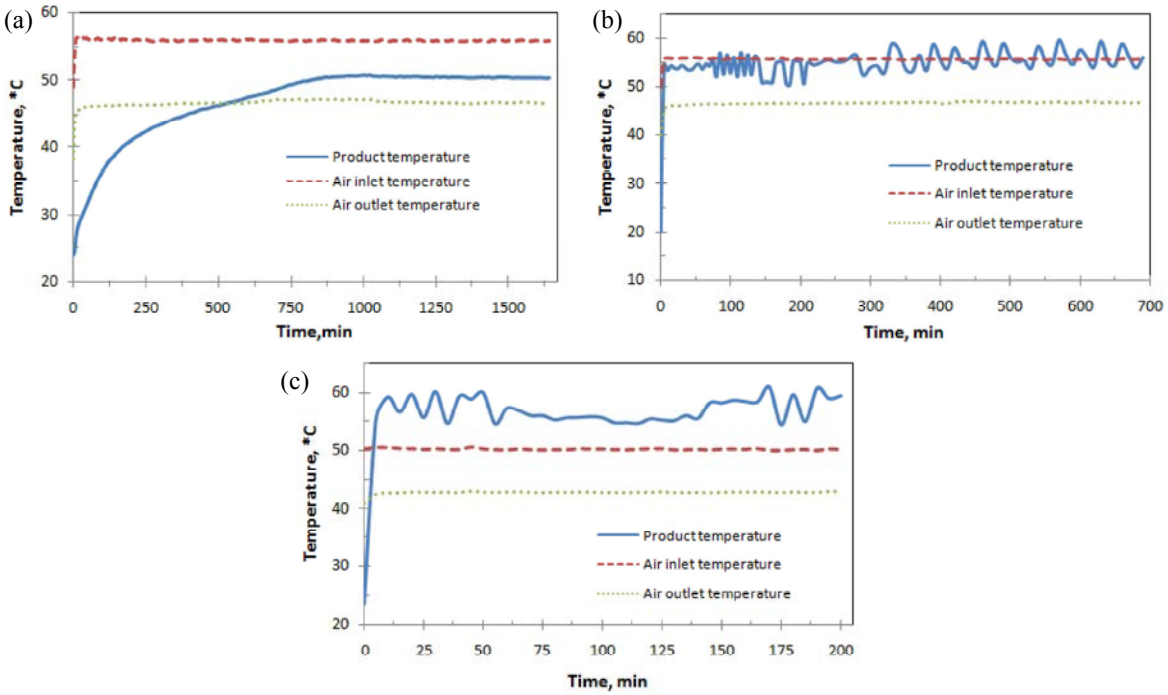

Fig. 5: Air inlet, air outlet and product temperatures progressions during: (a) hot air drying, (b) microwave-hot air drying and (c) microwave-vacuum drying

the set temperature of 55°C over the entire drying time of 27 hours. However, the product temperature of microwave-assisted drying (hot air and vacuum) immediately increased from the ambient temperature to the set temperature. Under these drying conditions, the product temperatures were maintained at the target temperature with the contribution of microwave energy.

The progression of air inlet, air outlet and product temperature during drying of red pitaya slices is shown in Figure 5. With the air inlet temperature of the unassisted hot air drying process set at 55°C, the product temperature slowly increased until it achieved a constant temperature (Figure 5a). However, the product temperature was still below the set points of about 50°C even though the system was run more than nine hours at the steady state temperature. This indicated that the heating process of hot air drying began from the surface of the samples.

The progression of air and product temperature of pitaya slices dried in microwave-hot air shown in Figure 5b, illustrates that product temperature was about the same as air inlet temperature (55°C) and higher than the in hot air alone. This occurred because the sample absorbed the microwave energy during the drying process to maintain the product temperature at the set point and the microwave was switch on only when the product temperature was below the set temperature. With this system, the product temperature was more uniform compared to the hot air drying system with no microwave assistance.

For the microwave-vacuum drying, the product temperature was fully controlled by the microwave energy applied to the system (Figure 5c). The air inlet temperature was set at 50°C to prevent condensation on the inside surface of the vacuum sample holder as previously mentioned.

Product Quality of Dried Pitaya: The quality attributes of red pitaya slices dried under hot air, microwave-hot air and microwave-vacuum drying are presented in Table 2. It was shown that the value of quality index of pitaya samples dried under microwave-vacuum was higher than the other two drying systems. Besides that, the pitaya slices dried in the microwave-vacuum drew up more water during the rehydration procedure than samples dried under the other systems.

Colour is one of the most important criteria for acceptability of a food. Undesirable changes in the colour of a food may decrease its quality and marketing value [15]. Table 2 shows the total colour changes of red pitaya slices dried in different drying methods. The least colour change was observed in the microwave-vacuum dried product because of the vacuum condition during the drying process and the shorter drying time.

Table 2: Quality attributes of red pitaya slices dried under hot air, microwave-hot air and microwave-vacuum

	Hot air	Microwave-hot Air	Microwave-vacuum
Quality index	1.2	1.2	2.0
Total color changes, ΔE	8.57	7.52	6.41
Water activity	0.423	0.431	0.462
Shrinkage (%)	84.73	85.57	81.04
Rehydration ratio	0.282	0.257	3.424
Ascorbic acid (mg g^{-1} FW)	0.212	0.685	0.838

The water activity of all dried pitaya samples was found to be lower than 0.7, which is often referred to as the limit for intermediate moisture foods. According to Beaudry *et al*. [24], foods having a water activity a_w between 0.4 and 0.65 are considered as dried products, whereas those having a water activity between 0.65 and 0.75 represent intermediate moisture foods. As shown in Table 2, no significant difference was observed for the water activity of pitaya dried in hot air, microwave-hot air and microwave-vacuum drying methods. This was because all the samples were dried until reaching the same final moisture content. All the dried products had values of a_w of below 0.7 which indicates that the growth of molds, bacteria and yeast is not promoted and enzymatic reactions are not likely to occur [24].

The effect of drying method on the shrinkage of red pitaya is shown in Table 2. The shrinkage of samples were 84.73, 85.57 and 81.04% for hot air, microwave-hot air and microwave-vacuum drying, respectively. From this comparison, the shrinkage of product from the three drying methods was not much different. As shown also in Table 2, the rehydration ratio of red pitaya samples dried by hot air, microwave-hot air and microwave-vacuum drying were 0.282, 0.257 and 3.424, respectively. The highest rehydration capacity was found for the microwave-vacuum dried sample which could be related to the lower shrinkage data. Qing-guo *et al.* [15] pointed out that a less shrunk structure has higher capacity to absorb water when reconstituted.

Since ascorbic acid (vitamin C) is relatively unstable to heat, oxygen and light, its retention can be used as an indicator for the quality of dried products. Cui *et al*. [28] stated that the higher the temperature, the longer the drying time, the more loss of vitamin C in the dried fruits and vegetables. The ascorbic acid contents in the product dried by hot air, microwave-hot air and microwave-vacuum dryers are presented in Table 2. It was observed that no significant loss of ascorbic acid in the pitaya occurred during microwave-vacuum drying, with the retentions of ascorbic acid of 44.6%. Ascorbic acid in the dried pitaya sample was better retained when subjected to microwave-vacuum drying due to the shorter drying time.

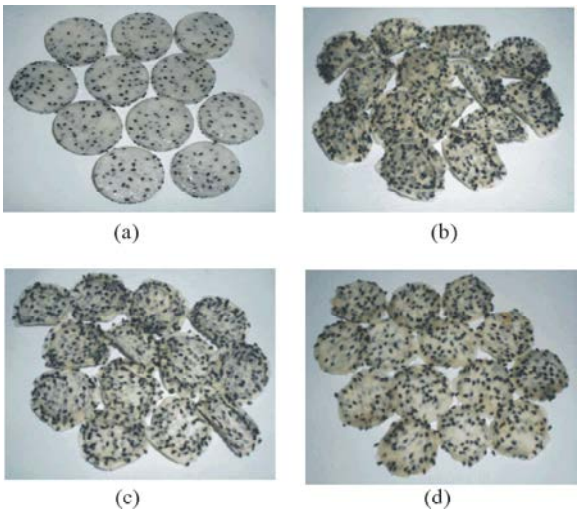

Fig. 6: Photographs of: (a) fresh pitaya slices, (b) hot air dried slices, (c) microwave-hot air dried slices and (d) microwave-vacuum dried slices

The lower ascorbic acid content in the dried pitaya samples for hot air and microwave-hot air drying was due to the oxidation and degradation of ascorbic acid in the presence of air.

The visual appearance of fresh red pitaya slices and of samples dried under hot air, microwave-hot air and microwave-vacuum drying is presented in Figure 6. Considerable reductions in size, as well as a slight darkening of the colour were observed in the dried product compared to the fresh samples. The darkening was more visible in hot air dried samples followed by the pitaya slices dried in a microwave-hot air. Dried product with the lightest colour was observed when drying under microwave-vacuum.

Dielectric Properties: The dielectric properties of materials vary with several different factors. In the present study, the dielectric properties of pitaya slices dried under the three different drying systems was measured and compared. Figure 7, which illustrates the relationship between dielectric constant (ϵ') and dielectric loss factor (ϵ") with shrinkage of pitaya slices at different moisture

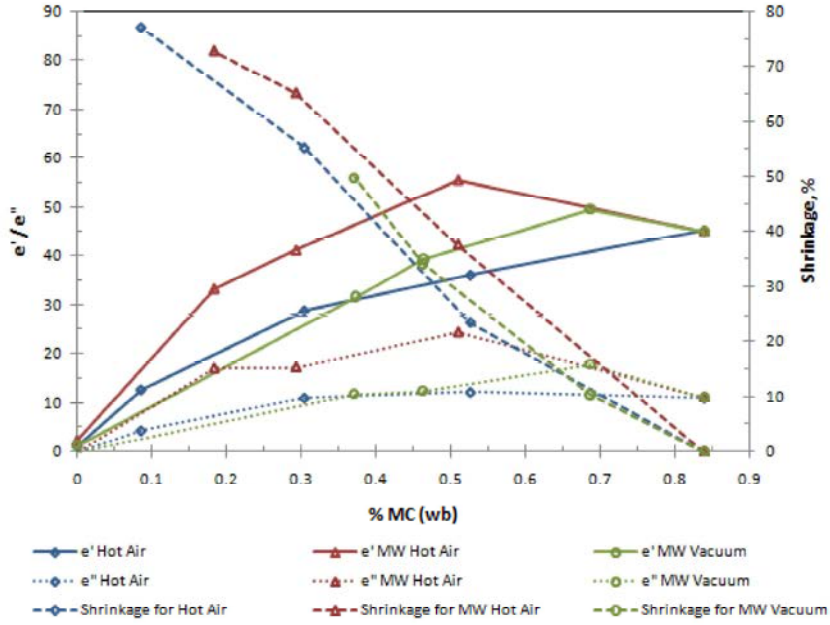

Fig. 7: Influence of dielectric constant (ϵ'), dielectric loss factor (ϵ") and volume shrinkage on the moisture content of red pitaya slices dried in three different drying systems: hot air dryer, microwave-hot air dryer and microwave-vacuum dryer

contents, clearly shows that the dielectric properties and shrinkage of pitaya slices obviously dependent on moisture content.

Moisture content is seen, as expected, to be inversely related to the shrinkage of red pitaya slices. However, shrinkage of dried pitaya slices was more pronounced under microwave-hot air drying compared to the other drying conditions. Different values of dielectric properties were obtained for dried red pitaya slices at the same moisture content for the different drying methods. This shows that dielectric properties and shrinkage of red pitaya slices also depends on the process applied to the samples and structure of the materials instead of just the moisture content as pointed out by Venkatesh and Raghavan [29].

In conclusion, fresh red pitaya slices were dried in three different drying systems: hot air dryer, microwave-hot air dryer and microwave-vacuum dryer. The addition of microwave energy to the hot air drying process enabled a reduction in drying time of over 50% compared to simple hot air drying; however, comparatively microwave-vacuum drying reduced drying time by 83% compared to simple hot air drying. The best product quality in terms of visual appearance was produced by microwave-vacuum drying. Microwave-vacuum drying was also able to retain 44.6% of the ascorbic acid content in the red pitaya fruit. Aside from visual appearance, rehydration ratio and ascorbic acid content, no significant differences in dried product quality were observed between the samples dried under hot air, microwave-hot air and microwave-vacuum drying.

ACKNOWLEDGEMENT

The authors would like to acknowledge the financial support received from the Malaysian Ministry of Science, Technology and Innovation through their National Science Fellowships, the Lembaga Zakat Selangor (Majlis Agama Islam Selangor, Malaysia) and Universiti Kebangsaan Malaysia through the research grant number DPP-2014-046 and FRGS/2/2013/TK05/UKM/02/3. The authors are also grateful to the Natural Sciences and Engineering Research Council of Canada and the Fonds Québécois de la Recherche sur la Nature et les Technologies of Québec, Canada for their financial contributions.

REFERENCES

1. Hoa, T.T., C.J. Clark, B.C. Waddell and A.B. Woolf, 2006. Post-harvest quality of Dragon fruit (*Hylocereus undatus*) following disinfesting hot air treatments. Postharvest Biology and Technology, 41(1): 62-69.

2. Lim, H.K., C.P. Tan, R. Karim, A.A Ariffin and J. Bakar, 2010. Chemical composition and DSC thermal properties of two species of *Hylocereus cacti* seed oil: *Hylocereus undatus* and *Hylocereus polyrhizus*. Food Chemistry, 119(4): 1326-1331.
3. Ariffin, A.A., J. Bakar, C.P. Tan, R.A. Rahman, R. Karim and C.C. Loi, 2009. Essential fatty acids of pitaya (dragon fruit) seed oil. Food Chemistry, 114(2): 561-564.
4. Dembitsky, V.M., S. Poovarodom, H. Leontowicz, M. Leontowicz, S. Vearasilp, S. Trakhtenberg and S. Gorinstein, 2011. The multiple nutrition properties of some exotic fruits: Biological activity and active metabolites. Food Research International, 44(7): 1671-1701.
5. Beltran-Orozco, M.C., T.G. Oliva-Coba, T. Gallardo-Velazquez and G. Osorio-Revilla, 2009. Ascorbic acid, phenolic content and antioxidant capacity of red, cherry, yellow and white types of pitaya cactus fruit (*Stenocereus stellatus* Riccobono). Agrociencia, 43: 153-161.
6. Rebecca, O.P.S., A.N. Boyce and S. Chandran, 2010. Pigment identification and antioxidant properties of red dragon fruit (*Hylocereus polyrhizus*). African Journal of Biotechnology, 9(10): 1450-1454.
7. Wu, L.C., H.W. Hsu, Y.C. Chen, C.C. Chiu, Y.I. Lin and J.A. Ho, 2006. Antioxidant and antiproliferative activities of red pitaya. Food Chemistry, 95(2): 319-327.
8. Mujumdar, A.S., 2001. Handbook of Industrial Drying. Marcel Dekker.
9. Moraveji, M.K., R. Davarnejad and M. Farjami, 2013. Investigation of some effective parameters on the fluidized bed grain dryers. Iranica Journal of Energy and Environment, 4(4): 391-397.
10. Azimi, A., T. Tovakoli, H.K. Beheshti and A. Rahimi, 2012. Experimental study on eggplant drying by an indirect solar dryer and open sun drying. Iranica Journal of Energy and Environment, 3(4): 347-353.
11. Askari, G.R., Z. Emam-Djomeh and S.M. Mousavi, 2009. An investigation of the effects of drying methods and conditions on drying characteristics and quality attributes of agricultural products during hot air and hot air/microwave-assisted dehydration. Drying Technology, 27(7/8): 831-841.
12. Ratti, C., 2001. Hot air and freeze-drying of high-value foods: a review. Journal of Food Engineering, 49(4): 311-319.
13. Chandrasekaran, S., S. Ramanathan and T. Basak, 2013. Microwave food processing-a review. Food Research International, 52(1): 243-261.
14. Zhang, M., J. Tang, A.S. Mujumdar and S. Wang, 2006. Trends in microwave-related drying of fruits and vegetables. Trends in Food Science and Technology, 17(10): 524-534.
15. Qing-guo, H., Z. Min, A.S. Mujumdar, D. Wei-hua and S. Jin-cai, 2006. Effects of different drying methods on the quality changes of granular edamame. Drying Technology, 24(8): 1025-1032.
16. Puspasari, I., M.Z.M. Talib, W.R.W. Daud and S.M. Tasirin, 2012. Drying kinetics of oil palm frond particles in an agitated fluidized bed dryer. Drying Technology, 30(6): 619-630.
17. Celma, A.R., S. Rojas and F. Lopez-Rodríguez, 2008. Mathematical modelling of thin-layer infrared drying of wet olive husk. Chemical Engineering and Processing: Process Intensification, 47(9-10): 1810-1818.
18. Hasibuan, R. and W.R.W. Daud, 2009. Quality changes of superheated steam-dried fibers from oil palm empty fruit bunches. Drying Technology, 27(2): 194-200.
19. Tulasidas, T.N., 1994. Combined convective and microwave drying of grapes. McGill University.
20. Hussain, A., Z. Li, D.R. Ramanah, C. Niamnuy and G.S.V. Raghavan, 2010. Microwave drying of ginger by online aroma monitoring. Drying Technology, 28(1): 42-48.
21. Prabhanjan, D.G. and H.S. Ramaswamy, 1995. Microwave assisted convective air drying. Journal of Food Engineering, 25(2): 283-293.
22. Sahlin, E., G.P. Savage and C.E Lister, 2004. Investigation of the antioxidant properties of tomatoes after processing. Journal of Food Composition and Analysis, 17(5): 635-647.
23. Ranganna, 2000. Handbook of Analysis and Quality Control for Fruit and Vegetable Products; Tata McGraw-Hill Publishing company Ltd.
24. Beaudry, C., G.S.V. Raghavan, C. Ratti and T.J. Rennie, 2004. Effect of four drying methods on the quality of osmotically dehydrated cranberries. Drying Technology, 22(3): 521-539.
25. Sunjka, P.S., T.J. Rennie, C. Beaudry and G.S.V. Raghavan, 2004. Microwave-convective and microwave-vacuum drying of cranberries: A comparative study. Drying Technology, 22(5): 1217-1231.
26. Therdthai, N. and W. Zhou, 2009. Characterization of microwave vacuum drying and hot air drying of mint leaves (*Mentha cordifolia* Opiz ex Fresen). Journal of Food Engineering, 91(3): 482-489.

27. Giri, S.K. and S. Prasad, 2007. Drying kinetics and rehydration characteristics of microwave-vacuum and convective hot-air dried mushrooms. Journal of Food Engineering, 78(2): 512-521.
28. Cui, Z.W., S.Y. Xu and D.W. Sun, 2004. Effect of microwave-vacuum drying on the carotenoids retention of carrot slices and chlorophyll retention of Chinese chive leaves. Drying Technology, 22(3): 563-575.
29. Venkatesh, M.S. and G.S.V. Raghavan, 2004. An overview of microwave processing and dielectric properties of agri-food materials. Biosystems Engineering, 88(1): 1-18.

NOMENCLATURE

COR	coefficient of rehydration
db	dry basis
m	mass of sample
MR	moisture ratio
QI	quality index
V	volume of sampe
X	moisture content
ΔE	total colour changes
*L**	colour parameter
*a**	colour parameter
*b**	colour parameter
ΔV	volume shrinkage

Subscript

eq	equilibrium
o	initial
rh	rehydrated sample
dh	dehydrated sample

Persian Abstract

DOI: 10.5829/idosi.ijee.2014.05.03.11

چکیده

تغییرات کیفیت برش خشک شده پیتایا قرمز (*Hylocereus undatus pitaya*) در هوای گرم، هوا گرم مایکروویو، خشک کن مایکروویو تحت خلاء مورد بررسی قرار گرفتند. پارامترهای کیفیت، رنگ، فعالیت آبی، انقباض(آب رفتگی)، نسبت جذب مجدد آب، مقدار اسید اسکوربیک و کیفیت بصری بازار بودند. مایکروویو خلاء پیتایا (*pitaya*) با بهترین کیفیت در مقایسه با هوای گرم و مایکروویو هوای گرم تولید نمود. پیتایای خشک در مایکروویو خلاء بالاترین نسبت جذب مجدد آب را داشت، در حالی که روش های دیگر نسبت جذب مجدد آبی مشابهی نشان دادند. اسید اسکوربیک در پیتایا خشک نیز بهتر حفظ شده بود هنگامی که با مایکروویو برقی خشک می شود. جدای از آن، زمان خشک کردن پیتایا خشک شده در مایکروویو خلاء را می تواند ۸۳ درصد در مقایسه با هوای گرم کاهش یابد.

Iranica Journal of Energy & Environment 5 (3): 323-336, 2014
ISSN 2079-2115
IJEE an Official Peer Reviewed Journal of Babol Noshirvani University of Technology
DOI: 10.5829/idosi.ijee.2014.05.03.12

BUT

Kinetic Evaluation of Simultaneous CNP Removal in an up-Flow Aerobic/Anoxic Sludge Fixed Film (UAASFF) Bioreactor

[1]A.M. Mansouri, [2]A.A.L. Zinatizadeh and [2]A. Akhbari

[1]Department of Analytical Chemistry, Faculty of Chemistry, Razi University, Kermanshah, Iran
[2]Water and Wastewater Research Center (WWRC), Department of Applied Chemistry, Faculty of Chemistry, Razi University, Kermanshah, Iran

Received: March 12, 2014; **Accepted** in Revised Form: June 11, 2014

Abstract: The kinetics of simultaneous removal of carbon, nitrogen and phosphorus from a synthetic wastewater in an innovative up-flow aerobic/anoxic sludge fixed film (UAASFF) bioreactor was investigated. The kinetic analysis was performed using the experimental data obtained in an earlier study where the UAASFF bioreactor was examined under different operating conditions by changing three independent variables, HRT, COD:N:P ratio and aeration time. In the analysis, different kinetic models (Monod, first-order, second-order and Stover-Kincannon models) were evaluated. The maximum removal efficiency of COD, total nitrogen (TN) and phosphorus (TP) were obtained to be 95.42, 79 and 79.1 %, respectively. All the models examined, gave high correlation coefficients for carbon, nitrogen and phosphorus removal. Biokinetic coefficients were determined as Y= 0.417-0.496 g VSS/g COD, k_d= 0.027-0.053 d^{-1}, μ_{max} =1.36 g VSS /g VSS.d, K_B=37.96 g/l.d, U_{max} =38.46 g/l.d, K_B(N) =0.271-7.2 g/l.d 6, U_{max}(N) =0.33-5.4 g/l.d, K_B (P)=0.09-0.89 g/l.d, U_{max} (P)=0.07-0.42 g/l.d.

Key words: Simultaneous nutrients removal kinetics · UAASFF bioreactor · Monod · Grau second-order model · Stover-Kincannon model

INTRODUCTION

Discharge of untreated wastewater containing nitrogen and phosphorus into receiving rivers result in environmental and human health problems such as fish poisoning by ammonia and eutrophication in water bodies. It is, therefore, necessary to remove these substances from wastewaters for reducing their harms to environments. Biological treatment has been accepted as one of the most feasible, eco-friendly and cost-effective options for the treatment of pollutants [1-3]. The performance of biological wastewater treatment systems can be improved by maintaining a high biomass concentration; because of the wastewater treatment capacity is proportional to the total biomass of the bioreactor.

In the recent years, substantial attention has been paid towards the compact high-rate bioreactors for wastewater treatment to meet the strict constraints with respect to space, odor, view and biosolids production. The integrated bioreactors which combine the aerobic and anaerobic processes in a single bioreactor are seen as a viable alternative and enhancing the overall removal efficiency [4]. A number of integrated bioreactors (such as; a naerobic-aerobic granular biofilm bioreactor, anoxic/oxic-membrane bioreactor (A/O-MBR), nano-filtration membrane bioreactor (NF-MBR), staged anaerobic-aerobic membrane bioreactor (MBR), rotating biological contactor and activated sludge (RBC-AS) and integrated anaerobic-aerobic fixed-film reactor (FFR)) have been developed which allow the coexistence of anaerobic and aerobic populations inside the same reactor [4-10].

Biomass concentration in biological reactors can be increased by variety techniques. Passive immobilization and intermittent aeration and effluent discharge in are two approaches for obtained this purpose [11-12]. The intermittent aeration strategy can also reduce the cost of treatment operation and demand for rbCOD contained in

Corresponding Author: A.M. Mansouri, Department of Analytical Chemistry, Faculty of Chemistry, Razi University, Kermanshah, Iran. Tel: +989188581130, Fax: +988314274559.

Please cite this article as: A.M. Mansouri, A.A.L. Zinatizadeh and A. Akhbari, 2014. Kinetic Evaluation of Simultaneous CNP Removal in an up-Flow Aerobic/Anoxic Sludge Fixed Film (UAASFF) Bioreactor. Iranica Journal of Energy and Environment, 5 (3): 323-336

the influent wastewater, so that PAOs will obtain sufficient rbCOD for anaerobic P release, which is beneficial to biological P removal. In addition, in an intermittently aerated bioreactor, the organic C stored by PAOs could be used by denitrifiers for denitrification in subsequent anoxic periods [13], resulting in less dependence of denitrification on the rbCOD content in the influent wastewater. Therefore, stable and efficient N and P removal can be achieved in intermittently aerated bioreactors. On the basis of the above consideration, an innovative up-flow aerobic/anoxic sludge fixed film (UAASFF) bioreactor with intermittent aeration as a hybrid reactor which is a combination of an activated sludge (AS) and an immobilized cell or fixed film (FF) reactor. The UAASFF was established and applied as a single treatment unit for carbon, nitrogen and phosphorus removal. The possibility to achieve high biomass concentration, no requirement for additional equipment to circulate the mixed liquor between aerobic and anaerobic compartments and, consequently, the application of short hydraulic retention time and wide variety COD:N:P ratio are the advantages of this type reactor.

Process modeling is an accepted route for describing the performance of biological treatment systems and predicting their performance. In order to achieve the correct design of a bioreactor as well as the reactor's maximum performance, the kinetic coefficients should be taken into consideration at the process of engineering design instead of using only empirical methods. The types of substrates and microorganisms and environment surrounding in a bioreactor are associated with value of the kinetic coefficients. Many models for the biomass growth processes have appeared in the wastewater treatment literature [14, 15]. Global parameters such as COD, BOD and NH_4 -N were used as substrate for evaluation under the assumption that the removal was exclusively due to aerobic biodegradation [16]. First-order substrate removal model [16-18] and second-order model often known as Optaken-Grau model are some of those which are used to test the kinetics of organic and nitrogen removal in bioreactors [19-20].

As the UAASFF system is involving a complex process (including anoxic and aerobic reactions in a single system with attached and suspended microbial growth), determination of the kinetic constants is of great importance in practical point of view. Therefore, this study is aimed to determine the biokinetic parameters of the process removing carbon, nitrogen and phosphorus using experimental data obtained under different operational conditions (varying HRT, aeration time and COD/N/P ratio). Different mathematical models including Monod, first-order, second-order and Stover-Kincannon model were employed to predict the kinetic coefficients.

Theoretical Development

Mass Balance Model: For an UAASFF reactor without biomass recycle, the rate of change of biomass in the system can be expressed as Eq. (1):

$$\frac{dX}{dt}V = QX_0 - [(Q - Q_w)X_e + Q_wX_w)] - VYr_{su} - Vk_dX \quad (1)$$

If it is assumed that the influent biomass concentration can be neglected and the condition is steady-state ($dX/dt = 0$), Eq. (2) which was derived by rearranging and simplifying the Eq. (1),

$$\frac{(Q - Q_w)X_e + Q_wX_w}{VX} = -Y\frac{r_{su}}{X} - k_d \quad (2)$$

The inverse of the term on the left-hand side of Eq. (2) is defined as the average solid retention time (SRT) and then Eq. (2) is rewritten as:

$$\frac{1}{SRT} = -Y\frac{r_{su}}{X} - K_d \quad (3)$$

In the Eq. (3), the term ($-r_{su}/X$) is known as the specific substrate utilization rate, U, which is calculated as follows:

$$U = \frac{r_{su}}{X} = \frac{Q(S_0 - S)}{VX} = \frac{S_0 - S}{(HRT).(X)} \quad (4)$$

By Substituting ($\mu=1/SRT$) and U into Eq. (3) will have:

$$\mu = YU - k_d \quad (5)$$

The kinetic parameters (Y, K_d) can be obtained by plotting Eq. (5).

The relationship between the specific growth rate, the rate limiting substrate concentration and SRT can be expressed by the Monod Eq. (4) as follows:

$$\mu = \frac{\mu_{max}.S}{K_s + S} \quad (6)$$

$$\mu = \frac{1}{SRT} + k_d \quad (7)$$

$$\frac{\mu_{max}.S}{K_s + S} = \frac{1}{SRT} + k_d \quad (8)$$

The value of μ_{max} and K_S are determined by plotting Eq. (9), which is derived by rearranging Eq. (8).

$$\frac{SRT}{1+k_d SRT} = \frac{K_s}{\mu_{max}} \cdot \frac{1}{S} + \frac{1}{\mu_{max}} \quad (9)$$

First-Order Substrate Removal Model: The rate of change in substrate concentration in the system with assuming the first order model for substrate removal could be expressed as follows:

$$-\frac{dS}{dt} = \frac{QS_0}{V} - \frac{QS}{V} - k_1 S \quad (10)$$

Under pseudo-steady-state conditions, the rate of change in substrate concentration due to accumulation (-d*S*/d*t*) is negligible and the equation given above can be modified as:

$$\frac{S_0 - S}{HRT} = k_1 S \quad (11)$$

The value of k_1 can be obtained by plotting ((S_0 - S)/HRT) versus S in Eq. (11).

Second-Order Substrate Removal Model: The general equation of a second-order model is given below [20] :

$$-\frac{dS}{dt} = k_{2(s)} \cdot \left(\frac{S}{S_0}\right)^2 \quad (12)$$

If Eq. (12) is integrated and then linearilized, Eq. (13) is resulted:

$$\frac{S_0 HRT}{S_0 - S} = HRT + \frac{S_0}{k_{2(s)} X} \quad (13)$$

If the second term of the right part of this equation is accepted as a constant, equation will be modified as below:

$$\frac{S_0 HRT}{S_0 - S} = a + bHRT \quad (14)$$

(S_0 -*S*)/S_0 expresses the substrate removal efficiency and is symbolized as *E*. Therefore, Eq. (15) can be written as follows:

$$\frac{HRT}{E} = a + bHRT \quad (15)$$

Stover-Kincannon Model: Stover-Kincannon is one of the most widely used mathematical models for determining the kinetic constants in immobilized systems. The model has been applied to continuously operated mesophilic and thermophilic upflow anaerobic filters for the treatment of paper-pulp liquors [21] and simulated starch wastewater [22], anaerobic filter for soybean wastewater treatment [22], nitrogen removal in an anammox non-woven membrane reactor [24] upflow aerobic immobilized biomass (UAIB) reactor treating simulated sugar-manufacturing wastewater [25] and anaerobic migrating blanket reactor treating a synthetic wastewater [26].

In this model, the substrate utilization rate is expressed as function of the organic loading rate by monomolecular kinetic for biofilm reactors such as rotating biological contactors and biological filters. Equations of the Stover-Kincannon model are as follows:

$$\frac{dS}{dt} = \frac{Q}{V}(S_0 - S) \quad (16)$$

$$\frac{dS}{dt} = \frac{U_{max}(QS_0/V)}{k_B + (QS_0/V)} \quad (17)$$

If $(dS/dt)^{-1}$ is taken as $V/[Q(S_0 - S)]$, which is the inverse of the removed substrate loading rate and this is plotted against the inverse of the total loading rate $V/Q.S_0$, a straight line portion of intercept $1/U_{max}$ and a slope of K_B/U_{max} resulted.

$$\left(\frac{dS}{dt}\right)^{-1} = \frac{V}{Q(S_0 - S)} = \frac{k_B}{U_{max}} \cdot \frac{V}{QS_0} + \frac{1}{U_{max}} \quad (18)$$

The substrate balance for the reactor at steady-state can be written as follows:

$$QS_0 = QS + V\frac{dS}{dt} \quad (19)$$

Substituting of Equation (17) into (19) gives

$$QS_0 = QS + \frac{U_{max}(QS_0/V)}{K_B + (QS_0/V))} * V \quad (20)$$

This expression can then be solved for either the effluent substrate concentration (Eq. (21)) or the removal efficiency of the reactor (Eq. (22)) by substituting kinetic constants U_{max} and K_B.

$$S = S_0 - \frac{U_{max} S_0}{K_B + (QS_0/V)} \quad (21)$$

$$E = \frac{S_O - S}{S_O} = \frac{U_{max}}{K_B + (QS_0/V)} \quad (22)$$

MATERIALS AND METHODS

Synthetic Wastewater (SWW): SWW was prepared based on the three different COD:N:P ratios (1000:250:50, 1000:83.3:35 and 1000:50:20). The synthetic wastewater was composed of glucose as simple carbon source, NH_4Cl as nitrogen source, KH_2PO_4 as phosphorus source and mineral nutrients such as $MgSO_4$ (0.2 g/l), $FeSO_4$ (0.01 g/l), $CaCl_2$ (0.2 g/l) and $NaHCO_3$ (0.073-1.45 g/l).

Bioreactor Configuration and Start up: A lab-scale UAASFF bioreactor was used in this study (Fig. 1). The glass bioreactor column was fabricated with an internal diameter of 5.2 cm and a liquid height of 122 cm. The working volume (total liquid volume excluding volume of the pall rings in fixed bed section) was 2500 ml. The column consisted of three sections; bottom, middle and top. The bottom part of the column, with a height of 80 cm was operated as an upflow activated sludge reactor, the middle part of the column with a height of 25 cm was operated as a fixed film (FF) reactor and the third part is for providing sufficient volume at the top of the reactor in order to continuous feeding and intermediate discharge. The middle section of the column was packed with a plastic media (supplied by JiangXi Transung Chemical Packing Co. China). The voidage of the packed-bed reactor was 85.45% and the specific surface area of the packing material was 500 m^2/m^3. The UAASFF reactor was operated under room temperature (20±2°C). In order to distribute the feed uniformly in the reactor, an influent liquid distributor was mounted at the base of the column. Air was introduced into the reactor with two bubble air diffusers at the bottom of the reactor. The air flow rate and the aeration time were controlled with an air flow-meter and timer that connected to the blower.

The reactor was inoculated with activated sludge taken from an aeration tank (municipal wastewater treatment plant, Kermanshah, Iran). The inoculum sludge had a sludge age of about 15 d, a mixed liquor volatile suspended solids (MLVSS) concentration of 5.8 g/l. After an initial dilution, 2.5 L activated sludge was seeded to the reactor, resulting in an initial MLVSS concentration of 3.8-4.0 g/l in the reactor.

Bioreactor Operation: In the first stage (reactor start-up), after adding the prepared inoculums, the bioreactor was operated under continuous flow regime. At intermittent aeration conditions at temperature, HRT, COD:N:P ratio and aeration time were 20±2°C, 6.5 h, 1000:83.3:35 and 40 min/h, respectively. It should be explained that each operation cycle was included three steps

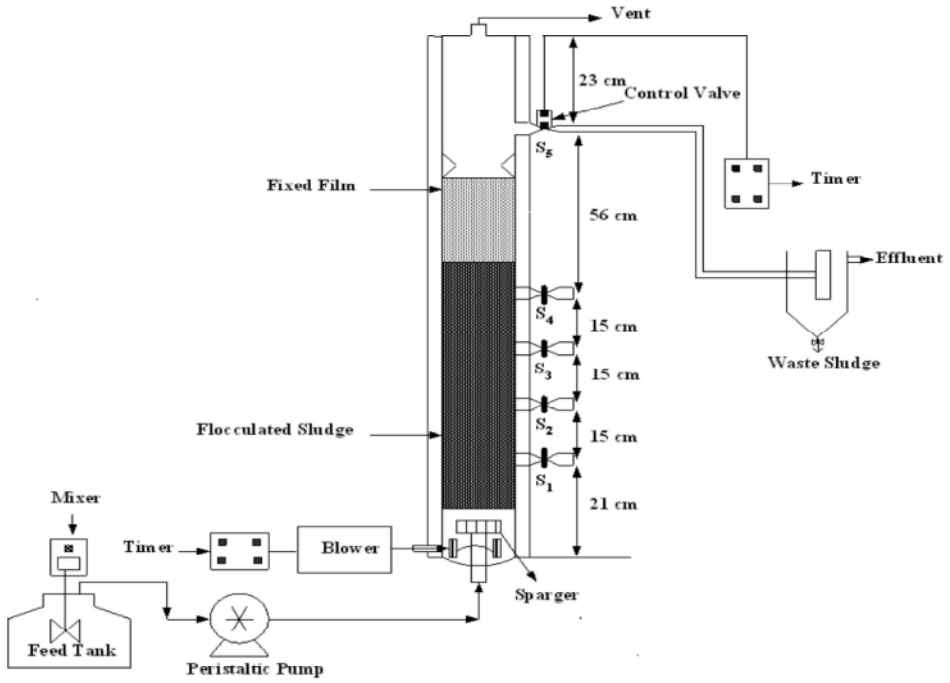

Fig. 1: Experimental set up

Table 1: Experimental range and levels of the independent variables

	Range and levels					
Variable1s	-1		0		1	
HRT(h)	2		4.25		6.50	
COD:N:P ratio	4		12		20	
Aeration time(min/h)	30		40		50	
	Aeration	Settling	Aeration	Settling	Aeration	Settling
	12 min	12 min	10 min	7 min	16 min	4 min

Table 2: Experimental data obtained under steady state conditions.

	Variables			Influent		Effluent									Responses			
Run	HRT h	COD:TKN:TP g:g:g	Aeration time min/h	Q_{in} l/d	X_i gVSS/l	Q_w l/d	X_e g/l	X_w g/l	COD_e g/l	TKN_e g/l	NO_{3in} g/l	NO_{3e} g/l	TN_e g/l	TP_e g/l	μ (1/SRT) d^{-1}	COD Rem. %	TN Rem. %	TP Rem. %
	2	1:0.25:0.05	30	30	4	0.74	0.011	8	0.406	0.138	0.017	0.003	0.139	0.03	0.62	59.4	45.3	39.2
1	4.25	1:0.25:0.05	30	14.11	4	0.48	0.006	8	0.134	0.111	0.017	0.004	0.112	0.017	0.39	86.6	55.9	65.6
	6.5	1:0.25:0.05	30	9.23	4	0.31	0.008	8	0.083	0.73	0.017	0.002	0.073	0.01	0.25	91.7	71	79.1
	2	1:0.05:0.02	30	30	4	0.84	0.009	8	0.35	0.031	0.017	0.001	0.032	0.012	0.70	65	41.2	41.3
2	4.25	1:0.05:0.02	30	14.11	4	0.49	0.006	8	0.134	0.026	0.017	0.003	0.028	0.007	0.40	86.6	50.3	65.6
	6.5	1:0.05:0.02	30	9.23	4	0.33	0.006	8	0.064	0.011	0.017	0.006	0.012	0.006	0.27	93.6	77.7	71.7
	2	1:0.083:0.035	40	30	4	0.77	0.11	6.5	0.316	047	0.017	0.001	0.048	0.023	0.82	68.4	45.2	34
3	4.25	1:0.083:0.035	40	14.11	4	0.71	0.011	6.5	0.117	0.027	0.017	0.007	0.029	0.014	0.47	88.3	66.81	59
	6.5	1:0.083:0.035	40	9.23	4	0.44	0.008	6.5	0.009	0.017	0.017	0.005	0.018	0.013	0.29	91	79	63.7
	2	1:0.25:0.05	50	30	4	0.28	0.35	5.5	0.27	0.117	0.017	0.003	0.012	0.037	0.98	73	53.6	25.4
4	4.25	1:0.25:0.05	50	14.11	4	0.63	0.12	5.5	0.146	0.093	0.017	0.016	0.097	0.029	0.51	85.4	61.7	41.7
	6.5	1:0.25:0.05	50	9.23	4	0.57	0.03	5.5	0.088	0.073	0.017	0.048	0.083	0.031	0.34	91.2	67.1	37.3
	2	1:0.05:0.02	50	30	4	0.29	0.35	5.5	0.248	0.018	0.017	0.019	0.023	0.015	0.99	75.2	57.3	23.3
5	4.25	1:0.05:0.02	50	14.11	4	0.65	0.12	5.5	0.146	0.016	0.017	0.016	0.019	0.012	0.52	85.4	63.9	37.3
	6.5	1:0.05:0.02	50	9.23	4	0.59	0.03	5.5	0.071	0.013	0.017	0.024	0.018	0.011	0.35	92.9	65.2	46.2

(aeration, settling and effluent discharge) which are intermittently carried out while the influent was continuously fed. This was continued until providing steady state condition. Intermittent effluent discharge was provided by using a programmable control valve at the bioreactor output. The time of discharge was adjusted by giving the time program with regard to the operating condition. The range studied for the HRT, COD:N:P ratio and intermittent cycling program for the aeration and settling time is presented in Table 1.

In the second stage, the UAASFF bioreactor was operated with synthetic wastewater under continuous flow regime and various experimental conditions by changing three independent variables viz. HRT, COD:N:P ratio, aeration time designed using Design Expert software (ver. 6.0) as shown in Table 2. The region of exploration for the process was taken as the area enclosed by hydraulic retention times (2, 4.25 and 6.5 h), COD: N: P ratios (1000:50:20, 1000:83.3:35 and 1000:250:50) and aeration times (30, 40 and 50 min/h) boundaries.

Chemical Analysis: The concentrations of chemical oxygen demand (COD), Total Kjeldahl nitrogen (TKN), nitrate, total nitrogen (TN), total phosphorus (TP), total suspended solids (TSS) were determined by using standard methods [27]. For COD, a colorimetric method 3with closed reflux method was developed. Spectrophotometer (DR 5000, Hach, Jenway, USA) at 600 nm was used to measure the absorbance of COD samples.Total Kjeldahl nitrogen (TKN) was determined by TKN meter Gerhardt model (Vapodest 10, Germany). The pH meter model HANNA-pH 211 was used to measure the pH.

RESULTS AND DISCUSSION

SCOD Removal

Process Description: The experimental values for SCOD removal obtained from a process performance studies were used to determine the kinetic coefficients. Table 2 summarizes the experimental conditions, effluent parameters and the process responses. Influent COD concentration was kept constant about 1000 mg/l. The range of HRT studied corresponds to food to microorganism (F/M) and feed flow rate 2.31-7.5 g COD/g VSS.d and 9.23-30 l/d, respectively. The maximum value of the COD removal was obtained to be 93.6% at COD: N: P ratio and aeration time 1000:50:20 and 30 min/h, respectively. The most significant factor effective on the COD removal was determined to be HRT. The effect of HRT at lower values of the aeration time was greater than those with higher aeration times. The interaction showed

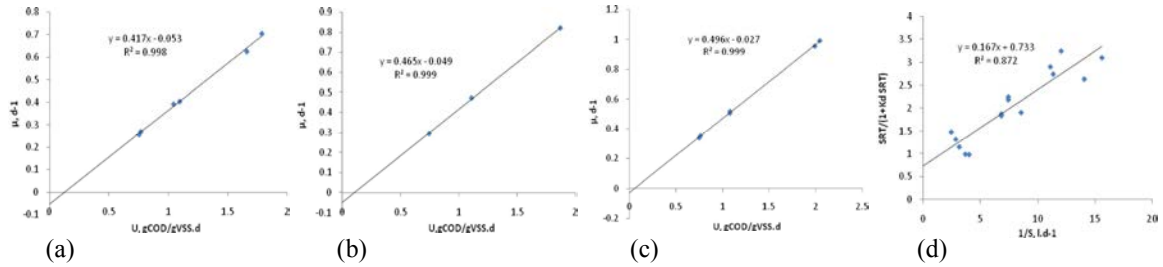

(a) (b) (c) (d)

Fig. 2: Estimation of the yield coefficient of biomass (Y) and bacteria decay rate (k_d) for SCOD removal in, (a) aeration time =30 min/h, (b) aeration time =40 min/h, (c), aeration time =50 min/h, (d) Estimation of the half velocity coefficient (K_s) and maximum rate of substrate degradation (Umax) for SCOD removal.

that HRT and aeration time played an important role in COD removal in the process. From the results presented in the Table 2, the response increased upon increasing the aeration time at lower HRT while at higher HRT, aeration time did not show significant effect on COD removal. It was attributed to sufficient aeration time at higher HRT which makes the response independent to aeration time in the design space studied. As a result, as the HRT increases, less aeration time is needed. The COD /N ratio (in the range of 4-20) did not show a strong effect on the process, as only a small difference is observed in the results obtained with different COD/N ratio. However, the response showed a little increase as the COD/N ratio was increased. Many methods have been used to describe the overall kinetics of organic removal in biological treatment systems. Here, the Monod model, first-order model, Stover-Kincannon model and second-order model (based on Substrate) were selected for describing COD removal rate in the UAASFF reactor.

Kinetics Evaluation for SCOD Removal

Mass Balance-based (Monod) Model: In order to estimate the cell yield coefficient (Y) and biomass decay coefficient (k_d), the relationship between the inverse SRT (μ =1/SRT) and the specific substrate utilization rate (U) (Eq. (5)) in the different conditions of aeration times for COD removal was plotted in the Fig. 2a-c. Y and k_d values were determined to be in the range of 0.417-0.496 g VSS g/COD and 0.027-0.053 d^{-1}, respectively, as shown in Table 3. As noted in the Table 3, an increase in aeration time (from 30 to 50 min/h) caused an increase in Y due to higher sludge production resulted from high COD consumption rate in the higher aeration time. Dissolved oxygen serves only as an electron acceptor for heterotrophic aerobes in wastewater.

The k_d is of little significance when the retention time is short, being an order of magnitude less than μ. However, when the system is operated in the endogenous growth phase, k_d is important in the calculation of the net amount of microorganisms produced and the oxygen utilization rate [28]. The lower values of k_d in this study resulted in short hydraulic retention time. The value of Y relates to concentration of biomass in the bioreactor and amount of excess sludge wasted. The higher values of Y obtained from the present work compared to the other study was because of short HRT (corresponding to higher OLR) and more biodegradability of substrate in this research.

The maximum growth rates (μ_{max}) and substrate saturation constant (K_S), were computed by plotting the experimental data as SRT/((1+k_d.SRT)) vs. 1/S (Fig. 2d). The values of kinetics coefficients, μ_{max} and K_S, were 1.36 g VSS produced /g VSS and 0.22 gCOD/l, respectively (Table 3). The K_s, as an apparent kinetic constant, represent the half velocity coefficient of bacteria which has reverse relationship with yield coefficient (Y) and bacteria decay rate (k_d) [29]. Also K_s determines how rapidly μ approaches μ_{max} and it is defined as the substrate concentration at which μ is equal to half of μ_{max} ($\mu=\mu_{max}/2$) [30]. This is the basis for all continuous flow treatment processes in biological wastewater treatment in which microorganisms are continuously cultivated but the overall rate of metabolism is controlled by the substrate concentration.

Table 4 shows the kinetic coefficients reported from different studies. As presented in Table 4, the value of the μ_{max} (1.36 d^{-1}) obtained in this study was higher than the μ_{max} value found by Carta-Escobar *et al*. [16] but smaller than the values reported by Kaewsuk *et al*. [28] (Table 4). The most likely reason for the differences in the kinetic coefficients compared with the values is the significant discrepancy in reactor configurations and wastewater composition [31]. According to the Monod equation, high μ_{max} value relates to the high substrate removal rate, indicating relatively high removal rate in the UAASFF bioreactor.

Table 3: Kinetic parameters for COD removal in UAASFF reactor

	Variables			Kinetic parameters: Mass balance (Monod) model								First order model	Stover-Kincannon model		Second order model		
Run	HRT h	COD: TKN:TP g:g:g	Aeration time min/h	Regression equation	R^2	Y gVSS/g COD	k_d gVSS/g VSS.d	Regression equation	R^2	μ_{max} g new cell/g cell.d	Ks gCOD/l	k_1 d^{-1}	K_B g.l.d^{-1}	Umax g.l.d^{-1}	$k_{2(s)}$ d^{-1}	a	b
1	2	1:0.25:0.05	30	Y=0.417x-0.053	0.99	0.417	0.053					12.09					
	4.25	1:0.25:0.05	30														
	6.5	1:0.25:0.05	30														
2	2	1:0.05:0.02	30														
	4.25	1:0.05:0.02	30														
	6.5	1:0.05:0.02	30														
3	2	1:0.083:0.035	40	Y=0.465x-0.049	0.99	0.465	0.049	Y=0.167x+0.733	0.91	1.36	0.22		37.65	38.46	5.95	0.042	0.928
	4.25	1:0.083:0.035	40									19.48					
	6.5	1:0.083:0.035	40														
	2	1:0.25:0.05	50														
4	4.25	1:0.25:0.05	50	Y=0.496 - 0.027	0.99	0.496	0.027					30.71					
	6.5	1:0.25:0.05	50														
	2	1:0.05:0.02	50														
5	4.25	1:0.05:0.02	50														
	6.5	1:0.05:0.02	50														

Table 4: Comparison of kinetic constants obtained from different models cited in the literature with the present results

Models	Substrate	Type of reactor	CODin g/l	HRT d	Kinetic parameters: Y	k_d	μ_{max}	Ks	Reference
Monod	Domestic wastewater	MBR	-	-	0.25 - 0.40	0.04-0.075	-	-	Huang *et al*., 2001
	Dairy wastewater	AS	-	2.3-2.4	0.26	0.032	0.440	0.141	Escobar *et al*., 2004
	Dairy wastewater	MSBR	2.5	10	0.23	0.14	1.69	0.174	Kaewsuk *et al*., 2010
	Synthetic wastewater	UAASFF	1	0.083-0.271	0.417-0.496	0.027-0.053	1.36	0.22	This study
						k1,d-1			
First-order	sugar-manufacturing wastewater	UAIB	0.75-4.5	0.5-1.0		14.549			Borghei *et al*., 2007
	Synthetic wastewater	UAASFF	1	0.083-0.271		12.09 -30.71			This study
					Umax			KB	
Stover-Kincannon	sugar-manufacturing wastewater	UAIB	0.75-4.5	0.5-1.0	101			106.8	Borghei *et al*., 2007
	Synthetic wastewater	MBBR	0.75-4.5	1	8.3			9.45	Borghei and Hosseiny, 2002
	Soybean wastewater	AF	7.5-11.45	1-1.45	83.3			85.5	Yu *et al*., 1998
	Synthetic wastewater	UAASFF	1	0.083-0.271	38.46			37.88	This study
					$k_2(s)$		a	b	
	Synthetic wastewater	UAIB	0.75-4.5	0.5-1.0	3.582		0.047	1.007	Borghei *et al*.,2008
Second order (Grau)	Molasses	RBC	2-15	0.5-2.0	10.81		0.033	1.192	Optaken ,1982
	Synthetic wastewater	UAASFF	1	0.083-0.271	5.95		0.042	0.928	This study

First Order Model: The majority of biological wastewater treatment processes are described by first-order kinetics. Reaction orders can differ when there is variation in the microorganisms, the substrate or environmental conditions and they must be measured experimentally. The BOD and COD removal has been traditionally modeled as a continuous first order reaction [32]. In this type of reaction, the rate of breakdown is at first rapid when the organic content is high, but gets progressively slower as the organic material is utilized.

Fig. 3a-c shows the correlation between the $(S_0\text{-}S)/HRT$ and the substrate concentration (S) in the bioreactor drawn based on the first-order equation (Eq. (11)). The data fitted well with an $R^2 > 0.93$. The high values of the determination coefficients (R^2) clearly indicate that first-order kinetics can be applied with good degree of precision. The values of first-order kinetic constant (k_1) were calculated to be in the range of 12.09 - 30.71 d^{-1} (Table 3). It was found that with an increase in the aeration time, the first-order kinetic constant (k_1) was increased favoring the biodegradation reaction of the substrate. As data presented in the Table 4, in a similar work, the first-order model was applied for the process kinetics of in a lab-scale upflow aerobic immobilized biomass (UAIB) reactor treating simulated sugar-manufacturing wastewater [25]. In this study, k_1 obtained 14.549 d^{-1} with correlation coefficient of 0.742. The difference between k_1 values obtained from the two studies might be attributed to the difference in type of the wastewater used as feed and the OLR applied. The results indicated that the UAASFF reactor described in this study was capable to biodegrade the organic matter up to 93 % at a low HRT (6.5 h).

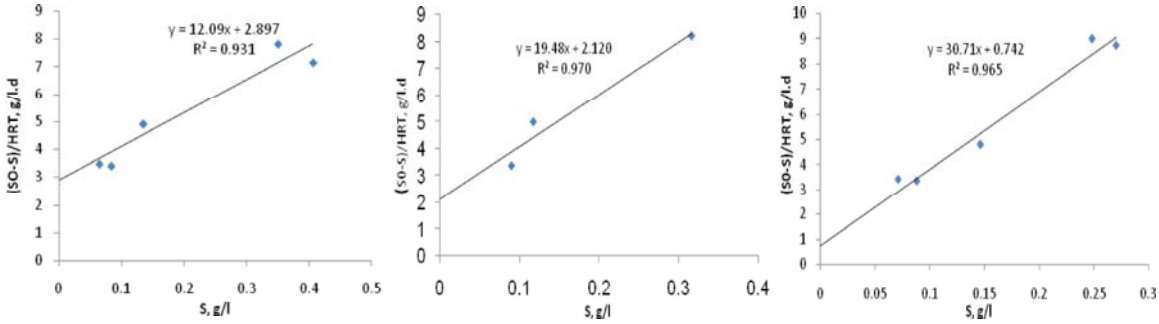

(a) (b) (c)

Fig. 3: First-order kinetics model plot for SCOD removal in, (a) aeration time =30 min/h , (c) aeration time= 40 min/h, (d) aeration time =50 min/h.

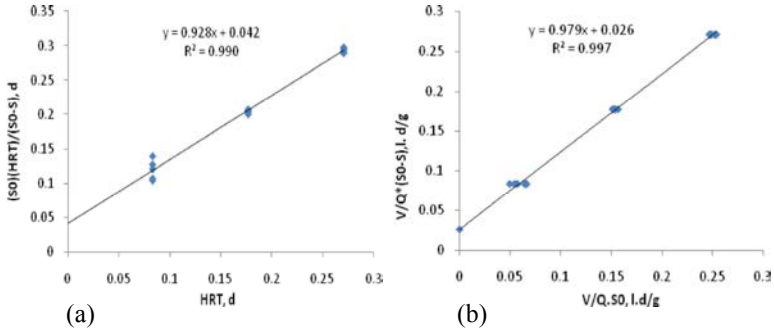

(a) (b)

Fig. 4: (a) Second-order kinetics model plot for SCOD removal (b) Stover-Kincannon model plot for SCOD removal.

Second-Order Model (Grau Model): The second-order model was also used to evaluate the rate of the biodegradation process occurred in the UAASFF bioreactor. In order to determine the kinetic coefficients (a, b and $k_{2(s)}$), Eq. (14) was plotted as shown in Fig. 4a. It must be noted that the substrate concentration is of high importance in second order reactions. Table 4 presents a comparable data for second-order kinetics from different studies [19, 25]. The values of $K_{2(s)}$ reported in the previous studies were in the range of 3.58-10.81 d^{-1}, where the value of $k_{2(s)}$ was 5.95(d^{-1}). The obtained results in this study, conforming the reported date in literature. The correlation coefficient (R^2) was 0.99, indicating the excellent agreement between the experimental and the modeled data.

Based on the Eq. (14), the relationship between effluent COD concentration and HRT is described as follows:

$$S = S_0(1 - \frac{HRT}{0.042 + 0.928HRT}) \quad (23)$$

and the substrate removal efficiency is represented by

$$E = \frac{HRT}{0.042 + 0.928HRT} \quad (24)$$

Stover-Kincannon Model: Stover-kincannon model investigates the effect of the influent OLR on the removed OLR. Fig. 4b shows the graph plotted between inverse the removed OLR, $V/(Q(S_0 - S))$, vs. inverse OLR_{in}, $V/(QS_0)$. According to Eq. (18), saturation constant (K_B) and maximum total substrate utilization rate (U_{max}) were calculated (Fig. 4b). The constant values for K_B and U_{max} were obtained 37.65 and 38.46 g/l.d, respectively (Table 4). It is resulted from the experimental data that the maximum removed OLR (OLR_{rem}) in the reactor was 22.56 g/l.d, implying that the reactor possessed an excellent COD removal capacity. The Stover- Kincannon model can also be used to determine the volume required to decrease the influent nutrient concentration from S_0 to S or to determine the effluent nutrient concentration for a given volume of the UAASFF bioreactor and influent nutrient concentration. From substrate mass balance equation (Eq. (21)), the following equation can be obtained:

$$S = S_0 - \frac{38.46S_0}{37.65 + (QS_0/V)} \quad (25)$$

The model developed for prediction of the total substrate removal efficiency in the present work is as follows:

$$E = \frac{38.46}{37.65 + (QS_0 / V)} \quad (26)$$

Consequently, the results of the kinetic studies obtained from the lab-scale experiments can be used for estimating treatment efficiency of a full-scale process under similar operational conditions. Therefore, the Stover-Kincannon model could be used in the design of the UAASFFF bioreactor. As seen in Table 4, a wide range of kinetic constants (U_{max} and K_B) were determined depending on the characteristics of the studied wastewaters and experimental conditions. Higher values of the constants have been reported for treating readily biodegradable substrates, such as molasses and glucose, while the lower values result from the presence of several recalcitrant inorganic compounds, complex components and other undesirable impurities in the wastewaters [22, 33-34]. The U_{max} value (38.46 g/l.d) obtained in this study was smaller than the value found by Borghei and his coworkers [25] (101 g/l.d) and larger than that obtained by Borghei and Hosseiny [35] (8.3 g/l.d). The wide range reported for U_{max} is attributed to different factors like type of reactor, OLR applied, wastewater characteristics and microorganisms used in the studies.

TN Removal

Process Description: During the course of the system's operation, the removal of the nitrogen contents was also monitored. The influent and effluent concentrations of TN, TKN and nitrate for steady state conditions are presented in Table 2. The concentration of ammonium nitrogen in this study was in the range of 50-250 mg/l. The performance of the UAASFF reactor under different HRT, COD:N:P ratio and aeration time is shown in Table 3. The results indicate that high efficiencies of TN removal were attained at high HRT and low aeration time. A reverse impact of the aeration time on TN removal was observed as the variable increased (Table 2). An increase in the aeration time (from 30 to 40 min/h) caused an increase in the response due to higher NO_3^- production as well as the favored condition for denitrification resulted from high DO consumption rate. Further increment in the variable (from 40 to 50 min/h) decreased the response. This was due to domination of nitrification over denitrifiction process, which was originated from much shortened time of settling. The maximum TN removal efficiency was found to be 79% at HRT, COD/N ratio and aeration time of 6.5 h, 12 and 40 min/h, respectively.

It has been argued that the TN removal process is so complex that it cannot be adequately described solely by the first-order reaction equation, with good degree of precision [24,36]. As the fraction of nitrifiers and denitrifiers in the biomass contents of the bioreactor was not investigated, so the Monod model could not be reliably employed to describe the TN removal process. Therefore, in this study the kinetic of the TN removal was studied using second-order and Stover-Kincannon models.

Kinetic Evaluation for TN Removal

Second-Order Substrate Removal Model: Grau second-order model coefficients were determined by plotting Eq. (14) (Fig. 5a-e). The values of $k_{2(s)}$, a and b are presented in Table 5. The R^2 of the second-order kinetic model was in the range of 0.79-1.0. Coefficients (a and b) for different aeration time and COD/N ratio studied are shown in Table 5. It is clear from the results that the both variables were effective on the $k_{2(s)}$. It was found that with an increase in aeration time, the average $k_{2(s)}$ was increased while with an increase in COD/N ratio the average $k_{2(s)}$ was decreased.

Stover-Kincannon Model: This model is capable of predicting substrate removal at any loading conditions, no matter which order kinetics [36]. Fig. 6a-e depicts the graphs plotted as inverse removed nitrogen loading rate, $[V/(Q(TN_{in} - TN_{out})]$, versus the inverse total nitrogen loading rate, $[V/(Q\ TN_{in})]$, at different conditions of aeration times (30, 40 and 50 min/h) and COD/N ratios (4, 12 and 20). As biokinetic data are presented in Table 5, the saturation constant (K_B) and the maximum utilization rate (U_{max}) for different conditions were computed to be in the ranges between 0.271-7.25 and 0.333-5.43 g/l.d, respectively.

The correlation coefficients (R^2) were over 0.87. The maximum values of K_B and U_{max} were determined to be 7.25 and 5.43 g/l.d, respectively. At aeration time and COD/N ratio of 50 min/h and 4 while the minimum values were obtained 0.271 and 0.333 at aeration time and COD/N ratio of 30 min/h and 12, respectively (Table 5). The results showed that K_B and U_{max} were very sensitive to aeration time and COD/N ratio such that with an increase in aeration time, the values of K_B and U_{max} were increased while an increase in COD/N ratios caused a decrease in the constants. It was attributed to that the nitrogen serves as an essential nutrient for all living organisms, including the heterotrophic bacteria that remove organic pollutants from wastewater. Therefore, as aeration time increases, a greater percentage of nitrogen is removed via bacterial growth and reproduction (i.e. assimilation into new cell mass).

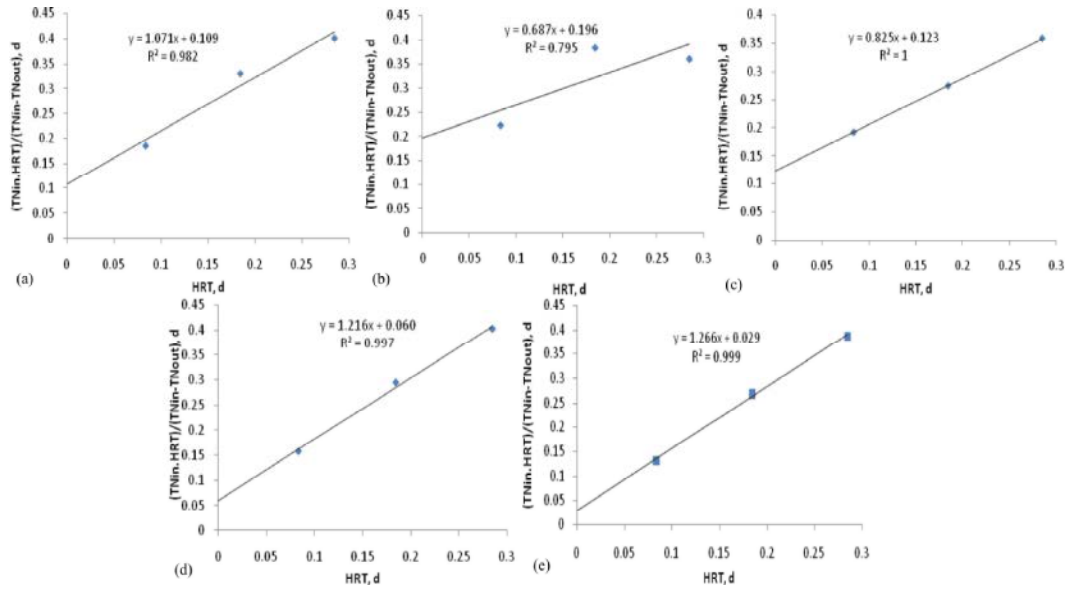

Fig. 5: Second-order kinetics model plots for TN removal in, (a) aeration time =30 min/h and COD/N ratio= 4, (b) aeration time= 30 min/h and COD/N ratio= 20, (c) aeration time = 40 min/h and COD/N = 12, (d) aeration time =50 min/h and COD/N ratio= 4, (e) aeration time =50 min/h and COD/N ratio= 4.

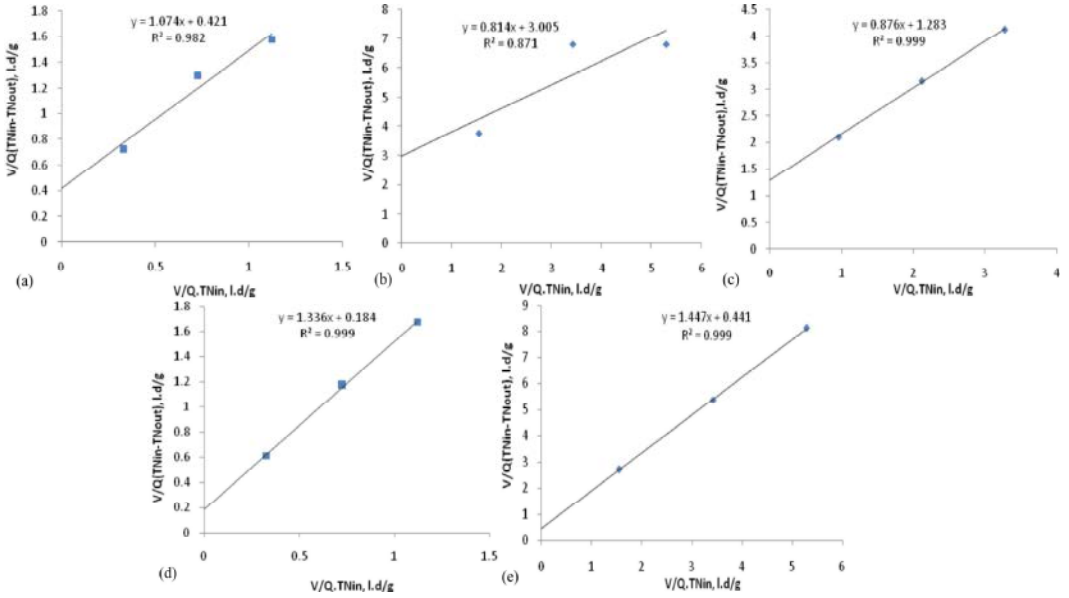

Fig. 6: Stover-Kincannon model plots for TN removal in, (a) aeration time =30 min/h and COD/N ratio= 4, (b) aeration time= 30 min/h and COD/N ratio= 20, (c) aeration time = 40 min/h and COD/N = 12, (d) aeration time =50 min/h and COD/N ratio= 4, (e) aeration time =50 min/h and COD/N ratio= 4.

The Kinetic coefficients K_B and U_{max} for TN removal (0.271-7.25 and 0.333-5.43 g/l.d respectively) were lower than the values found by Jin and Zheng [36] (12 and 12.4 g/l.d, respectively). This could be attributed to the relatively high nitrogen loading rate applied to the bioreactor in this study.

TP Removal

Process Description: Removal of phosphorus in wastewater is closely dependent upon the phosphorus release in anaerobic conditions and on the subsequent uptake process of the excess phosphorus including that contained in wastewater in aerobic conditions.

Table 6: Kinetic parameters for biological phosphorus removal in UAASFF reactor

	Variables			Models: Second order model					Models: Stover-Kin cannon model			
Run	HRT h	COD:TKN:TP g:g:g	Aeration time min/h	Regression equation	R^2	$k_{2(s)}$ d^{-1}	a	b	Regression equation	R^2	Umax $g.l.d^{-1}$	K_B $g.l.d^{-1}$
1	2 4.25 6.5	1:0.25:0.05	30	Y=0.69x+0.152	0.99	0.08	0.152	0.69	Y=0.69x+3.05	0.99	0.33	0.31
2	2 4.25 6.5	1:0.05:0.02	30	Y=0.94x+0.117	0.99	0.04	0.117	0.94	Y=0.94x+5.86	0.99	0.16	0.17
3	2 4.25 6.5	1:0.083:0.035	40	Y=0.96x+0.153	0.98	0.057	0.153	0.96	Y=0.96x+4.38	0.98	0.23	0.22
4	2 4.25 6.5	1:0.25:0.05	50	Y=2.12x+0.117	0.96	0.11	0.117	2.12	Y=2.12x+2.36	0.96	0.42	0.89
5	2 4.25 6.5	1:0.05:0.02	50	Y=1.22x-0.256	0.99	0.019	0.256	1.2	Y=1.22x-12.8	0.99	0.07	0.09

This basic information indicates that control of anaerobic (or anoxic) and aerobic conditions are of great importance to biological phosphorus removal. In the present study, as the system is intermittently aerated, a micro anaerobic environment seems to be provided in the biofloc formed in the process. The maximum observed phosphorus removal efficiency was about 79.1 % at COD:P ratio and aeration time 20 and 30 min/h, respectively. While, the minimum value of the response (23.3 %) was obtained at COD:P ratio and aeration time 50 and 50 min/h, respectively. As shown in Table 3, the response decreased upon increasing the aeration time. An increase in aeration time causes a decrease in the anaerobic time when the PAOs accumulate polyhydroxy butyrate (PHB) from volatile fatty acids (VFAs) produced. In this process, glucose as the individual source of VFAs requires sufficient time for acidification [37]. The reason for the decrease in phosphorous removal at high aeration time was due to the presence of nitrate, which inhibits the fermentation processes producing VFAs in the anaerobic zone.

Kinetic Evaluation for TP Removal

Grau Second-order Substrate Removal Model: The second-order kinetic coefficients ($k_{2(s)}$, a and b) are summarized as shown in Table 6. Very high agreement was found between the experimental and the model data (R^2=0.96). The second-order substrate removal rate constant values $k_{2(s)}$ ($a = P_{in}/(k_{2(S)}X)$, were in the range of 0.04-0.11d^{-1} (Table 6). Almost the same trend in $k_{2(s)}$ as what obtained for TN removal was found for P removal with smaller amount, indicating slower reaction rate compared to N removal rate.

Stover-Kincannon Model: Stover-Kincannon model was also used to assess the kinetic P removal process. The different coefficient (U_{max} and K_B) were computed as presented in Table 6. Determination coefficient showed very good regression (R^2=0.96). The values of U_{max} and K_B were in the range of 0.07-0.42 g1/l.d and 0.09-0.89 g/l.d, respectively. From the results, the maximum values of U_{max} and K_B were obtained to be 0.42 and 0.89 g P/l.d for aeration time and COD/P ratio 50 min/h and 20, respectively; while the minimum values of these parameters were 0.07 g/l.d and 0.09 g/l.d for aeration time and COD/P ratio, 50 min/h and 50, respectively.

CONCLUSION

Kinetic analysis of the UAASFF bioreactor using the experimental data obtained under different HRT, COD: N: P ratio and aeration time was successfully preformed. The maximum removal efficiencies of COD, TN and TP were obtained 93.6, 79 and 79.1 %, respectively. All the models examined, gave high correlation coefficients, for carbon, nitrogen and phosphorus removal. The maximum U_{max} for COD, TN and TP were found to be 22.56, 5.43 and 0.42 g/l.d, respectively. From the obtained biokinetic data suggesting that the reactor possessed an excellent COD, N and P removal capacity.

ACKNOWLEDGEMENT

The financial supports provided by Razi University, Kermanshah, is greatly acknowledged. The authors acknowledge the laboratory equipments provided by Water and Power Industry Institute for Applied and Scientific Higher Education (Mojtama-e-gharb), Kermanshah that has resulted in this article. The authors also wish to thank Mrs. S. Kiani for her assistant (Technical Assistant of Water and Wastewater Laboratory).

Nomenclature

TKN	Total Kjeldahl nitrogen	g/l
MLVSS	Mixed liquor volatile suspended solids	g/l
rbCOD	Readily biodegradable chemical oxygen demand	g/l
TN	Total nitrogen	g/l
VSS	Volatile suspended solid	g/l
SRT	Solid retention time	d^{-1}
OLR	Organic loading rate	g/l.d
Y	Growth yield coefficient	g VSS/g COD
k_d	Microbial decay rate constant	d^{-1}
μ_{max}	Maximum specific biomass growth rate	g VSS produced /g VSS present. d
K_s	Half-velocity constant	g/l
U_{max}	Maximum substrate utilization rate constant	g/l.d
K_B	Saturation constant	g/l.d
r_{su}= ds/dt	Rate of change in the substrate concentration due to utilization	g/l. d
X	Biomass concentration	g/l
S_0	Influent substrate concentration	g/l
S	Substrate concentration	g/l
μ	Specific biomass growth rate	g VSS produced /g VSS present. d
k_1	First-order substrate removal rate constant	d^{-1}
$k_{2(S)}$	Second -order substrate removal rate constant	d^{-1}
Q_0	Influent flow rate	l/d
Q	Effluent flow rate	l/d
Q_w	Waste sludge flow rate	l/d
X_e	Effluent biomass concentration	g/l
X_w	Effluent biomass concentration	g/l
V	Reactor volume	L
U= r_{su}/x	Specific substrate utilization rate	g COD/g VSS. d

REFERENCES

1. Pérez, J., J.L. Montesinos and F. Gòdia, 2006. Gas-liquid mass transfer in an up-flow cocurrent packed-bed biofilm reactor. Biochemical Engineering Journal, 31(3): 188-196.
2. Chong, N.M. and T.Y. Lin, 2007. Measurement of the degradation capacity of activated sludge for a xenobiotic organic. Bioresource Technology, 98(5): 1124-1127.
3. Asadi, A. and A. Ziantizadeh, 2011. Statistical Analysis and Optimization of an Aerobic SBR Treating an Industrial Estate Wastewater Using Response Surface Methodology (RSM). Iranica Journal of Energy & Environment, 2(4): 356-365.
4. Tartakovsky, B., M.F. Manuel and S. Guiot, 2005. Degradation of trichloroethylene in a coupled anaerobic-aerobic bioreactor: Modeling and experiment. Biochemical Engineering Journal, 26(1): 72-81.
5. Shen, C. and S. Guiot, 1996. Long-term impact of dissolved O2 on the activity of anaerobic granules. Biotechnology and Bioengineering, 49(6): 611-620.
6. Miguez, C.B., C.F. Shen, D. Bourque, S.R. Guiot and D. Groleau, 1999. Monitoring methanotrophic bacteria in hybrid anaerobic-aerobic reactors with PCR and a catabolic gene probe. Applied and Environmental Microbiology, 65(2): 381-388.
7. Moosavi, G., A. Mesdaghinia, K. Naddafi, A. Mahvi and J. Nouri, 2005. Feasibility of development and application of an up-flow anaerobic/aerobic fixed bed combined reactor to treat high strength wastewaters. Journal of Applied Sciences, 5(1): 169-171.
8. Kootenaei, F.G. and H.A. Rad, 2013. Treatment of Hospital Wastewater by Novel Nano-Filtration Membrane Bioreactor (NF-MBR). Iranica Journal of Energy and Environment, Special Issue on Nanotechnology, 4(1): 60-67.
9. Del Pozo, R. and V. Diez, 2005. Integrated anaerobic-aerobic fixed-film reactor for slaughterhouse wastewater treatment. Water Research, 39(6): 1114-1122.
10. Akhbari, A., A. Zinatizadeh, P. Mohammadi, M. Irandoust and Y. Mansouri, 2011. Process modeling and analysis of biological nutrients removal in an integrated RBC-AS system using response surface methodology. Chemical Engineering Journal, 168(1): 269-279.
11. Zare, H., G. Najafpour, H. Heydarzadeh, M. Rahimnejad and A. Tardast, 2012. Performance and Kinetic Evaluation of Ethyl Acetate Biodegradation in a Biofilter Using Pseudomonas Putida. Iranica Journal of Energy & Environment, 3(5): 14-18.

12. Ra, C., K. Lo, J. Shin, J. Oh and B. Hong, 2000. Biological nutrient removal with an internal organic carbon source in piggery wastewater treatment. Water Research, 34(3): 965-973.
13. Artan, N. and D. Orhon, Mechanism and design of1 sequencing batch reactors for nutrient removal2005: Iwa Publishing.
14. Beltrán, F.J., J.F. García-Araya and P.M. Álvarez, 2000. Estimation of Biological Kinetic Parameters from a Continuous Integrated Ozonation-Activated Sludge System Treating Domestic Wastewater. Biotechnology progress, 16(6): 1018-1024.
15. Akhbari, A., A. Zinatizadeh, P. Mohammadi, Y. Mansouri, M. Irandoust and M. Isa, 2012. Kinetic modeling of carbon and nutrients removal in an integrated rotating biological contactor-activated sludge system. International Journal of Environmental Science and Technology, 9(2): 371-378.
16. Carta-Escobar, F., J. Pereda-Marin, P. Alvarez-Mateos, F. Romero-Guzmán and M. Durán Barrantes, 2005. Aerobic purification of dairy wastewater in continuous regime: Part II: Kinetic study of the organic matter removal in two reactor configurations. Biochemical Engineering Journal, 22(2): 117-124.
17. Stover, E.L. and D.F. Kincannon, 1982. Rotating biological contactor scaleup and design. In: Proceedings of the 1st International Conference on Fixed Film Biological Processes, Kings Island, Ohio.
18. Vavilin, V.A., S.V. Rytov, L.Y. Lokshina, J.A. Rintala and G. Lyberatos, 2001. Simplified hydrolysis models for the optimal design of two-stage anaerobic digestion. Water Research, 35(17): 4247-4251.
19. Ardestani, F., 2011. Investigation of the Nutrient Uptake and Cell Growth Kinetics with Monod and Moser Models for Penicillium brevicompactum ATCC 16024 in Batch Bioreactor. Iranica Journal of Energy & Environment, 2(2): 117-121.
20. Grau, P., M. Dohanyos and J. Chudoba, 1975. Kinetics of multicomponent substrate removal by activated sludge. Water Research, 9(7): 637-642.
21. Ahn, J.H. and C. Forster, 2002. A comparison of mesophilic and thermophilic anaerobic upflow filters treating paper-pulp-liquors. Process Biochemistry, 38(2): 256-261.
22. Ahn, J.H. and C. Forster, 2000. Kinetic analyses of the operation of mesophilic and thermophilic anaerobic filters treating a simulated starch wastewater. Process Biochemistry, 36(1): 19-23.
23. Yu, H., F. Wilson and J.H. Tay, 1998. Kinetic analysis of an anaerobic filter treating soybean wastewater. Water Research, 32(11): 3341-3352.
24. Ni, S.Q., P.H. Lee and S. Sung, 2010. The kinetics of nitrogen removal and biogas production in an anammox non-woven membrane reactor. Bioresource Technology, 101(15): 5767-5773.
25. Borghei, S., M. Sharbatmaleki, P. Pourrezaie and G. Borghei, 2008. Kinetics of organic removal in fixed-bed aerobic biological reactor. Bioresource Technology, 99(5): 1118-1124.
26. Kuşçu, Ö.S. and D.T. Sponza, 2009. Kinetics of para-nitrophenol and chemical oxygen demand removal from synthetic wastewater in an anaerobic migrating blanket reactor. Journal of Hazardous Materials, 161(2): 787-799.
27. APHA, 1999.Standard Methods for the Examination of Water and Wastewater, 19th ed. American Public Health Association, Washington, DC.
28. Kaewsuk, J., W. Thorasampan, M. Thanuttamavong and G.T. Seo, 2010. Kinetic development and evaluation of membrane sequencing batch reactor (MSBR) with mixed cultures photosynthetic bacteria for dairy wastewater treatment. Journal of Environmental Management, 91(5): 1161-1168.
29. Metcalf, Eddy, 2003. Tochobanoglous, Wastewater Engineering: Treatment and Reuse, fourth ed. New York, McGraw-Hill Higher Education.
30. Gray, N.F., 2004. Biology of wastewater treatment, Second Edition, London WC2H 9HE.
31. Işik, M. and D.T. Sponza, 2005. Substrate removal kinetics in an upflow anaerobic sludge blanket reactor decolorising simulated textile wastewater. Process Biochemistry, 40(3): 1189-1198.
32. Droste, R.L., 1997. Theory and Practice of Water and Wastewater Treatment. Wiley, New York.
33. Yuceer, S., 2006. Investigated effect of temperature to substrate removal kinetic in anaerobic filter. M.Sc Thesis, Cukurova University, Institute of Science, Department of Environmental Engineering, Adana.
34. Sponza, D.T. and A. Uluköy, 2008. Kinetic of carbonaceous substrate in an upflow anaerobic sludge sludge blanket (UASB) reactor treating 2, 4 dichlorophenol (2, 4 DCP). Journal of Environmental Management, 86(1): 121-131.
35. Borghei, S.M. and S.H. Hosseiny, 2002. Modeling of organic removal in a moving bed biofilm reactor (MBBR). Scientica Iranica, 9: 53-58.
36. Jin, R.C. and P. Zheng, 2009. Kinetics of nitrogen removal in high rate anammox upflow filter. Journal of Hazardous Materials, 170(2): 652-656.
37. Tchobanoglous, G.F.L. and H.D. Burton, 2003. Stensel, Treatment and reuse Wastewater engineering. 4th Ed. McGraw Hill, New York.

Persian Abstract

DOI: 10.5829/idosi.ijee.2014.05.03.12

چکیده

در این مطالعه، حذف همزمان کربن، نیتروژن و فسفر از فاضلاب سنتزی در یک بیوراکتور با جریان رو به بالای هوازی/انوکسیک با فیلم ثابت لجن (UAASFF) مورد بررسی قرار گرفت. تحلیل سینتیکی با استفاده از داده های آزمایشگاهی به دست آمده از مطالعه قبلی که در آن بیوراکتور UAASFF تحت شرایط راهبری مختلف با تغییر سه متغیر مستقل HRT ، نسبت COD:N:P و زمان هوادهی مورد آزمایش قرار گرفته بود، انجام شد. در این تحلیل مدل های مختلف سینتیکی (مونود، درجه اول، درجه دوم؛ و استوور کین کنن) مورد ارزیابی قرار گرفتند. حداکثر راندمان حذف برای COD، نیتروژن کل (TN) و فسفر کل(TP) به ترتیب ۹۵/۴۲، ۷۹ و ۷۹/۱٪ به دست آمد. تمام مدل های آزمایش شده، ضرایب همبستگی بالایی را برای حذف کربن، نیتروژن و فسفر نشان دادند. ضرائب سینتیکی به دست آمده در این مطالعه به صورت زیر می باشند:

Y= 0.417-0.496 g VSS/g COD, k_d= 0.027-0.053 d^{-1}, μ_{max} =1.36 g VSS /g VSS.d, K_B=37.96 g/l.d, U_{max}=38.46 g/l.d, $K_B(N)$ =0.271-7.2 g/l.d 6, $U_{max}(N)$ =0.33-5.4 g/l.d, $K_B(P)$=0.09-0.89 g/l.d, $U_{max}(P)$=0.07-0.42 g/l.d